universität wien

DISSERTATION / DOCTORAL THESIS

Titel der Dissertation / Title of the Doctoral Thesis

„Towards a Plant-on-a-Bench“

verfasst von / submitted by

Dipl.-Ing. Hande Barkan Öztürk

angestrebter akademischer Grad / in partial fulfilment of the requirements for the degree of

Doktorin der Naturwissenschaften (Dr.rer.nat)

Wien, 2022 / Vienna, 2022

Studienkennzahl lt. Studienblatt / degree program code as it appears on the student record sheet:	UA 796 605 419
Dissertationsgebiet lt. Studienblatt / field of study as it appears on the student record sheet:	Chemie
Betreut von / Supervisor:	Univ.-Prof. Dr. Alexander Bismarck

Abstract

Macroporous polymers produced by polymerisation of the monomer containing continuous phase (CP) of high internal phase emulsions (HIPEs), known as polyHIPEs, have been explored for many diverse applications, e.g., filters, membranes, sorbents and scaffolds for tissue engineering. I investigated micromixing of fluids in the tailorable, interconnected pore structure of polyHIPEs, which can be assembled to realise miniaturised unit operations leading to a plant-on-a-bench system suitable for continuous flow chemistry.

Miniaturised unit operations were realised by designing and fabricating polyHIPE micromixers with tailored morphological features and physical properties. The residence time distribution of polyHIPE micromixers was determined using a tracer method and was found to be in good agreement with the axial dispersion model. Moreover, the effectiveness of polyHIPE micromixers was demonstrated using two competitive parallel reactions. The yield of the slower saponification reaction (2.5%) was found to be significantly lower compared with a commercial Kenics® static mixer which proofs the effective micromixing within the polyHIPEs. Utilising the effective mixing performance of polyHIPE micromixers allowed for continuous emulsification of a monomer containing continuous and an aqueous internal phase resulting in HIPEs. Using the polyHIPE micromixer, it was possible to generate HIPEs with adjustable volume fractions and droplet diameters that could be polymerised into polyHIPEs. Continuous alteration of the ratio between the continuous and the internal phase of the generated HIPEs is also possible using these micromixers, which after polymerisation of the monomer phase resulted in polyHIPEs with a porosity gradient.

To perform continuous organic flow reactions, polyHIPE microreactors were fabricated using hypercrosslinked polyHIPEs having a surface area of 850 m^2/g and a Pd surface loading serving as heterogeneous catalyst. However, due to the lack of functional groups on their surface, which form complexes with Pd and thereby immobilising it, the model hydrogenation reaction could not be performed. However, using a solvent stitching approach and Scholl coupling reaction allowed for simultaneous hypercrosslinking and functionalisation of the polyHIPEs leading to the incorporation of triphenylphosphine moieties into the polymer network, which results in upto 7 wt.% P functionalisation. Unfortunately, during these reactions the polyHIPE monoliths

fractured into pieces. Nevertheless, these pieces were found to have efficient catalytic activities after Pd loading for a model Suzuki-Miyaura coupling reaction, allowing yields of up to 98% after a reaction time of only 30 min resulting in turnover frequencies of up to 2440 h^{-1}.

The final operation unit of a plant-on-a-bench is a continuous liquid-liquid extraction unit with settler. This could be fabricated by combining hydrophilic and hydrophobic polyHIPEs within a micromixer and connect it to a minisettler. The microextractor-minisettler was used for the extraction of a hydrogenation reaction product from its simulated reaction medium into ethyl acetate within a polyHIPE micromixer connected to a gravity-based minisettler. The extraction efficiency of the polyHIPE-microextractor-minisettler unit reached 98%, while that of control experiments performed using a blank tube or static mixer was only 78%.

I designed and fabricated polyHIPE micromixers and microextraction units, which could be useful for the intensification of continuous flow reactions in miniaturised operating units, and demonstrated their efficiency.

Zusammenfassung

Makroporöse Polymere, die durch Polymerisation der monomerhaltigen, kontinuierlichen Phase (CP) von *High Internal Phase Emulsions* (HIPEs) hergestellt werden, werden PolyHIPEs genannt und kommen für verschiedenste Anwendungen z.B. als Filter, Membranen, Sorptionsmittel und *Scaffolds* für die Gewebezüchtung in Frage. Ich untersuchte das *Micromixing* von Flüssigkeiten in PolyHIPEs mit einer maßgeschneiderten, offenporigen Porenstruktur, die als miniaturisierte Reaktoren bzw. Betriebseinheiten zu einem *Plant-on-a-Bench*-System zusammengesetzt werden können, das für die kontinuierliche Durchflusschemie geeignet ist.

Die miniaturisierten Durchflussreaktoren wurden durch die gezielte Synthese von PolyHIPE-*Micromixern* mit auf die Anwendungsanforderungen zu geschneiderten Morphologien und physikalischen Eigenschaften hergestellt. Die Verweilzeitverteilung in den PolyHIPE-*Micromixer* wurde unter Verwendung eines Tracer-Verfahrens bestimmt und es wurde festgestellt, dass sie in guter Übereinstimmung mit dem axialen Dispersionsmodell steht. Darüber hinaus wurde anhand von zwei kompetitiven Parallelreaktionen die Wirksamkeit von polyHIPE-*Micromixern* im Vergleich zum handelsüblichen Kenics® -Statikmischer getestet. Es wurde festgestellt, dass die Ausbeute der langsameren Verseifungsreaktion (2,5 %) in PolyHIPE-*Micromixern* verglichen mit dem Kenics® -Statikmischer signifikant niedriger war, was die Effektivität des *Micromixings* in PolyHIPEs beweist. Die Nutzung der effektiven Mischleistung von PolyHIPE-*Micromixern* ermöglichte das kontinuierliche Emulgieren einer wässrigen, internen Phase in einer kontinuierlichen Monomerphase was zu HIPEs führte. Mit dem PolyHIPE-*Micromixer* war es möglich, HIPEs mit einstellbaren Volumenanteilen und Tröpfchendurchmessern zu erzeugen, die zu polyHIPEs polymerisiert werden konnten. Darüber hinaus ist durch die Verwendung von PolyHIPE-*Micromixern* auch eine kontinuierliche Änderung des Volumenverhältnisses zwischen der internen und der kontinuierlichen Phase der erzeugten HIPEs möglich, was nach der Polymerisation der Monomerphase zu PolyHIPEs mit einem Porositätsgradienten führt.

Um kontinuierliche organische Durchflussreaktionen durchführen zu können, wurden zunächst PolyHIPE-*Microreaktor* unter Verwendung von *hypercrosslinked* PolyHIPEs mit einer Oberfläche von 850 m^2/g hergestellt und Pd als heterogenem Katalysator auf

deren Porenoberfläche abgeschieden. Aufgrund des Mangels an funktionellen Gruppen auf der PolyHIPE-Oberfläche, die mit Pd Komplexe bilden und es somit immobilisieren können, konnte die Modellhydrierungsreaktion nicht effektiv durchgeführt werden. Aus diesem Grund wurde der Lösungsmittel-Stitching-Ansatz und die Scholl-Kupplungsreaktion zum gleichzeitigen *Hypercrosslinking* und Funktionalisieren der PolyHIPEs verwendet, was den Einbau von Triphenylphosphin-Einheiten in das Polymernetzwerk ermöglichte, was zu einer P-Funktionalisierung der Oberfläche von bis zu 7 Gew.-% führte. Leider zerbrachen die polyHIPE-Monolithen während dieser Reaktionen in Stücke. Dennoch wurde festgestellt, dass diese Stücke nach Pd-Beladung für eine Modell-Suzuki-Miyaura-Kupplungsreaktion effiziente katalytische Aktivitäten aufweisen. Dies führt zu Ausbeuten von bis zu 98 % nach einer Reaktionszeit von nur 30 min und entspricht zu *Turnover*-Frequenzen von bis zu 2440 h^{-1}.

Die letzte Betriebseinheit einer Plant-on-a-Bench ist eine kontinuierliche Flüssig-Flüssig-Extraktionseinheit mit Abscheider. Dies wurde durch das Zusammenführen von hydrophilen und hydrophoben PolyHIPEs zu einem *Micromixer*, der mit einem Miniabscheider verbunden ist, realisiert. Dieser *Microextractor*-Miniabscheider wurde für die Überführung eines Hydrierungsreaktionsprodukts aus einem simulierten Reaktionsmedium in Ethylacetat verwendet, wobei der Miniabscheider Schwerkraft getrieben war. Die Extraktionseffizienz des PolyHIPE- *Microextractor*-Miniabscheider betrug 98 %, während die der Kontrollexperimente, die unter Verwendung eines leeren Röhrchens oder eines Statikmischers durchgeführt wurden, nur 78 % betrug.

Ich entwarf und stellte PolyHIPE-*Micromixer* und *Microextraktor-unit* her, die für die Intensivierung von kontinuierlichen Durchflussreaktionen in miniaturisierten Betriebseinheiten nützlich sein könnten, und demonstrierte ihre Effektivität.

Acknowledgment

My PhD would not have been possible without the support of many people. Many thanks and heartful gratitude to my supervisor, Prof. Alexander Bismarck, who read my numerous manuscripts and helped me to find solutions to many troubles, even in my own sentences. Your insightful feedback, faith and meticulous editing brought me to the end of my PhD, but not to the end of our scientific journey.

I am grateful to my co-supervisor Dr. Angelika Menner for her encouraging and motivating guidance. Thank you for providing opportunities for me to grow professionally. Owing to your organisational helps and advice made possible to finish my PhD. Without you we would have so much trouble.

I am fortunate that Ass. Prof. Robert Woodward joined our team during my PhD. Special thanks to you that you made my third paper possible, and for your valuable suggestions, which still did not satisfy Alex so I had to go back to lab.

I would like to thank Dr. Andreas Mautner for his help in my endless XPS measurements. I would also like to acknowledge to Mag. Dr. Franz Jirsa, Privatdoz., who helped a lot to characterise my samples.

I am fortunate to have been a part of the PaCE group. I would especially like to thank Dr. Qixiang Jiang for being willing to discuss scientific challenges and having time for my questions not only during my masters but also during my PhD.

Many thanks to all other members of our research group for all their support, encouraging and having lots of fun. But special thanks my beloved friends Emina Muratspahic, Neptun Yousefi and Amy Ho, who were always by my side on the ups and downs. Even though we had many downs, still we had so much fun together.

I would like to express my gratitude to Claudia Mitterer, who is always there to help us with almost everything in the laboratories. She made our experiments possible. I am also thankful to Angela Weber for her incredible help with organisational matters.

I am grateful for the help of all BSc and exchange students (Seo Hee Son, Maximillian Spitaler, Simona Kiskyte, Alena Chugreeva, Barbara Wagner, Felix Fronek, Salome Boizet, Agathe Le Guen, Martin Gostner, Joanna Delorme, Bilgesu Apaydin) for their contribution to my thesis and their support while working with me.

Last, but not least, I am grateful to my husband, Burak Öztürk, who always believed in me and thanks to him I have started my PhD journey. Thank you that you were always there, and always will be. I am thankful to my parents, whose constant love and support. Thank you for my brother, who was always there for me. I would also like to deeply thank my old friends in Turkey and new friends in Vienna. They bring joy to my life.

List of Scientific Publications

Publication 1: Barkan-Öztürk, H.; Menner, A.; Bismarck, A. Emulsion-Templated Macroporous Polymer Micromixers. *Ind. Eng. Chem. Res.* **2021**, *60* (39), 14013–14025. https://doi.org/10.1021/acs.iecr.1c01949.

HBÖ performed all experimental work and analysed the data. AM conceptualization, supervision, revision of draft, AM and AB supervised the work. All authors contributed to manuscript review and editing.

Publication 2: Barkan-Öztürk, H.; Menner, A.; Bismarck, A. Polymerised High Internal Phase Emulsion Micromixers for Continuous Emulsification. Chem. Eng. Sci. 2021, 117296. https://doi.org/10.1016/j.ces.2021.117296.

HBÖ performed all experimental work and analysed the data. AM conceptualization, supervision, revision of draft, AM and AB supervised the work. All authors contributed to manuscript review and editing.

Publication 3: Barkan-Öztürk, H.; Menner, A.; Woodward, R.; Bismarck, A. Simultaneous hypercrosslinking and functionalization of polyHIPEs for catalyst supports, submitted 2022.

All authors conceptualized the work, HBÖ performed all experimental work and analysed the data. HBÖ, RW and AB wrote the manuscript and designed the figures. AM, RW and AB supervised the work. All authors contributed to manuscript review and editing.

Publication 4: Barkan-Öztürk, H.; Delorme, J.; Menner, A.; Bismarck, A. Liquid-liquid extraction using combined hydrophilic-hydrophobic emulsion templated macroporous polymer micromixer-settlers. Submitted 2022.

All authors conceptualized the work, HBÖ performed all experimental work and analysed the data. JD performed experimental work. HBÖ, and AB wrote the manuscript and designed the figures. AM and AB supervised the work. All authors contributed to manuscript review and editing.

Oral presentations and papers at conferences:

Barkan-Öztürk, H., Menner, A., Bismarck, A., Plant-on-a-Bench. Danube Vltava Sava Polymer Meeting (DVSPM), Vienna, 2017.

Barkan-Öztürk, H., Menner, A., Bismarck, A., Emulsion templated macroporous polymer as micromixer. 18th European Conference on Composite Materials (ECCM18). Athens, 2018.

Barkan-Öztürk, H., Menner, A., Bismarck, A., 3D-Printing Compressible Macroporous Polymer Using Poly-Pickering-HIPE as Micromixer. 18th International Conference on Composite Materials (ICCM18). Amsterdam, 2018.

Barkan-Öztürk, H., Menner, A., Bismarck, A., The Micromixer Properties of PolyHIPEs. MOF19. Paris, 2019.

Barkan-Öztürk, H., Woodward, R., Bismarck, A., Hypercrosslinked polyHIPEs as Pd-catalyst supports. Polymer Meeting. Graz, 2021.

Barkan-Öztürk, H., Menner, A., Bismarck, A., Liquid-Liquid extraction using hydrophilic & hydrophobic polyHIPE micromixers. European Polymer Meeting, Prague, 2022.

List of Symbols and Abbreviations

Symbol	Parameter	Unit
D_i	Inner diameter	mm
d_p	Average pore diameter	µm
d_{pt}	Average pore diameter	µm
k	Permeability	Darcy ($x10^{-12}$ m^2)
k_La	overall volumetric mass transfer coefficient	s^{-1}
P	Porosity	%
Re_p	Pore Reynolds number	-
N	number of average pore throats per pore	-
Q_{tot}	Total flow rate	mL/min
V	Volume	cm^3
ε	Energy dissipation rate	m^2/s^3
η	Apparent viscosity	Pa s
ρ_f	Foam density	gr/cm^3
ρ_s	Skeletal density	gr/cm^3

Abbreviations

3D	Three dimensional
4-AAP	4-aminoacetophenone
4-NAP	4-nitroacetophenone
AF	Ammonium formate
AIBN	Azobisisobutyronitrile
Ca	Capillary number
CEC	Capillary electrochromatography
CMP	Bis(chloromethyl)-biphenyl
CNC	Computer numerical control
CP	Continuous phase
DCE	1,2-dichloroethane
DCM	Dichloromethane
DoI	Degree of Interconnectivity
DVB	Divinylbenzene
EGDMA	Ethylene glycol dimethacrylate
EHA	2-ethylhexyl acrylate
GMA	Glycidyl methacrylate
HCPs	hypercrosslinked polymers
HDK H20	Hydrophobic pyrogenic silica particles
HEMA	Hydroxyethyl methacrylate

HIPEs	High internal phase emulsions
HLB	Hydrophilic-lypophilic balance
IP	Internal phase
LIPEs	Low internal phase emulsions
L-L	Liquid-liquid
MBAA	N,N′ -methylene bisacrylamide
MIPEs	Medium internal phase emulsions
o/w	Oil-in-water
$Pd(OAc)_2$	Palladium acetate
PI	Process intensification
PPh_3	Triphenylphosphine
PUDA	Polyurethane diacrylate
Re	Reynolds number
RTD	Residence time distribution
SEM	Scanning electron microscopy
SM	Static mixer
Span 80	Sodium monosorbitol
St	Styrene
TFEMA	2,2,2-trifluoroethyl methacrylate
TLC	Thin-layer chromatography
UV	Ultraviolet
w/o	Water-in-oil
We	Weber number

Table of Content

1 Introduction

Continuous flow processing is an innovative technology (Figure 1-1), which can be applied to many chemical reactions of relevance to various industrial fields producing significant benefits in terms of process and chain efficiency, lower capital and operating expenses, better product quality, less waste and improved process safety.[1,2] In order to scale up chemical reactions to industrial scale, continuous processing needs to be investigated and developed in lab-scale. Therefore, miniaturised equipment needs to be designed, fabricated, and tested to perform unit operations, such as mixing, chemical transformation, extraction, separation, crystallisation and distillation, continuously. For instance, during mixing operations, chemical reactions or extraction can be performed in micromixers or static mixers.

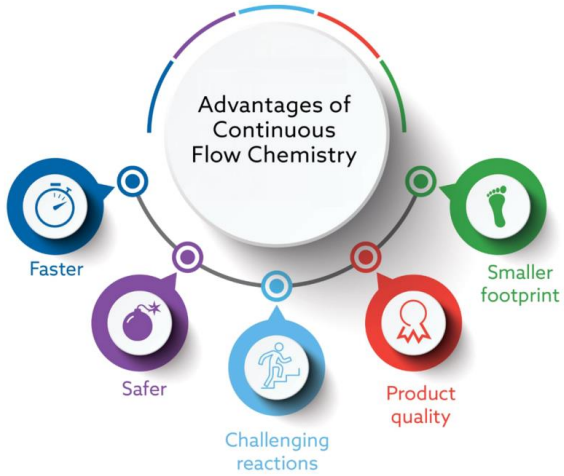

Figure 1-1. What is driving the adoption of continuous flow chemistry for chemical synthesis? (Reprinted from Baumann, M. et al.,[2] Copyright 2020 with permission from American Chemical Society).

Over the years, applications of micromixers have grown rapidly due to the advantages they present, including better control of physical reaction parameters, reduced reagent utilization, fast and controllable mixing processes, lower energy consumption and therefore, lower costs.[3,4] The small dimensions of micromixers results in a large surface area to volume ratio, which provides efficient mass and heat transfer rates.[5] As a result of those advantages, we can say that, micromixers have significant role to play in the development of continuous flow reactions.

In micromixers mixing of two or more fluids occurs by molecular diffusion mainly in laminar flow while mixing at macro scale occurs by turbulent movement.[6] The

transition between laminar and turbulent flow is conveniently described by the Reynolds (*Re*) number, which is the ratio of inertial to viscous forces within the fluid. Relying only on diffusion to mix fluids is inconvenient for large-scale mixing as very long channels or tubes would be needed. Therefore, mixing is commonly enhanced by chaotic advection, which is achieved by increasing the deformation of the boundary between fluids by stretching resulting in an increased interfacial area.[7] In order to achieve chaotic advection, the *Re* should be higher than one,[4] micromixer channel design is of great importance to increase the interface between fluids while reducing channel length and thus the mixing time. Most reported micromixers have been produced by injection moulding of cyclic olefin copolymer,[8] moulding Polydimethylsiloxane onto a plasma etched silica substrates[9] or by machining polycarbonates.[10] However, special instrumentations and clean room facilities are necessary to build micromixing devices using time consuming and challenging processes, resulting in high costs. Moreover, the channel dimensions cannot be lower than hundreds of micrometres due to physical limitations.[8] For this reason interconnected, high porosity macroporous polymers, whose pore size can be tuned from hundreds to a few µm, were explored as valuable option for the production of micromixers,[11,12] microreactors[13] as well as extraction units.[14]

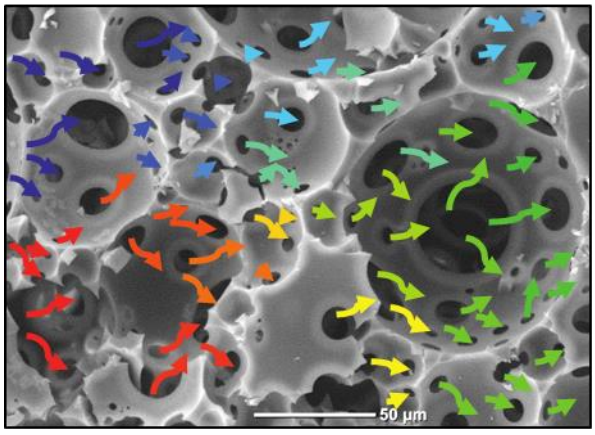

Figure 1-2. Typical SEM image of an emulsion templated macroporous polymers, illustrating the chaotic advection of two co-flowing im/miscible fluids passing through its interconnected pore space, causing mixing.

Macroporous polymers can be produced using a variety of techniques, including chemical or physical blowing,[15,16] phase separation[17,18] or templating methods.[19–21] Since a tailored interconnected macroporous structure is of great importance for the fabrication of micromixers, emulsion templating methods offer significant advantages

over other polymer foaming processes. Emulsion templating commonly employed High Internal Phase Emulsions (HIPEs), defined emulsions with an internal phase volume ratio >74%, which after polymerisation of the continuous emulsions phase consisting of or containing monomers and removal of the internal templating phase results in high porosity macroporous polymers, called poly(merised)HIPEs.[22] Emulsion templating methods offer a number of advantages for the fabrication of micromixers; for instance the morphological properties of porous polymers can be easily tailored during the emulsification process by changing the emulsification conditions (choice of emulsifier and energy input)[23,24] and their and mechanical properties can be tuned by monomer selection[25,26] and incorporation of suitable reinforcements.[27,28] Chemically inert scaffolds for micromixers can be realised by monomer selection from the large catalogue of monomers, that can be polymerised in emulsions. Moreover, post-processing of interconnected macroporous polymers allows for the introduction of various functionalities to alter their surface properties, such wettability, specific surface area, etc. Moreover, it is possible to load catalysts onto their interior surface for use in catalysed chemical reactions. PolyHIPEs are great candidates for the fabrication of micromixers and extraction units to mix liquids in their interconnected pore network (Figure 1-2) as well as catalyst support for heterogeneous catalysis.

1.1 Scope of the thesis

Emulsion templating is a suitable method to produce macroporous polymers with desired morphology and mechanical properties.[29] Therefore, the aim of my PhD thesis is to design, build and demonstrate unit operations, which will be useful for the realisation of a miniature plant-on-a-bench system suitable to test continuous flow chemistry. To reach this aim, the following objectives were defined:

1. to optimize the morphological properties of polyHIPEs for micromixing applications,
2. to quantify the micromixing performance of polyHIPE micromixers,
3. to demonstrate the usefulness of polyHIPE micromixers for the continuous emulsification of two immiscible liquid phases,

4. to simultaneously functionalise and hypercrosslink polyHIPEs to introduce ligands enabling catalyst loading and increasing surface area,
5. to realise a polyHIPE micromixer heterogeneous catalyst support for continuous hydrogenation reactions, and
6. to design and fabricate an effective polyHIPE extraction unit to separate reaction educts and products continuously.

1.2 Structure of the thesis

The brief introduction and aims & objectives will be followed by a literature review detailing the advance of porous polymers produced by emulsion templating methods and their application areas highlighting the research gaps required to further the development porous polymer-based micromixers. Chapter 3 will briefly summarise the experimental methods. Chapter 4 will be the executive summary of my research findings detailed in appended publications I to IV. Chemically stable polyHIPEs were designed and fabricated into micromixers and their micromixing performance quantified by the Residence Time Distribution and competitive parallel reactions (**Publication I**). In order to prove the effective micromixing in the polyHIPE micromixers, HIPEs were generated by mixing monomer containing continuous phase and aqueous internal phase in various ratios and flow rates. Thereby, I showed that the Degree of Interconnectivity of openness of polyHIPEs has impact on the droplet breakup, which allows to produce continuous emulsions having desired internal volume phase fraction and droplet size (**Publication II**). In the following work (**Publication III**), polyHIPEs were hypercrosslinked and simultaneously functionalized with phosphine moieties with various hypercrosslinking methods to accomplish heterogeneous catalyst loaded polyHIPE microreactors. However, due to the strong reaction conditions monolithic polyHIPEs were broken either during the quenching of the hypercrosslinking reaction or purification. Nevertheless, successful phosphine functionalisation was achieved and allowed to stable Pd-loading, which was tested with model Suzuki-Miyaura cross-coupling reaction by reaching 2440 h^{-1} turnover frequency. Furthermore, I also hypercrosslinked polyHIPEs using bischloromethyl biphenyl, which resulted in increased surface area (up to 850 m^2/g) and improved mechanical properties. However, due to lack of ligand in the chemical structure of

hypercrosslinked polyHIPEs, stable and catalytically active Pd loading could not be achieved. Their results were explained in the summary of my research. As a final step of realising plant-on-a-bench operation units, micromixer-setter was fabricated using polyHIPE extraction unit consist of both hydrophilic and hydrophobic polyHIPEs and homemade settler (**Publication IV**). Hydrogenation reaction simulation was extracted in polyHIPE extraction unit and separated continuously.

2 Literature Review

2.1 Process Intensification: from microfluidics towards plant-on-a-bench

Process intensification (PI) is a strategy to minimise the size of chemical plants to achieve a given production objective with significantly reduced capital cost of the system.[30] Process intensification involves development of innovative equipment and advanced techniques that results in momentous enhancements in chemical processing while reducing substance volume, thus waste, and energy consumption (Figure 2-1). PI results in cheaper, safer, and sustainable chemical processes.[31] The four principles of PI are;[32]

1. to enhance the effectiveness of intra- and intermolecular interactions toward ideal reactions,
2. to supply the same process environment to each molecule,
3. to adjust the driving forces and resistances in the most favourable way and enhance specific surface areas,
4. to maximise synergistic effects from all process units.

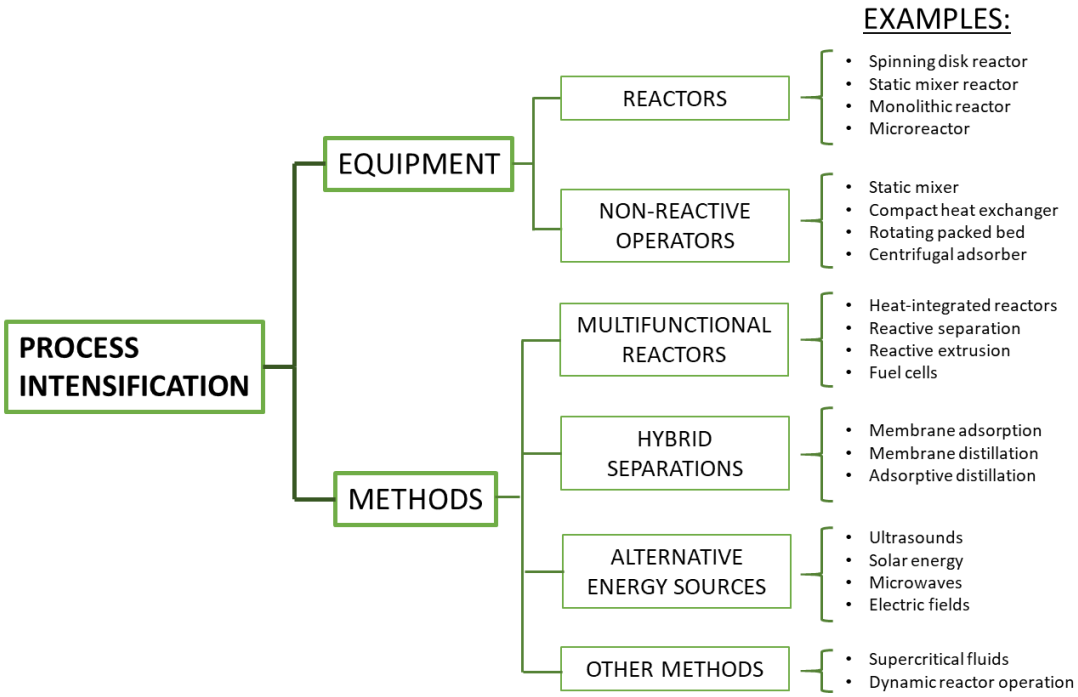

Figure 2-1. Components of Process Intensification (adapted from "Reactive separations for process intensification: an industrial perspective", Stankiewicz, A., 2003).[31]

Multifunctional reactors and microtechnology have significant importance in downscaling chemical plants by replacing large, expensive, and energy-intensive equipment or processes.[33] Multifunctional reactors are designed to simultaneously perform several processes, such as mixing and catalytic reaction. The main aim of multifunctional reactors is to optimise mass, heat and momentum transfer within a single flow cell leading to lower reaction volumes, better temperature control, and reduction in pressure requirements.[2,30] Figure 2-2 shows an example of a multifunctional reactor developed by Bayat et al.[34], which allows to couple the highly exothermic methanol synthesis with the endothermic cyclohexane dehydrogenation with a Pt/Al_2O_3 catalyst. They further modified this reactor by addition of zeolite 4A particles acting as water adsorbent, which offers significant advantages over the conventional sorption-enhanced reaction process because the water adsorbent can be continuously regenerated using a solid regenerator.[34]

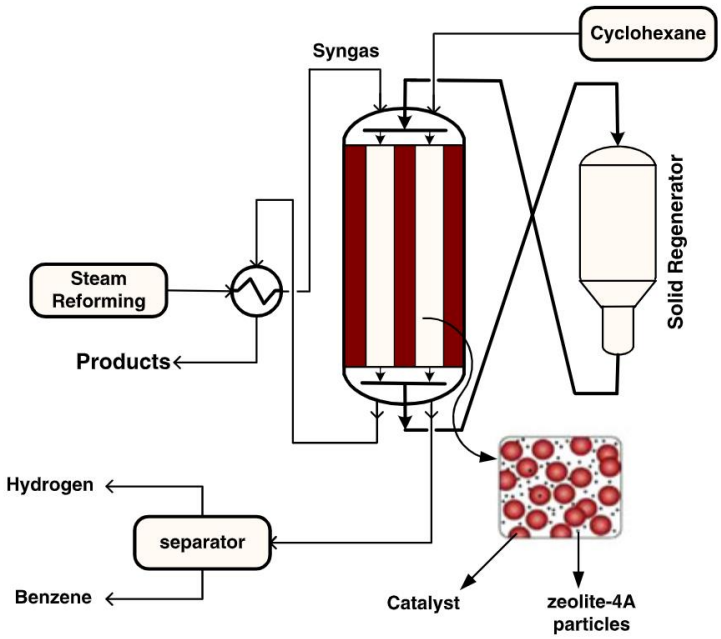

Figure 2-2. Schematic flow diagram of a thermally coupled multifunctional reactor for simultaneous production of methanol and hydrogen. (Reprinted from Bayat, M., et al.,[34] copyright 2013, with permission from John Wiley & Sons, Ltd.).

Many studies focus on continuous flow chemistry, which is an important part of process intensification. Recent studies showed that economical and sustainable processes can be achieved by transforming a batch into a continuous process.[35,36] For instance, Snead and Jamison synthesised and purified diphenhydramine hydrochloride, an active pharmaceutical ingredient, by continuous flow chemistry, which produced a number of advantages, such as real-time inline purification, solvent minimisation, resulting in lower waste, reduced costs and hazards.[37]

Incorporation of micromixers and microreactors into continuous chemical reactions is a way to intensify production processes because of enhanced surface-to-volume ratios as result of decreased characteristic dimensions of the system.[5,36] Micromixers are mixing units, where fluids can interact with each other by molecular diffusion in sub-millimeter channels.[38] Due to the high specific surface area reacting species are homogenized at molecular scale, which leads to better reaction control, improved selectivity, and higher reaction rates.[32,39] Micromixers are classified as active and passive, depending on the mixing mechanism. In active micromixers fluids are mixed by external energy input, such as acoustic, magnetic or electric fields.[40] Passive micromixers rely on manipulation of fluid flow by channel geometry and/or interfacial forces to enhance interfacial area between the fluids, thus resulting enhanced mixing.[38]

Mixing in passive micromixers occurs mainly by molecular diffusion in the laminar range, when the Reynolds number, which is the ratio between inertial forces and viscous forces, is much below 2200. However, relying only on molecular diffusion to achieve effective mixing requires longer microchannels resulting in extended mixing time. The interfacial area between the fluids governing the mixing efficiency can be enhanced by generating chaotic advection using obstacles added to flow channel, which reduces diffusion length. Clever micro-channel design to reorienting flow can also used to be enhance the mixing efficiency (Figure 2-3).[8,38]

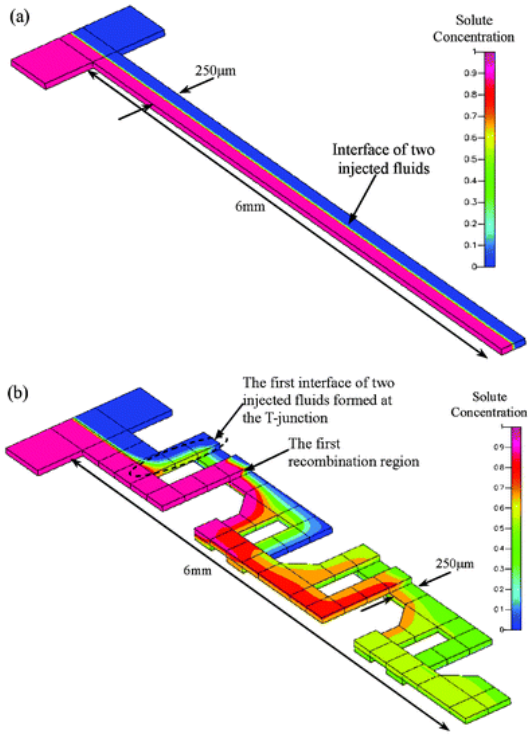

Figure 2-3. Mixing simulation of two different micromixers: A) t-type micromixer and B) serpentine laminated micromixer. (Reprinted from Kim, D. S., et al.,[8] copyright 2005, with permission from The Royal Society of Chemistry).

Interfacial forces, as expressed by the Capillary number, which is the ratio of viscous forces and interfacial forces, are one of the most important parameters affecting the flow pattern in the microchannel. In case of parallel flow in the micromixer, mass transfer through the interface is proportional to the interfacial area. The interfacial area is increased by generating plug flow or slug flow in the micromixer by increasing the flow rate, also resulting in internal circulation within the slug (Figure 2-4).[41,42] The highest mass transfer occurs in bubbly or droplet flow having the largest interfacial area. Such flows can be generated by further increasing the flow rate or adding obstacles into the microchannel.[42–44] The generation of droplet flow pattern by increasing flow

rate results in higher energy dissipation.[43] Reorienting flow by adding obstacles or special channel design requires sophisticated techniques and are limited by machine tolerance.[45] The flow pattern of dispersed and continuous phases depends on the wettability of the channel, unlike in batch mixing. Channel wettability can be tailored by combining different materials or applying coatings, which allows to control the dispersion type affecting mass transfer.[46]

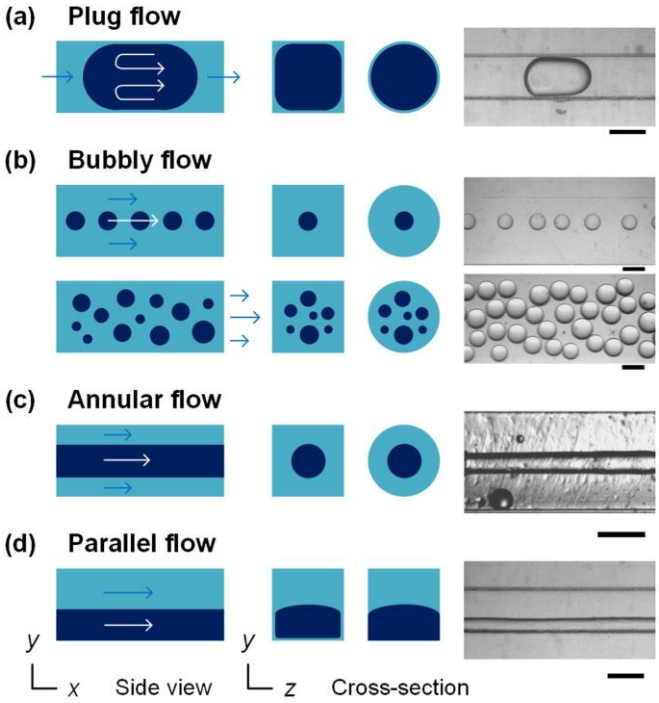

Figure 2-4. Flow patterns generated in microchannels; schematic representations on the left and photographs of the flow on the right. (Reprinted from Wang, K., et al.,[42] copyright 2017, with permission from Elsevier).

Micromixers were fabricated from various materials, e.g., poly(methyl methacrylate), glass, polycarbonate, stainless steel, etc., using an array of techniques, such as etching, moulding, and CNC milling. Helical channels (serpentine, spiral, curved), split-and-recombination structures, a combination of helical and split-and-recombination channels, patterned groves and two-layer crossing channel are the main the micromixer designs.[47] The internal structure of interconnected macroporous polymers, for instance polyHIPEs, combine these channel types and thus could be a suitable alternative to those microchannel micromixers. Fluids passing through the pores of polyHIPEs are forced through pore throats, which results in mixing both in axial and radial direction.[11,48]

2.2 Porous Polymers

Porous polymers are of significant interest for several application areas due to their tailorable strength/weight ratio, low thermal conductivity, well-defined porosity and easy processability.[19,49] As a result they have found applications both in daily life, as the synthetic sponges, shoes soles or foam cups, and in various industries, for instance in the automobile,[50] aerospace, construction sectors,[51] but also as scaffolds for tissue engineering.[52–54] Among porous polymers, polyurethane foams have the largest global market share valued as US$ 70.67 billion in 2020, while polystyrene foams are in second place.[55] Besides classifying porous polymers based on the polymer used, they can also be classified by their pore structure as open or closed porous polymers, which results in various application areas.[49] Most polymer foams are produced from polymer by physical or chemical blowing, or by using expandable or hollow beads (syntactic foams).[56]

According to IUPAC, porous polymers can be characterized by their pore size; microporous polymers are polymer foams with pore sizes < 2 nm in diameter, while mesoporous polymers pore size in the range of 2–50 nm, and macroporous polymers have pores > 50 nm in diameter.[57] Porous polymers having both micro- and mesoporous structure are also called nanoporous polymers, which have been investigated recently because of their potential applications as catalyst support,[58,59] for gas sorption/separation,[60,61] and electrical conductive porous materials.[62] Nanoporous polymers possessing a highly ordered structure can be synthesised by covalent linking small building blocks,[63] which resulted in new polymer classes, such as covalent organic frameworks,[64,65] conjugated microporous polymers,[66] porous aromatic frameworks,[67] hypercrosslinked polymers (HCPs),[62,68] etc. Among these polymers, HCPs are receiving increased interest due to their extraordinary advantages such as simple and versatile synthetic methods which are suitable for diverse reagents requiring only mild synthesis conditions, easy functionalization, high surface area, low cost.[69] The synthesis of HCPs is based on Friedel-Crafts alkylation employing a Lewis acid catalyst in mild conditions, which led to the formation of crosslinks between aromatic moieties of the building blocks resulting in intrinsic porosity.[69,70]

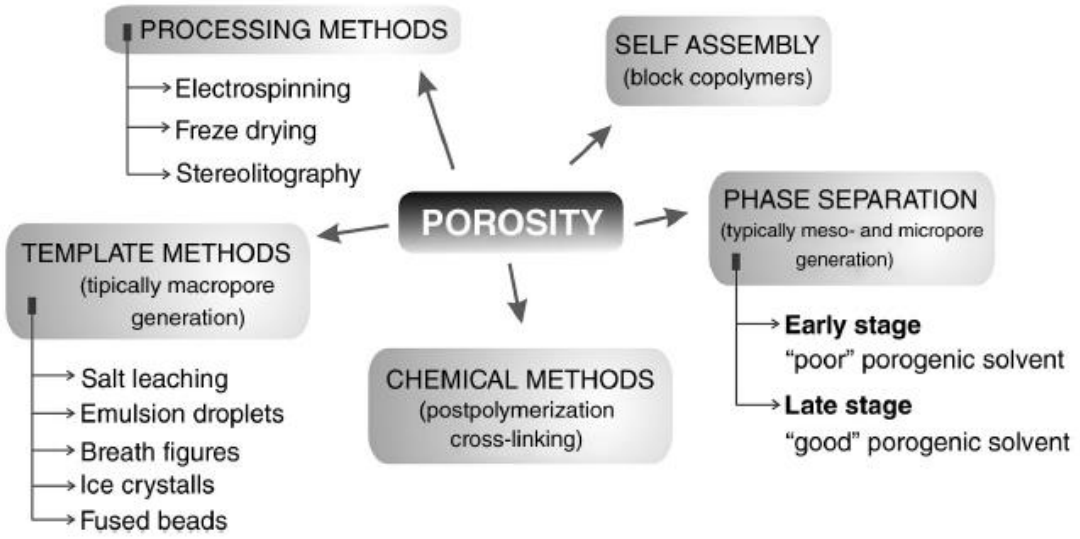

Figure 2-5. Techniques to introduce porosity in polymer monoliths (Reprinted from Pulko, I. and Krajnc, P.,[71] Copyright (2017), with permission from John Wiley & Sons, Inc.)

Macroporous polymers, which with pore sizes ranging from 50 nm to 1 mm, have been widely investigated for many industrial applications, e.g. as stationary phase in chromatography,[72,73] support for catalysts,[74,75] sensors and adsorbents,[76,77] as well as supports for cell growth and drug delivery systems.[78] Macroporous polymers can be produced using range of methods including particle sintering, use of blowing agents, phase separation, particle leaching and colloidal templating (Figure 2-5).[19,71] In order to produce macroporous polymers with desired properties, such as pore size (distribution), porosity, permeability and mechanical properties, the method of production is of great importance. Emulsion templating is an effective route to synthesize macroporous polymer foams with tailored mechanical and morphological properties in any desired shape.[79] However, it has the disadvantage that large amounts of water have to be removed from the porous polymer precursor requiring significant amount of energy.

2.3 Emulsion templated macroporous polymers

2.3.1 Formation of emulsions

Emulsions are heterogeneous mixtures in which one immiscible liquid is dispersed in another in the form of droplets. Emulsions can be either water-in-oil (w/o), where the dispersed phase is an aqueous phase, or oil-in-water (o/w) in which oil is the dispersed phase. The formation of w/o or o/w emulsions depends on factors, such as the viscosity

ratio of the liquid phases, volume fraction of the two phases, emulsifier type and concentration, pH and temperature.[80] Emulsions can also be classified by the dispersed (or internal) phase volume ratios; high internal phase emulsions (HIPEs) have an internal phase ratio of > 74.05 vol.%, medium internal phase emulsions (MIPEs) from 30 vol.% to 74.5 vol.% and low internal phase emulsions < 30 vol.%.[22,81,82]

Emulsion can be easily formed by applying a shear force to break-up droplets increasing the interfacial area, which results in the dispersion of one liquid phase in another.[80] However, if not stabilised by suitable emulsifiers droplets will coalescence to decrease their interfacial area to minimise their interfacial energy. Suitable emulsifiers can be surface active agent, also called surfactant, or nanoparticles. Surfactants promote emulsion stability by reducing the interfacial tension by absorbing at the o/w interface owing to their amphiphilic structure. Their hydrophilic-lypophilic balance (HLB) determines which phase will be dispersed and which continuous.[83] W/o emulsions can be created with surfactants with HLB values ranging from 2 to 6, while surfactants with HLB values between 8-18 are required to stabilise o/w emulsions.[84]

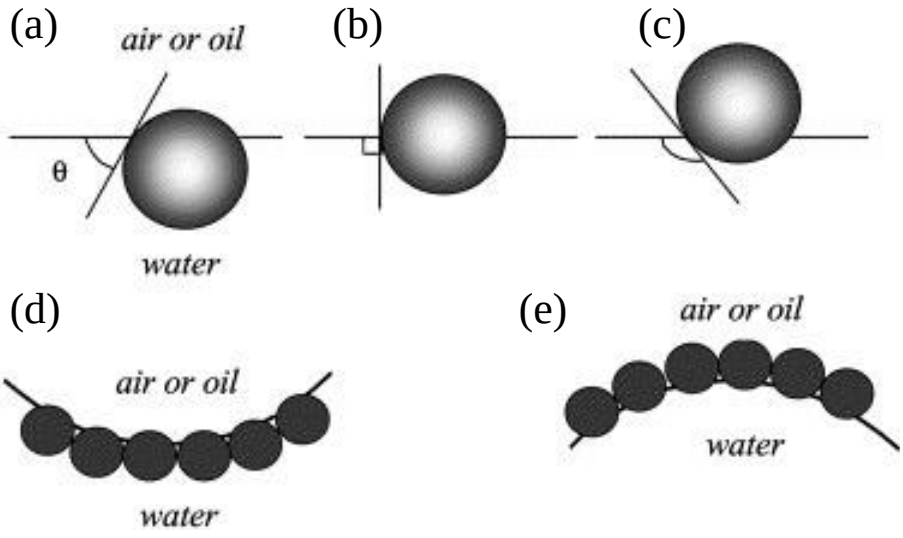

Figure 2-6. Schematic of particles with different wettability as expressed by their contact angle resting at an oil-water interface (a) 90° > θ, hydrophilic spherical particle. (b) θ = 90° (c) 180° > θ > 90°, hydrophobic spherical particle. (d) Possible positioning of hydrophilic particles at oil-in-water interface. (e) Possible positioning for hydrophobic particles at water-in-oil interface. Reprinted from Binks, B.P.,[85] copyright 2002, with permission from Elsevier.

Alternatively nano-sized particles can also be used to stabilise emulsions. Particulate stabilised emulsions are also called Pickering emulsions. Such emulsions form by particulate adsorption at the w/o interfaces. The oil/water wettability of particles determines whether o/w or w/o emulsions form (Figure 2-6).[85,86] Particles form a dense

layer at the interface between immiscible phases, which allows to generate droplets and coalesce of the droplets avoided by acting of the particle layer as mechanical barrier (Figure 2-7).[24,27,87,88]

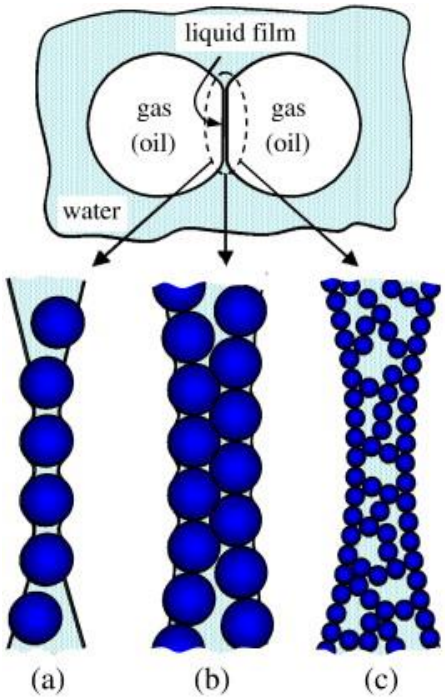

Figure 2-7. Stabilisation mechanisms in particle stabilised emulsion: (a) monolayer of bridging hydrophilic particles; (b) close-packed particles generating a bilayer and (c) aggregated particles inside the liquid film separating droplets or bubbles. Reprinted from Horozov, T.[88], copyright 2008, with permission from Elsevier.

2.3.2 Stability of emulsion templates

HIPE stability is affected by many different aspects, including the molecular structure of the components comprising the phases and of the surfactant, the surfactant content,[27] the emulsion phase volume fraction, formulation of the dispersed phase, and the temperature.[89] The common destabilisation process occurs by coalescence of dispersed phase droplets, which is mainly driven by van der Waals attractions. Flocculated droplets may lead to droplet coalescence which occurs when the thin film between the neighbouring droplets rapture driving emulsion destabilisation.[80] Sedimentation or creaming, caused by density differences between the liquid phases in the emulsion, can also contribute to droplet coalescence and then phase separation. Sedimentation or creaming is not yet destabilisation, but results in a concentration gradient along the emulsion.[80] Destabilisation of emulsion can also occur by Ostwald ripening, which is driven by differences in the (Laplace) pressure of curvature resulting in solubility differences of molecules around dispersed droplets of varying size. Ostwald ripening

results in the disappearance of small droplets at the expense of larger droplets.[90] Ostwald ripening can be reduced by the dissolution of electrolytes in the aqueous emulsion phase.

2.3.3 Preparation of macroporous polymers by emulsion templating

Macroporous polymers having desired mechanical and morphological properties can be produced by polymerisation of the monomer containing continuous phase of emulsion templates, and subsequent removal of the internal phase.[22] Depending on the use of HIPEs, MIPEs or LIPEs as the templates, the resulting macroporous polymers are named polyHIPEs, polyMIPEs and polyLIPEs, respectively. The morphology of the emulsion template at the gel point of the polymerisation represents the structure of resultant macroporous polymers.[22,82] The porosity of macroporous polymers can be easily altered by changing the internal volume phase ratio of the emulsion template. Moreover, the mechanical performance of polyHIPEs is determined by the porosity of the porous polymer and mechanical properties of the polymer itself.[81]

Since pores of emulsion templated macroporous polymers are replica of the droplets in the emulsion templates, the average pore size and pore size distribution can be tailored by changing the droplet size. The surfactant-to-monomer ratio has great impact on the droplet size of the emulsion template; increasing the surfactant amount results in lower average droplet sizes.[84] Moreover, at a fixed surfactant concentration smaller emulsion droplets can be produced by increasing the energy input during the emulsification, e.g. increasing the agitation rate and/or time[91] or increasing the flow rate of immiscible phases during emulsification with micromixers.[92–94] Typically the average pore sizes in poly-Pickering-HIPEs are larger as compared to polyHIPEs produced by polymerisation of surfactant stabilised emulsion templates, since the interaction between particles hinders the generation of smaller droplets in particle stabilised emulsions.[24]

Another important morphological property of macroporous polymers is the size and the structure of interconnecting pore throats, which some authors also call windows.[21,22] As mentioned before, due to the presence of densely packed droplets in HIPEs, they are in close contact with their neighbours. The formation of interconnects between pores, is governed by the competition between polymerisation-induced surfactant depletion attraction and the strength of interfacial films (Figure 2-8).[95] Moreover, weak

interfacial areas between droplets in HIPEs result in pore throat formation in polyHIPEs by rapturing the flattened interfacial areas during polymerisation[21] or purification[22].[95] Owing to the presence of pore throats polyHIPEs possess a permeable structure, which allows to use them in various applications requiring fluid transfer. Formation of pore throats in polyHIPEs depends on the phase volume fraction, emulsifier type and concentration and droplet size.[81] It was shown that polyMIPEs exhibited either very small and/or fewer pore throats compared to polyHIPEs.[96]

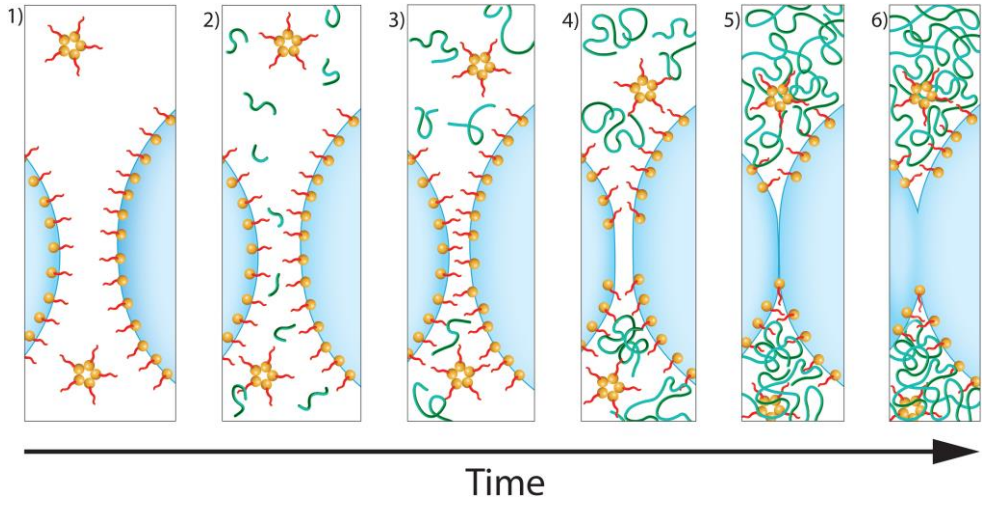

Figure 2-8. Schematic representation of pore throat formation during polymerisation of HIPEs starting with excluding growth of oligomers (stage 2) in the interdroplet layer causing interlayer droplet drainage (stage 4&5) resulting in film thinning. (Reprinted from Foudazi, R.,[95] copyright 2021 with permission from Elsevier)

Pickering-emulsion stability is affected by particle size, concentration and interaction between particles.[86,97] Poly-Pickering-HIPEs possess typically closed pore structures, because of the high energy required to detach particles from the interface. Also particles reinforce the film separating droplets/pores creating mechanically stronger films.[24,86,97] However, drainage or rapturing of the film separating droplets can be achieved by adding a small amount of surfactant at the end of emulsification, which also adsorbed at the o/w and particle/o interface displacing particles weaking the interfacial film.[24]

Besides morphological properties, mechanical properties of polyHIPEs can also be tailored by changing the internal phase volume fraction, emulsifier type, monomer type and monomer-to-crosslinker ratio. PolyHIPEs have been synthesized from HIPEs by free radical polymerisation of monomers such as styrene and meth/acrylates.[89] Poly(styrene-co-divinylbenzene)HIPEs are the most frequently studied emulsion templated macroporous polymers, because of the ease to produce HIPEs and simplicity

of polymerisation, low cost and chemical stability.[29,98] Poly(St-co-DVB)HIPEs are very brittle and friable, which hinders the applicability of these polyHIPEs.[81] The incorporation of nanoparticles into the forming polymer improves their stiffness and strength.[48,97] The friable nature of poly(St-co-DVB)HIPEs can be addressed by using different crosslinkers resulting in less brittle polyHIPEs.[26,99] Flexible, less brittle and friable polyHIPEs were produced by using acrylate-based monomers.[100] Cameron and Sherrington[101] reduced the brittleness of poly(St-co-DVB)HIPEs by using 2-ethylhexyl acrylate (EHA) as comonomer, which also reduced the glass transition temperature.

HIPEs are highly viscous and paste-like emulsions, which allows to process them with different methods, including moulding,[81] casting[102] and even as ink for 3D printing.[26,100,103] By dispersing HIPEs in immiscible solvents allows for production of macroporous polymer beads.[104–106] PolyHIPE beads can be produced by using multiple emulsions,[107] sedimentation polymerisation,[104] phase inversion[108] or microfluidic fabrication.[109] Monolithic macroporous polymers can be described as a single piece of continuous porous polymer fabricated by moulding. Depending on the HIPE formulation they possess an interconnected or closed cell pore structure.[81,97] As a result of those advantages of emulsion templating method, desired macroporous polymers can be produced relatively easily and have explored for many potential application areas, hence polyHIPEs have been intensively investigated by many groups (Figure 2-9).

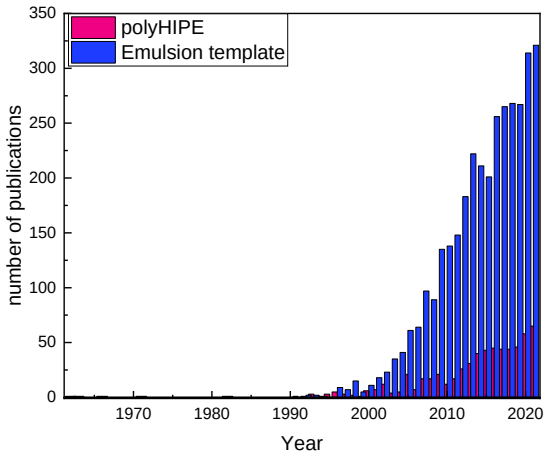

Figure 2-9. Number of publications dealing with polyHIPEs and emulsion templates since the first publication by Von Bonin and Bartl in 1962.

2.4 Applications of PolyHIPEs

Despite the fact that the first publication describing polyHIPEs appeared in 1961 and increasing interest in the past 30 years it is striking that polyHIPEs have not found significant industrial uptake. As far as I am aware of the only industrial application of polyHIPEs is the superabsorbent insert of diapers, which was commercialised rather recently by Procter and Gamble.[110] Nevertheless, polyHIPEs have been explored for numerus applications ranging from tissue engineering[53,54,111] to inserts in energy harvesting systems.[26] More popular application areas will be reviewed further below.

Because of their interconnected pore structure and wide choice of monomers, which after polymerisation result in biocompatible materials, polyHIPEs have been explored as scaffolds for tissue engineering or cell culture. Tissue engineering aims to repair, restore and/or replace damaged tissue and has the potential to extend the life time and/or quality of life of humans.[52] In order to use a material as scaffold for bone replacement or repair, it has to have an interconnected pore structure to allow for tissue ingrowth, transport of nutrients to and metabolic waste products fro the growing cells. Furthermore, the scaffold should be at least bioinert, but ideally bioactive and possess similar mechanical properties as the tissue to be engineered.[112] Commonly acrylate-based materials are widely used in tissue engineering or for biomedical applications, because of their biocompatibility and tailorable mechanical performance. Various polyHIPEs have been synthesised and explored as (injectable) scaffolds for variety of tissue types.[111] Moreover, HIPEs because of their liquid nature high viscosity at low shear rate and low viscosity at printing and fast UV-polymerisation, are potential candidates for bioinks to create complex tissue engineered structures.[113] For this reason, isobornyl acrylate is often preferred monomer to prepare polyHIPEs with adjustable morphological and mechanical properties to use in this case for bone repair.[114] Fumarate based materials were shown to have potential as bone graft biomaterial, thus Sears et al.[113]synthesised polyHIPEs from propylene fumarate dimethacrylate for use as scaffold for bone replacement.

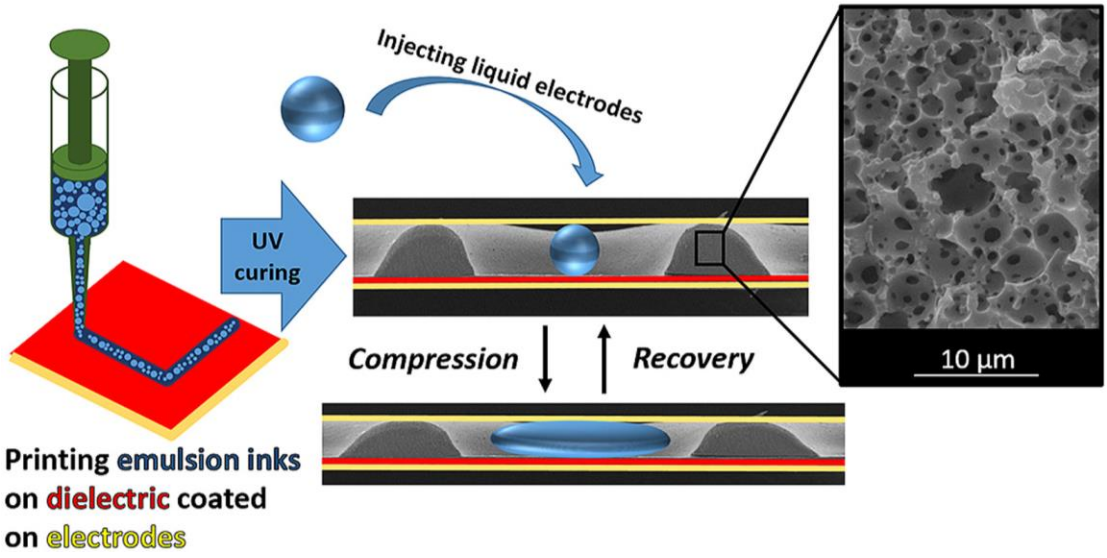

Figure 2-10. Flexible and compressible polyHIPEs were used by printing HIPEs and subsequently UV-polymerising as spring/spacer element for capacitive energy harvesting. Copied from [26], open access under CC-BY license.

Jiang et al.[26] disclosed a flexible and reversibly compressible macroporous polymer, which was produced by emulsion templating for use as spring element in an energy harvester (Figure 2-10). Previous research focused on mechanical-to-electrical energy harvester based on the reverse electrowetting phenomenon, but the system needed a spring/spacer element to allow for reversible and continuous wetting-dewetting.[115] To produce such spring/spacer element, a highly interconnected macroporous polymers was fabricated by polymerisation of a printed emulsion template pattern. Polyurethane diacrylate was chosen as crosslinker as it allowed for a very flexible and reversibly compressible material. Moreover, its high viscosity and fast UV induced polymerisation allowed to print desired patterns, which could be polymerised into a spring/spacer element containing mercury droplets enabling electrowetting.[26]

2.4.1 PolyHIPEs as catalyst supports

Two key benefits of polyHIPEs are their interconnected, permeable pore structure and chemical stability allowing them to be used as support for catalysts for organic synthesis, and for immobilisation of enzymes used for protein synthesis for batch and continuous processes.[74] Noble-metal nanoparticles are effective heterogeneous catalysts, but need to be supported on suitable macroscopic and/or porous materials to retain their activity. PolyHIPEs are good candidate materials for use as catalyst support and as it is relatively easy to introduce suitable moieties to anchor catalyst particles to

their surfaces. Furthermore, their pore structure is easily accessible for functionalisation.[116–118] Desforges et al.[116] fabricated amine group containing polyHIPEs for use as Pd catalyst support for Suzuki-Miyaura cross-coupling reactions. The stability and catalytic effectiveness of Pd nanoparticles resulted in yields of 90% after a reaction time of 70 h (Figure 2-11). Grinding the polyHIPE into powder improved the yield to 100% after a reaction time of only 24 h.[116] The low surface area of these functionalised polyHIPEs resulted in long reaction times, thus making necessary to grind the support to enhance the catalytic activity. In another study, polyHIPEs were first hypercrosslinked, then functionalised with a Schiff base ligand to support cupper(II) ions for use as catalyst for the epoxidation of cyclohexene.[119] Hypercrosslinking and chemical functionalisation of polyHIPEs doubled catalyst stability and activity due to the increased surface area.[119]

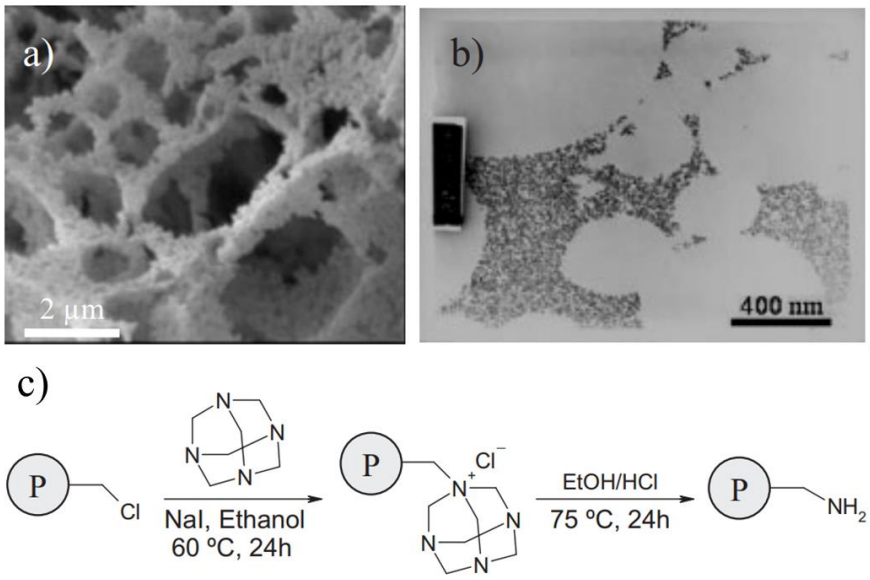

Figure 2-11. Pd nanoparticle coated polyHIPE as catalyst in Suzuki Miyaura coupling reaction. A) SEM image of polyHIPEs, B) Transmission electron microscope image of Pd nanoparticles on polyHIPE surface, and C) surface functionalisation of polyHIPE (P) by a primary amine. Reprinted from Desforges et al.,[116] copyright 2005, with permission from John Wiley and Sons.

Dendritic amphiphiles impregnated noble-metal nanoparticles were used to stabilise emulsion templates, which after polymerisation were embedded into the surfaces of pore walls. These nanoparticles decorated polyHIPEs could be used as heterogeneous catalyst for the reduction of 4-nitrophenol to 4-aminophenol.[117] (Figure 2-12).

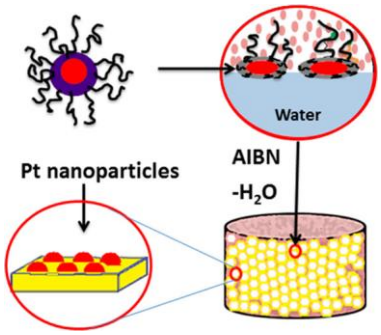

Figure 2-12. Pt-loaded polyHIPEs were produced by polymerisation of HIPEs stabilise using in situ produced Pt nanoparticles, which shows catalytic activity as evaluated by reduction of 4-nitrophenol. Reprinted from Liu et al.,[117] copyright 2015, with permission from American Chemical Society.

PolyHIPEs can also be used to perform biochemical reactions. Ruan et al.[120] fabricated an easily regenerable enzyme reactor by immobilising the enzyme TPCK-Trypsin on poly(St-co-DVB-co-glutaraldehyde)HIPEs. Because of the functional groups in polyglutaraldehyde, the enzyme could be immobilised on the surface of the monolith at a high immobilization rate.[120]

2.4.2 PolyHIPEs as membranes and adsorbents

A porous material can act as a filter medium as long as the following conditions are met; it must be permeable and have pore sizes smaller than the contaminant rejected, mechanically robust, chemically stable, wetted by the solution/solvent, does not undergo undesired side reactions. Furthermore, it should be easily fabricated into desired shapes.[121] PolyHIPEs are ideal candidates for filtration applications because their mechanical and wetting properties can be tailored by monomer/crosslinker choice and the fact that their pore structure, i.e. their characteristic pore and pore throat diameters, can be adjusted by choice of emulsifiers (surfactants vs. particles) and by energy input during emulsification.[122] They have been used as medium in filtration systems capturing pollutants by either adsorption or chemisorption[28,123] or by rejecting particles by sieving.[124,125] Malakian et al.[124] fabricated polyHIPE microfiltration membranes having a hydrophobic bulk and hydrophilic surface. This membrane system allowed for effective separation of microalgae from aqueous solution (Figure 2-13).

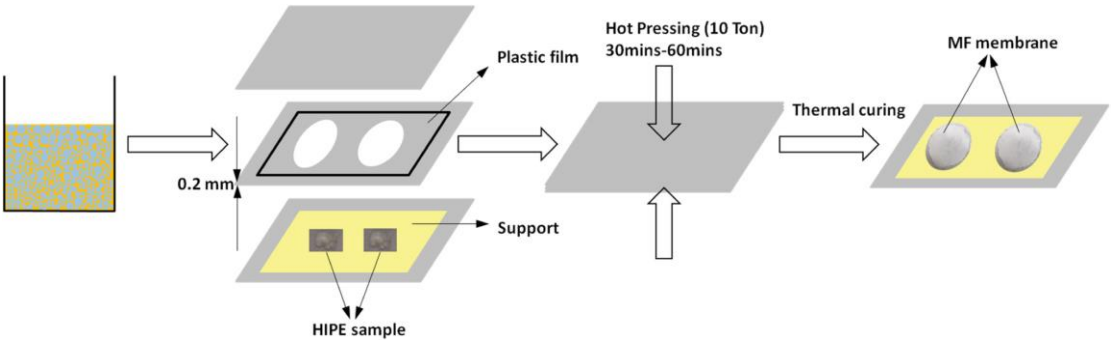

Figure 2-13. Schematic of the polyHIPE membrane fabrication process: a thin layer of HIPE is casted on a support, a polyHIPE is obtained by polymerisation during hot pressing resulting in a microfiltration (MF) membrane. (Reprinted from Malakian et al.,[124] with permission from Elsevier).

Oil/water separation after oil spillages was demonstrated using hybrid polyHIPEs produced by polymerisation of HIPE organogels, which were stabilised by triblock ionomer modified magnetic Fe_3O_4 nanoparticles.[126] The adsorbent can be collected using magnetic fields. They studied the separation of oil and found that hybrid polyHIPEs adsorbed spilled oil from the mixture in a few seconds, quicker than the reported common oil-adsorbents.[126] The adsorbed oil could be recovered by centrifuging allowing the material to be reused for at least 20 cycles without significant loss of adsorption performances.[127]

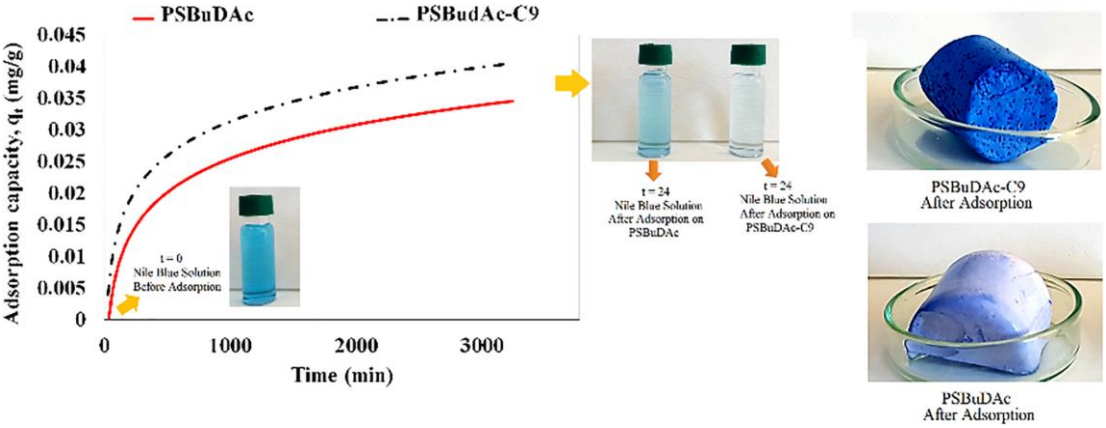

Figure 2-14. Adsorption performance of cellulose nanocrystals loaded polyHIPE monoliths against cationic Nile dye in aqueous environment. (Reprinted from Eslek, A. et al.,[28] with permission from Elsevier)

Eslek et al.[28] produced polyHIPE filter medium for waste water treatment. The mechanical properties of polyHIPEs were improved by incorporation of cellulose nanocrystals into the polymer phase, which was achieved by CNC dispersion in the continuous phase during emulsification. Moreover, the use of crosslinker 1,4-butanediol diacrylate resulted in reduced friability and brittleness of the produced

polyHIPEs as compared to poly(St-co-DVB)HIPEs. The adsorption performance of these polyHIPEs was tested by absorption of Nile blue from water (Figure 2-14).

Another important pollutant source are heavy metal ions, which can easily enter the food chain if polluted water is used for agriculture or food processing.[123] To remove heavy metal ions from water sources, various separation methods, such as chemical precipitation, adsorption, membrane filtration or ion exchange, are being used. Chemical precipitation of heavy metals is the most widespread technique especially in developing countries. However, it has also many disadvantages; it is a slow process as the precipitated settles poorly, and produces excessive sludge.[128] Adsorption is an effective and economical method because of its reversibility and, therefore, adsorbents recently attracted more attention.[129]

PolyHIPEs are good candidates as adsorbents to remove heavy metal ions from wastewater. In order to achieve rapid contact between adsorbent and wastewater containing heavy metal ions, Han et al.[130] produced poly(GMA)HIPEs and grafted polyacrylic acid to the surface of the highly interconnected porous monolith. Glycidyl methacrylate (GMA) is attracting considerable interest as monomer in HIPEs, because of its hydrophobicity and reactive epoxy group, which can be functionalised with nucleophile attack.[131] Han et al.[130] showed that copper ions were effectively removed from wastewater with a maximum adsorption capacity of 35.30 mg/g, which remained stable over seven ad/desorption cycles.[130] This adsorption capacity is high to conventional adsorption materials, which have an adsorption capacity of 12.3 mg/g.[132] Mert et. al.[133] showed that Ag(I), Cu(II) and Cr(III) can be removed from an aqueous solution using amine functionalised polyHIPEs.

Porous hydrogels can be produced by polymerisation of inverse (o/w) HIPEs. Such hydrogel polyHIPEs have been used to remove heavy metal ions from wastewater; Cu^{2+} and Pb^{2+} can be separated from aqueous solution using an acrylic acid grafted chitosan polyHIPE.[134] Adsorption of metal ions occurred within 5 min with an adsorption capacity of 302 mg/g for Cu^{2+} and 612 mg/g for Pb^{2+} at a solution concentration of 50 mg/g. This materials had excellent reusability.[134]

2.4.3 Applications of polyHIPE in chromatography

Monolithic stationary phases have become popular in chromatography because of their ability to separate macromolecules at high flow rates as a result of their higher permeability compared with common packed bed stationary phases.[135] The Krajnc group synthesised poly(GMA)HIPE monoliths, which were modified by attaching diethyl amine or diethylenediamine to poly(GMA) epoxy groups. These polyHIPEs were used to separate standard protein mixture containing myoglobin, conalbumine and trypsin inhibitor.[136,137] Diethyl amine functionalised poly(GMA-co-EGDMA)HIPEs were also used as stationary phase in liquid chromatography to separate different proteins.[138] These polyHIPE columns could be reused over 300 times without any loss in permeability and separation performance.[138]

PolyHIPEs were also used as stationary phase in capillary electrochromatography (CEC) because of their low back pressure at high flow rates and superior mass transport compared with common packed bed phases.[139] Poly(isodecylacrylate-co-DVB)HIPEs were used as CEC column to separate variety of alkylbenzenes. Ionisable sulphate groups stemming from the initiator used induced electroosmotic flow (EOF) without the need for any additional moieties inducing EOF. EOF is necessary in CEC to drive mobile phase and analytes. Even though successfully separation of alkylbenzenes was achieved, the column had a short life time, because it swelled after 24 h storage in organic mobile phase.[139] Afterwards, the same group tried to replace isodecylacrylate with styrene, because of the chemical stability of crosslinked polystyrene. Effective separation of various alkylbenzenes was shown to be possible using this monolithic column.[140]

Khodabandeh et al.[141] demonstrated the possibility to separate small molecules using hydrophilic macroporous polymers prepared by polymerisation of emulsion templates stabilized by an amphiphilic diblock copolymer (Figure 2-15). The polyethylene glycol part of diblock copolymer stabiliser embedded into the polymer network enables retention of polar hydroxybenzoic acids in liquid chromatography, while the polystyrene component is responsible for hydrophobic interactions needed to separate non-polar alkylbenzenes in reverse phase mode.[141]

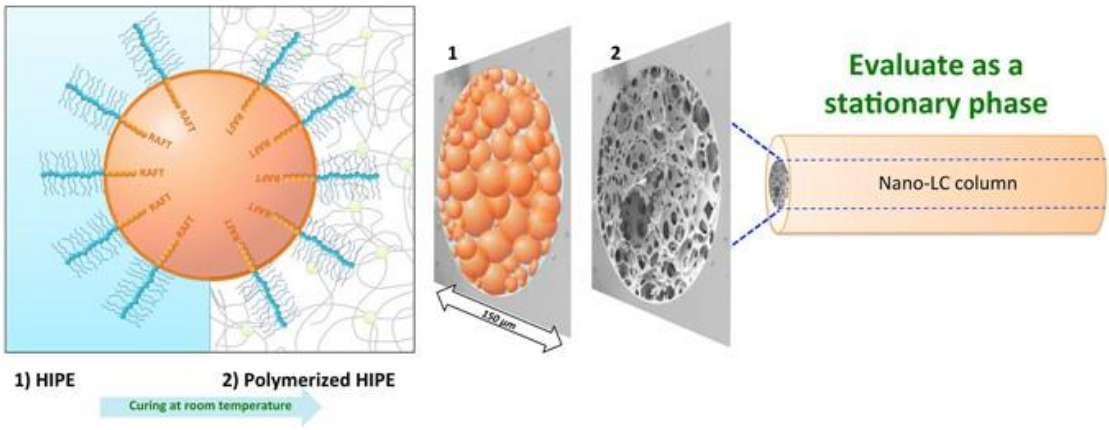

Figure 2-15. Capillary format polyHIPEs prepared by polymerisation of HIPEs stabilised using polyethylene glycol-based brush-type amphiphilic macro-RAFT agents. These polyHIPEs were used as stationary phase for high-performance liquid chromatography. Copied from [141], open access under CC-BY license.

Thin-layer chromatography (TLC) is used to identify and monitor analytes qualitatively.[142,143] New stationary phases for TLC have been developed to improve separation properties. Due to the highly viscous, liquid nature of HIPEs, TLC separation layers can be easily produced by casting.[144] Yin et al.[143] produced polyHIPE layers for use as stationary phase in thin layer chromatography and demonstrated the separation of plant extract.

3 Summary of Publications: Experiments

3.1 Materials

Styrene ≥99%, divinylbenzene (DVB) 80%, sodium monosorbitol (Span 80), α, α′-azo-isobutyronitrile (AIBN), calcium chloride dihydrate ($CaCl_2 \cdot 2H_2O$) ≥99%, ethylhexyl acrylate (EHA), ethylene glycol dimethacrylate (EGDMA), 2-hydroxyethyl methacrylate (HEMA), N,N'-methylene bisacrylamide (MBAA), ammonium persulfate (APS), the surfactant poly-(ethylenglycole)-block-poly-(propyleneglycole)-block-poly-(ethyleneglycole) (Kolliphor® P 188 (P188)), cyclohexane, N,N,N′,N′-tetramethylethylenediamine (TEMED), 2,2-dimethoxypropane (DMP), sodium hydroxide (NaOH), sodium borohydride ($NaBH_4$), potassium chloride (KCl), 1,2-dichloroethane (DCE), aluminium chloride ($AlCl_3$), iron chloride ($FeCl_3$), dimethoxy methane (DMM), 4,4-bis(chloromethyl)-1,1-biphenyl (CMP), trifluoro-methanesulfonic acid (trifilic acid), triphenylphosphine (PPh_3), palladium acetate ($Pd(OAc)_2$), 4-aminoacetophenone (4-AAP), 4-nitroacetophenone (4-NAP), triethylene silane, ammonium formate (AF), bromobenzene, phenylboronic acid and tripotassium phosphate (K_3PO_4) were all purchased from Sigma-Aldrich. Ethanol, methanol, acetone, hydrochloric acid (HCl, 37%), isopropanol, ethyl acetate, chloroform, dichloromethane (DCM) were purchased from Fischer Chemicals (Vienna, Austria), Araldite Rapid adhesive® from Rapid Electronics Ltd. (Essex, UK), Araldite 2020 from Farnell Element14 (Salzburg, Austria), shrink tubing from Conrad Electronic GmbH (Vienna, Austria), 3/8" Kenics static mixer (12 helix) from Cole-Parmer (Germany), and 1/16" PTFE tubes from VWR (Vienna, Austria). Hydrophobic pyrogenic silica particles (HDK H20) were kindly provided by Wacker Chemie AG (Germany) and polyurethane diacrylate "Ebecryl 8402" (PUDA) by Cytec (Diegem, Belgium). All materials were used as received.

3.2 Experimental part

In publication I, II, III and IV hydrophobic poly(-Pickering-)(St-co-DVB)HIPEs were prepared by polymerisation of the continuous phase (CP) of HIPEs or Pickering-HIPEs containing monomers (for w/o HIPEs). In addition, Publication IV reports on preparation of hydrophilic poly(HEMA-co-MBAA)HIPEs produced by polymerisation

of the CP (for o/w HIPEs) comprising a monomer solution. Their preparations and characterisation (morphological, mechanical and chemical characterisations, including SEM, skeletal and foam densities, gas permeability, N_2 adsorption isotherms, X-ray photoelectron spectroscopy, Fourier-transform infrared spectroscopy, solid-state ^{13}C cross polarization (CP) and ^{31}P high power decoupling (HPDEC) magic angle spinning (MAS) NMR spectra.) are explained in detail in publications I - IV. Moreover, experimental details of the simultaneous hypercrosslinking and functionalisation of poly(St-co-DVB)HIPEs are given in publication III. In the following chapter, the highlights of the publications I-IV are presented, which mainly are the characterisation of Pd@polyHIPEs catalyst support and polyHIPE micromixers on the way of their use as unit operators in a Plant-on-a-Bench.

3.3 Characterisation of polyHIPE unit operators

3.3.1 Effectiveness of polyHIPE micromixers-Publication I

3.3.1.1 Fabrication of polyHIPE micromixers

To fix inlet tubes two 5 mm deep holes were drilled into the top of the monolith (Figure 3-1/1). Two 1/16 inch PTFE tubes were inserted into the holes and sealed with highly viscous Araldite® Rapid two-phase epoxy resin. Two different micromixer outlet positions were tested: outlet holes were either drilled into monolith bottom or into the side wall 5 mm above the bottom (Figure 3-1/1) and equipped with PTFE tubes. After fixing inlet and outlet tubes, the surface of the monolith was covered with highly viscous epoxy resin to create an impermeable barrier (Figure 3-1/2). After curing the epoxy resin, the sealed monolith was placed into a high-temperature heat shrink tube to provide extra protection (Figure 3-1/3). The tubes were additionally sealed with Araldite 2020 (Figure 3-1/3) and the resin cured in a convection oven at 70 °C for 4 h.

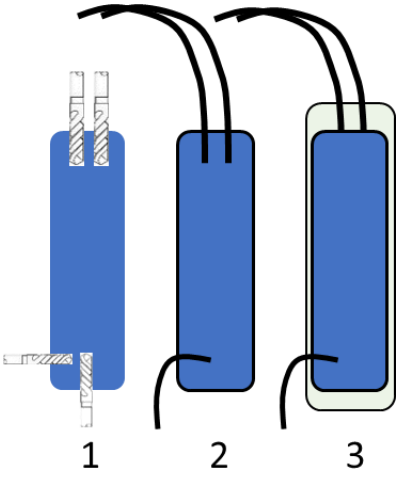

Figure 3-1. Fabrication of polyHIPE micromixers; 1) drilling 5 mm deep holes, 2) placing two inlet tubes on the upper and one outlet tube (either in flow or perpendicular to the flow direction) into the porous monolith followed by sealing the outer surface with an epoxy resin, 3) further protecting the monolith with a shrink tubing and sealing the upper and bottom part of micromixer with epoxy resin.

3.3.1.2 Effectiveness of polyHIPE micromixers

The effectiveness of polyHIPE micromixers were determined by the residence time distribution (RTD) and two competitive parallel reactions (4th Bourne). Their details were explained in publication I.

Residence time distribution of polyHIPE micromixers

Briefly, RTD of polyHIPE micromixers and commercial Kenics© static mixer were determined using a tracer (0.2 mL, 25 mg/mL KCl aqueous solution), which was injected as pulse flow into a micromixer through which continuously flew water. The tracer concentration was monitored at the outlet of the micromixer using a refractometer (DnDc, WGE Dr Bures, Dallgow-Doeberitz, Germany) as a function of time.

The measured refractive index was converted into concentration $c(t)$ using the pre-determined calibration curve. The RTD function E(t) was calculated as follows:[145]

$$E(t) = \frac{c(t)}{\int_0^\infty c(t)dt} \qquad \text{(Eq. 1)}$$

The axial dispersion number (D_{ax}/uL) describes the flow spreading rate in the micromixer due to a laminar velocity profile, the molecular diffusion, etc.[146] The axial dispersion model for a dispersion number larger than 0.01 (Eq. 2) was introduced using open-open boundary conditions, representing a conventional and commonly used

experimental device.[146] D_{ax}/uL can be determined from the parameters of the RTD curve by using the axial dispersion model:

$$E(t) = \frac{1}{t_m\sqrt{4\pi\left(\frac{D_{ax}}{uL}\right)\left(\frac{t}{t_m}\right)}} exp\left[-\frac{\left(1-\frac{t}{t_m}\right)^2}{4\left(\frac{D_{ax}}{uL}\right)\left(\frac{t}{t_m}\right)}\right] \qquad \text{(Eq. 2)}$$

where D_{ax} is the dispersion coefficient, L the length of the investigated device, u the velocity of the main flow and t_m the mean residence time.

Two competitive parallel reactions (4th Bourne)

The micromixing efficiencies of polyHIPE micromixers and the static mixer were determined using the 4th Bourne reactions (R1 & R2) by monitoring the acetone yield resulting from the slower saponification reaction of DMP (R2) using a UV−vis spectrophotometry (Agilent 8453, Agilent Technologies Österreich GmbH, Vienna, Austria).

4th Bourne reactions:

$$HCl + NaOH \rightarrow NaCl + H_2O \qquad (k_1 = 1.3 \times 10^{11} m^3 kg^{-1} mol^{-1} s^{-1}\ at\ 25°\ C)(R1)$$

$$CH_3(OCH_3)_2CH_3 + H_2O \xrightarrow{H^+} CH_3COCH_3 + CH_3OH \qquad (k_2 = 700 m^3 kg^{-1} mol^{-1} s^{-1} at\ 25°\ C)\ (R2)$$

3.3.2 Continuous emulsification using polyHIPE micromixers-Publication II

The details of the continuous emulsification using polyHIPE micromixers were explained in the publication II. Briefly, continuous HIPE production using polyHIPE micromixers, of which micromixing performance were characterised in publication I, was performed by injecting a CP containing monomer/crosslinker, surfactant, and initiator via inlet 1 and an aqueous IP via inlet 2 using two syringe pumps (PHD Ultra, Harvard Apparatus, UK, and Masterflex® Touch-Screen Syringe Pump, Cole-Parmer, Germany). Various flow rates and IP:CP ratios were tested. Generated HIPEs were either photopolymerised subsequently (in case of using acrylates as monomers) or collected in a centrifuge tube and polymerised in an oven at 70 °C for 4 h (in case of using St and DVB as monomers). The morphology as well as density and porosity of the resulting polyHIPEs was investigated like conventional polyHIPEs via SEM and pycnometry.

3.3.3 Model reactions using Pd@polyHIPE microreactor and pieces

3.3.3.1 Preparation of Pd@polyHIPE heterogeneous catalysts

Pd catalyst was immobilised on hypercrosslinked and functionalised coarse powder poly-Pickering-HIPEs (0.5 g) (after solvent stitching and Scholl coupling reaction) by soaking the pieces in 6 mL DCM solution containing $Pd(OAc)_2$ (0.046 g, 0.41 mmol) and stirring under reflux for 2 h. The polyHIPE pieces were collected using tweezers, dried in a fume hood and washed with acetone to remove physisorbed Pd^{II}. The catalyst support was dried at 70 °C in an oven. In order to load Pd into the knitted poly-Pickering-HIPE micromixers, 10 mL of $Pd(OAc)_2$ solution was flushed through the micromixer at a flow rate of 0.6 mL/min. Afterwards, these micromixers were placed into an oven at 70 °C to evaporate the solvent. Pd^{II} was reduced to Pd^0 by injecting $NaBH_4$ dissolved in water, which resulted in H_2 production. Afterwards, water was passed through the micromixer to remove any side products. The Pd-loaded poly-Pickering-HIPE microreactors were dried in an oven at 70 °C overnight.

3.3.3.2 Hydrogenation reaction using Pd@polyHIPE microreactor

Catalytic properties of knitted polyHIPE microreactors were investigated using a model hydrogenation reaction of 4-NAP with various hydrogen sources (ammonium formate, sodium borohydride, triethylene silane) (Figure 3-2) by placing a microreactor into a sand bath at 80 °C. 4-NAP (0.05 M in EtOH) and the hydrogen source (0.6 or 1.2 M in H_2O) were injected using syringe pumps at a flow rate of 0.2 or 0.3 mL/min. The exit stream was collected and extracted with EtOAc. The EtOAc was removed from the extraction phase using a rotary evaporator and the recovered solid was characterised by ^1H NMR. The yield of the reaction was determined by calculating the proportional ratio of the peak area of product to the peak areas of educt and product.

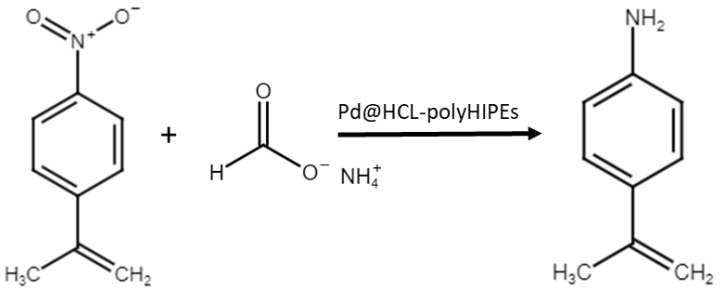

Figure 3-2. Hydrogenation reaction of 4-NAP with ammonium formate as H_2 source using Pd-coated hypercrosslinked polyHIPEs.

3.3.3.3 Suzuki-Miyaura coupling reaction using Pd@polyHIPE pieces-Publication III

Catalytic properties of Pd@polyHIPE pieces were tested using a model Suzuki-Miyaura reaction of bromobenzene (1 mmol) with phenylboronic acid (1.1 mmol) in the presence of K_3PO_4 (3mmol) in 4 mL H_2O-EtOH (v/v = 1:1) at 80 °C for 30 min (Figure 3-3). Afterwards, the Pd@polyHIPE catalyst was removed using tweezers and washed with water, EtOH and EtOAc, then reused five more times. EtOAc was used to extract the product/educt mixture from the aqueous reaction phase; purification and characterisation was carried out as described above. The fabrication of the Pd@polyHIPE catalyst, its use in a Suzuki-Miyaura reaction and the following assessment of the effectiveness of the Pd@polyHIPE catalysts were discussed in detail in the publication III.

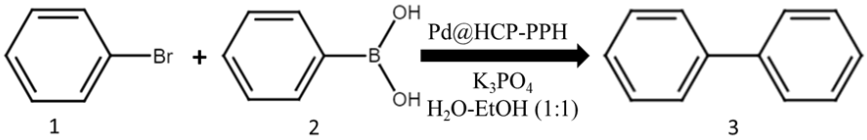

Figure 3-3. The model Suzuki-Miyaura coupling reaction of bromobenzene with phenylboronic acid at 80 °C with Pd loaded hypercrosslinked and functionalised polyHIPEs.

3.3.4 Continuous liquid-liquid extraction using polyHIPE microextractor-settler-Publication IV

The Liquid-liquid (L-L) extraction of caffeine (1g/L aqueous solution) and 4-AAP from its simulated reaction medium (4-NAP (0.05 M)/4-AAP (0.05 M)/AF (0.6 M); 1:1:2 (v/v/v)), respectively, with EtOAc was performed using polyHIPE micromixers fabricated either from a single polyHIPE monolith or a combination of a hydrophilic and a hydrophobic polyHIPE as microextractor. The two liquid phases were injected into the microextractor using a double syringe pump at a flow rate of 0.2 or 0.3 mL/min. The exit stream was separated continuously using a home-made minisettler (view publication IV) and collected in vials. Afterwards, the phases were characterised using UV-Vis spectroscopy to determine the caffeine or 4-AAP concentration. The Reynolds number of the polyHIPE extraction units was determined using the following equation:

$$Re = \frac{\rho_c d_p u_{tot}}{\mu_c} \qquad (Eq. 3)$$

where d_p is average pore size of polyHIPEs, u_{tot} is the total superficial velocity and μ_c is dynamic viscosity and ρ_c the density of CP.

The extraction efficiency *E* was calculated as follows:

$$E = \frac{C_{i_{out},E} - C_{i_{in},E}}{C_{i^{eq},E} - C_{i_{in},E}} \qquad (Eq. 4)$$

where $C_{i_{out},E}$ is the caffeine or 4-AAP concentration in the extracted ethyl acetate phase collected at the oil-outlet of the minisettler, $C_{i_{in},E}$ is their concentration in the extraction solvent (ethyl acetate) and $C_{i^{eq},E}$ is their equilibrium concentration.

The overall volumetric mass transfer coefficient $k_L a$ characterises the mass transfer performance of droplets generated in the extraction units and calculates as follows:[147,148]

$$k_L a = \frac{1}{\tau} \ln\left(\frac{C_{i^{eq},R} - C_{i_{in},R}}{C_{i^{eq},R} - C_{i_{out},R}}\right) \qquad (Eq. 5)$$

where τ is the extraction time determined by the ratio of extraction unit volume and volumetric flow rate, $C_{i_{in},R}$ is the $C_{4\text{-AAP}}$ in the inlet of the raffinate phase (simulated reaction medium) and $C_{i_{out},R}$ is the remaining $C_{4\text{-AAP}}$ in the outlet of the raffinate phase.

The energy dissipation rate ε of the polyHIPE extraction units, the blank tube and a Kenics mixer were calculated from pressure drop (ΔP) monitored during the experiments:

$$\varepsilon = \frac{\Delta P Q_{tot}}{\rho_c V_R} \qquad (Eq. 6)$$

where Q_{tot} is the total volumetric flow rate during L-L extraction, ρ_c is the density of CP of the extracted mixture and V_R the extractor volume. Further details regarding the experiments and calculations are given in publication IV.

4 Summary of Publications: Results and Discussion

4.1 Macroporous polymer micromixers (Publication I)

In order to realise the operating units of a Plant-on-a-Bench, chemically stable and mechanically robust polyHIPEs were produced by polymerisation of the monomer containing continuous HIPE phase and subsequent removal of internal templating phase. Poly(St-co-DVB)HIPEs are the most investigated polyHIPEs, however they suffer from weak mechanical properties, in particular they are brittle and friable. Their mechanical properties can be improved by polymerisation of HIPEs stabilised using hydrophobic silica nanoparticles to which surfactant was added prior to polymerisation resulting in the formation of particle reinforced, open porous polyHIPEs (Figure 4-1). These polyHIPEs can be turned into micromixers without difficulty. The degree of interconnectivity (*DoI*) of the open porous polyHIPE monoliths can be tailored by the addition of increasing amounts of surfactant to the Pickering-HIPE template without significantly affecting the porosity and average pore diameters of the resulting polyHIPEs (Table 4-1). The increased *DoI* resulted in an increased permeability of the polyHIPEs.

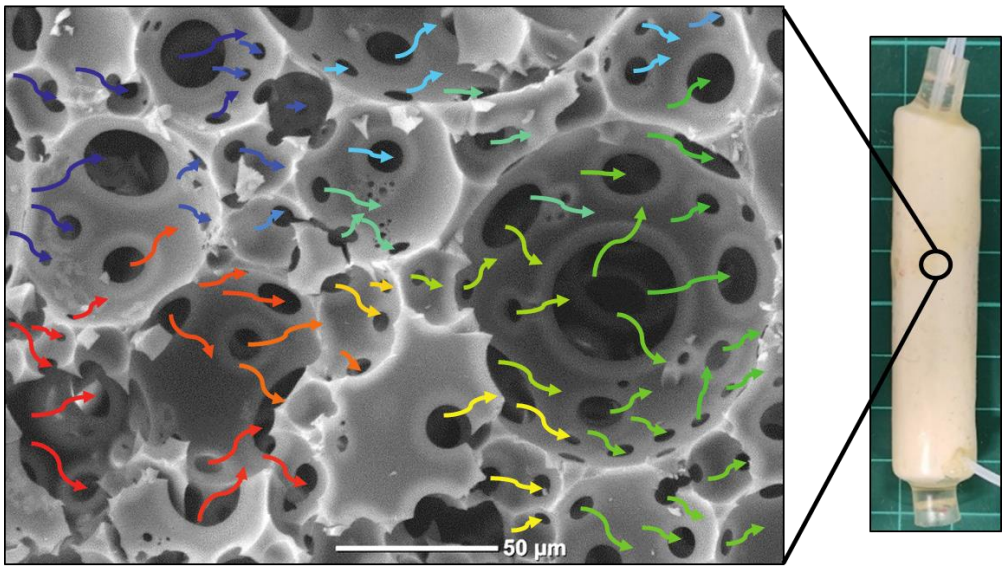

Figure 4-1. Schematic of the fluid flow (left) through the pore structure of polyHIPE micromixer (right); the pore throats act as orifices in a series of connected parallel tubes.

The pore Reynolds number Re_p of polyHIPE micromixers ranged between 1.8 and 4.5 (Table 4-1), indicating laminar flow. Re_p decreased with increasing *DoI* of the

monoliths because of fewer obstacles redirecting the fluid flow. Comiti et al.[149] showed for packed bed reactors that the limiting Re_p for laminar flow is 4.3 for Newtonian fluids. Re_p for our polyHIPE micromixers were smaller than *Re* of tubular reactors (ID 0.4 mm, *Re* = 80),[150] commercial static mixers (Statmix6 and ST-mixer *Re* = 20 and *Re* = 5 at $Q = 0.5$ mL/min, respectively)[151] and the Kenics® mixer, which I used as reference (Re = 122). In those static mixers, the mixing performance increased by formation of chaotic flow at higher Re. However, our polyHIPE micromixers consist of multiple interconnected microchannels, where pore throats act as both obstacles (orifices) and split and recombination channels. A parallel channel design is also used in commercial SAR micromixers to improve their mixing performance.[38]

Table 4-1. Effect of increasing surfactant amounts added to the primary Pickering-HIPE templates on the morphology descriptors of poly-Pickering-HIPEs: average pore $\boldsymbol{d_p}$ and pore throat diameter $\boldsymbol{d_{pt}}$, degree of interconnectivity (or openness) $\boldsymbol{DoI}$, porosity $\boldsymbol{P}$, and gas permeability $\boldsymbol{k}$, pore Reynolds number $\boldsymbol{Re_p}$ for water pumped through the poly-Pickering-HIPEs at $\boldsymbol{Q}$ = 0.6 mL/min.

Sample	d_p/ µm	d_{pt} / µm	DoI /·10^{-2}	P / %	k / D	Re_p / -
P0	89 ± 27	0	0	80.5 ± 0.5	0	-
P5	78 ± 38	12 ± 9	2.8 ± 0.6	84.3 ± 0.4	0.4 ± 0.1	4.5 ± 0.2
P10	80 ± 29	20 ± 12	4.3 ± 0.2	86.7 ± 1.2	1.5 ± 0.2	4 ± 0.3
P15	96 ± 33	17 ± 10	4.6 ± 0.7	87.2 ± 0.5	3.2 ± 0.5	3 ± 0.3
P20	68 ± 30	13 ± 8	6 ± 0.8	88.2 ± 1.2	3.7 ± 0.1	1.8 ± 0.2

The residence time distribution (RTD) of polyHIPE micromixers (Figure 4-1) was investigated using a tracer method, which allows for quantification of the deviation from ideal plug flow. Micromixing properties of polyHIPE micromixers were compared with that of a Kenics® static mixer (as this was quantified and published before);[150] polyHIPE micromixers possessed an RTD which was less spread and skewed than that of the commercial static mixer. By modelling the RTD of polyHIPE micromixers based on axial dispersed flow (Figure 4-2), I showed that the fabricated micromixers were in good agreement with that of commercial split-and-recombination micromixers. The axial dispersion number of polyHIPE micromixers was dependent on the *DoI* of the polyHIPE monoliths (Table 4-2). The micromixing performance of polyHIPE micromixers can be adjusted by tailoring the morphology of polyHIPEs.

Table 4-2. Axial dispersion number D_{ax}/uL and the coefficient of determination R^2 obtained by fitting of the axial dispersion model to the RTD of polyHIPE micromixers and the Kenics static mixer at volumetric flow rates of 0.6 mL/min and 1.2 mL/min.

sample name	D_{ax}/uL ($\cdot 10^{-2}$)		R^2	
	0.6 mL/min	1.2 mL/min	0.6 mL/min	1.2 mL/min
P5	4 ± 0.5	3 ± 0.05	0.96	0.95
P10	6 ± 0.2	2 ± 0.04	0.62	0.93
P15	6 ± 0.1	3 ± 0.06	0.72	0.96
P20	8 ± 0.2	4 ± 0.2	0.71	0.79
static mixer	-	8.8 ± 0.3	-	0.92

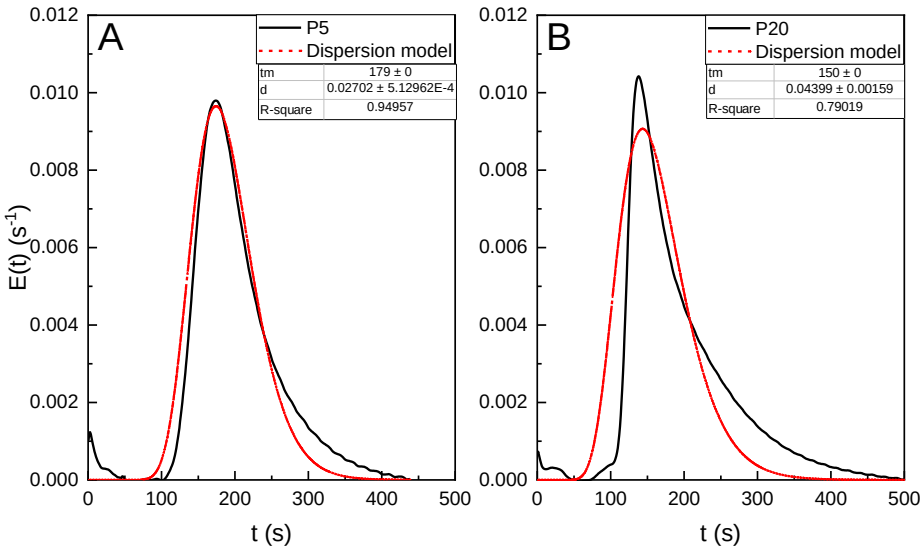

Figure 4-2. Residence time distribution of A) P5 micromixer (produced by polymerisation of Pickering-HIPE to which 5 vol% surfactant was added), and B) P20 micromixer (20 vol% surfactant was added) and the fitted axial dispersion model.

Moreover, the effectiveness of polyHIPE micromixers was tested by two competitive parallel reactions (4th Bourne reaction). The 4th Bourne reaction consists of the very fast neutralisation of NaOH and slower acid catalysed saponification reaction of dimethoxypropane for which HCl is the common reactant. In case of effective mixing, only neutralisation should take place consuming all HCl, thus no acetone and methanol, the products of the saponification reaction, should not be observed.

Regardless of the degree of interconnectivity, all polyHIPE micromixers resulted in a dimethoxypropane decomposition yield of approximately 2.5%, whilst the Kenics static mixer had an acetone yield of 17% indicating a worse mixing performance. Together

with the RTD, these results show that polyHIPEs are good candidates for the fabrication of micromixer because of their adjustable morphology, interconnected macroporous structure, chemical stability, high permeability resulting in a low backpressure, which was found as 54.3 mbar for the polyHIPE micromixer fabricated using polyHIPE having the lowest *DoI*.

4.2 Continuous emulsification using emulsion templated macroporous polymers (Publication II)

PolyHIPE micromixers, for which micromixing properties were quantified in the first publication, were used for the continuous production of HIPEs. This was achieved by simultaneous injection of a continuous monomer-crosslinker phase and an aqueous IP having significantly different viscosities. Mixing of two-phase flow in the polyHIPE micromixer was investigated. The literature reported successful continuous emulsification using microfluidic devices.[93,152] Droplet-breakup takes place in these devices either in channel/tube junctions (for T-junctions or impinging jets) or at orifices in co-flow devices, which makes it difficult to produce emulsions with high phase volume ratios. Moreover, the productivity of such microfluidic devices is rather low. On the contrary, in polyHIPE micromixers, droplet breakup occurs by increased shear and pressure gradients caused by forcing the fluid through the pore throats of polyHIPEs resulting in droplet elongation and breakup.

Three different CP formulations, namely St-DVB, EHA-PUDA, and EHA-EGDMA, were used to demonstrate continuous emulsification using polyHIPE micromixers for production of HIPEs with various internal phase volume fractions (Figure 4-3) (without the need for forced sedimentation of low volume fraction precursor emulsions as is often the case with microfluidic devices).[10,44] The polymerisation of the produced HIPEs results in typical polyHIPEs having a porosity determined by the IP ratio and varying degrees of interconnectivity. The porosity of the resultant polyHIPEs was controlled by varying the flow rate ratio of IP and CP during emulsification using polyHIPE micromixers, which allowed to produce polyHIPEs with a porosity gradient. Such polyHIPEs could be of interest for applications in tissue engineering[153] or as separation medium.[154]

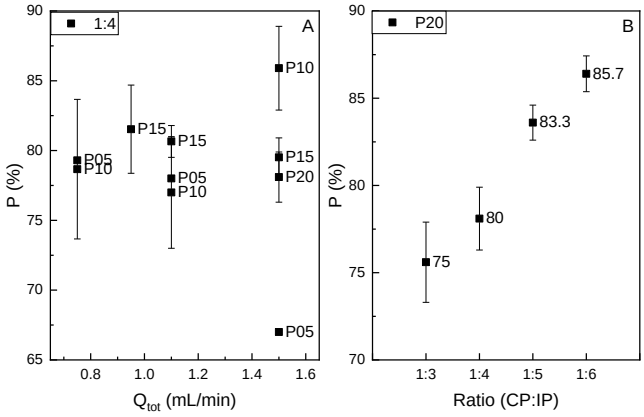

Figure 4-3. Porosities of poly(PUDA-co-EHA)HIPEs made by polymerisation of HIPEs created using various polyHIPE micromixers operated at flow rate ratio of 1:4 (CP:IP) (A), and of poly(PUDA-co-EHA)HIPEs made by continuous emulsification using P20 demonstrating that porosity can be controlled by changing the injection flow rate ratio of CP:IP (B).

Furthermore, I demonstrated that continuous emulsification of acrylate monomers containing a photoinitiator (in EHA-PUDA CP formulation) in polyHIPE micromixers fitted to a 3D printer allows to print HIPEs in desired patters. These printed HIPEs can be photopolymerised during printing using a UV-pen to create (fix) the desired macroporous material (Figure 4-4).

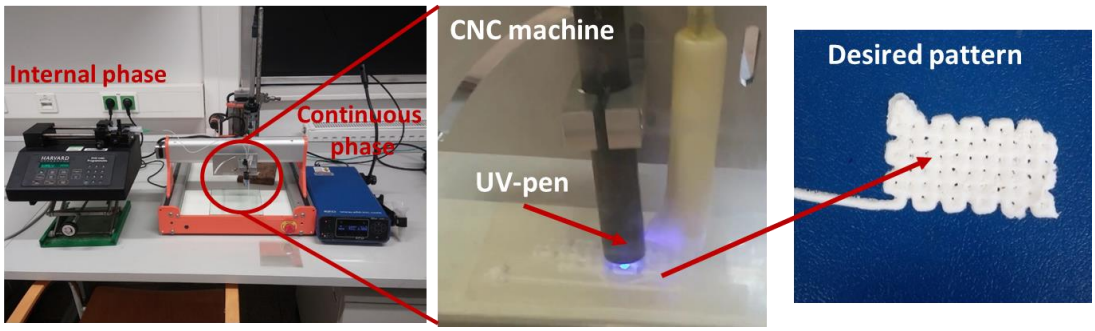

Figure 4-4. HIPEs generation using polyHIPE micromixer connected to the movable head of a CNC machine to print desired pattern which can subsequently be photopolymerised using a UV-pen resulting in structured polyHIPEs.

Besides the emulsion phase volume fraction, which controls porosity of the resulting polyHIPEs, it was possible to tailor pore and pore throat diameters by using polyHIPE micromixers with different permeability; the lower the *DoI* the higher the shear applied to droplets causing breakup, which results in the formation of smaller droplets acting as template for polymerisation thus smaller pore diameters of the resulting polyHIPEs after polymerisation (Figure 4-5).

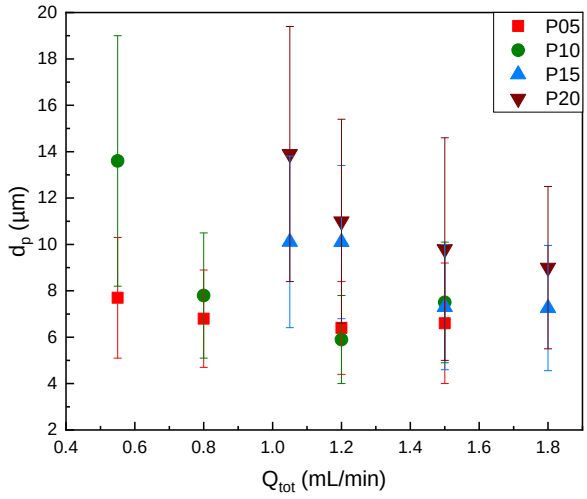

Figure 4-5. Average pore size of poly(EHA-co-PUDA)HIPEs produced by polymerisation of HIPEs generated using polyHIPE micromixers having various permeabilities as a function of total flow rate.

The literature reports the formation of methacrylate-based HIPEs, which were produced using a flow focusing microfluidic device. PolyHIPEs produced by polymerisation of these HIPE templates had d_p of 70-120 µm,[44] which was much larger than the average d_p of polyHIPEs that I produced by polymerisation of acrylate-based HIPEs formed in polyHIPE micromixers (Figure 4-5). Moreover, I could show that the average d_p of resulting polyHIPEs decreased with increasing flow rates because of higher shear forces acting on the droplets during emulsification in poly-Pickering-HIPE micromixers (Figure 4-5). Kiss et al.[155] generated o/w emulsions using SMX commercial static mixers in the laminar flow regime. They showed that the droplet diameter decreased from 220 µm to 90 µm with increasing flow velocities.[156] The less complex structure of the SMX static mixers caused larger droplet sizes when compared with the droplet diameters of HIPEs produced using polyHIPE micromixers, even though approximately a hundred times higher flow velocities were tested in SMX static mixers.[155] PolyHIPE micromixers are effective to continuously generate emulsions with desired phase volume fractions and smaller droplet diameters as possible with commercial micromixers.

4.3 Hypercrosslinked and functionalized polyHIPEs as Pd catalyst support in Suzuki-Miyaura cross-coupling reactions (Publication III)

En route to accomplish a Plant-on-a-Bench design, one of my objectives was to fabricate polyHIPE microreactors, which serve as micromixers but simultaneously as catalyst support for a Pd catalyst required for the hydrogenation of 4-nitroacetophenone. Even though poly(St-co-DVB)HIPEs are chemically stable and suitable to micromix fluids, they lack functional moieties to serve as ligands for the catalyst and possess low surface areas (~10 m^2/g). Therefore, I initially explored hypercrosslinking approaches of aromatic moieties in the polyHIPE structure. Friedel-Crafts alkylation with various external crosslinkers in the presence of Lewis acid or Brønsted acid catalysts was attempted to increase the available surface area of polyHIPEs. Knitting of poly-Pickering-HIPEs with bis(chloromethyl)-biphenyl (CMP) as external crosslinker and trifilic acid as catalyst increased the surface area of polyHIPEs from 10 m^2/g to approximately 850 m^2/g as a result of the formation of micro- and mesoporosity in the pore walls (Figure 4-6), while preserving the monolithic form and macropore structure of polyHIPEs (Figure 4-7). CMP knitted polyHIPEs were used for the fabrication of micromixer as described above. The hierarchical pore structure of micromixer was loaded with Pd in an attempt to create a microreactor.

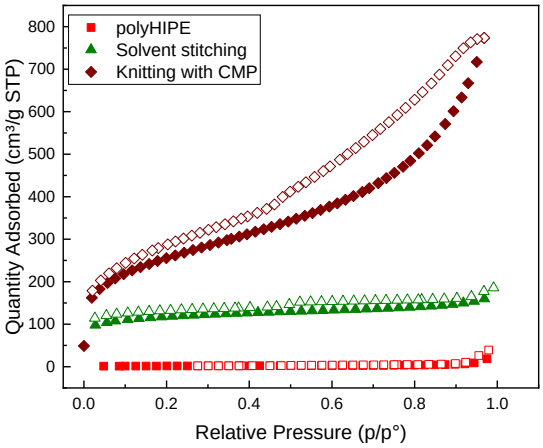

Figure 4-6. N_2 adsorption isotherm of polyHIPEs, hypercrosslinked polyHIPEs with solvent stitching approach and hypercrosslinked polyHIPEs with knitting of CMP external crosslinker.

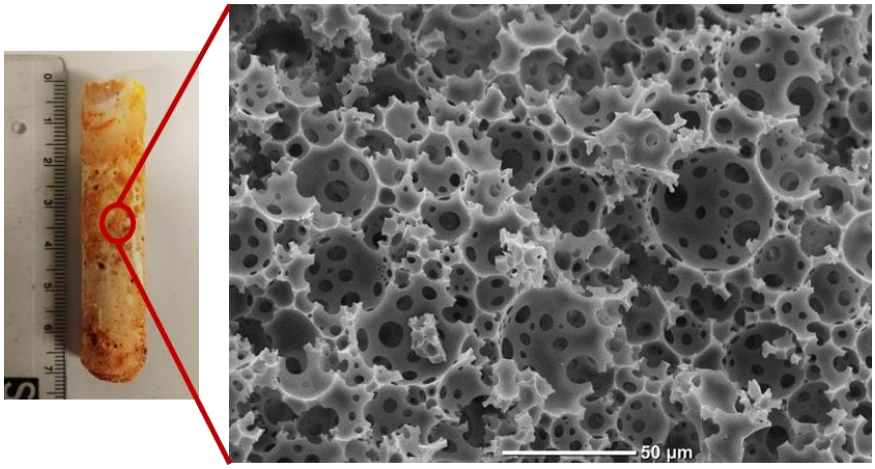

Figure 4-7. Photograph of CMP knitted poly-Pickering-HIPEs and its characteristic SEM image.

Pd@polyHIPE microreactors were used for the hydrogenation of 4-NAP in the presence of various hydrogen sources, which should yield 4-AAP (Figure 3-2). The highest yield achieved was 70%. Unfortunately, when reusing these microreactors the reaction yield dropped to as low as 30%. Even though knitted polyHIPEs possess significantly higher surface areas than polyHIPEs it was not possible to fix Pd to their hypercrosslinked surfaces; Pd leaching was observed and the remaining Pd oxidised to PdO (Figure 4-8B), which is catalytically inactive. This indicates the need for the incorporation of ligand moieties into polyHIPE surfaces. Therefore, the incorporation of triphenylphosphine (PPh_3) moieties–known to be a suitable ligand to form stable Pd complexes–was studied. Unfortunately, none of the knitting reactions with an external crosslinker was found to be effective to incorporate PPh_3 into the polymer network.

In order to hypercrosslink and simultaneously incorporate PPh_3 moieties into poly(St-co-DVB)HIPEs produced by polymerisation of hydrophobic silica particle and surfactant-stabilised HIPEs, which were found to be much more resilient than common polyHIPEs (see ESI publication III), solvent stitching and Scholl coupling reaction approaches in the presence of a Lewis acid ($AlCl_3$ instead of $FeCl_3$) catalyst were tested. DCM or DCE were used as external crosslinker for solvent stitching. The Scholl coupling reaction involves the elimination of two aryl-bound hydrogen atoms accompanied by the formation of a new aryl–aryl bond. During these hypercrosslinking reactions, PPh_3 was also added to the reaction mixture. The success of simultaneous functionalisation and hypercrosslinking was seen by an incorporation of up to 7.6% P into the polymer network and an increase of the surface area up to 410 m^2/g (Figure 4-6). The macroporous structure of polyHIPEs was preserved after the post-

functionalisation but unfortunately the monoliths cracked and/or broke after the reaction, which was probably caused by quenching of highly reactive $AlCl_3$ within the rigid structures resulting in rapid vapour release. However, the remaining polyHIPE pieces were mechanically robust and remained intact after loading them with $Pd(OAc)_2$ dissolved in DCM (Figure 4-8). Therefore, I explored the use of Pd@polyHIPE as heterogeneous catalyst for a batch model Suzuki-Miyaura coupling reaction (Figure 3-3).

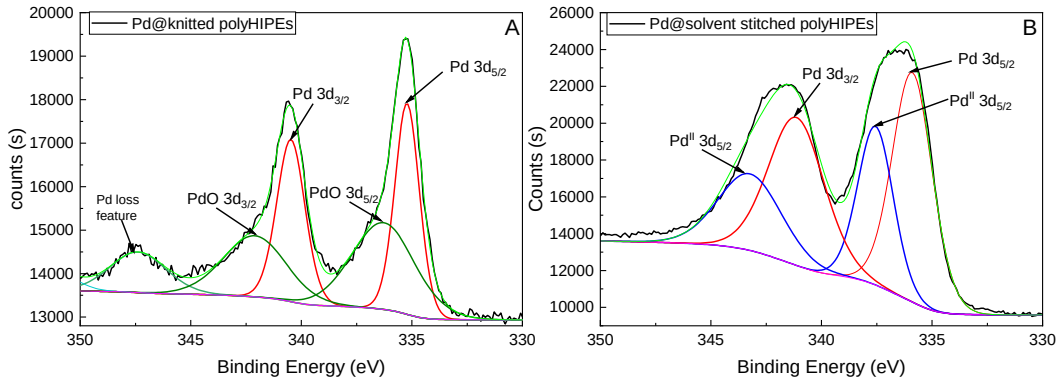

Figure 4-8. HR XP spectra of Pd-loaded on A) knitted but non-functionalised polyHIPE and B) hypercrosslinked and P-functionalised polyHIPE produced by solvent stitching.

Pd was found to be complexed by the phosphine moieties simultaneously introduced during hypercrosslinking of polyHIPEs. In this case no Pd leaching was observed after reusing the catalyst support six times. In the literature, functionalised, high surface area nanoporous polymers loaded with Pd were investigated several times as heterogeneous catalyst.[58,116,157] However, the fine powder form of these nanoporous polymers required tedious filtration steps for both the preparation of Pd loaded supports and after each reaction cycle. The coarse powder form of hypercrosslinked and functionalised polyHIPEs allowed for simple catalyst recovery from the reaction mixture using tweezers. The Pd@polyHIPE catalysts could be reused at least six times (more cycles were not tested because of time constraints). These polyHIPEs were resistant against repeated impact with the magnetic bar during reactions. Pd-loaded polyHIPEs displayed outstanding catalytic performance for the chosen model Suzuki-Miyaura coupling reaction reaching turnover frequencies of up to 2440 h^{-1} (Figure 4-9).

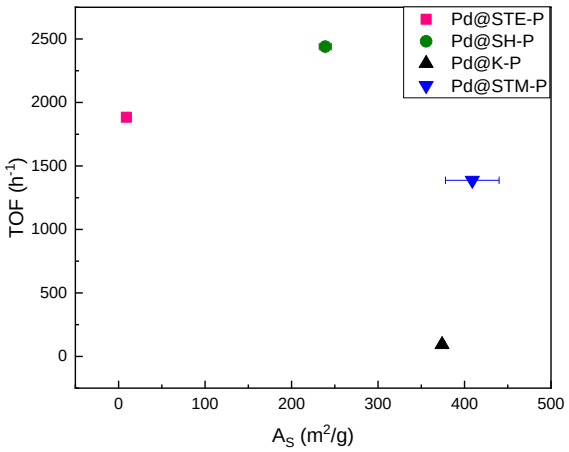

Figure 4-9. Turnover frequency of Suzuki Miyaura coupling reaction using Pd@polyHIPE pieces as a function of the specific surface areas of those hypercrosslinked and/or P functionalised polyHIPEs.

4.4 Liquid-liquid extraction of 4-aminoacetophenone using hydrophilic and hydrophobic polyHIPE micromixers (Publication IV)

A Plant-on-a-Bench design for continuous flow reactions requires besides the micromixer/microreactor a separation unit to recover the product from the reaction medium. This can be achieved using a liquid-liquid (L-L) extraction unit combined with a settler allowing for separation of the phases. As already demonstrated by Tebboth et al.[14] and above in paper I and II, the effective micromixing performance of polyHIPE micromixers makes them great candidates for the fabrication of a microextraction unit to recover continuously the product of 4-NAP hydrogenation reaction. L-L extraction of 4-AAP from the aqueous reaction mixture was investigated using polyHIPE micromixers combined with a gravity based minisettler (Figure 4-10A). L-L extraction is only effective if it is possible to generate a large interface between dispersed droplets and continuous phase as mass transfer during extraction occurs through this interface. In order to investigate whether the droplet type (o/w or w/o) affects the extraction efficiency I produced hydrophilic micromixers or micromixers consisting of a combination of hydrophilic and hydrophobic polyHIPEs. I started with hydrophilic micromixers as Tebboth et al. investigated hydrophobic polyHIPE micromixers before for the L-L extraction of caffeine, which served also as control for my work. The combination of hydrophilic and hydrophobic polyHIPEs within a single microextraction unit allows to switch the droplet dispersion type from o/w or w/o or

vice versa during extraction because of the preferential wettability (water or oil-wet) of the polyHIPE parts.

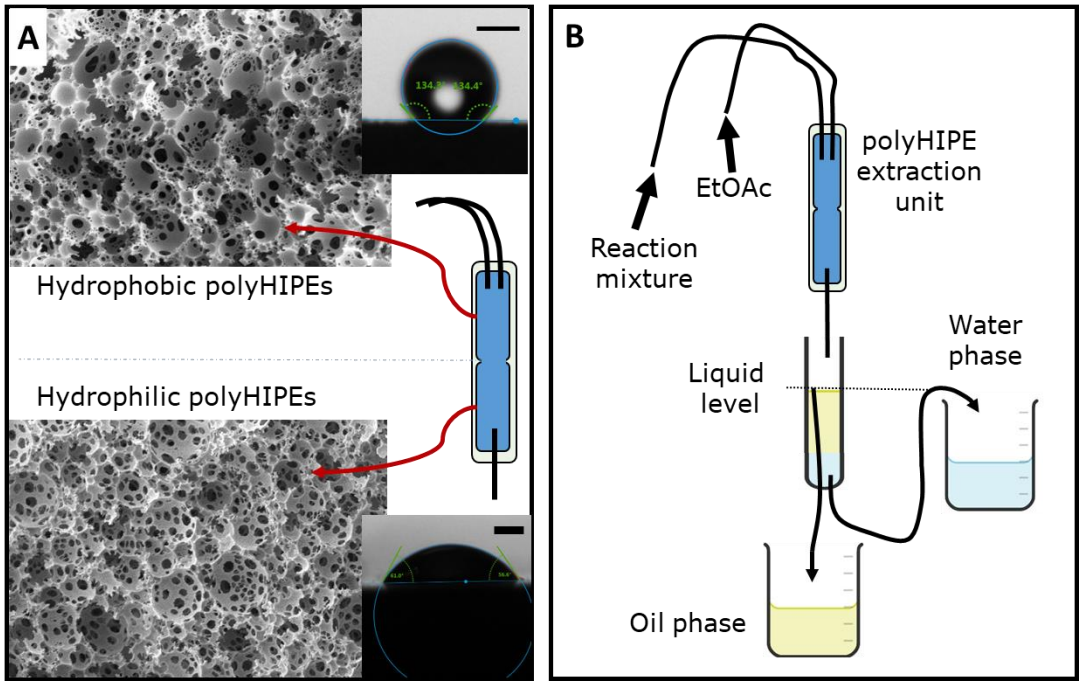

Figure 4-10. A) PolyHIPE extraction unit fabricated by combination of hydrophobic poly(St-co-TFEMA-co-DVB)HIPEs (SEM image and contact angle) used as top part in the micromixer and hydrophilic poly(HEMA-co-MBA)HIPEs (SEM image and contact angle) used as bottom part of the micromixer, B) Schematic of the L-L micromixer-minisettler unit used for the extraction of 4-AAP in to EtOAc from an aqueous mixture.

The 4-AAP extraction efficiency achieved when using a combined polyHIPE micromixer-settler was compared with polyHIPE micromixer-settlers fabricated only using hydrophilic or -phobic polyHIPEs of the same length and pore volume (Figure 4-10). Combined polyHIPE micromixer-settlers had improved extraction efficiencies compared to hydrophobic polyHIPE extraction units, however, had a similar extraction efficiency compared to hydrophilic polyHIPE micromixers. Nevertheless, combined polyHIPE micromixers possessed a higher permeability compared to hydrophilic polyHIPE micromixers because a smaller section of hydrophilic polyHIPE swelled in water affecting permeability, which renders the combined microextractor more attractive. I compared the extraction efficiency with those achieved in a blank tube and a commercial Kenics® static mixer having same internal volume. Significantly higher extraction efficiencies were obtained using polyHIPE micromixer-settlers, which proves effective micromixing, thus mass transfer in polyHIPE micromixing units (Figure 4-11).

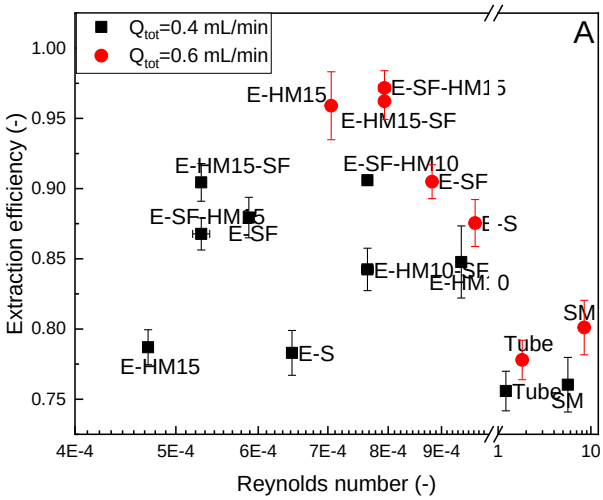

Figure 4-11. L-L extraction efficiency of 4-AAP from its simulated reaction mixture using polyHIPE micromixer-settlers, and static mixer (SM) and blank tube (tube) at Q_{tot} = 0.4 and 0.6 mL/min.

The literature reports various types of micromixer extraction units; L-L extraction of $CuSO_4$ from aqueous solution into kerosene with di-(2-ethylhexyl)phosphoric acid (D2EHPA) was investigated using a twisted micromixer. The overall volumetric mass transfer coefficient k_La increased approximately from 1 s^{-1} to 8 s^{-1} when increasing Re from 77 to 460, however at an expense of the extraction efficiency which decreased from 97% to 60%.[158] Even though they report much higher k_La compared to my findings (Figure 4-12A), their energy dissipation rate was also significantly higher (1200-100000 Pa/s) than the energy dissipation rate of my extraction units (0.03-0.28 m^2/s^3). L-L extraction in a four-stage oscillating micromixer with minisettler was tested to extract Zr(IV) from an aqueous solution.[159] The recirculation of fluids caused by the Coanda effect was achieved by forcing the fluid into the mixing chambers through much smaller channels at high enough speed. This mixing behaviour is similar to that in porous polyHIPEs in which fluid enters pores through much smaller pore throats. However, the extraction efficiency achieved using the four-stage oscillating micromixer with minisettler was only between ~20-45%. They reported a lower k_La compared with the polyHIPE micromixer-settlers, even though the extraction was performed at significantly higher flow rates.

Mass transfer efficiency of polyHIPE micromixers was significantly higher compared to other commercial and reported micromixers, which was likely due to the presence of many more connected mixing chambers (pores) within the polyHIPE structure. Higher overall volumetric mass transfer coefficients k_La were reported for L-L extraction of a

single compounds using commercial micromixers compared to the polyHIPE micromixer-settler but in some cases still resulted in much lower extraction efficiencies because their significantly lower extraction times. Energy dissipation rates to generate droplet flow in microchannel microextractors can be as high as 100 m^2/s^3,[43] while the energy dissipation rates in polyHIPE micromixer-settlers were lower than 0.28 m^2/s^3 (Figure 4-12B).

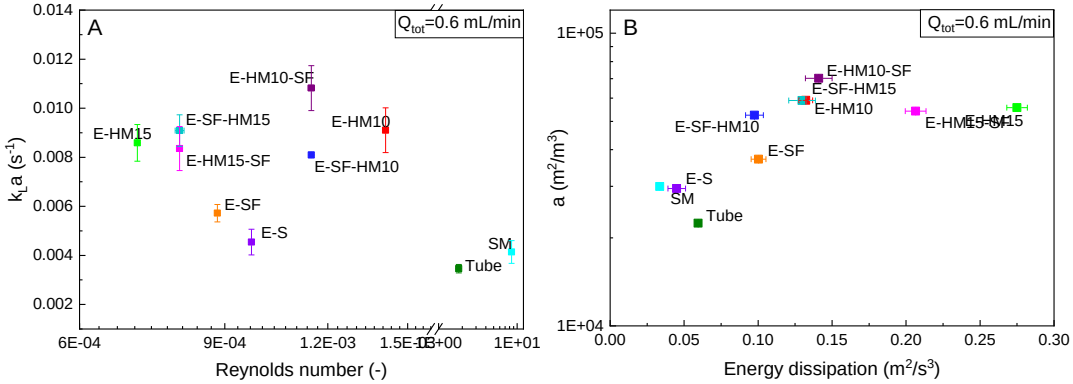

Figure 4-12. A) Overall volumetric mass transfer coefficient k_La of polyHIPE micromixer-settlers, a Kenics static mixer (SM) and a blank tube, used as controls, as function of Reynolds number, and B) interfacial area produced in the microextractors as function of energy dissipation at a total flow rate of Q_{tot} = 0.6 mL/min.

5 Conclusions and Future Work

5.1 Conclusions

Emulsion templated macroporous polymers were investigated with aim to use them for design of micromixers, microreactors and microextractors to be used as unit operations in a future Plant-on-a-Bench. Chemically stable polyHIPEs with an interconnected pore structures were synthesised to fabricate effective micromixers, which can be used to continuously mix fluids by molecular diffusion and chaotic advection. I showed that poly(St-co-DVB)HIPEs produced by polymerisation of HIPEs stabilised with hydrophobic silica particles and surfactant are great candidates for the fabrication of micromixers. I optimised the design of polyHIPE micromixers, which could be relatively easy built by inserting inlet and outlet tubes into polyHIPEs, followed by coating the surface of the polyHIPE with epoxy resin and further protection with a shrink tube. Fluids injected through the inlet tubes pass from macropore to macropore in polyHIPEs being forced through pore throats, which acting as constrictions, causing the fluids to mix both in radial and axial directions. Four polyHIPEs with identical average macropore diameters and porosities but increasing degrees of interconnectivity, and thus permeability, were synthesised, turned into micromixers and their micromixing behaviour investigated. The residence time distribution (RTD) of polyHIPE micromixers was determined using a tracer method. An axial dispersion model was fitted to the RTD and was in good agreement with commercial split and recombination micromixers. Additionally, the effectiveness of polyHIPE micromixers was investigated using two competitive parallel (4th Bourne) reactions. By determining the yield of slower reaction product, successful micromixing in polyHIPE micromixers was confirmed. The micromixing performance of polyHIPE micromixers was much better as compared with a commercial (Kenics) static mixer.

The micromixer performance of polyHIPE micromixers were utilised to continuously emulsify two immiscible liquids. A CP consisting of monomer, crosslinker and surfactant was mixed insight the pore structure of polyHIPE micromixers with an aqueous IP at various flow rates and CP:IP ratios. By changing the flow ratio during emulsification, the volume phase fraction of the generated emulsions could be adjusted. In contrast to many microfluidic devices it was possible to continuously generate HIPEs

(with emulsion phase volume ratios up to 88%) directly within polyHIPE micromixers without the need for forced sedimentation to produce HIPEs. The generated HIPEs could be polymerised into polyHIPEs (when using acrylate monomers even right after ejection from the mixer, allowing to pattern porous structures by 3D printing of HIPEs) with direct control over their porosity, which also allows for the preparation of graded porous polyHIPEs by simply changing the flow ratio of IP:CP during HIPE production in the polyHIPE micromixers. Moreover, the morphology of polyHIPEs used to build micromixers had direct impact on the HIPE droplet size, which is reflected in the pore size of the resultant porous polymers. Increasing the degree of interconnectivity of polyHIPEs resulted in lower shear forces exerted on the emulsion droplets and thus in larger droplets, which in turn result in polyHIPEs with larger average pore sizes. The usefulness of polyHIPE micromixers to continuously generate HIPE templates was tested using three different emulsion formulations with various IP:CP viscosity ratios. Because of the chemical stability of poly(St-co-DVB)HIPEs, micromixers could be reused several times without observing any obvious change of their morphology.

After demonstration of effective micromixing in polyHIPE micromixers, I attempted to turn them into microreactors loaded with catalyst. Due to lack of functional moieties and/or the low surface area of polyHIPEs it was impossible to stabilise catalyst on their macroporous surfaces. Therefore, poly(St-co-DVB)HIPEs were hypercrosslinked to increase their surface area. The aromatic moieties within monolithic polyHIPEs were knitted using an external crosslinker resulting in a surface area of ~850 m^2/g. Despite the much-increased surface area it was impossible to anchor the Pd catalyst to their surface. Therefore, I choose solvent stitching, in which solvent was used as external crosslinker, and Scholl coupling reaction not only to increase the surface area of polyHIPEs but also to incorporate phosphine moieties, which was not possible by knitting with an external crosslinker. Triphenylphosphine is known to be a ligand, which can complex Pd, resulting in stable and active catalyst. The simultaneous hypercrosslinking and PPh_3 functionalisation using solvent stitching and Scholl coupling reactions, resulted in the incorporation of 4 to 7 wt.% of P. Unfortunately, the polyHIPE monoliths fractured into a coarse powder during the reaction, which was used for Pd loading. Owing to the size of coarse polyHIPE pieces, they could be collected easily using tweezers allowing for simple catalyst recovery. Because of the successful introduction of phosphine moieties, stable Pd complexes formed on those polyHIPEs.

The catalytic activity of Pd@polyHIPE was determined using a model Suzuki-Miyaura reaction; reaction yields of 98% were achieved after a reaction time of only 30 min.

The final operation unit of a Plant-on-a-Bench for continuous flow reactions is a continuous L-L extraction and settler unit. This was designed and fabricated using polyHIPE micromixers. In the microextractor design, water- and oil-wet polyHIPEs were combined to investigate the effect of the droplet dispersion type (o/w or w/o) on the mass transfer and thus extraction efficiency. I investigated the L-L extraction of 4-aminoacetophenone, the product of the 4-nitroacetophenone hydrogenation reaction, from an aqueous reaction medium with ethyl acetate using a polyHIPE microextraction unit combined with gravity-based minisettler. The L-L extraction unit fabricated using a combination of hydrophilic and hydrophobic polyHIPE allowed for an extraction efficiency of 98%. The interfacial area between the two immiscible liquid phases produced in the polyHIPE extraction unit was as high as 17900 m^2/m^3 but the energy dissipation rate as low as 0.1 m^2/s^3. The extraction efficiency and interfacial area was comparable to values reported in the literature but at much lower energy dissipation rate. The developed polyHIPE micromixer-settler unit is a great candidate for continuous flow reactions allowing to intensify such processes.

5.2 Future work

The developments described in this thesis lay the groundwork for the development of a Plant-on-a-Bench assembled with miniaturised operation units, which could be realised with emulsion templated macroporous polymers. PolyHIPEs having tailored permeability and wettability were fabricated as micromixers and their effectiveness was investigated. Even though they had excellent micromixing performance, they still possessed mean residence times exceeding those of most commercially available micromixers. Therefore, shorter polyHIPE micromixers should be fabricated and tested.

In conventional microfluidic mixing units, fluid reorientation in microchannels achieved by insertion of obstacles into the mixing channel. It should be possible to polymerise HIPEs in microchannels to produce tailor-made obstacles, which could allow for improved mixing in such channel micromixers.

I demonstrated continuous emulsion generation in polyHIPE micromixers having various permeabilities. However, the droplet break-up mechanism could not be clarified completely because of the transparency of the polyHIPE micromixer. In order to understand it better, viscosity ratio between internal and continuous phases can be altered, thus changing critical Capillary number affecting droplet break-up. The droplet diameter of the resulting emulsion should be investigated systematically, which will be helpful to understand the mixing mechanism in polyHIPEs.

Furthermore, polyHIPE micromixers can be used to generate HIPEs continuously, which could be used to subsequently create more complex printed "porous structures". This could be realised by fitting such micromixer to a 3D printer allows for HIPE production during printing with photopolymerisation of the monomer containing phase. By tailoring the viscosity and emulsion volume phase fraction of the generated HIPE, many different desired materials can be produced in very short times.

Another important milestone of my project was to fabricate a polyHIPE microreactor by loading their porous surface with a heterogeneous catalyst. However, because of the lack of suitable ligand sites to stabilise the catalyst on the hypercrosslinked polyHIPE monoliths, I could not accomplish this. Nevertheless, the solvent stitching approach and Scholl reaction are promising tools to incorporate chemical functionalities into the polymer network. By improving the reaction and quenching method it should be possible to realise hypercrosslinked and functionalised monolithic polyHIPEs, suitable for loading with heterogeneous catalyst. These can be used to produce as microreactors.

Furthermore, knitted high surface area polyHIPEs should be tested as catalyst support with another metals, which do not oxidise as fast as Pd, which could also enable the production of polyHIPE microreactors.

As a final point of my project, after accomplishing stable catalyst loading on polyHIPE monoliths, microreactor, extraction unit and minisettler should assembled into a plant-on-a-bench and tested to perform continuous flow reactions. This might open up opportunities for process intensification of flow reactions. PolyHIPEs could play an important role as part of operating units in continuous flow synthesis.

6 References

(1) Dimian, A. C.; Bildea, C. S.; Kiss, A. A. Process Intensification. In *Computer Aided Chemical Engineering*; Elsevier, 2014; Vol. 35, pp 397–448. https://doi.org/10.1016/B978-0-444-62700-1.00010-3.

(2) Baumann, M.; Moody, T. S.; Smyth, M.; Wharry, S. A Perspective on Continuous Flow Chemistry in the Pharmaceutical Industry. *Org. Process Res. Dev.* **2020**, *24* (10), 1802–1813. https://doi.org/10.1021/acs.oprd.9b00524.

(3) Capretto, L.; Cheng, W.; Hill, M.; Zhang, X. Micromixing Within Microfluidic Devices. In *Microfluidics*; Lin, B., Ed.; Springer Berlin Heidelberg: Berlin, Heidelberg, 2011; Vol. 304, pp 27–68. https://doi.org/10.1007/128_2011_150.

(4) Nimafar, M.; Viktorov, V.; Martinelli, M. Experimental Investigation of Split and Recombination Micromixer in Confront with Basic T- and O- Type Micromixers. *Int. J. Mech. Appl.* **2012**, *2* (5), 61–69. https://doi.org/10.5923/j.mechanics.20120205.02.

(5) Akwi, F. M.; Watts, P. Continuous Flow Chemistry: Where Are We Now? Recent Applications, Challenges and Limitations. *Chem. Commun.* **2018**, *54* (99), 13894–13928. https://doi.org/10.1039/C8CC07427E.

(6) Kelley, D. H.; Ouellette, N. T. Separating Stretching from Folding in Fluid Mixing. *Nat. Phys.* **2011**, *7* (6), 477–480. https://doi.org/10.1038/nphys1941.

(7) Ruijin, W.; Beiqi, L.; Dongdong, S.; Zefei, Z. Investigation on the Splitting-Merging Passive Micromixer Based on Baker's Transformation. *Sens. Actuators B Chem.* **2017**, *249*, 395–404. https://doi.org/10.1016/j.snb.2017.04.087.

(8) Kim, D. S.; Lee, S. H.; Kwon, T. H.; Ahn, C. H. A Serpentine Laminating Micromixer Combining Splitting/Recombination and Advection. *Lab. Chip* **2005**, *5* (7), 739. https://doi.org/10.1039/b418314b.

(9) Liu, Y.; Deng, Y.; Zhang, P.; Liu, Z.; Wu, Y. Experimental Investigation of Passive Micromixers Conceptual Design Using the Layout Optimization Method. *J. Micromechanics Microengineering* **2013**, *23* (7), 075002. https://doi.org/10.1088/0960-1317/23/7/075002.

(10) Costantini, M.; Colosi, C.; Guzowski, J.; Barbetta, A.; Jaroszewicz, J.; Święszkowski, W.; Dentini, M.; Garstecki, P. Highly Ordered and Tunable PolyHIPEs by Using Microfluidics. *J. Mater. Chem. B* **2014**, *2* (16), 2290. https://doi.org/10.1039/c3tb21227k.

(11) Tebboth, M.; Kogelbauer, A.; Bismarck, A. Effectiveness of Emulsion-Templated Macroporous Polymer Micromixers Characterized by the Bourne Reaction. *Ind. Eng. Chem. Res.* **2015**, *54* (22), 5974–5981. https://doi.org/10.1021/acs.iecr.5b00493.

(12) Barkan-Öztürk, H.; Menner, A.; Bismarck, A. Emulsion-Templated Macroporous Polymer Micromixers. *Ind. Eng. Chem. Res.* **2021**, *60* (39), 14013–14025. https://doi.org/10.1021/acs.iecr.1c01949.

(13) Brown, J. F.; Krajnc, P.; Cameron, N. R. PolyHIPE Supports in Batch and Flow-Through Suzuki Cross-Coupling Reactions. *Ind. Eng. Chem. Res.* **2005**, *44* (23), 8565–8572. https://doi.org/10.1021/ie048843c.

(14) Tebboth, M.; Kogelbauer, A.; Bismarck, A. Liquid–Liquid Extraction within Emulsion Templated Macroporous Polymers. *Ind. Eng. Chem. Res.* **2015**, *54* (29), 7284–7291. https://doi.org/10.1021/acs.iecr.5b01346.

(15) Reglero Ruiz, J. A.; Vincent, M.; Agassant, J.-F.; Sadik, T.; Pillon, C.; Carrot, C. Polymer Foaming with Chemical Blowing Agents: Experiment and Modeling. *Polym. Eng. Sci.* **2015**, *55* (9), 2018–2029. https://doi.org/10.1002/pen.24044.
(16) Jalalian, M.; Jiang, Q.; Bismarck, A. Air Templated Macroporous Epoxy Foams with Silica Particles as Property-Defining Additive. *ACS Appl. Polym. Mater.* **2019**, *1* (3), 335–343. https://doi.org/10.1021/acsapm.8b00084.
(17) Rusakov, D.; Menner, A.; Spieckermann, F.; Wilhelm, H.; Bismarck, A. Morphology and Properties of Foamed High Crystallinity PEEK Prepared by High Temperature Thermally Induced Phase Separation. *J. Appl. Polym. Sci.* **2022**, *139* (1), 51423. https://doi.org/10.1002/app.51423.
(18) Rusakov, D.; Menner, A.; Bismarck, A. High-Performance Polymer Foams by Thermally Induced Phase Separation. *Macromol. Rapid Commun.* **2020**, *41* (11), 2000110. https://doi.org/10.1002/marc.202000110.
(19) Wu, D.; Xu, F.; Sun, B.; Fu, R.; He, H.; Matyjaszewski, K. Design and Preparation of Porous Polymers. *Chem. Rev.* **2012**, *112* (7), 3959–4015. https://doi.org/10.1021/cr200440z.
(20) Menner, A.; Powell, R.; Bismarck, A. Open Porous Polymer Foams via Inverse Emulsion Polymerization: Should the Definition of High Internal Phase (Ratio) Emulsions Be Extended? *Macromolecules* **2006**, *39* (6), 2034–2035. https://doi.org/10.1021/ma052705x.
(21) Cameron, N. R.; Sherrington, D. C.; Albiston, L.; Gregory, D. P. Study of the Formation of the Open-Cellular Morphology of Poly(Styrene/Divinylbenzene) PolyHIPE Materials by Cryo-SEM. *Colloid Polym. Sci.* **1996**, *274* (6), 592–595. https://doi.org/10.1007/BF00655236.
(22) Menner, A.; Powell, R.; Bismarck, A. Open Porous Polymer Foams via Inverse Emulsion Polymerization: Should the Definition of High Internal Phase (Ratio) Emulsions Be Extended? *Macromolecules* **2006**, *39* (6), 2034–2035. https://doi.org/10.1021/ma052705x.
(23) Tebboth, M.; Kogelbauer, A.; Bismarck, A. Highly Permeable Macroporous Polymers via Controlled Agitation of Emulsion Templates. *Chem. Eng. Sci.* **2015**, *137*, 786–795. https://doi.org/10.1016/j.ces.2015.06.047.
(24) Ikem, V. O.; Menner, A.; Horozov, T. S.; Bismarck, A. Highly Permeable Macroporous Polymers Synthesized from Pickering Medium and High Internal Phase Emulsion Templates. *Adv. Mater.* **2010**, *22* (32), 3588–3592. https://doi.org/10.1002/adma.201000729.
(25) Jiang, Q.; Menner, A.; Bismarck, A. Emulsion-Templated Macroporous Polymer/Polymer Composites with Switchable Stiffness. *Pure Appl. Chem.* **2014**, *86* (2). https://doi.org/10.1515/pac-2014-5001.
(26) Jiang, Q.; Barkan, H.; Menner, A.; Bismarck, A. Micropatterned, Macroporous Polymer Springs for Capacitive Energy Harvesters. *Polymer* **2017**, *126*, 419–424. https://doi.org/10.1016/j.polymer.2017.04.018.
(27) Menner, A.; Verdejo, R.; Shaffer, M.; Bismarck, A. Particle-Stabilized Surfactant-Free Medium Internal Phase Emulsions as Templates for Porous Nanocomposite Materials: Poly-Pickering-Foams. *Langmuir* **2007**, *23* (5), 2398–2403. https://doi.org/10.1021/la062712u.
(28) Eslek, A.; Kekevi, B.; Mert, H. H.; Mert, E. H. Emulsion Templated Polymer Monoliths Containing Cellulose Nanocrystals: Synthesis and Adsorption Properties. *J. Appl. Polym. Sci.* **2022**, *139* (11), 51802. https://doi.org/10.1002/app.51802.

(29) Kenneth J. Lissant. Continuous Process for the Prepartion of Emulsion. US 3565817.
(30) Dautzenberg, F. M.; Mukherjee, M. Process Intensification Using Multifunctional Reactors. *Chem. Eng. Sci.* **2001**, *56* (2), 251–267. https://doi.org/10.1016/S0009-2509(00)00228-1.
(31) Stankiewicz, A. Reactive Separations for Process Intensification: An Industrial Perspective. *Chem. Eng. Process. Process Intensif.* **2003**, *42* (3), 137–144. https://doi.org/10.1016/S0255-2701(02)00084-3.
(32) Stankiewicz, A.; Van Gerven, T.; Stefanidis, G. *The Fundamentals of Process Intensification*; Wiley-VCH: Weinheim, 2019.
(33) Charpentier, J.-C. In the Frame of Globalization and Sustainability, Process Intensification, a Path to the Future of Chemical and Process Engineering (Molecules into Money). *Chem. Eng. J.* **2007**, *134* (1–3), 84–92. https://doi.org/10.1016/j.cej.2007.03.084.
(34) Bayat, M.; Hamidi, M.; Dehghani, Z.; Rahimpour, M. R.; Shariati, A. Hydrogen/Methanol Production in a Novel Multifunctional Reactor with *in Situ* Adsorption: Modeling and Optimization: Multifunctional Sorption-Enhanced Methanol Reactor. *Int. J. Energy Res.* **2014**, *38* (8), 978–994. https://doi.org/10.1002/er.3092.
(35) Benaskar, F.; Ben-Abdelmoumen, A.; Patil, N. G.; Rebrov, E. V.; Meuldijk, J.; Hulshof, L. A.; Hessel, V.; Krtschil, U.; Schouten, J. C. Cost Analysis for a Continuously Operated Fine Chemicals Production Plant at 10 Kg/Day Using a Combination of Microprocessing and Microwave Heating. *J. Flow Chem.* **2011**, *1* (2), 74–89. https://doi.org/10.1556/jfchem.2011.00015.
(36) Roberge, D. M.; Zimmermann, B.; Rainone, F.; Gottsponer, M.; Eyholzer, M.; Kockmann, N. Microreactor Technology and Continuous Processes in the Fine Chemical and Pharmaceutical Industry: Is the Revolution Underway? *Org. Process Res. Dev.* **2008**, *12* (5), 905–910. https://doi.org/10.1021/op8001273.
(37) Snead, D. R.; Jamison, T. F. End-to-End Continuous Flow Synthesis and Purification of Diphenhydramine Hydrochloride Featuring Atom Economy, in-Line Separation, and Flow of Molten Ammonium Salts. *Chem. Sci.* **2013**, *4* (7), 2822. https://doi.org/10.1039/c3sc50859e.
(38) Nguyen, N.-T. *Micromixers: Fundamentals, Design, and Fabrication*, 2nd ed.; Micro & nano technologies series; Elsevier/William Andrew: Amsterdam ; Boston, 2012.
(39) Mao, Z.; Yang, C. Micro-Mixing in Chemical Reactors: A Perspective. *Chin. J. Chem. Eng.* **2017**, *25* (4), 381–390. https://doi.org/10.1016/j.cjche.2016.09.012.
(40) Bayareh, M.; Ashani, M. N.; Usefian, A. Active and Passive Micromixers: A Comprehensive Review. *Chem. Eng. Process. - Process Intensif.* **2020**, *147*, 107771. https://doi.org/10.1016/j.cep.2019.107771.
(41) Kashid, M. N.; Harshe, Y. M.; Agar, D. W. Liquid−Liquid Slug Flow in a Capillary: An Alternative to Suspended Drop or Film Contactors. *Ind. Eng. Chem. Res.* **2007**, *46* (25), 8420–8430. https://doi.org/10.1021/ie070077x.
(42) Wang, K.; Luo, G. Microflow Extraction: A Review of Recent Development. *Chem. Eng. Sci.* **2017**, *169*, 18–33. https://doi.org/10.1016/j.ces.2016.10.025.
(43) Plouffe, P.; Roberge, D. M.; Sieber, J.; Bittel, M.; Macchi, A. Liquid–Liquid Mass Transfer in a Serpentine Micro-Reactor Using Various Solvents. *Chem. Eng. J.* **2016**, *285*, 605–615. https://doi.org/10.1016/j.cej.2015.09.115.

(44) Dabrowski, M. L.; Jenkins, D.; Cosgriff-Hernandez, E.; Stubenrauch, C. Methacrylate-Based Polymer Foams with Controllable Connectivity, Pore Shape, Pore Size and Polydispersity. *Phys. Chem. Chem. Phys.* **2020**, *22* (1), 155–168. https://doi.org/10.1039/C9CP03606G.
(45) Lapierre, F.; Cameron, N. R.; Zhu, Y. Ready… Set, Flow: Simple Fabrication of Microdroplet Generators and Their Use in the Synthesis of PolyHIPE Microspheres. *J. Micromechanics Microengineering* **2015**, *25* (3), 035011. https://doi.org/10.1088/0960-1317/25/3/035011.
(46) Shui, L.; van den Berg, A.; Eijkel, J. C. T. Interfacial Tension Controlled W/O and O/W 2-Phase Flows in Microchannel. *Lab Chip* **2009**, *9* (6), 795–801. https://doi.org/10.1039/B813724B.
(47) Raza, W.; Hossain, S.; Kim, K.-Y. A Review of Passive Micromixers with a Comparative Analysis. *Micromachines* **2020**, *11* (5), 455. https://doi.org/10.3390/mi11050455.
(48) Barkan-Öztürk, H.; Menner, A.; Bismarck, A. Emulsion Templated Macroporous Polymer Micromixers. *Ind. Eng. Chem. Res.* **2021**, *Submitted*.
(49) Liu, P. S. *Porous Materials: Processing and Applications*, 1st edition.; Elsevier: Waltham, MA, 2014.
(50) Mills, N. Chapter 1 - Introduction to Polymer Foam Microstructure. In *Polymer Foams Handbook*; Mills, N., Ed.; Butterworth-Heinemann: Oxford, 2007; pp 1–18. https://doi.org/10.1016/B978-075068069-1/50002-7.
(51) Jalalian, M.; Jiang, Q.; Coulon, A.; Storb, M.; Woodward, R.; Bismarck, A. Mechanically Whipped Phenolic Froths as Versatile Templates for Manufacturing Phenolic and Carbon Foams. *Mater. Des.* **2019**, *168*, 107658. https://doi.org/10.1016/j.matdes.2019.107658.
(52) Amini, A. R.; Laurencin, C. T.; Nukavarapu, S. P. Bone Tissue Engineering: Recent Advances and Challenges. *Crit. Rev. Biomed. Eng.* **2012**, *40*, 363–408. https://doi.org/10.1615/critrevbiomedeng.v40.i5.10.
(53) Cox, S. C.; Thornby, J. A.; Gibbons, G. J.; Williams, M. A.; Mallick, K. K. 3D Printing of Porous Hydroxyapatite Scaffolds Intended for Use in Bone Tissue Engineering Applications. *Mater. Sci. Eng. C* **2015**, *47*, 237–247. https://doi.org/10.1016/j.msec.2014.11.024.
(54) Barbetta, A.; Dentini, M.; Zannoni, E. M.; De Stefano, M. E. Tailoring the Porosity and Morphology of Gelatin-Methacrylate PolyHIPE Scaffolds for Tissue Engineering Applications. *Langmuir* **2005**, *21* (26), 12333–12341. https://doi.org/10.1021/la0520233.
(55) *Polyurethane Market Size, Share & Trends Analysis Report By Product (Flexible Foam, Rigid Foam), By End Use (Construction, Electronics & Appliances), By Region (APAC, North America), And Segment Forecasts, 2021 - 2028*; 978-1-68038-262–4; 2021; p 105.
(56) Jin, F.-L.; Zhao, M.; Park, M.; Park, S.-J. Recent Trends of Foaming in Polymer Processing: A Review. *Polymers* **2019**, *11* (6), 953. https://doi.org/10.3390/polym11060953.
(57) Rouquerol, J.; Avnir, D.; Fairbridge, C. W.; Everett, D. H.; Haynes, J. M.; Pernicone, N.; Ramsay, J. D. F.; Sing, K. S. W.; Unger, K. K. Recommendations for the Characterization of Porous Solids (Technical Report). *Pure Appl. Chem.* **1994**, *66* (8). https://doi.org/10.1351/pac199466081739.

(58) Li, B.; Guan, Z.; Yang, X.; Wang, W. D.; Wang, W.; Hussain, I.; Song, K.; Tan, B.; Li, T. Multifunctional Microporous Organic Polymers. *J. Mater. Chem. A* **2014**, *2* (30), 11930. https://doi.org/10.1039/C4TA01081G.
(59) Xu, W.; Liu, C.; Xiang, D.; Luo, Q.; Shu, Y.; Lin, H.; Hu, Y.; Zhang, Z.; Ouyang, Y. Palladium Catalyst Immobilized on Functionalized Microporous Organic Polymers for C–C Coupling Reactions. *RSC Adv.* **2019**, *9* (59), 34595–34600. https://doi.org/10.1039/C9RA07303E.
(60) Wang, S.; Zhang, C.; Shu, Y.; Jiang, S.; Xia, Q.; Chen, L.; Jin, S.; Hussain, I.; Cooper, A. I.; Tan, B. Layered Microporous Polymers by Solvent Knitting Method. *Sci. Adv.* **2017**, *3* (3), e1602610. https://doi.org/10.1126/sciadv.1602610.
(61) Liu, G.; Wang, Y.; Shen, C.; Ju, Z.; Yuan, D. A Facile Synthesis of Microporous Organic Polymers for Efficient Gas Storage and Separation. *J. Mater. Chem. A* **2015**, *3* (6), 3051–3058. https://doi.org/10.1039/C4TA05349D.
(62) Woodward, R. T.; Jobbe-Duval, A.; Marchesini, S.; Anthony, D. B.; Petit, C.; Bismarck, A. Hypercrosslinked PolyHIPEs as Precursors to Designable, Hierarchically Porous Carbon Foams. *Polymer* **2017**, *115*, 146–153. https://doi.org/10.1016/j.polymer.2017.03.042.
(63) Huang, J.; Turner, S. R. Hypercrosslinked Polymers: A Review. *Polym. Rev.* **2018**, *58* (1), 1–41. https://doi.org/10.1080/15583724.2017.1344703.
(64) Furukawa, H.; Yaghi, O. M. Storage of Hydrogen, Methane, and Carbon Dioxide in Highly Porous Covalent Organic Frameworks for Clean Energy Applications. *J. Am. Chem. Soc.* **2009**, *131* (25), 8875–8883. https://doi.org/10.1021/ja9015765.
(65) Côté, A. P.; Benin, A. I.; Ockwig, N. W.; O'Keeffe, M.; Matzger, A. J.; Yaghi, O. M. Porous, Crystalline, Covalent Organic Frameworks. *Science* **2005**, *310* (5751), 1166–1170. https://doi.org/10.1126/science.1120411.
(66) Dawson, R.; Adams, D. J.; Cooper, A. I. Chemical Tuning of CO2 Sorption in Robust Nanoporous Organic Polymers. *Chem. Sci.* **2011**, *2* (6), 1173. https://doi.org/10.1039/c1sc00100k.
(67) Lu, W.; Verdegaal, W. M.; Yu, J.; Balbuena, P. B.; Jeong, H.-K.; Zhou, H.-C. Building Multiple Adsorption Sites in Porous Polymer Networks for Carbon Capture Applications. *Energy Environ. Sci.* **2013**, *6* (12), 3559. https://doi.org/10.1039/c3ee42226g.
(68) Woodward, R. T. The Design of Hypercrosslinked Polymers from Benzyl Ether Self-Condensing Compounds and External Crosslinkers. *Chem. Commun.* **2020**, *56* (36), 4938–4941. https://doi.org/10.1039/D0CC01002B.
(69) Tan, L.; Tan, B. Hypercrosslinked Porous Polymer Materials: Design, Synthesis, and Applications. *Chem. Soc. Rev.* **2017**, *46* (11), 3322–3356. https://doi.org/10.1039/C6CS00851H.
(70) Davankov, V.; Tsyurupa, M.; Ilyin, M.; Pavlova, L. Hypercross-Linked Polystyrene and Its Potentials for Liquid Chromatography: A Mini-Review. *J. Chromatogr. A* **2002**, *965* (1–2), 65–73. https://doi.org/10.1016/S0021-9673(01)01583-7.
(71) Pulko, I.; Krajnc, P. Porous Polymer Monoliths by Emulsion Templating: POROUS POLYMER MONOLITHS BY EMULSION TEMPLATING. In *Encyclopedia of Polymer Science and Technology*; John Wiley & Sons, Inc., Ed.; John Wiley & Sons, Inc.: Hoboken, NJ, USA, 2017; pp 1–28. https://doi.org/10.1002/0471440264.pst653.

(72) Bolton, K. F.; Canty, A. J.; Deverell, J. A.; Guijt, R. M.; Hilder, E. F.; Rodemann, T.; Smith, J. A. Macroporous Monolith Supports for Continuous Flow Capillary Microreactors. *Tetrahedron Lett.* **2006**, *47* (52), 9321–9324. https://doi.org/10.1016/j.tetlet.2006.10.113.

(73) Desire, C. T.; Hilder, E. F.; Arrua, R. D. Monolithic High-Performance Liquid Chromatography Columns. In *Encyclopedia of Analytical Chemistry*; Meyers, R. A., Ed.; John Wiley & Sons, Ltd: Chichester, UK, 2017; pp 1–37. https://doi.org/10.1002/9780470027318.a9386.

(74) Ruckenstein, E.; Hong, L. Binding Catalytic Sites to the Surface of Porous Polymers and Some Catalytic Applications. *Chem. Mater.* **1992**, *4* (1), 122–127. https://doi.org/10.1021/cm00019a026.

(75) Tan, L.; Tan, B. Functionalized Hierarchical Porous Polymeric Monoliths as Versatile Platforms to Support Uniform and Ultrafine Metal Nanoparticles for Heterogeneous Catalysis. *Chem. Eng. J.* **2020**, *390*, 124485. https://doi.org/10.1016/j.cej.2020.124485.

(76) Wang, G.; Liu, X.; Zhang, J.; Sui, W.; Jang, J.; Si, C. One-Pot Lignin Depolymerization and Activation by Solid Acid Catalytic Phenolation for Lightweight Phenolic Foam Preparation. *Ind. Crops Prod.* **2018**, *124*, 216–225. https://doi.org/10.1016/j.indcrop.2018.07.080.

(77) Yang, J.; Ye, Y.; Li, X.; Lü, X.; Chen, R. Flexible, Conductive, and Highly Pressure-Sensitive Graphene-Polyimide Foam for Pressure Sensor Application. *Compos. Sci. Technol.* **2018**, *164*, 187–194. https://doi.org/10.1016/j.compscitech.2018.05.044.

(78) Jiang, Q.; Menner, A.; Bismarck, A. Emulsion-Templated Macroporous Polymer/Polymer Composites with Switchable Stiffness. *Pure Appl. Chem.* **2014**, *86* (2). https://doi.org/10.1515/pac-2014-5001.

(79) Silverstein, M. S. Emulsion-Templated Porous Polymers: A Retrospective Perspective. *Polymer* **2014**, *55* (1), 304–320. https://doi.org/10.1016/j.polymer.2013.08.068.

(80) Colloid Stability. In *Emulsions, Foams, and Suspensions*; Wiley-VCH Verlag GmbH & Co. KGaA: Weinheim, FRG, 2006; pp 117–154. https://doi.org/10.1002/3527606750.ch5.

(81) Menner, A.; Haibach, K.; Powell, R.; Bismarck, A. Tough Reinforced Open Porous Polymer Foams via Concentrated Emulsion Templating. *Polymer* **2006**, *47* (22), 7628–7635. https://doi.org/10.1016/j.polymer.2006.09.022.

(82) Lissant, K. J. The Geometry of High-Internal-Phase-Ratio Emulsions. *J. Colloid Interface Sci.* **1966**, *22* (5), 462–468.

(83) Cases, J. M.; Villieras, F. Thermodynamic Model of Ionic and Nonionic Surfactants Adsorption-Abstraction on Heterogeneous Surfaces. *Langmuir* **1992**, *8* (5), 1251–1264. https://doi.org/10.1021/la00041a005.

(84) Williams, J. M. High Internal Phase Water-in-Oil Emulsions: Influence of Surfactants and Cosurfactants on Emulsion Stability and Foam Quality. *Langmuir* **1991**, *7* (7), 1370–1377. https://doi.org/10.1021/la00055a014.

(85) Binks, B. P. Particles as Surfactants—Similarities and Differences. *Curr. Opin. Colloid Interface Sci.* **2002**, *7* (1–2), 21–41. https://doi.org/10.1016/S1359-0294(02)00008-0.

(86) Binks, B. P.; Lumsdon, S. O. Catastrophic Phase Inversion of Water-in-Oil Emulsions Stabilized by Hydrophobic Silica. *Langmuir* **2000**, *16* (6), 2539–2547. https://doi.org/10.1021/la991081j.

(87) Walstra, P. Principles of Emulsion Formation. *Chem. Eng. Sci.* **1993**, *48* (2), 333–349. https://doi.org/10.1016/0009-2509(93)80021-H.
(88) Horozov, T. Foams and Foam Films Stabilised by Solid Particles. *Curr. Opin. Colloid Interface Sci.* **2008**, *13* (3), 134–140. https://doi.org/10.1016/j.cocis.2007.11.009.
(89) *Porous Polymers*; Silverstein, M. S., Cameron, N. R., Hillmyer, M. A., Eds.; Wiley: Hoboken, N.J, 2011.
(90) Taylor, P. Ostwald Ripening in Emulsions. *Adv. Colloid Interface Sci.* **1998**, *75* (2), 107–163. https://doi.org/10.1016/S0001-8686(98)00035-9.
(91) Tebboth, M.; Kogelbauer, A.; Bismarck, A. Highly Permeable Macroporous Polymers via Controlled Agitation of Emulsion Templates. *Chem. Eng. Sci.* **2015**, *137*, 786–795. https://doi.org/10.1016/j.ces.2015.06.047.
(92) Barkan-Öztürk, H.; Menner, A.; Bismarck, A. Polymerised High Internal Phase Emulsion Micromixers for Continuous Emulsification. *Chem. Eng. Sci.* **2021**, 117296. https://doi.org/10.1016/j.ces.2021.117296.
(93) Stubenrauch, C.; Menner, A.; Bismarck, A.; Drenckhan, W. Emulsion and Foam Templating-Promising Routes to Tailor-Made Porous Polymers. *Angew. Chem. Int. Ed.* **2018**, *57* (32), 10024–10032. https://doi.org/10.1002/anie.201801466.
(94) Akay, G.; Noor, Z. Z.; Dogru, M. Process Intensification in Water-in-Crude Oil Emulsion Separation by Simultaneous Application of Electric Field and Novel Demulsifier Adsorbers Based on Polyhipe Polymers. In *Microreactor Technology and Process Intensification*; Wang, Y., Holladay, J. D., Eds.; ACS Symposium Series; American Chemical Society: Washington, DC, 2005; Vol. 914, pp 378–392. https://doi.org/10.1021/bk-2005-0914.ch023.
(95) Foudazi, R. HIPEs to PolyHIPEs. *React. Funct. Polym.* **2021**, *164*, 104917. https://doi.org/10.1016/j.reactfunctpolym.2021.104917.
(96) Wu, R.; Menner, A.; Bismarck, A. Macroporous Polymers Made from Medium Internal Phase Emulsion Templates: Effect of Emulsion Formulation on the Pore Structure of PolyMIPEs. *Polymer* **2013**, *54* (21), 5511–5517. https://doi.org/10.1016/j.polymer.2013.08.029.
(97) Menner, A.; Ikem, V.; Salgueiro, M.; Shaffer, M. S. P.; Bismarck, A. High Internal Phase Emulsion Templates Solely Stabilised by Functionalised Titania Nanoparticles. *Chem. Commun.* **2007**, No. 41, 4274. https://doi.org/10.1039/b708935j.
(98) Williams, J. M.; Wrobleski, D. A. Spatial Distribution of the Phases in Water-in-Oil Emulsions. Open and Closed Microcellular Foams from Cross-Linked Polystyrene. *Langmuir* **1988**, *4* (3), 656–662. https://doi.org/10.1021/la00081a027.
(99) Jiang, Q.; Menner, A.; Bismarck, A. One-Pot Synthesis of Supported Hydrogel Membranes via Emulsion Templating. *React. Funct. Polym.* **2017**, *114*, 104–109. https://doi.org/10.1016/j.reactfunctpolym.2017.03.003.
(100) Owen, R.; Sherborne, C.; Paterson, T.; Green, N. H.; Reilly, G. C.; Claeyssens, F. Emulsion Templated Scaffolds with Tunable Mechanical Properties for Bone Tissue Engineering. *J. Mech. Behav. Biomed. Mater.* **2016**, *54*, 159–172. https://doi.org/10.1016/j.jmbbm.2015.09.019.
(101) Cameron, N. R.; Sherrington, D. C. Preparation and Glass Transition Temperatures of Elastomeric PolyHIPE Materials. *J. Mater. Chem.* **1997**, *7* (11), 2209–2212. https://doi.org/10.1039/a702030i.

(102) Pulko, I.; Smrekar, V.; Podgornik, A.; Krajnc, P. Emulsion Templated Open Porous Membranes for Protein Purification. *J. Chromatogr. A* **2011**, *1218* (17), 2396–2401. https://doi.org/10.1016/j.chroma.2010.11.069.
(103) Sušec, M.; Ligon, S. C.; Stampfl, J.; Liska, R.; Krajnc, P. Hierarchically Porous Materials from Layer-by-Layer Photopolymerization of High Internal Phase Emulsions. *Macromol. Rapid Commun.* **2013**, *34* (11), 938–943. https://doi.org/10.1002/marc.201300016.
(104) Zhang, H.; Cooper, A. I. Synthesis of Monodisperse Emulsion-Templated Polymer Beads by Oil-in-Water-in-Oil (O/W/O) Sedimentation Polymerization. *Chem. Mater.* **2002**, *14* (10), 4017–4020. https://doi.org/10.1021/cm0206643.
(105) Kramer, S.; Krajnc, P. Hierarchically Porous Microspheres by Thiol-Ene Photopolymerization of High Internal Phase Emulsions-in-Water Colloidal Systems. *Polymers* **2021**, *13* (19), 3366. https://doi.org/10.3390/polym13193366.
(106) Ferrer, J.; Jiang, Q.; Menner, A.; Bismarck, A. An Approach for the Scalable Production of Macroporous Polymer Beads. *J. Colloid Interface Sci.* **2022**, *616*, 834–845. https://doi.org/10.1016/j.jcis.2022.02.053.
(107) Desforges, A.; Arpontet, M.; Deleuze, H.; Mondain-Monval, O. Synthesis and Functionalisation of PolyHIPE® Beads. *React. Funct. Polym.* **2002**, *53* (2–3), 183–192. https://doi.org/10.1016/S1381-5148(02)00172-4.
(108) Li, Z.; Liu, H.; Zeng, L.; Liu, H.; Yang, S.; Wang, Y. Preparation of High Internal Water-Phase Double Emulsions Stabilized by a Single Anionic Surfactant for Fabricating Interconnecting Porous Polymer Microspheres. *Langmuir* **2014**, *30* (41), 12154–12163. https://doi.org/10.1021/la502564r.
(109) Gokmen, M. T.; Van Camp, W.; Colver, P. J.; Bon, S. A. F.; Du Prez, F. E. Fabrication of Porous "Clickable" Polymer Beads and Rods through Generation of High Internal Phase Emulsion (HIPE) Droplets in a Simple Microfluidic Device. *Macromolecules* **2009**, *42* (23), 9289–9294. https://doi.org/10.1021/ma9018679.
(110) Young, G. A.; Lavon, G. D.; Taylor, G. W. High Efficiency Absorbent Articles for Incontinence Management. EP0598823B1, March 12, 1997.
(111) Aldemir Dikici, B.; Claeyssens, F. Basic Principles of Emulsion Templating and Its Use as an Emerging Manufacturing Method of Tissue Engineering Scaffolds. *Front. Bioeng. Biotechnol.* **2020**, *8*.
(112) Yuan, B.; Zhou, S.; Chen, X. Rapid Prototyping Technology and Its Application in Bone Tissue Engineering. *J. Zhejiang Univ.-Sci. B* **2017**, *18* (4), 303–315. https://doi.org/10.1631/jzus.B1600118.
(113) Sears, N.; Dhavalikar, P.; Whitely, M.; Cosgriff-Hernandez, E. Fabrication of Biomimetic Bone Grafts with Multi-Material 3D Printing. *Biofabrication* **2017**, *9* (2), 025020. https://doi.org/10.1088/1758-5090/aa7077.
(114) Owen, R.; Sherborne, C.; Paterson, T.; Green, N. H.; Reilly, G. C.; Claeyssens, F. Emulsion Templated Scaffolds with Tunable Mechanical Properties for Bone Tissue Engineering. *J. Mech. Behav. Biomed. Mater.* **2016**, *54*, 159–172. https://doi.org/10.1016/j.jmbbm.2015.09.019.
(115) Krupenkin, T.; Taylor, J. A. Reverse Electrowetting as a New Approach to High-Power Energy Harvesting. *Nat. Commun.* **2011**, *2* (1). https://doi.org/10.1038/ncomms1454.
(116) Desforges, A.; Backov, R.; Deleuze, H.; Mondain-Monval, O. Generation of Palladium Nanoparticles within Macrocellular Polymeric Supports: Application

to Heterogeneous Catalysis of the Suzuki-Miyaura Coupling Reaction. *Adv. Funct. Mater.* **2005**, *15* (10), 1689–1695. https://doi.org/10.1002/adfm.200500146.

(117) Liu, H.; Wan, D.; Du, J.; Jin, M. Dendritic Amphiphile Mediated One-Pot Preparation of 3D Pt Nanoparticles-Decorated PolyHIPE as a Durable and Well-Recyclable Catalyst. *ACS Appl. Mater. Interfaces* **2015**, *7* (37), 20885–20892. https://doi.org/10.1021/acsami.5b06283.

(118) Yuan, W.; Chen, X.; Xu, Y.; Yan, C.; Liu, Y.; Lian, W.; Zhou, Y.; Li, Z. Preparation and Recyclable Catalysis Performance of Functional Macroporous PolyHIPE Immobilized with Gold Nanoparticles on Its Surface. *RSC Adv.* **2018**, *8* (11), 5912–5919. https://doi.org/10.1039/C8RA00089A.

(119) Moghe, K.; Sutar, A. K.; Kang, I. K.; Gupta, K. C. Poly(Vinylbenzyl Chloride-Co-Divinyl Benzene) PolyHIPE Monolith-Supported o-Hydroxynaphthaldehyde Propylenediamine Schiff Base Ligand Complex of Copper(II) Ions as a Catalyst for the Epoxidation of Cyclohexene. *RSC Adv.* **2019**, *9* (53), 30823–30834. https://doi.org/10.1039/C9RA05811G.

(120) Ruan, G.; Wu, Z.; Huang, Y.; Wei, M.; Su, R.; Du, F. An Easily Regenerable Enzyme Reactor Prepared from Polymerized High Internal Phase Emulsions. *Biochem. Biophys. Res. Commun.* **2016**, *473* (1), 54–60. https://doi.org/10.1016/j.bbrc.2016.03.049.

(121) *Filters and Filtration Handbook*, 5. ed.; Sutherland, K., Ed.; Elsevier, Butterworth-Heinemann: Amsterdam, 2008.

(122) Tebboth, M.; Menner, A.; Kogelbauer, A.; Bismarck, A. Polymerised High Internal Phase Emulsions for Fluid Separation Applications. *Curr. Opin. Chem. Eng.* **2014**, *4*, 114–120. https://doi.org/10.1016/j.coche.2014.03.001.

(123) Chavan, A. A.; Li, H.; Scarpellini, A.; Marras, S.; Manna, L.; Athanassiou, A.; Fragouli, D. Elastomeric Nanocomposite Foams for the Removal of Heavy Metal Ions from Water. *ACS Appl. Mater. Interfaces* **2015**, *7* (27), 14778–14784. https://doi.org/10.1021/acsami.5b03003.

(124) Malakian, A.; Zhou, M.; Zowada, R. T.; Foudazi, R. Synthesis and *in Situ* Functionalization of Microfiltration Membranes via High Internal Phase Emulsion Templating. *Polym. Int.* **2019**, *68* (7), 1378–1386. https://doi.org/10.1002/pi.5828.

(125) Vásquez, L.; Davis, A.; Gatto, F.; Ngoc An, M.; Drago, F.; Pompa, P. P.; Athanassiou, A.; Fragouli, D. Multifunctional PDMS PolyHIPE Filters for Oil-Water Separation and Antibacterial Activity. *Sep. Purif. Technol.* **2021**, *255*, 117748. https://doi.org/10.1016/j.seppur.2020.117748.

(126) Zhang, T.; Wu, Y.; Xu, Z.; Guo, Q. Hybrid High Internal Phase Emulsion (HIPE) Organogels with Oil Separation Properties. *Chem Commun* **2014**, *50* (89), 13821–13824. https://doi.org/10.1039/C4CC06674J.

(127) Zhang, N.; Zhong, S.; Zhou, X.; Jiang, W.; Wang, T.; Fu, J. Superhydrophobic P (St-DVB) Foam Prepared by the High Internal Phase Emulsion Technique for Oil Spill Recovery. *Chem. Eng. J.* **2016**, *298*, 117–124. https://doi.org/10.1016/j.cej.2016.03.151.

(128) Barakat, M. A. New Trends in Removing Heavy Metals from Industrial Wastewater. *Arab. J. Chem.* **2011**, *4* (4), 361–377. https://doi.org/10.1016/j.arabjc.2010.07.019.

(129) Fu, F.; Wang, Q. Removal of Heavy Metal Ions from Wastewaters: A Review. *J. Environ. Manage.* **2011**, *92* (3), 407–418. https://doi.org/10.1016/j.jenvman.2010.11.011.
(130) Han, J.; Du, Z.; Zou, W.; Li, H.; Zhang, C. Fabrication of Interfacial Functionalized Porous Polymer Monolith and Its Adsorption Properties of Copper Ions. *J. Hazard. Mater.* **2014**, *276*, 225–231. https://doi.org/10.1016/j.jhazmat.2014.05.035.
(131) Huš, S.; Kolar, M.; Krajnc, P. Separation of Heavy Metals from Water by Functionalized Glycidyl Methacrylate Poly (High Internal Phase Emulsions). *J. Chromatogr. A* **2016**, *1437*, 168–175. https://doi.org/10.1016/j.chroma.2016.02.012.
(132) Huang, S.-H.; Chen, D.-H. Rapid Removal of Heavy Metal Cations and Anions from Aqueous Solutions by an Amino-Functionalized Magnetic Nano-Adsorbent. *J. Hazard. Mater.* **2009**, *163* (1), 174–179. https://doi.org/10.1016/j.jhazmat.2008.06.075.
(133) Mert, E. H.; Kaya, M. A.; Yıldırım, H. Preparation and Characterization of Polyester–Glycidyl Methacrylate PolyHIPE Monoliths to Use in Heavy Metal Removal. *Des. Monomers Polym.* **2012**, *15* (2), 113–126. https://doi.org/10.1163/156855511X615001.
(134) Zhu, Y.; Zheng, Y.; Wang, F.; Wang, A. Monolithic Supermacroporous Hydrogel Prepared from High Internal Phase Emulsions (HIPEs) for Fast Removal of Cu2+ and Pb2+. *Chem. Eng. J.* **2016**, *284*, 422–430. https://doi.org/10.1016/j.cej.2015.08.157.
(135) Masini, J. C.; Svec, F. Porous Monoliths for On-Line Sample Preparation: A Review. *Anal. Chim. Acta* **2017**, *964*, 24–44. https://doi.org/10.1016/j.aca.2017.02.002.
(136) Krajnc, P.; Leber, N.; Štefanec, D.; Kontrec, S.; Podgornik, A. Preparation and Characterisation of Poly(High Internal Phase Emulsion) Methacrylate Monoliths and Their Application as Separation Media. *J. Chromatogr. A* **2005**, *1065* (1), 69–73. https://doi.org/10.1016/j.chroma.2004.10.051.
(137) Jerenec, S.; Šimić, M.; Savnik, A.; Podgornik, A.; Kolar, M.; Turnšek, M.; Krajnc, P. Glycidyl Methacrylate and Ethylhexyl Acrylate Based PolyHIPE Monoliths: Morphological, Mechanical and Chromatographic Properties. *React. Funct. Polym.* **2014**, *78*, 32–37. https://doi.org/10.1016/j.reactfunctpolym.2014.02.011.
(138) Yao, C.; Qi, L.; Yang, G.; Wang, F. Preparation of Sub-Micron Skeletal Monoliths with High Capacity for Liquid Chromatography. *J. Sep. Sci.* **2010**, *33* (4–5), 475–483. https://doi.org/10.1002/jssc.200900655.
(139) Tunç, Y.; Gölgelioğlu, Ç.; Hasirci, N.; Ulubayram, K.; Tuncel, A. Acrylic-Based High Internal Phase Emulsion Polymeric Monolith for Capillary Electrochromatography. *J. Chromatogr. A* **2010**, *1217* (10), 1654–1659. https://doi.org/10.1016/j.chroma.2010.01.020.
(140) Tunc, Y.; Gölgelioğlu, Ç.; Tuncel, A.; Ulubayram, K. Polystyrene-Based High Internal Phase Emulsion Polymer Monolithic Stationary Phase for Capillary Electrochromatography. *Sep. Sci. Technol.* **2012**, *47* (16), 2444–2449. https://doi.org/10.1080/01496395.2012.672846.
(141) Khodabandeh, A.; Arrua, R. D.; Mansour, F. R.; Thickett, S. C.; Hilder, E. F. PEO-Based Brush-Type Amphiphilic Macro-RAFT Agents and Their

Assembled PolyHIPE Monolithic Structures for Applications in Separation Science. *Sci. Rep.* **2017**, *7* (1). https://doi.org/10.1038/s41598-017-08423-x.
(142) Bernard-Savary, P.; Poole, C. F. Instrument Platforms for Thin-Layer Chromatography. *J. Chromatogr. A* **2015**, *1421*, 184–202. https://doi.org/10.1016/j.chroma.2015.08.002.
(143) Yin, D.; Guan, Y.; Gu, H.; Jia, Y.; zhang, Q. Polymerized High Internal Phase Emulsion Monolithic Material: A Novel Stationary Phase of Thin Layer Chromatography. *RSC Adv.* **2017**, *7* (12), 7303–7309. https://doi.org/10.1039/C6RA27609A.
(144) Menner, A.; Powell, R.; Bismarck, A. Open Porous Polymer Foams via Inverse Emulsion Polymerization: Should the Definition of High Internal Phase (Ratio) Emulsions Be Extended? *Macromolecules* **2006**, *39* (6), 2034–2035. https://doi.org/10.1021/ma052705x.
(145) Fogler, H. S. *Elements of Chemical Reaction Engineering*; Prentice Hall: Boston, 2016.
(146) Levenspiel, O. *Chemical Reaction Engineering*, 3rd ed.; Wiley: New York, 1999.
(147) Kaske, F.; Dick, S.; Pajoohi, S. A.; Agar, D. W. The Influence of Operating Conditions on the Mass Transfer Performance of a Micro Capillary Contactor with Liquid–Liquid Slug Flow. *Chem. Eng. Process. Process Intensif.* **2016**, *108*, 10–16. https://doi.org/10.1016/j.cep.2016.06.010.
(148) Xu, J. H.; Tan, J.; Li, S. W.; Luo, G. S. Enhancement of Mass Transfer Performance of Liquid–Liquid System by Droplet Flow in Microchannels. *Chem. Eng. J.* **2008**, *141* (1–3), 242–249. https://doi.org/10.1016/j.cej.2007.12.030.
(149) Comiti, J.; Sabiri, N. E.; Montillet, A. Experimental Characterization of Flow Regimes in Various Porous Media — III: Limit of Darcy's or Creeping Flow Regime for Newtonian and Purely Viscous Non-Newtonian Fluids. *Chem. Eng. Sci.* **2000**, *55* (15), 3057–3061. https://doi.org/10.1016/S0009-2509(99)00556-4.
(150) Gobert, S. R. L.; Kuhn, S.; Braeken, L.; Thomassen, L. C. J. Characterization of Milli- and Microflow Reactors: Mixing Efficiency and Residence Time Distribution. *Org. Process Res. Dev.* **2017**, *21* (4), 531–542. https://doi.org/10.1021/acs.oprd.6b00359.
(151) Boskovic, D.; Loebbecke, S. Modelling of the Residence Time Distribution in Micromixers. *Chem. Eng. J.* **2008**, *135*, S138–S146. https://doi.org/10.1016/j.cej.2007.07.058.
(152) Kim, N.; Murphy, M. C.; Soper, S. A.; Nikitopoulos, D. E. Liquid–Liquid Segmented Flows in Polycarbonate Microchannels with Cross-Sectional Expansions. *Int. J. Multiph. Flow* **2014**, *58*, 83–96. https://doi.org/10.1016/j.ijmultiphaseflow.2013.09.002.
(153) Costantini, M.; Jaroszewicz, J.; Kozoń, Ł.; Szlązak, K.; Święszkowski, W.; Garstecki, P.; Stubenrauch, C.; Barbetta, A.; Guzowski, J. 3D-Printing of Functionally Graded Porous Materials Using On-Demand Reconfigurable Microfluidics. *Angew. Chem. Int. Ed.* **2019**, *58* (23), 7620–7625. https://doi.org/10.1002/anie.201900530.
(154) Naebe, M.; Shirvanimoghaddam, K. Functionally Graded Materials: A Review of Fabrication and Properties. *Appl. Mater. Today* **2016**, *5*, 223–245. https://doi.org/10.1016/j.apmt.2016.10.001.

(155) Kiss, N.; Brenn, G.; Pucher, H.; Wieser, J.; Scheler, S.; Jennewein, H.; Suzzi, D.; Khinast, J. Formation of O/W Emulsions by Static Mixers for Pharmaceutical Applications. *Chem. Eng. Sci.* **2011**, *66* (21), 5084–5094. https://doi.org/10.1016/j.ces.2011.06.065.
(156) Chabanon, E.; Sheibat-Othman, N.; Mdere, O.; Valour, J. P.; Urbaniak, S.; Puel, F. Drop Size Distribution Monitoring of Oil-in-Water Emulsions in SMX+ Static Mixers: Effect of Operating and Geometrical Conditions. *Int. J. Multiph. Flow* **2017**, *92*, 61–69. https://doi.org/10.1016/j.ijmultiphaseflow.2017.03.001.
(157) Li, B.; Guan, Z.; Wang, W.; Yang, X.; Hu, J.; Tan, B.; Li, T. Highly Dispersed Pd Catalyst Locked in Knitting Aryl Network Polymers for Suzuki-Miyaura Coupling Reactions of Aryl Chlorides in Aqueous Media. *Adv. Mater.* **2012**, *24* (25), 3390–3395. https://doi.org/10.1002/adma.201200804.
(158) Jafari, O.; Rahimi, M.; Kakavandi, F. H. Liquid–Liquid Extraction in Twisted Micromixers. *Chem. Eng. Process. Process Intensif.* **2016**, *101*, 33–40. https://doi.org/10.1016/j.cep.2015.12.013.
(159) Xie, T.; Ma, Y.; Xu, C. Passive Continuous-Flow Microextraction/Stripping System with High Throughput. *Chem. Eng. Sci.* **2020**, *223*, 115745. https://doi.org/10.1016/j.ces.2020.115745.
(160) Mitcheson, P. D.; Yeatman, E. M.; Rao, G. K.; Holmes, A. S.; Green, T. C. Energy Harvesting From Human and Machine Motion for Wireless Electronic Devices. *Proc. IEEE* **2008**, *96* (9), 1457–1486. https://doi.org/10.1109/JPROC.2008.927494.

7 Publications

I&EC research
Industrial & Engineering Chemistry Research

Publication I

pubs.acs.org/IECR

Article

Emulsion-Templated Macroporous Polymer Micromixers

Hande Barkan-Öztürk, Angelika Menner, and Alexander Bismarck*

Cite This: *Ind. Eng. Chem. Res.* 2021, 60, 14013−14025

Read Online

ACCESS | Metrics & More | Article Recommendations | Supporting Information

ABSTRACT: Micromixers were fabricated from emulsion-templated macroporous polymers, known as polymerizing high internal-phase emulsions (polyHIPEs). Micromixers are mixing elements containing submillimeter channels, in which mixing occurs by molecular diffusion in the laminar flow regime. PolyHIPEs possess an interconnected pore structure with connected channels, which are ideal to mix liquids. We investigated the residence time distribution of polyHIPE micromixers in comparison to a helix static mixer using a tracer method, which allows for quantifying the deviation from ideal plug flow. The axial dispersed flow was modeled, and the obtained axial dispersion number is in good agreement with that of commercial split-and-recombination micromixers. Two competitive parallel reactions (4th Bourne reaction) were performed to characterize the efficiency of micromixing of polyHIPE mixers. We show that polyHIPE micromixers are more efficient than a commercial helix static mixer.

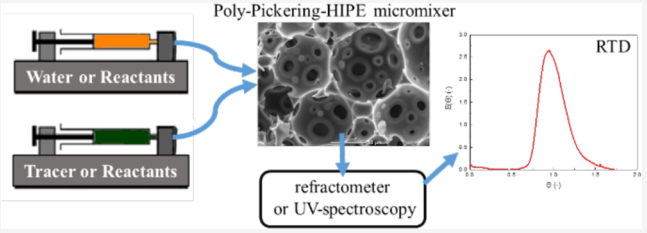

INTRODUCTION

Mixing of fluids is important for both laboratory and industry processes for a plethora of reasons, including chemical and biological reactions.[1] Mixing is classified by the mixing scale either as macromixing or micromixing (Figure 1). Macromixing takes place by driving the largest scales of motion in a fluid in turbulent flow. The smallest scale of motion is called micromixing, where molecular diffusion becomes important to mix the fluids in the submillimeter range.[1] Macro- and microscale mixing are distinguished by the dimensionless Reynolds number (Re), which is the ratio of inertial forces and viscous forces in the fluid.[1] At low Re, laminar flow dominates in submillimeter mixing channels resulting in micromixing. The Re range between 10^2 and 10^4 is considered to be the transition region between laminar and turbulent flow inside channels.[2] Mixers capable of micromixing are known as micromixers.[1,2]

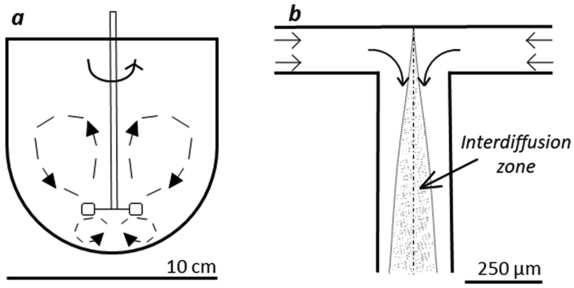

Figure 1. Fluid mixing processes: (a) macromixing by turbulent motion in a vessel equipped with an impeller stirrer and (b) micromixing by molecular diffusion in a T-shape micromixer. Adapted with permission from ref 1. Copyright 2012, Elsevier.

Micromixers operate, control, and process small fluid volumes in continuous flow, resulting in less waste.[1,3,4] They possess high surface-to-volume ratios due to their small channel dimensions, which produce many benefits over macroscale mixing.[1,4] Micromixers provide better process control during mixing as a result of controlling flow properties by viscous ($\mu \cdot u/D$) rather than inertial effects allowing for rapid diffusive mixing, which results in higher yields at a lower energy input compared to macroscale mixing techniques.[1,2] Owing to these advantages, micromixers have found many applications, for instance in chemical and biochemical screening,[2,5] for the continuous production of emulsions,[6] synthesis of pharmaceuticals,[7] and continuous nanoparticle production.[8] Micromixers belong to the top 10 chemical innovations to render our world more sustainable, according to the list published in 2019 by IUPAC.[9]

Y and T type micromixers are the most common types of micromixers consisting of two inlet channels, which merge to form a microchannel (Figure 1B).[1] The fluids entering from the inlet channels are mixed in the microchannel by molecular diffusion, which takes place in the interfacial zone between the two coflowing fluids. However, the fluids away from the interfacial zone need some time to interact, due to the lack of

Received: May 21, 2021
Revised: August 23, 2021
Accepted: August 26, 2021
Published: September 28, 2021

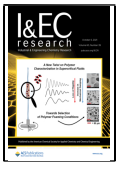

https://doi.org/10.1021/acs.iecr.1c01949
Ind. Eng. Chem. Res. 2021, 60, 14013−14025

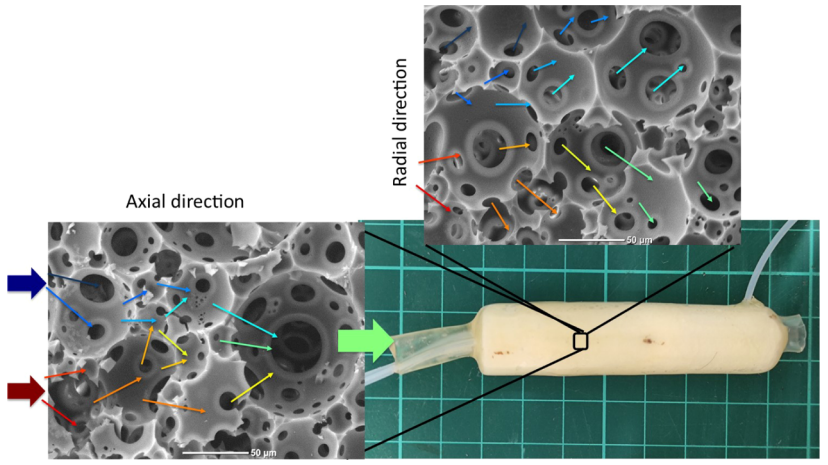

Figure 2. Fluid flow and thus mixing through axial and radial directions along the interconnected poly-Pickering-HIPE micromixer.

turbulence, and thus, long channels are required to achieve complete mixing.[10] Many researchers showed that the micromixing performance in an empty tube can be enhanced by adding obstacles to the wall or by inserting a helical structure into the tube.[10,11] These obstacles redirect the flow and produce irregularities, generating chaotic advection resulting in more efficient mixing.[10,11] Moreover, the micromixing performance can be improved by designing channel splits, which recombine the flow at different points along the microchannel.[1] Although the addition of obstacles or split-and-recombination (SAR) channels enhances mixing, the production of these microchannels is expensive and requires special instrumentation and expertise.[12] In contrast, Tebboth et al.[13,14] explored interconnected macroporous polymers as micromixers, and Brown et al.[15] used polymerizing high internal-phase emulsions (polyHIPEs) as catalyst supports and microreactors for flow through processing. Mixing occurs in pores of the polyHIPEs, while the flow is split and recombined by pore throats interconnecting various pores in radial and axial directions along the porous monolith (Figure 2). This allows micromixers with desired diameters and lengths to be produced simply from emulsion-templated macroporous polymers with minimal design effort and low cost.

Emulsion-templated macroporous polymers, called polyHIPEs, are particularly interesting for specialty applications, such as scaffolds for tissue engineering,[16,17] stationary chromatography phases,[18,19] and filters.[20,21] PolyHIPEs are synthesized by polymerization of the continuous phase of high or medium internal phase emulsions containing monomer(s). The removal of the aqueous internal phase results in pores.[22] Emulsions are called HIPEs if the emulsion phase volume ratio exceeds 74%.[23,24] The morphology of polyHIPEs can be tailored by changing the internal phase ratio to alter their porosity, energy input which affects pore sizes,[25,26] or by selection of the emulsifier type and concentration,[27] which enables to control pore interconnectivity. The formation of pore throats, forming the interconnects between pores, is governed by the competition between polymerization-induced surfactant depletion attraction and the strength of interfacial films. The weak interfacial areas result in pore throats in polyHIPEs of the same size as the flattened interfacial areas between droplets in HIPEs.[28] Owing to those pore throats, an interconnected permeable structure forms. Moreover, molecular surfactants act as plasticizers that negatively affect the mechanical properties of polyHIPEs.[29] Hydrophobic nanoparticles are alternative emulsifiers that can be used to stabilize water-in-oil emulsions.[30,31] Macroporous polymers produced by polymerization of nanoparticle-stabilized emulsions, called poly-Pickering-HIPEs, have better mechanical properties than traditional polyHIPEs, produced from surfactant-stabilized emulsions.[29] However, they are typically closed celled and thus impermeable.[29,30] We already demonstrated[29,31] that pore throat formation during the synthesis of poly-Pickering-HIPEs can be initiated by addition of a small amount of surfactants at the end of the emulsification process, which promotes the formation of permeable structures. The mechanical properties and chemical stability of polyHIPEs are determined by monomer choice.[32] Due to the liquid nature of the template, HIPEs can be shaped, allowing to produce net-shaped polyHIPEs, such as monoliths,[13] micrometer- to millimeter-sized beads,[21] or membranes.[33] HIPEs can also be directly polymerized inside a capillary[15,34] or printed and polymerized using additive manufacturing.[35]

Herein, we report the design, fabrication, and evaluation of micromixers from permeable poly-Pickering-HIPEs. We characterized the deviation from ideal plug flow in micromixers by the residence time distribution (RTD), which also allows to determine the existence of dead-zones in a micromixer and the homogeneity of the mixing by monitoring an inert tracer flow through the micromixer.[36] Moreover, the effectiveness of our micromixers was tested by two competitive parallel reactions (4th Bourne reaction), which share a common reactant (HCl) but have different reaction kinetics.[37] The first reaction is an instantaneous neutralization reaction

$$\mathrm{HCl} + \mathrm{NaOH} \rightarrow \mathrm{NaCl} + \mathrm{H_2O}$$
$$(k_1 = 1.3 \times 10^{11}\ \mathrm{m^3\ kg^{-1}\ mol^{-1}\ s^{-1}}\ \text{at}\ 25\ ^\circ\mathrm{C})$$

and second reaction is an acid (HCl)-catalyzed saponification of dimethoxypropane (DMP), which is much slower than the neutralization reaction.

$$\mathrm{CH_3(OCH_3)_2CH_3} + \mathrm{H_2O} \xrightarrow{\mathrm{H^+}} \mathrm{CH_3COCH_3} + \mathrm{CH_3OH}$$
$$(k_2 = 700\ \mathrm{m^3\ kg^{-1}\ mol^{-1}\ s^{-1}}\ \text{at}\ 25\ ^\circ\mathrm{C})$$

If micromixing is effective, only the neutralization reaction takes place so that the common reactant is solely consumed in this reaction. If the fluids are not effectively mixed, some HCl

https://doi.org/10.1021/acs.iecr.1c01949
Ind. Eng. Chem. Res. 2021, 60, 14013−14025

will be consumed also in the slower saponification reaction, yielding acetone and methanol.[37] The micromixing performance is monitored by quantifying the concentration of the reaction products to determine which reaction occurred. The micromixing behavior of poly-Pickering-HIPE micromixers will be evaluated and compared with a commercial static mixer (3/8″ 12 helix Kenics static mixer, Cole-Parmer, Germany).

EXPERIMENTAL PART

Materials. Styrene ≥99%, divinylbenzene (DVB) 80%, sodium monosorbitol (Span 80), α,α′-azoisobutyronitrile (AIBN), calcium chloride dihydrate ($CaCl_2 \cdot 2H_2O$) ≥99%, 2,2-DMP, ethanol ≥99.8%, sodium hydroxide (NaOH), hydrochloric acid (HCl, 37%), potassium chloride (KCl), and copper sulfate ($CuSO_4$) were purchased from Sigma-Aldrich. Hydrophobic pyrogenic silica particles (HDK H20) were kindly provided by Wacker Chemie AG (Germany). Araldite rapid adhesive and Araldite 2020 were purchased from RS Components Ltd. (Corby, UK). All materials were used as received.

Preparation of Poly-Pickering-HIPEs. Poly-Pickering-HIPEs were prepared by polymerization of the continuous monomer phase of Pickering-HIPEs. The continuous phase was produced by homogenizing a 1:1 mixture of styrene/DVB containing 3% (w/v) of HDK H20 in a free-standing centrifuge tube (VWR, Vienna, Austria) using a high-speed homogenizer (Kinematica POLYTRON PT 1600 E, Malters, Switzerland) for 15 min at 15,000 rpm. Afterward, the suspension was transferred into a glass mixing vessel, and 1 mol % AIBN (with respect to the monomer double bonds) was added. AIBN was dissolved in the monomer phase by stirring at 400 rpm. Subsequently, an aqueous solution of 40 g/L $CaCl_2 \cdot 2H_2O$ (in total 40 mL) was added dropwise into the continuous phase while stirring at the same rate with an anchor paddle attached to an overhead stirrer (Phoenix Instruments RSO-20D, Garbsen, Germany). The internal phase volume ratio was 80%. After addition of the internal phase, the Pickering-HIPEs were agitated further for 3 min at 400 rpm, yielding a stable emulsion. Thereafter, 5, 10, 15, or 20 vol % of Span 80 (with respect to the continuous phase) were added into the emulsion template, and the emulsion was mixed for 30 s at 400 rpm to dissolve the surfactant. One of the Pickering-HIPE was poured into the mold without adding surfactant. The emulsions were then poured into molds with diameters of either 6 mm [poly(tetrafluoroethylene) (PTFE) tube, VWR, Vienna, Austria] or 12 mm (centrifuge tubes, VWR) and polymerized at 70 °C for 4 h in a convection oven. After polymerization, the monoliths were purified by Soxhlet extraction, first with distilled water to remove $CaCl_2$, then with acetone to remove residual surfactants and unreacted monomers. The monoliths were kept in the fume hood overnight for the acetone to evaporate slowly before they were dried in a convention oven at 70 °C for 24 h. The poly-Pickering-HIPEs were named P0, P5, P10, P15, and P20 with respect to the surfactant volume which was added to their emulsion template.

Fabrication of Poly-Pickering-HIPE Micromixers. Micromixers were produced from poly-Pickering-HIPE monoliths with diameters of 6 and 12 mm prepared by polymerization of Pickering-HIPEs, to which either 5 or 10% surfactant was added (P5 and P10, respectively). For P15 and P20, only 12 mm diameter monoliths were used for micromixer fabrication. The conical tip at the base of the monolith was removed, and two inlet holes with diameters of 2 mm were drilled 5 mm deep into the top of the monolith. An outlet hole with the same diameter and depth of 5 mm was drilled into the wall of the 12 mm diameter monolith 5 mm above its base. For 6 mm diameter monoliths, the outlet hole was only 3 mm deep (stage 1 in Figure 3). PTFE tubes (outer diameter 1/16″, VWR, Vienna, Austria) were sealed into the holes using Araldite Rapid adhesive, which cured in 30 min at room temperature (stage 2, as shown in Figure 3). The adhesive was also used to coat the surface of the monolith to avoid fluid bypassing the poly-Pickering-HIPEs (stage 3, as shown in Figure 3). Afterward, the monolith was sealed with a high-temperature shrink tube (Conrad, Vienna, Austria) using a heat gun to provide extra protection (stage 4, as shown in Figure 3). The top of the micromixer was sealed using epoxy resin (Araldite 2020), which also provided stability to the inlet tubes (stage 4, as shown in Figure 3). The device was placed into a convection oven at 70 °C for 4 h to cure the epoxy resin.

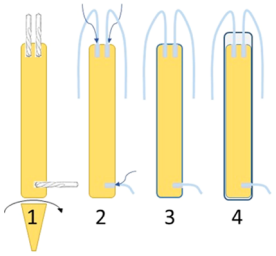

Figure 3. Schematic showing the fabrication of poly-Pickering-HIPE micromixers: (1) removal of the conical base of the monolith and drilling inlet/outlet holes, (2) inserting and sealing tubes, (3) sealing the outer surface of the porous monolith with adhesive, and (4) finally sealing the micromixer in a shrink tube and the top with adhesive.

Characterization of Poly-Pickering-HIPEs. *Morphology of Poly-Pickering-HIPEs.* The morphology of poly-Pickering-HIPEs was investigated using scanning electron microscopy (SEM, JCM-6000, JEOL GmbH, Eching, Germany) operated in a high vacuum mode with an acceleration voltage of 15 kV. Fractured sample surfaces were gold-coated (JFC-1200 JEOL GmbH, Eching, Germany) prior to imaging. SEM images were analyzed using the software package ImageJ (https://imagej.nih.gov/ij/download.html) to measure pore and pore throat diameters, and at least 150 individual pore throats and pore diameters per sample were analyzed. The average degree of interconnectivity (DoI) or openness was calculated, as described by Pulko and Krajnc[38]

$$\mathrm{DoI} = \frac{N \cdot d_{pt}^{\,2}}{d_p^{\,2} \cdot 4} \tag{1}$$

where N is the number average of pore throats per pore, d_{pt} is the average pore throat diameter, and d_p is the average pore diameter.

Density of Poly-Pickering-HIPEs. The skeletal density ρ_s of poly-Pickering-HIPEs was determined using helium displacement pycnometry (Accupyc II 1340, Micrometrics, Aachen, Germany). About 0.1 g of poly-Pickering-HIPE was ground to powder, weighed, and analyzed. The foam density ρ_f of the poly-Pickering-HIPEs was determined using an envelope density analyzer (GeoPyc 1360, Micrometrics Ltd., Aachen, Germany). The porosity of the poly-Pickering-HIPEs was calculated as follows

https://doi.org/10.1021/acs.iecr.1c01949
Ind. Eng. Chem. Res. 2021, 60, 14013−14025

$$P\ (\%) = \left(1 - \frac{\rho_f}{\rho_s}\right)\cdot 100 \tag{2}$$

Gas Permeability of Poly-Pickering-HIPEs. The gas permeability of the monoliths was determined by pressure rise measurements using a home built device.[39] In brief, poly-Pickering-HIPEs with a diameter of 12 mm were prepared as described and cut to a length of 25 mm, coated with Araldite rapid. These coated samples were placed into a cylindrical PTFE mold with a diameter of 25 mm, and Araldite 2020 was poured to the space between the sample and mold to seal the sample to avoid crossflow, and the epoxy resin was cured at 70 °C for 4 h. For each formulation, two samples were prepared, and their gas permeability was measured from both sides of the sample by increasing the inlet pressure from 0.3 to 2.5 bar. 10 individual measurements were taken for each inlet pressure. After reaching constant pressure with the help of a vacuum pump (−0.6 bar), nitrogen was passed through the sample, and the pressure rise was recorded. The permeability coefficient K was calculated, as described by Manley et al.[39] Further details are provided in Supporting Information (eq S1 and Figure S1).

Tortuosity and Flow Behavior of Poly-Pickering-HIPEs. Tortuosity of poly-Pickering-HIPE monoliths was determined based on the AC electrical conductivity of an electrolyte solution in a non-conductive sample.[40,41] The AC impedance of electrolyte solution (0.01 M $CuSO_4$)-filled poly-Pickering-HIPEs was measured using a frequency response analyzer (Reference 600 Gamry Instruments, C3 Prozess und Analysentechnik GmbH, Munich, Germany) in a custom-made measurement cell. 1.3 mm thick poly-Pickering-HIPEs disks were soaked in electrolyte solution and positioned between two copper electrodes in the measurement cell. The measurement was performed by varying the AC signal frequency from 1 Hz to 100 kHz applying 1 mV at 25 °C. The resistance R of the electrolyte-filled poly-Pickering-HIPEs was determined by Randles fitting to the Nyquist plots (see Supporting Information, Figure S2). The conductivity κ_p of the disks was calculated as follows[41]

$$\kappa_p = \frac{l}{R\cdot A} \tag{3}$$

where l is the length and A is the area of the poly-Pickering-HIPEs. The tortuosity T of poly-Pickering-HIPEs was calculated as follows

$$T = \frac{P\cdot\kappa}{\kappa_p} \tag{4}$$

where P is the porosity of the poly-Pickering-HIPE and κ is the conductivity of electrolyte solution.

Carman introduced the average flow velocity u_p through a porous medium[42]

$$u_p = \frac{u_s\cdot T}{P} \tag{5}$$

where u_s is the superficial velocity of fluids injected into the porous medium using a syringe pump (PHD Ultra, Harvard Apparatus, UK), which made it possible to determine the Re number for porous media (Re_p) as follows[42,43]

$$Re_p = \frac{u_p\rho d_p}{\mu} \tag{6}$$

where ρ is the fluid density, d_p is the average pore diameter of poly-Pickering-HIPEs, and μ is the kinetic viscosity of the fluid.

Micromixing Properties of Poly-Pickering-HIPEs. *Determination of the Residence Time Distribution.* The RTD of poly-Pickering-HIPE micromixers and a commercial static mixer was determined using an inert tracer injected into water flowing though the micromixer. The tracer concentration in the exit stream was monitored by refractive index measurements as a function of time using a differential refractometer (DnDc, WGE Dr Bures, Dallgow-Doeberitz, Germany). The measured refractive index is proportional to the concentration of the non-reactive KCl tracer. Therefore, the refractive index increment (dn/dc) was determined using KCl solutions with concentrations of 2, 4, 6, 8, and 10 mg/mL in order to determine the concentration of a solution with unknown concentration from the measured refractive index. A syringe pump (PHD Ultra, Harvard Apparatus, UK) was used to feed demineralized water through one of the inlet tubes continuously at rates of 0.6, 0.9, or 1.2 mL/min. 0.2 mL of tracer (25 mg/mL KCl) was injected by hand through the other inlet as the pulse input into the steady-state flow of water. The outlet tube was connected to the sample inlet of the refractometer, and the second inlet of the refractometer was filled with demineralized water. The refractive index of mixing fluids flowing through the micromixers was monitored over time until the signal stabilized. The measured refractive index was converted to concentration $c(t)$ using the calibration curve (see Supporting Information, Figure S3). The RTD function $E(t)$ was determined using[36]

$$E(t) = \frac{c(t)}{\int_0^\infty c(t)\mathrm{d}t} \tag{7}$$

The mean residence time t_m and average residence time τ were calculated as follows[36]

$$t_m = \int_0^\infty tE(t)\mathrm{d}t \tag{8}$$

$$\tau = \frac{PV}{Q} \tag{9}$$

where t is the time of each measured $c(t)$, P is the porosity, V is the pore volume of the monolith, and Q is the volumetric flow rate. The variance σ[10,36] and coefficient of variance or spread CoV[10] were calculated using eqs 10 and 11, respectively, to quantify the degree of mixing

$$\sigma^2 = \int_0^\infty (t-t_m)E(t)\mathrm{d}t \tag{10}$$

$$\mathrm{CoV} = \frac{\sigma}{t_m} \tag{11}$$

These two values describe the deviation from ideal plug flow. A spread (CoV) of a symmetric RTD is equal to zero and indicates ideal plug flow. In the presence of axial flow, CoV is larger than 0.[10]

The skewness s describes the extent to which a distribution skewed in one direction from the mean and is defined as[36]

$$s^3 = \frac{1}{\sigma^{3/2}}\int_0^\infty (t-t_m)^3E(t)\mathrm{d}t \tag{12}$$

The axial dispersion number (D_{ax}/uL) characterizes the spreading rate of flow in the micromixer as a result of a laminar

https://doi.org/10.1021/acs.iecr.1c01949
Ind. Eng. Chem. Res. 2021, 60, 14013−14025

velocity profile, molecular diffusion, and so forth.[44] In the axial dispersion number, D_{ax} is the dispersion coefficient, L is the length of the investigated device, and u is the velocity of the main flow. Levenspiel[44] introduced an axial dispersion model for a dispersion number larger than 0.01 using open−open boundary conditions, representing a conventional and commonly used experimental device. D_{ax}/uL was determined by fitting of eq 13 to the RTD curve

$$E(t) = \frac{1}{t_m\sqrt{4\pi\left(\frac{D_{ax}}{uL}\right)\left(\frac{t}{t_m}\right)}} \cdot \exp\left[-\frac{\left(1-\frac{t}{t_m}\right)^2}{4\left(\frac{D_{ax}}{uL}\right)\left(\frac{t}{t_m}\right)}\right] \quad (13)$$

Micromixing Efficiency of Poly-Pickering-HIPEs. The micromixing efficiencies of both poly-Pickering-HIPE micromixers and the commercial static mixer were investigated using two competitive parallel reactions by monitoring the acetone yield resulting from the decomposition of DMP. A syringe pump equipped with double syringes (Masterflex Touch-Screen Syringe Pumps, Cole-Parmer, Wertheim, Germany) was used to continuously inject a 1:1 mixture of DMP (0.2 M)/NaOH (0.38 M) and HCl (0.36 M) at flow rates of 0.3 or 0.6 mL/min into the (micro)mixers. The outlet tube of the flow cells was connected to a quartz flow cell (Hellma Analytics, Müllheim, Germany) with an internal volume of 0.05 mL. The absorbance of acetone at 265 nm was monitored every 0.5 s for 500 s using UV−vis spectrophotometry (Agilent 8453, Agilent Technologies Österreich GmbH, Vienna, Austria) at room temperature. The concentration of acetone in the effluent was calculated using the Lambert−Beer law

$$[C_{acetone}] = \frac{A}{\varepsilon l} \quad (14)$$

where A is the absorbance, l is the optical path length, and ε is the molar extinction coefficient of acetone at 265 nm (13.718 L mol^{-1} cm^{-1}) determined using a known concentration of acetone in H_2O (see Supporting Information, Figure S4).

RESULTS AND DISCUSSION

Macroporous poly(St-*co*-DVB) monoliths were produced by polymerization of the continuous phase of Pickering-HIPEs and subsequent removal of the templating phase resulting in an interconnected porous structure (Figure 4). These poly-Pickering-HIPEs were stable to thermal degradation in a nitrogen atmosphere up to 350 °C (Figure S5). The thermal conductivity of poly(St-*co*-DVB)HIPEs with a similar porosity was reported to be 0.2 W/m K.[45] Together, this indicates that this material could be potentially used even for exothermic reactions. All poly-Pickering-HIPEs (P5-20) had within error the same average pore and pore throat diameters (Table 1) despite the fact that the amount of the surfactant which was added to the Pickering-HIPEs to induce pore throat formation was increased from 5 to 20 vol %. However, it has to be noted that DoI or openness of the poly-Pickering-HIPEs increased significantly from DoI = 0.028 (P5) to 0.06 (P20) with increasing surfactant amount added to the emulsion template (Table 1) which indicates that the number of pore throats per pore increased rather than the pore throat diameters. Zhu et al.[46] followed the generation of pore throats in poly-Pickering-HIPEs during the polymerization of Pickering-HIPEs to which the surfactant was added by laser scanning confocal microscopy. The addition of the surfactant into a Pickering

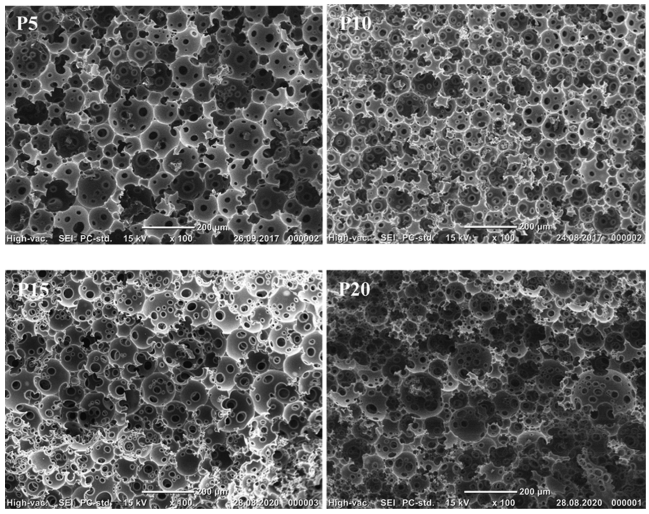

Figure 4. Characteristic SEM images of poly-Pickering-HIPEs (P5, P10, P15, and P20) prepared by polymerization of the continuous phase of Pickering-HIPE templates to which increasing amounts of the surfactant was added.

emulsion causes the particles which stabilized the primary emulsion to be displaced from the film region between neighboring droplets, thus weakening the film.[46] These weaker films between neighboring droplets in the emulsion templates ruptured during polymerization of the monomer phase, resulting in pore throats, thus increasing the surfactant amount added to the primary emulsion template resulted in the formation of more pore throats per pore during the polymerization, which consequently resulted in a higher DoI. The reference poly-Pickering-HIPE, which was produced without adding the surfactant, has a closed pore structure (Figure S6). The fluids passing through poly-Pickering-HIPEs pass pores and pore throats having a range of diameters and directions (Figure 4). The tortuosity of the poly-Pickering-HIPEs is larger than 1 (Table 1), but it decreased with increasing DoI. The increased openness (DoI) and decreasing tortuosity of the poly-Pickering-HIPEs resulted in an increased gas permeability from 400 mD (P5) to 3.7 D (P20) (Table 1).

The skeletal density of all poly-Pickering-HIPEs was identical (1.12 g/cm^3) because they were all produced from the same formulation (with the exception of the surfactant added to the primary emulsion template, which does not take part in the reaction), thus having the same composition. The porosity of the poly-Pickering-HIPEs was higher than the internal phase ratio of the emulsion templates, which was caused by the loss of the surfactant acting as a porogen, and of non-reacted monomers during the purification. The porosity of the monoliths increased with increasing the surfactant amount from 84.3 to 88.2% (Table 1).

The pore Reynolds number Re_p of water passing through poly-Pickering-HIPE monoliths at a flow rate of 0.6 mL/min were between 1.8 and 4.5 (Table 1), thus indicating a laminar flow regime. Re_p decreased with increasing openness (affecting the tortuosity) of the monoliths because fewer obstacles affected the flowing fluid. Comiti et al.[43] showed for packed bed reactors that the limiting Re_p for the laminar flow is 4.3 for Newtonian fluids. Re_p for water passing our poly-Pickering-HIPEs was smaller than Re of tubular reactors (0.4 mm diameter, Re = 80),[10] commercial static mixers Statmix6 and ST-mixer (Re = 20 and Re = 5 at Q = 0.5 mL/min,

https://doi.org/10.1021/acs.iecr.1c01949
Ind. Eng. Chem. Res. 2021, 60, 14013−14025

Table 1. Effect of Increasing Surfactant Amounts Added to the Primary Pickering-HIPE Templates on the Morphology Descriptors of Poly-Pickering-HIPEs: Average Pore d_p and Pore Throat Diameter d_{pt}, Degree of Interconnectivity (or Openness) DoI, Porosity P, Tortuosity T, Gas Permeability k, and Pore Reynolds Number Re_p for Water Pumped through the Poly-Pickering-HIPEs with Q = 0.6 mL/min

sample	d_p/μm	d_{pt}/μm	DoI/10^{-2}	P/%	T/-	k/D	Re_p/-
P0	89 ± 27	0	0	80.5 ± 0.5	0	0	
P5	78 ± 38	12 ± 9	2.8 ± 0.6	84.3 ± 0.4	3.7 ± 0.4	0.4 ± 0.1	4.5 ± 0.2
P10	80 ± 29	20 ± 12	4.3 ± 0.2	86.7 ± 1.2	3.1 ± 0.5	1.5 ± 0.2	4 ± 0.3
P15	96 ± 33	17 ± 10	4.6 ± 0.7	87.2 ± 0.5	2.6 ± 0.4	3.2 ± 0.5	3 ± 0.3
P20	68 ± 30	13 ± 8	6 ± 0.8	88.2 ± 1.2	1.5 ± 0.2	3.7 ± 0.1	1.8 ± 0.2

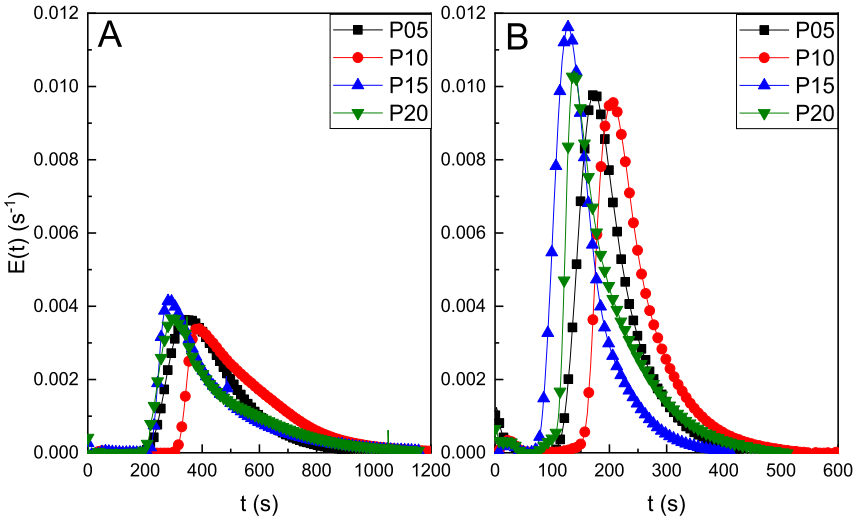

Figure 5. RTD curves of P5, P10, P15, and P20 poly-Pickering-HIPE micromixers at Q = 0.6 mL/min (A) and Q = 1.2 mL/min (B).

respectively),[47] and the (Kenics) static mixer, which was used as reference (Re = 122, calculated for water at Q = 1.2 mL/min using the hydraulic tube diameter). In those static mixers, the mixing performance increased due to the creation of chaotic flow at higher Re. However, poly-Pickering-HIPE micromixers consist of multiple microchannels, which are interconnected with each other by pore throats. Therefore, pore throats acted not only as obstacles but also as splitting and recombination channels. Such a design is also applied in commercial SAR micromixers to improve their mixing performance.[1] Our poly-Pickering-HIPE micromixers exhibited very low back pressures due to their highly interconnected pore structure. The back pressure was determined to be 54.3 mbar using the hydrostatic pressure of a water column for the micromixer with the lowest DoI and permeability (P5) (see Supporting Information, eq S3). The back pressure increased linearly with increasing flow rate up to 4.8 mL/min (Figure S7). The RTD was determined to analyze the mixing efficiency of our poly-Pickering-HIPE micromixers using an inert tracer method. The relationship between the RTD $E(t)$ and time the tracer spend in the poly-Pickering-HIPE micromixers is depicted in Figure 5; an increasing flow rate resulted in sharpening of $E(t)$ for all poly-Pickering-HIPE micromixers. With an increasing flow rate, the RTD became narrower, which indicated the enhanced liquid dispersion in poly-Pickering-HIPE micromixers (Figure 5B). Moreover, with increasing permeability of the poly-Pickering-HIPE micromixers, RTD shifted to lower times at the same flow rate (Figure 5 and Table 1). Please note that the small peak at the beginning of the measurements was due to the sudden increase in the volumetric flow rate caused by injecting the entire tracer volume (0.2 mL) at once. The same behavior was observed when injecting pure water instead of the KCl tracer.

The RTD curves of all micromixers have asymmetric bell shapes with tailing, which represents the deviation from an ideal plug flow reactor (Figures 5 and6).[10,44] The low fluid velocities near the wall of the micromixer caused $E(t)$ curves to broaden and tailing. Such tailing was not only observed in

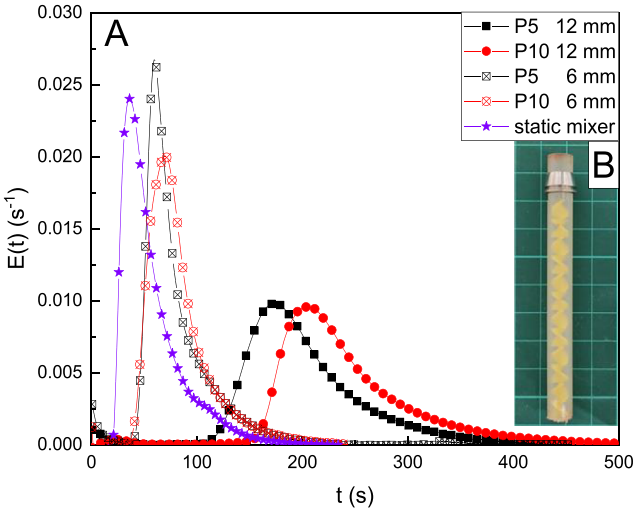

Figure 6. RTD curves of P5 and P10 poly-Pickering-HIPE micromixers with a diameter of 12 and 6 mm and the Kenics helical static mixer at Q = 1.2 mL/min (A), and a photo of the Kenics helical static mixer (B).

https://doi.org/10.1021/acs.iecr.1c01949
Ind. Eng. Chem. Res. 2021, 60, 14013−14025

Table 2. Mean Residence Time t_m, Axial Dispersion Number D_{ax}/uL, and the Coefficient of Determination R^2 Obtained by Fitting of the Axial Dispersion Model to the RTD of Poly-Pickering-HIPE Micromixers and the Kenics Static Mixer at Two Different Volumetric Flow Rates

	t_m (s)		D_{ax}/uL ($\times 10^{-2}$)		R^2	
sample name	0.6 mL/min	1.2 mL/min	0.6 mL/min	1.2 mL/min	0.6 mL/min	1.2 mL/min
P5[a]	370	179	4 ± 0.5	3 ± 0.05	0.96	0.95
P10[a]	400	212	6 ± 0.2	2 ± 0.04	0.62	0.93
P15[a]	307	133	6 ± 0.1	3 ± 0.06	0.72	0.96
P20[a]	310	150	8 ± 0.2	4 ± 0.2	0.71	0.79
P5[b]	129	62	3 ± 0.01	3 ± 0.1	0.92	0.9
P10[b]	138	73	3 ± 0.03	4 ± 0.08	0.99	0.97
static mixer		40		8.8 ± 0.3		0.92

[a]Micromixers fabricated with 12 mm diameter monoliths. [b]Micromixers fabricated with 6 mm diameter monoliths.

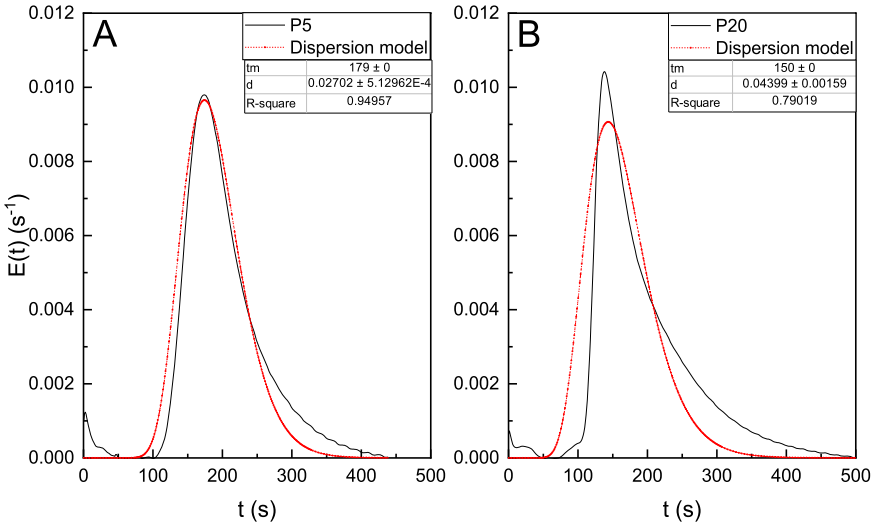

Figure 7. Fits of the axial dispersion model to the RTD ($E(t)$) of P5 (A) and P20 (B) micromixers with diameters of 12 mm at Q = 1.2 mL/min.

open cell millireactors[48] but also in commercial multichannel chip reactors and static mixers.[10,49] Even though $E(t)$ of poly-Pickering-HIPE micromixers showed tailing, they do not contain any irregularities or non-uniform peaks, which would indicate fluid maldistribution, such as recirculation, flow in parallel channels, or bypassing of the micromixer.[44,49] Méndez-Portillo et al.[49] quantified the RTD of commercial SAR micromixers, whose RTD curves showed irregularities as a result of recirculation, when the velocity ratio between the mainstream and tracer injection was ≤1. In order to compare the RTD of our poly-Pickering-HIPE micromixers with the SAR mixers characterized by Méndez-Portillo et al.,[49] we did test them at a velocity ratio between the tracer and the mainstream flow of <2 but did not observe any irregularities (Figure S8). Because of the interconnected structure of poly-Pickering-HIPEs, fluid can also interact with each other in the radial direction, and thus, problems causing the maldistribution of fluid were avoided.

Poly-Pickering-HIPEs with diameters of 6 and 12 mm (Figure 6) were fabricated in order to investigate the radial dispersion of our P5 and P10 micromixers. Micromixers with diameter 6 mm had significantly shorter residence times than the 12 mm diameter micromixers (Table 2) since the dispersion of fluids in the radial direction was limited. Those thinner micromixers also possessed an asymmetrical RTD with tailing. The poly-Pickering-HIPEs consisted of multiple pores and pore throats in radial and axial directions forming many parallel but interconnected mixing channels, which could have caused the tailing in the RTD. Furthermore, the RTD curves were compared with that of a 3/8″ diameter 12 helix Kenics static mixer. The static mixer could only be tested at a flow rate of 1.2 mL/min. The peak of $E(t)$ of the static mixer occurred slightly earlier than that of the 6 mm poly-Pickering-HIPE micromixers, which is due to its simpler single channel structure (Figure 6).

To investigate the scalability, micromixers were also fabricated from 25 mm diameter poly-Pickering-HIPEs. The RTD could not be determined for 60 mm long micromixers due to their high back pressure (too high for our syringe pump), but it could be analyzed for 30 mm long micromixers. The RTD curve was showing very high tailing and asymmetry due to the high radial dispersion in larger diameter micromixers (Figure S9). Therefore, we did not further characterize these mixers.

From RTD of micromixers operated at different flow rates (Figure 5) and two diameters (Figure 6), the mean residence time (t_m) of poly-Pickering-HIPE micromixers and the static mixer was determined (Table 2). Increasing the flow rate and decreasing the diameter of the micromixers resulted in decreasing t_m. However, the measured t_m of the micromixers was slightly lower than the calculated τ for a flow rate of 1.2 mL/min (τ = 240 ± 5 s). Since all poly-Pickering-HIPEs had the same porosity and dimensions, τ was the same for all micromixers. The deviation between τ and t_m was higher for

https://doi.org/10.1021/acs.iecr.1c01949
Ind. Eng. Chem. Res. 2021, 60, 14013−14025

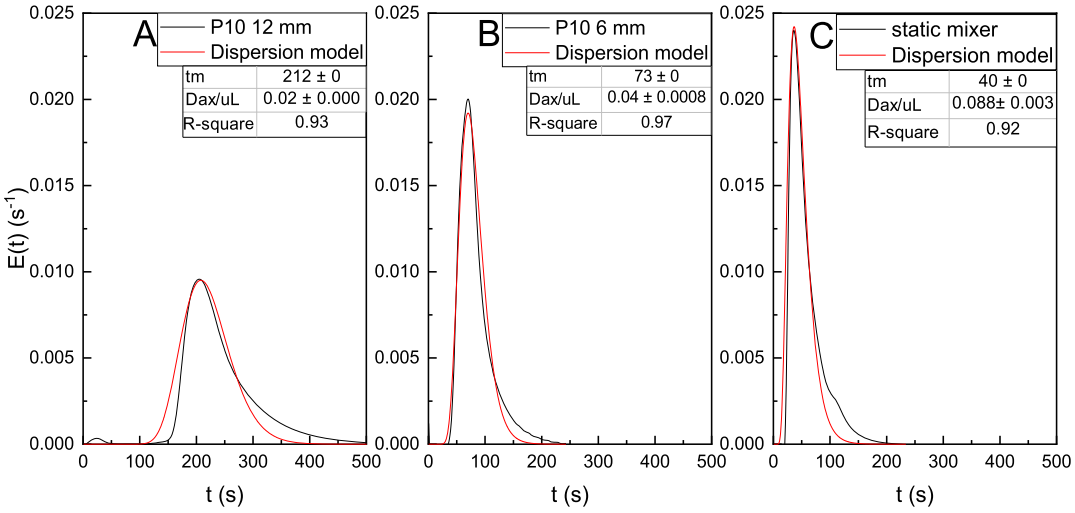

Figure 8. Fits of the axial dispersion model to the RTD [$E(t)$] of micromixers with diameters of 12 mm (A) and 6 mm (B) micromixers fabricated using P10 and of the Kenics static mixer (C).

micromixers operated at a lower flow rate and increased with increasing DoI of the poly-Pickering-HIPE micromixers. The smaller t_m was caused by the dead volumes around the inlet and outlet tubes. The Kenics static mixer had a significantly smaller mean residence time (40 s) than the P5 and P10 micromixers of similar diameters (62 and 73 s, respectively). As a result of the single channel helical design of the static mixer, the dispersion of the tracer was faster.

Levenspiel[44] showed that the axial dispersion model (eq 13) can be fitted to the RTD if the axial dispersion number $D_{ax}/uL > 0.01$. D_{ax} describes the degree of back mixing during flow, which is different from mixing in the radial direction occurring due to molecular diffusion.[44] Figure 7 shows the fitted axial dispersion model to the RTD of P5 and P20 micromixers. The dispersion model fitted for RTD of P5 micromixer reasonably well. However, a larger deviation between the dispersion model and the RTD was observed for the P20 micromixer. The large DoI of the P20 monolith allowing for increased radial dispersion was responsible for the observed deviation between model and the measured RTD. The coefficient of determination R^2 of the fitted models was lowest for P20 at a 1.2 mL/min flow rate (Table 2). The reason for this behavior could be the high DoI of P20, which allowed for mixing in the radial direction. Therefore, the fluctuation increased as a result of the difference in the flow velocities between the pore walls and the center of pores within the micromixer, thus causing the higher deviation from the dispersion model (Table 2).

Table 2 shows the axial dispersion number of micromixers at different flow rates and t_m, which were determined by fitting the dispersion model to the RTD. Furthermore, at a flow rate of 0.6 mL/min, we observed broadening of the $E(t)$ curves for all micromixers (Figure 5) and as a result, the axial dispersion number increased as well (Table 2 and Figure S10). However, for micromixer P5, we observed the lowest deviation at a flow rate of 0.6 mL/min. This micromixer had the lowest DoI, which limited the spread of the liquid in the radial direction. Levenspiel[44] stated that the axial dispersion model can be employed only if $D_{ax}/uL < 1$. The obtained average values for D_{ax}/uL were in the range of 0.02−0.08 for poly-Pickering-HIPE micromixers (Table 2), indicating that the mixing performance in the poly-Pickering-HIPE micromixers is diffusion controlled under our experimental conditions. The axial dispersion number (D_{ax}/uL) increased with the decreasing flow rate, resulting in the increased asymmetry and tailing of the $E(t)$ curves, which indicates decreasing dispersion, which would result in an increasing reaction control.

The P10 micromixers with diameters of 12 and 6 mm had axial dispersion numbers of 4×10^{-2} and 2×10^{-2} at 1.2 mL/min with R^2 of 0.93 and 0.97, respectively (Figure 8A,B). However, the axial dispersion number of the P10 micromixer with a diameter of 12 mm increased with the decreasing flow rate (Table 2) as a result of larger number of interacting flow channels along the micromixer. Furthermore, we compared the dispersion model of our P10 micromixers with that of the commercial static mixer, for which the deviation from the model is higher, especially in the tail part of the curve (Figures 8C and6). The axial dispersion number for the static mixer is 8.8×10^{-2}, which is an indication of the increased spread of the RTD caused by velocity differences in the radial direction of the static mixer (Table 2). Gobert et al.[10] used the convection model to describe the RTD of the Kenics static mixer, which however, does not produce a decent fit. Therefore, we also choose to use the dispersion model to describe the static mixer. This model describes the experimental RTD with a lower deviation than the convection model. Additionally, Gobert et al.[10] used the axial dispersion model to describe commercial SAR chip micromixers. They report axial dispersion numbers that are approximately three times lower than ours. The reason for the higher axial dispersion numbers of poly-Pickering-HIPE micromixers is that they have larger pore throat diameters, resulting in a higher DoI between possible flow paths (Figure 2), which results not only in increased radial dispersion but also increased fluctuation between the pore walls and the pore centers within the micromixers compared to SAR chip micromixers, consisting of parallel microchannels. The dispersion model of the rest of the poly-Pickering-HIPE micromixers can be found in the Supporting Information (Figure S10).

The dimensionless RTD, $E(\Theta)$, of 12 mm diameter poly-Pickering-HIPE micromixers operated at a flow rate of 1.2 mL/min are shown in Figure 9. An increasing DoI of the monolithic poly-Pickering-HIPE micromixers resulted in a

https://doi.org/10.1021/acs.iecr.1c01949
Ind. Eng. Chem. Res. 2021, 60, 14013−14025

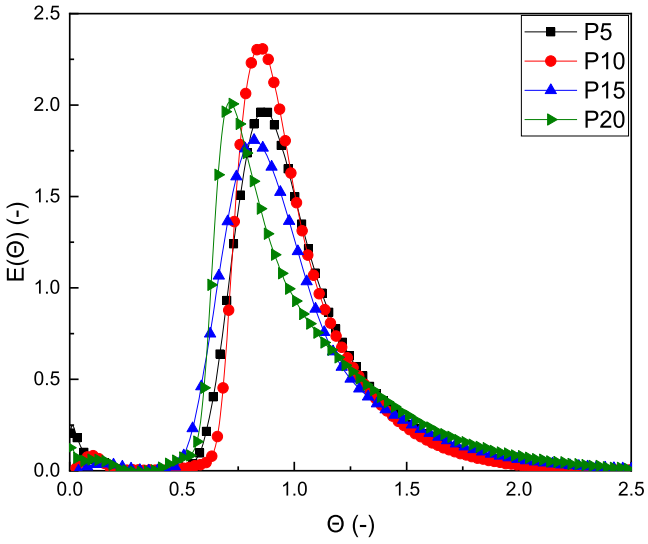

Figure 9. Dimensionless RTD $E(\Theta)$ of the poly-Pickering-HIPE micromixers having diameters of 12 mm and P5, P10, P15, and P20 at a flow rate of 1.2 mL/min. Please note that the perturbation at the beginning of the measurement was caused by the injection pulse of the tracer.

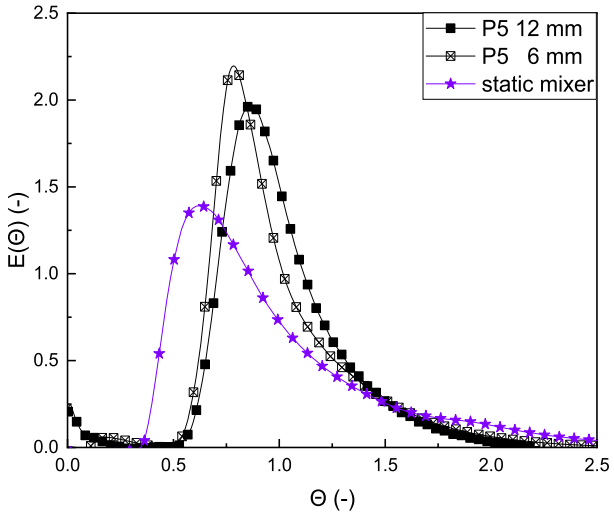

Figure 10. Dimensionless RTD $E(\Theta)$ of the P5 micromixers having diameters of 6 and 12 mm and the Kenics static mixer operated at Q = 1.2 mL/min.

larger spread of the RTD (see also Figure 5). The flow entering the micromixers with a high DoI can be easily divided over several possible parallel paths compared to that in micromixers with a lower DoI. Moreover, the radial dispersion between those parallel flow paths through their pore throats was higher in micromixers with a higher DoI, which resulted in larger spread in the RTD. A large RTD spread was shown in the literature for many SAR-type micromixers.[10,49,50]

When operating the micromixers at Q = 0.6 mL/min, we observed that the RTD shifted to a shorter dimensionless time (Figure S11) and an increased asymmetry of the curve resulting in a higher skewness of the RTD (Figure 11). Even lower volumetric flow rates result in a smaller difference in the flow velocities between the pore walls and the pore center parts in the micromixer but resulted in a higher asymmetry (i.e. skewness), which was already shown in the literature.[49−51]

The dimensionless RTD, $E(\Theta)$, of P5 micromixers having diameters of 6 and 12 mm and the Kenics static mixer are shown in Figure 10. By decreasing the diameter of the micromixers, $E(\Theta)$ shifted to shorter dimensionless times, even though the skewness of the micromixer having a diameter of 6 mm was significantly smaller than that of 12 mm diameter micromixers (Figure 11B). Regardless of the flowrate and, hence Re, the CoV ($\overline{\mathrm{CoV}}$ = 0.41) of the P5 micromixer with a diameter of 6 mm diameter and P20 with 12 mm diameter is larger than all of other poly-Pickering-HIPE micromixers ($\overline{\mathrm{CoV}}$ = 0.31), indicating less tailing and thus a flow behavior closer to plug flow. However, all micromixers have a much smaller spread and less tailing than the static (Kenics) mixer (Figure 10). The static mixer created vortices, which helped improve the mixing performance when compared to an empty tube.[10] However, it also causes flow velocity differences throughout the mixer, which cause asymmetry and tailing. The interconnected structure of poly-Pickering-HIPE micromixers reduced the flow velocity differences, as compared with the static mixer.

CoV of poly-Pickering-HIPE micromixers having diameters of 6 and 12 mm as a function of Re_p were compared with the commercial static (Kenics) mixer (Figure 11A). The flow through a P20 micromixer having the largest DoI and consequently the lowest Re_p possessed the largest deviation from the dispersion model (Table 2). Micromixer P20 had the highest CoV because of its high radial dispersion caused by the high openness (DoI) of its pore structure (Figure 11A). A decreasing DoI of the 12 mm diameter micromixers, reducing the axial dispersion, resulted in an increased Re_p, which caused CoV to reduce. The commercial static mixer (Re = 122) has the highest CoV (Figure 11A) because of the higher diffusion distance in this mixer due to its simpler channel structure, which reduced the contribution to radial mixing, thus increasing the axial dispersion number D_{ax}/uL (Table 2). We determined the same CoV for this static mixer as reported in the literature,[10] showing the reliability of our measurement technique. Moreover, analyzing the skewness is helpful to estimate the differences between RTD. All curves had a positive skewness, as seen in Figure 11B. The higher the skewness, the greater the asymmetry and tailing of the RTD (Figure 5). The skewness of the RTD of poly-Pickering-HIPE micromixers decreased with increasing Re_p, due to the smaller radial dispersion of liquids along the micromixers (Figure 11B). The 6 mm diameter micromixers had the lowest skewness because of the small distance between the central part of the micromixers and their wall and thus a smaller flow velocity difference across the mixers.

Figure 12 shows that the acid-catalyzed decomposition yield of DMP is lower when the reaction mixture is passed through poly-Pickering-HIPE micromixers (on average 2.5%) in contrast to the spiral static mixer resulting in a decomposition yield of 17%. This indicated that fluids mixed more efficiently and more homogeneously within the pores of macroporous polymers resulting in more consistent decomposition yields. As discussed previously, the axial dispersion number and CoV of the static mixer were highest compared with the poly-Pickering-HIPE micromixers (Table 2 and Figure 11A). Tebboth et al.[13] compared the mixing performance for the same competitive reaction for polyHIPE flow cells to a spiral static mixer and found a yield of the acid-catalyzed DMP decomposition of 22.2%. The reason for the higher yield (compared to ours) was the lower total flow rate of the

https://doi.org/10.1021/acs.iecr.1c01949
Ind. Eng. Chem. Res. 2021, 60, 14013−14025

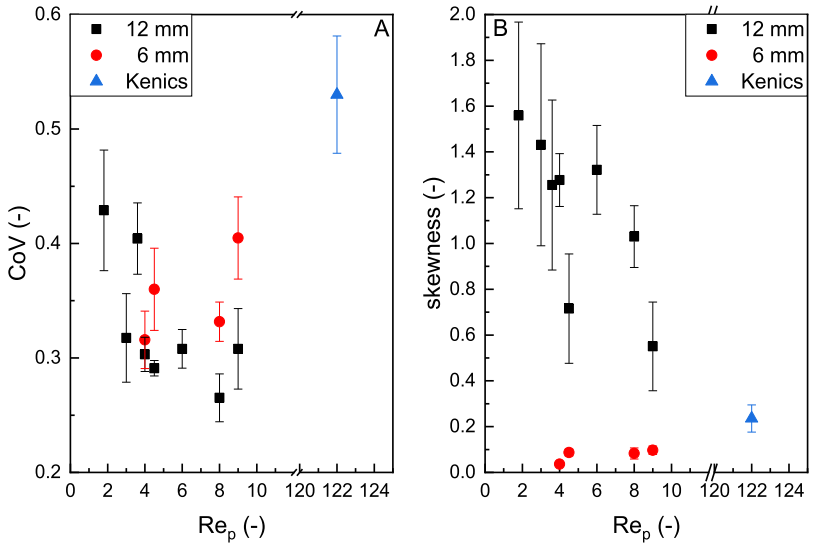

Figure 11. Spread expressed as CoV (A) and skewness *s* (B) of poly-Pickering-HIPE micromixers as a function of Re_p for micromixers with diameters of 6 and 12 mm operated at Q = 0.6 and 1.2 mL/min compared with the Kenics static mixer (blue triangle) operated only at Q = 1.2 mL/min.

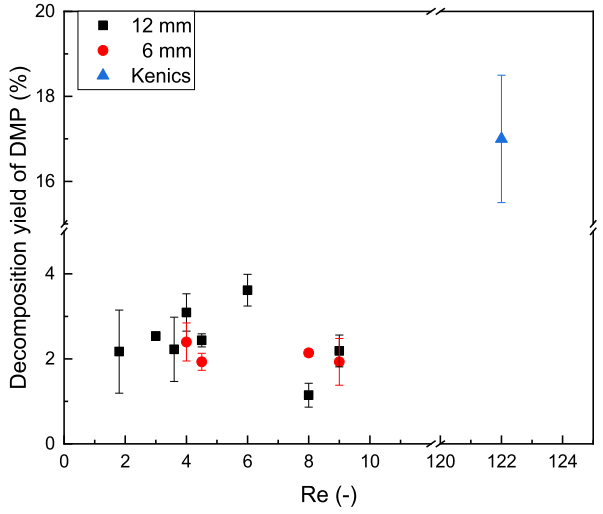

Figure 12. Acid-catalyzed decomposition yield of DMP as a result of competitive parallel reactions occurring in poly-Pickering-HIPE micromixers having various Re_p, diameters of 6 and 12 mm operated at flow rates of 0.6 and 1.2 mL/min, and the Kenics static mixer operated at a flow rate of 1.2 mL/min as a function of the mean residence time Re_p.

reaction mixture, which was 1 mL/min, and the time elapsed between sample collection and HPLC analysis.

Tebboth et al.[13] investigated the micromixing performance of a poly-Pickering-HIPE flow cell, with a similar morphology to P5. They reported a DMP decomposition yield of 23.1% when operating the flow cell at a total flow rate of 1 mL/min. The main reason for this difference in the decomposition yield is the micromixer design. In their case, fluids were directly pumped from the top of the monolith placed into a steel tube and collected at the bottom end. We, however, placed inlet and outlet tubes directly into the monolith which resulted in improved mixing of the fluids, especially before exiting the micromixer (Figure 3). Our design was the result of testing these micromixers to create stable emulsions; when testing the micromixers without an outlet tube, that is, collecting the emulsion directly at the bottom end of the micromixer, we did not obtain a stable emulsion. However, highly stable and viscous emulsions were produced using the current design (Figure 3). Details will be reported at the later stage.

CONCLUSIONS

Macroporous polymers with increasing DoI were produced by polymerization of particle-stabilized emulsions to which surfactants were added and characterized with respect to their suitability as micromixers. The DoI increased with increasing amount of surfactants, which were added to the primary Pickering-HIPE prior to polymerization. With increasing DoI, the tortuosity decreased, while gas permeability of the poly-Pickering-HIPEs increased indicating less resistance to fluid flow, which is also reflected in the decreasing Re_p for water pumped through the micromixer. We used these poly-Pickering-HIPEs to produce micromixers whose mixing performance was characterized by RTD and two competitive parallel reactions. The axial dispersion numbers were determined by fitting the appropriate Levenspiel axial dispersion model to the RTD. The axial dispersion numbers were in the order of D_{ax}/uL = 0.03 to 0.08, depending on the morphology and dimensions of the polyHIPE monoliths used in the micromixer. An increasing openness of the polyHIPE monoliths resulted in increased axial dispersion numbers. The fluid flow through the most effective micromixer (P10-12 mm) with the lowest CoV (0.27) and low axial dispersion number (0.02) operated at a flowrate of 1.2 mL/min approached plug flow. Increasing the openness of the polyHIPEs used in the micromixers resulted in lower Re_p and reduced mixing performance because of increased radial mixing, which caused tailing. Poly-Pickering-HIPE micromixers were compared with a commercial 12 helix Kenics static mixer and had a better mixing performance. The Kenics static mixer had a spread CoV = 0.53 and axial dispersion number of 0.09, which was in agreement with literature data. Moreover, their micromixing performance was also tested using the 4th Bourne competitive parallel reactions, and all polyHIPE micromixers had DMP decomposition yields of about 2.5%, while the yield in the

https://doi.org/10.1021/acs.iecr.1c01949
Ind. Eng. Chem. Res. 2021, 60, 14013−14025

static Kenics mixer was 17%, again indicating a poorer mixing performance.

■ ASSOCIATED CONTENT

Supporting Information

The Supporting Information is available free of charge at https://pubs.acs.org/doi/10.1021/acs.iecr.1c01949.

Additional experimental details, materials, methods, and supporting results, such as thermal stability, morphology, further axial dispersion fits, and measured back pressures of micromixers (PDF)

■ AUTHOR INFORMATION

Corresponding Author

Alexander Bismarck − *Polymer and Composite Engineering (PaCE) Group, Institute of Material Chemistry and Research, Faculty of Chemistry, University of Vienna, Vienna 1090, Austria; Department of Chemical Engineering, Imperial College London, London SW7 2AZ, U.K.;* orcid.org/0000-0002-7458-1587; Email: alexander.bismarck@univie.ac.at

Authors

Hande Barkan-Öztürk − *Polymer and Composite Engineering (PaCE) Group, Institute of Material Chemistry and Research, Faculty of Chemistry, University of Vienna, Vienna 1090, Austria*

Angelika Menner − *Polymer and Composite Engineering (PaCE) Group, Institute of Material Chemistry and Research, Faculty of Chemistry, University of Vienna, Vienna 1090, Austria*

Complete contact information is available at: https://pubs.acs.org/10.1021/acs.iecr.1c01949

Author Contributions

All authors conceptualized the work, H.B.Ö. performed all experimental work and analyzed the data. H.B.Ö. and A.B. wrote the manuscript and designed the figures. A.M. and A.B. supervised the work. All authors contributed to manuscript review and editing.

Funding

H.B.Ö. gratefully acknowledges financial support by the University of Vienna.

Notes

The authors declare no competing financial interest.

■ ACKNOWLEDGMENTS

We acknowledge the financial support from the Faculty of Chemistry, University of Vienna.

■ ABBREVIATIONS

$C(t)$	tracer concentration (mol L^{-1})
D	Darcy (1 D = 9.87 × 10^{-13} m^2)
D_h	hydraulic pipe diameter (m)
D_{ax}	axial dispersion coefficient (m^2 s^{-1})
d_p	average pore diameter (μm)
d_{pt}	average pore throat diameter (μm)
$E(t)$	exit age distribution function (s^{-1})
k_i	reaction rate constant (m^3 kg^{-1} mol^{-1} s^{-1})
K	permeability coefficient (m^2 s^{-1})
k	gas permeability (D)
P	porosity (%)
Q	flow rate (mL/min)
s	skewness (s)
t	time (s)
t_m	mean residence time (s)
u	linear flow velocity (m s^{-1})
u_p	average pore flow velocity (m s^{-1})
T	tortuosity (-)
A	absorbance (-)

■ GREEK LETTERS

μ	dynamic viscosity (Pa·s)
ρ	fluid density (g cm^{-3})
σ	variance (s)
τ	average residence time (s)
ε	molar extinction coefficient (L mol^{-1} cm^{-1})
ρ_s	skeletal density (g cm^{-3})
ρ_f	foam density (g cm^{-3})
κ_p	conductivity (S cm^{-1})
Θ	normalized time
$E(\Theta)$	normalized exit age distribution function

■ DIMENSIONLESS GROUPS

D_{ax}/uL	axial dispersion number
Re	Reynolds number
Re_p	pore Reynolds numbers

■ ACRONYMS

AIBN	α,α'-azoisobutyronitrile
CoV	covariance
DMP	2,2-dimethoxypropane
DoI	degree of interconnectivity also called openness
DVB	divinyl benzene
HDK H20	hydrophobic pyrogenic silica particles
HIPE	high internal phase emulsion
polyHIPE	polymerized high internal phase emulsion
RTD	residence time distribution
SAR	split-and-recombination micromixer
SEM	scanning electron microscopy

■ REFERENCES

(1) Nguyen, N.-T. *Micromixers: Fundamentals, Design, and Fabrication*, Micro & Nano Technologies Series; 2nd ed., Elsevier/William Andrew: Amsterdam; Boston, 2012; p 351.

(2) Brody, J. P.; Yager, P.; Goldstein, R. E.; Austin, R. H. Biotechnology at Low Reynolds Numbers. *Biophys. J.* **1996**, *71*, 3430−3441.

(3) Huebner, A.; Sharma, S.; Srisa-Art, M.; Hollfelder, F.; Edel, J. B.; deMello, A. J. Microdroplets: A Sea of Applications? *Lab Chip* **2008**, *8*, 1244.

(4) Adeosun, J. T.; Lawal, A. Numerical and Experimental Studies of Mixing Characteristics in a T-Junction Microchannel Using Residence-Time Distribution. *Chem. Eng. Sci.* **2009**, *64*, 2422−2432.

(5) Song, H.; Bringer, M. R.; Tice, J. D.; Gerdts, C. J.; Ismagilov, R. F. Experimental Test of Scaling of Mixing by Chaotic Advection in Droplets Moving through Microfluidic Channels. *Appl. Phys. Lett.* **2003**, *83*, 4664−4666.

(6) Kiss, N.; Brenn, G.; Pucher, H.; Wieser, J.; Scheler, S.; Jennewein, H.; Suzzi, D.; Khinast, J. Formation of O/W Emulsions by Static Mixers for Pharmaceutical Applications. *Chem. Eng. Sci.* **2011**, *66*, 5084−5094.

(7) Britton, J.; Jamison, T. F. The Assembly and Use of Continuous Flow Systems for Chemical Synthesis. *Nat. Protoc.* **2017**, *12*, 2423−2446.

(8) Sharada, S.; Suryawanshi, P. L.; Kumar, P. R.; Gumfekar, S. P.; Narsaiah, T. B.; Sonawane, S. H. Synthesis of Palladium Nanoparticles Using Continuous Flow Microreactor. *Colloids Surf., A* **2016**, *498*, 297−304.
(9) Gomollón-Bel, F. Ten Chemical Innovations That Will Change Our World: IUPAC Identifies Emerging Technologies in Chemistry with Potential to Make Our Planet More Sustainable. *Chem. Int.* **2019**, *41*, 12−17.
(10) Gobert, S. R. L.; Kuhn, S.; Braeken, L.; Thomassen, L. C. J. Characterization of Milli- and Microflow Reactors: Mixing Efficiency and Residence Time Distribution. *Org. Process Res. Dev.* **2017**, *21*, 531−542.
(11) Rasouli, M. R.; Abouei Mehrizi, A.; Lashkaripour, A. Numerical Study on Low Reynolds Mixing of T-Shaped Micro-Mixers with Obstacles. *Transp. Phenom. Nano Micro Scales* **2015**, *3*, 68−76.
(12) Lapierre, F.; Cameron, N. R.; Zhu, Y. Ready Set, Flow: Simple Fabrication of Microdroplet Generators and Their Use in the Synthesis of PolyHIPE Microspheres. *J. Micromech. Microeng.* **2015**, *25*, 035011.
(13) Tebboth, M.; Kogelbauer, A.; Bismarck, A. Effectiveness of Emulsion-Templated Macroporous Polymer Micromixers Characterized by the Bourne Reaction. *Ind. Eng. Chem. Res.* **2015**, *54*, 5974−5981.
(14) Tebboth, M.; Kogelbauer, A.; Bismarck, A. Liquid−Liquid Extraction within Emulsion Templated Macroporous Polymers. *Ind. Eng. Chem. Res.* **2015**, *54*, 7284−7291.
(15) Brown, J. F.; Krajnc, P.; Cameron, N. R. PolyHIPE Supports in Batch and Flow-Through Suzuki Cross-Coupling Reactions. *Ind. Eng. Chem. Res.* **2005**, *44*, 8565−8572.
(16) Whitely, M.; Rodriguez-Rivera, G.; Waldron, C.; Mohiuddin, S.; Cereceres, S.; Sears, N.; Ray, N.; Cosgriff-Hernandez, E. Porous PolyHIPE Microspheres for Protein Delivery from an Injectable Bone Graft. *Acta Biomater.* **2019**, *93*, 169−179.
(17) Richardson, S. A.; Rawlings, T. M.; Muter, J.; Walker, M.; Brosens, J. J.; Cameron, N. R.; Eissa, A. M. Covalent Attachment of Fibronectin onto Emulsion-Templated Porous Polymer Scaffolds Enhances Human Endometrial Stromal Cell Adhesion, Infiltration, and Function. *Macromol. Biosci.* **2019**, *19*, 1800351.
(18) Desire, C. T.; Hilder, E. F.; Arrua, R. D. Monolithic High-Performance Liquid Chromatography Columns. In *Encyclopedia of Analytical Chemistry*; Meyers, R. A., Ed.; John Wiley & Sons, Ltd: Chichester, U.K., 2017; pp 1−37.
(19) Desire, C. T.; Arrua, R. D.; Mansour, F. R.; Bon, S. A. F.; Hilder, E. F. Effect of Shearing Stress on the Radial Heterogeneity and Chromatographic Performance of Styrene-Based Polymerised High Internal Phase Emulsions Prepared in Capillary Format. *RSC Adv.* **2019**, *9*, 7301−7313.
(20) Tebboth, M.; Menner, A.; Kogelbauer, A.; Bismarck, A. Polymerised High Internal Phase Emulsions for Fluid Separation Applications. *Curr. Opin. Chem. Eng.* **2014**, *4*, 114−120.
(21) Pulko, I.; Kolar, M.; Krajnc, P. Atrazine Removal by Covalent Bonding to Piperazine Functionalized PolyHIPEs. *Sci. Total Environ.* **2007**, *386*, 114−123.
(22) Lissant, K. J. Continuous Process for the Preparation of Emulsions. U.S. Patent 3,565,817 A, 1968.
(23) Menner, A.; Haibach, K.; Powell, R.; Bismarck, A. Tough Reinforced Open Porous Polymer Foams via Concentrated Emulsion Templating. *Polymer* **2006**, *47*, 7628−7635.
(24) Cameron, N. R. High Internal Phase Emulsion Templating as a Route to Well-Defined Porous Polymers. *Polymer* **2005**, *46*, 1439−1449.
(25) Stubenrauch, C.; Menner, A.; Bismarck, A.; Drenckhan, W. Emulsion and Foam Templating-Promising Routes to Tailor-Made Porous Polymers. *Angew. Chem., Int. Ed.* **2018**, *57*, 10024−10032.
(26) Menner, A.; Powell, R.; Bismarck, A. Open Porous Polymer Foams via Inverse Emulsion Polymerization: Should the Definition of High Internal Phase (Ratio) Emulsions Be Extended? *Macromolecules* **2006**, *39*, 2034−2035.
(27) Ng, N.; Rogers, M. A. Surfactants. *Encyclopedia of Food Chemistry*; Elsevier, 2019; pp 276−282.
(28) Foudazi, R. HIPEs to PolyHIPEs. *React. Funct. Polym.* **2021**, *164*, 104917.
(29) Wong, L. L. C.; Ikem, V. O.; Menner, A.; Bismarck, A. Macroporous Polymers with Hierarchical Pore Structure from Emulsion Templates Stabilised by Both Particles and Surfactants. *Macromol. Rapid Commun.* **2011**, *32*, 1563−1568.
(30) Menner, A.; Verdejo, R.; Shaffer, M.; Bismarck, A. Particle-Stabilized Surfactant-Free Medium Internal Phase Emulsions as Templates for Porous Nanocomposite Materials: Poly-Pickering-Foams. *Langmuir* **2007**, *23*, 2398−2403.
(31) Ikem, V. O.; Menner, A.; Horozov, T. S.; Bismarck, A. Highly Permeable Macroporous Polymers Synthesized from Pickering Medium and High Internal Phase Emulsion Templates. *Adv. Mater.* **2010**, *22*, 3588−3592.
(32) Kimmins, S. D.; Cameron, N. R. Functional Porous Polymers by Emulsion Templating: Recent Advances. *Adv. Funct. Mater.* **2011**, *21*, 211−225.
(33) Jiang, Q.; Menner, A.; Bismarck, A. One-Pot Synthesis of Supported Hydrogel Membranes via Emulsion Templating. *React. Funct. Polym.* **2017**, *114*, 104−109.
(34) Khodabandeh, A.; Arrua, R. D.; Mansour, F. R.; Thickett, S. C.; Hilder, E. F. PEO-Based Brush-Type Amphiphilic Macro-RAFT Agents and Their Assembled PolyHIPE Monolithic Structures for Applications in Separation Science. *Sci. Rep.* **2017**, *7*, 7847.
(35) Jiang, Q.; Barkan, H.; Menner, A.; Bismarck, A. Micro-patterned, Macroporous Polymer Springs for Capacitive Energy Harvesters. *Polymer* **2017**, *126*, 419−424.
(36) Fogler, H. S. *Elements of Chemical Reaction Engineering*; Prentice Hall: Boston, 2016; pp 872−885.
(37) Baldyga, J.; Bourne, J. R.; Walker, B. Non-Isothermal Micromixing in Turbulent Liquids: Theory and Experiment. *Can. J. Chem. Eng.* **1998**, *76*, 641−649.
(38) Pulko, I.; Krajnc, P. High Internal Phase Emulsion Templating − A Path To Hierarchically Porous Functional Polymers. *Macromol. Rapid Commun.* **2012**, *33*, 1731−1746.
(39) Manley, S. S.; Steindl, P.; Hewitt, G. F.; Bismarck, A. An Integrated Method for Measuring Gas Permeability and Diffusivity of Porous Solids. *Chem. Eng. Sci.* **2020**, *223*, 115725.
(40) Łukowski, J.; Kaczmarek, M. Laboratory Methods of Determination of Pore Structure Parameters: Formation Factor and Tortuosity of Permeable Media by Electric Methods. *Eng. Trans.* **2002**, *50*, 267.
(41) Danninger, D.; Hartmann, F.; Paschinger, W.; Pruckner, R.; Schwödiauer, R.; Demchyshyn, S.; Bismarck, A.; Bauer, S.; Kaltenbrunner, M. Stretchable Polymerized High Internal Phase Emulsion Separators for High Performance Soft Batteries. *Adv. Energy Mater.* **2020**, *10*, 2000467.
(42) Carman, P. C. *Flow of Gases through Porous Media*; Academic Press, 1956; p 69.
(43) Comiti, J.; Sabiri, N. E.; Montillet, A. Experimental Characterization of Flow Regimes in Various Porous Media — III: Limit of Darcy's or Creeping Flow Regime for Newtonian and Purely Viscous Non-Newtonian Fluids. *Chem. Eng. Sci.* **2000**, *55*, 3057−3061.
(44) Levenspiel, O. *Chemical Reaction Engineering*, 3rd ed.; Wiley: New York, 1999; pp 293−304.
(45) Zhou, W.; Zhang, Y.; Wang, J.; Li, H.; Xu, W.; Li, B.; Chen, L.; Wang, Q. Lightweight Porous Polystyrene with High Thermal Conductivity by Constructing 3D Interconnected Network of Boron Nitride Nanosheets. *ACS Appl. Mater. Interfaces* **2020**, *12*, 46767−46778.
(46) Zhu, W.; Zhu, Y.; Zhou, C.; Zhang, S. Pickering Emulsion-Templated Polymers: Insights into the Relationship between Surfactant and Interconnecting Pores. *RSC Adv.* **2019**, *9*, 18909−18916.
(47) Boskovic, D.; Loebbecke, S. Modelling of the Residence Time Distribution in Micromixers. *Chem. Eng. J.* **2008**, *135*, S138−S146.

https://doi.org/10.1021/acs.iecr.1c01949
Ind. Eng. Chem. Res. 2021, 60, 14013−14025

(48) Saber, M.; Pham-Huu, C.; Edouard, D. Axial Dispersion Based on the Residence Time Distribution Curves in a Millireactor Filled with β-SiC Foam Catalyst. *Ind. Eng. Chem. Res.* **2012**, *51*, 15011−15017.
(49) Méndez-Portillo, L. S.; Fradette, L.; Dubois, C.; Tanguy, P. A. Characterization of the Hydrodynamics and Mixing Performance of a Split-and-Recombination (SAR) Prototype Microreactor and a Multilamination Commercial Microreactor. *Ind. Eng. Chem. Res.* **2012**, *51*, 994−1005.
(50) Bošković, D.; Loebbecke, S.; Gross, G. A.; Koehler, J. M. Residence Time Distribution Studies in Microfluidic Mixing Structures. *Chem. Eng. Technol.* **2011**, *34*, 361−370.
(51) Hutter, C.; Zenklusen, A.; Lang, R.; von Rohr, P. R. Axial Dispersion in Metal Foams and Streamwise-Periodic Porous Media. *Chem. Eng. Sci.* **2011**, *66*, 1132−1141.

https://doi.org/10.1021/acs.iecr.1c01949
Ind. Eng. Chem. Res. 2021, 60, 14013−14025

Supporting Information

Emulsion Templated Macroporous Polymer Micromixers

Hande Barkan-Öztürk,[1] Angelika Menner,[1] Alexander Bismarck[1,2,]*

[1] Polymer and Composite Engineering (PaCE) Group, Institute of Material Chemistry and Research, Faculty of Chemistry, University of Vienna, Währinger Strasse, 42, 1090, Vienna, Austria.

[2] Department of Chemical Engineering, Imperial College London, South Kensington Campus, London SW7 2AZ, United Kingdom

* Corresponding author: Alexander Bismarck, e-mail: alexander.bismarck@univie.ac.at

Gas permeability of poly-Pickering-HIPEs. The permeability coefficient *K* was calculated as described by Manley et al.:[1]

$$K = \frac{Q_2 P_2 L}{\Delta P A} = \frac{V\left(\frac{dP_2}{dt}\right)L}{P_1 A} = \frac{k}{\mu} P_m + \frac{4}{3} K_0 \sqrt{\frac{8RT}{\pi M}} \#(S1)$$

where, Q_2 is the volumetric flow rate downstream, P_2 the downstream pressure, ΔP the pressure difference across the samples, A cross-sectional area of sample, L length of sample, P_1 beginning pressure, μ fluid viscosity, V a known volume, K_0 the slip coefficient, M the molecular weight of the transport species, R the gas constant, T the absolute temperature and t the time. The viscous permeability k was derived from the gradient of the linear plot of the permeability coefficient K vs. P_m (mean pressure) (**Figure S1**).

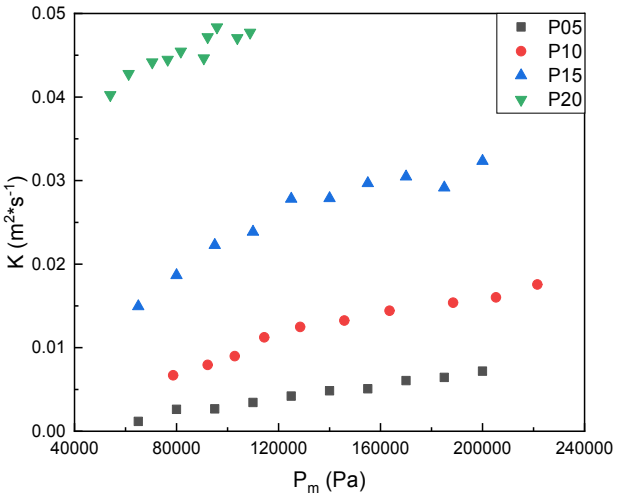

Figure S1: Permeability coefficient K of poly-Pickering-HIPEs (P05-P20) as function of mean pressure P_m

Impedance Spectroscopy. The impedance of poly-Pickering-HIPEs was determined using a custom-made measurement cell as described in previous work studied by our group.[2] Briefly, the measured impedance response is modeled using the equivalent circuit by substituting constant phase elements (CPEs) with impedance and exponents $\alpha < 1$:

$$Z_{CPE_1} = \frac{Q_i}{(i\omega)^{\alpha_1}} \#(S2)$$

where Q_i is related to the electrode capacitance, ω is the angular frequency, i imaginary number.

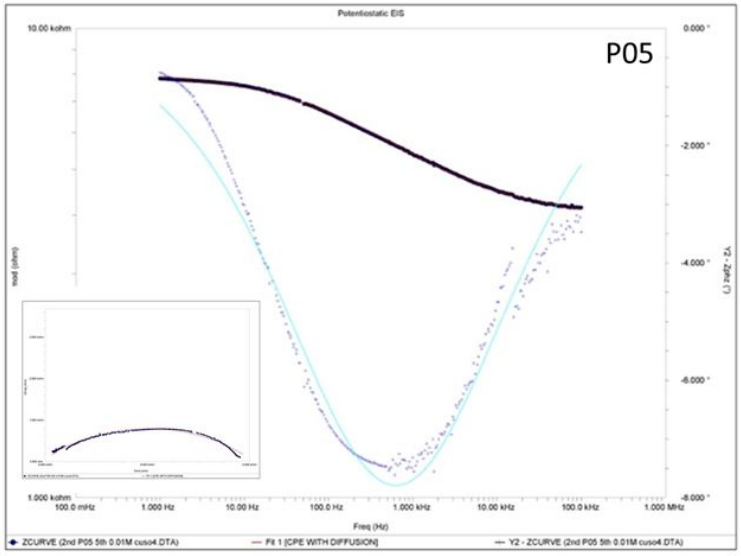
Potentiostatic EIS
P05
10.00 kohm
1.000 kohm
100.0 mHz
1.000 Hz
10.00 Hz
100.0 Hz
1.000 kHz
10.00 kHz
100.0 kHz
1.000 MHz
Freq (Hz)
0.000 °
-2.000 °
-4.000 °
-6.000 °
-8.000 °
Zmod (ohm)
YZ - ZPhz (°)
ZCURVE (2nd P05 5th 0.01M cuso4.DTA)
Fit 1 [CPE WITH DIFFUSION]
Y2 - ZCURVE (2nd P05 5th 0.01M cuso4.DTA)

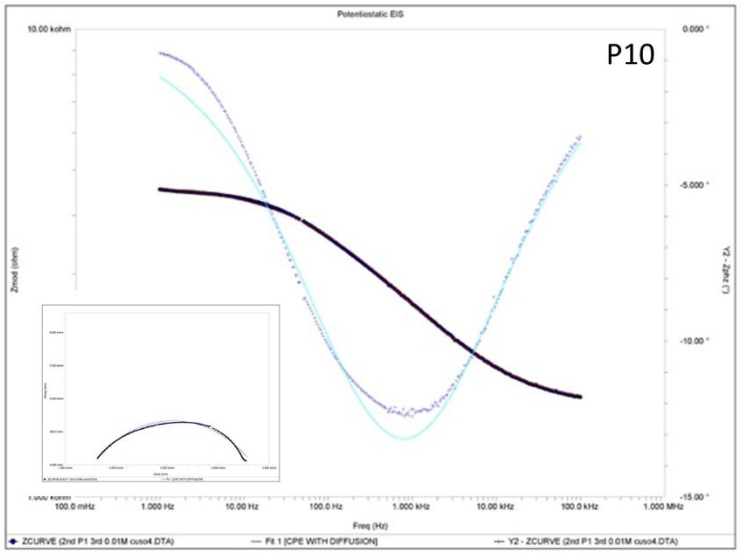
Potentiostatic EIS
P10
10.00 kohm
100.0 mHz
1.000 Hz
10.00 Hz
100.0 Hz
1.000 kHz
10.00 kHz
100.0 kHz
1.000 MHz
Freq (Hz)
0.000 °
-5.000 °
-10.00 °
-15.00 °
Zmod (ohm)
YZ - ZPhz (°)
ZCURVE (2nd P1 3rd 0.01M cuso4.DTA)
Fit 1 [CPE WITH DIFFUSION]
Y2 - ZCURVE (2nd P1 3rd 0.01M cuso4.DTA)

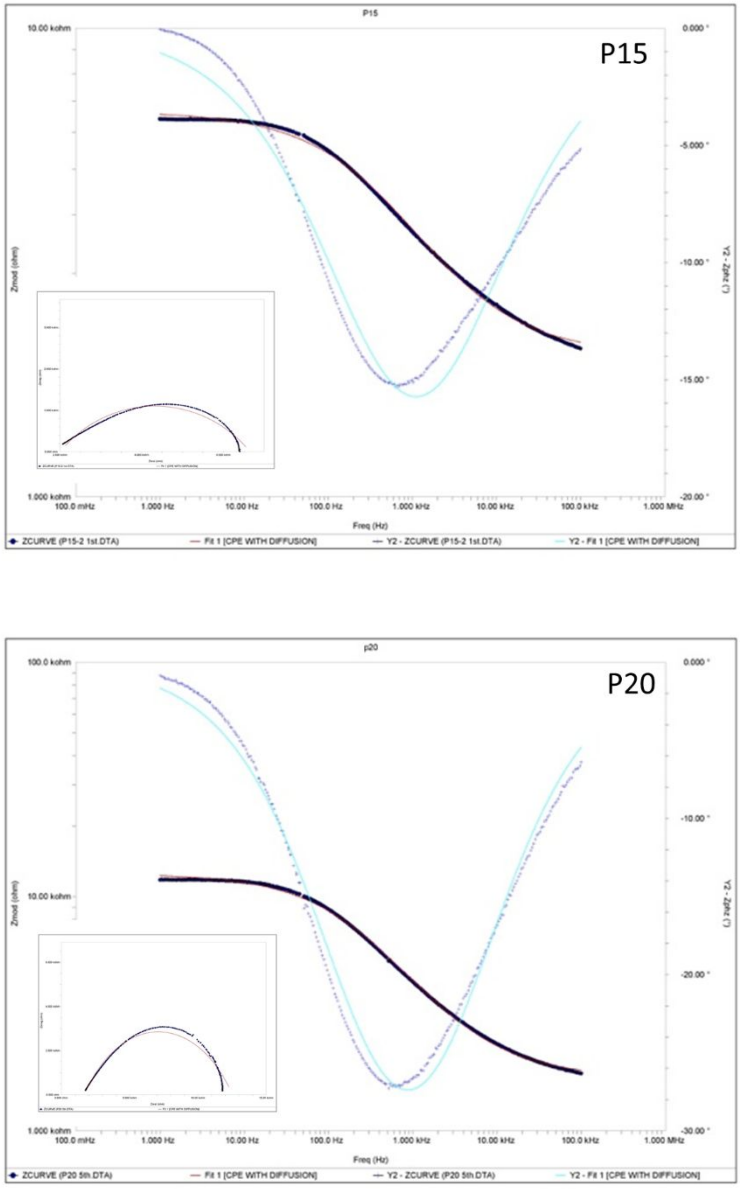

Figure S2. The impedance spectrum (1 Hz to 100 kHz) of poly-Pickering-HIPEs as well as the corresponding regression with an equivalent-circuit model and their Nyquist plot (on the corner of the image)

Determination of the RTD.

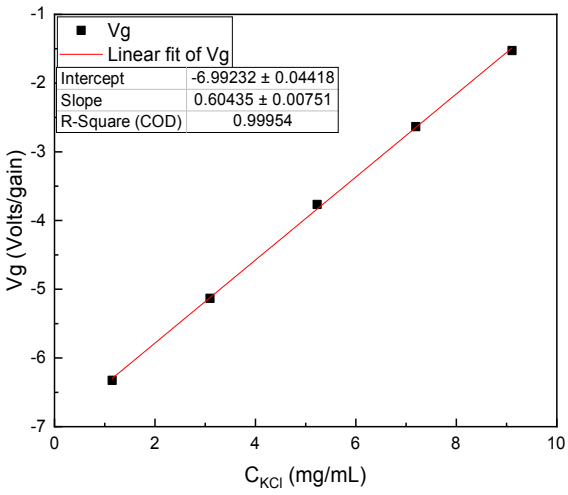

Figure S3: Refractive index increment (dn/dc) of KCl solutions with various concentrations obtained from the refractive index measurement (Vg)

Calibration curve of acetone by UV-Vis Spectroscopy

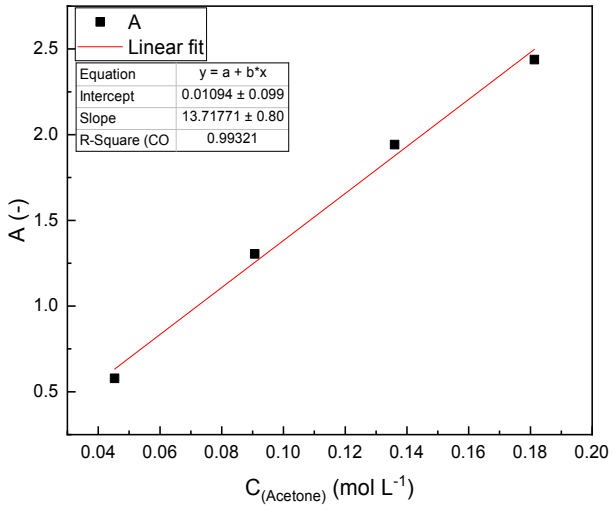

Figure S4. Absorbance of known acetone concentrations in water

Thermal Gravimetric Analysis (TGA) of Poly-Pickering-HIPE monolith

Thermal gravimetric analysis (TGA) of poly-Pickering-HIPEs was performed from room temperature to 800˚C using a TA instrument Discovery TGA (Discovery SA, TA Instrument, Eschborn, Germany) at a heating rate of 10˚C/min in a nitrogen atmosphere.

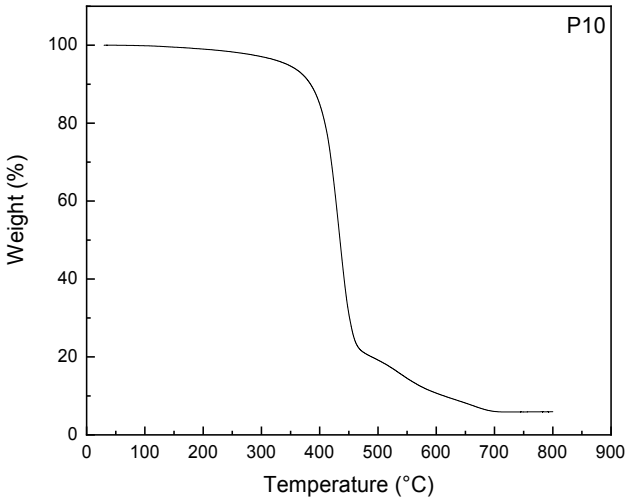

Figure S5. TGA of P10 monolith from 30˚C to 800˚C under N_2 atmosphere

The morphology of poly-Pickering-HIPE

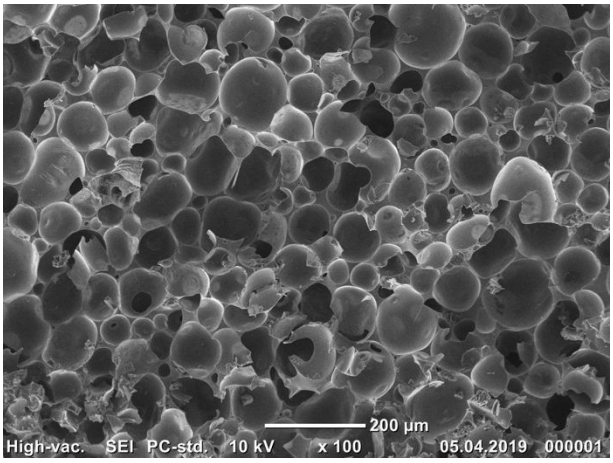

Figure S6. A typical SEM image of poly-Pickering-HIPE produced by polymerization of Pickering-HIPE stabilized with 3 w% HDK H20

Pressure drop measurement over poly-Pickering-HIPE micromixers

A titration burette filled with 60 mL water was connected to P5 poly-Pickering-HIPE micromixer to determine its backpressure and the outlet tube was open to atmospheric pressure. The valve of the burette was opened, and water flowed through the micromixer. Water flow stopped, when the hydrostatic pressure of the water column became equal to the backpressure of the micromixer. The hydrostatic pressure p applied to the micromixer was calculated as follows:

$$p = \rho \cdot g \cdot h \ \#(S3)$$

where ρ is the density of water (997 kg/m^3), g the acceleration due to gravity and h height of the remaining water column. The pressure drop was found as 54.3 mbar for the micromixer fabricated from poly-Pickering-HIPE having the lowest DoI and gas permeability.

The pressure drop of poly-Pickering-HIPE micromixers were determined by injecting water from 0.6 to 4.8 mL/min using a HPLC pump (1290 Infinity HPLC, Agilent Technologies, Österreich GmbH, Vienna, Austria). The pressure drop p of P5 micromixer was derived from the gradient of the linear plot of the pressure p vs. flow rate (Figure S7).

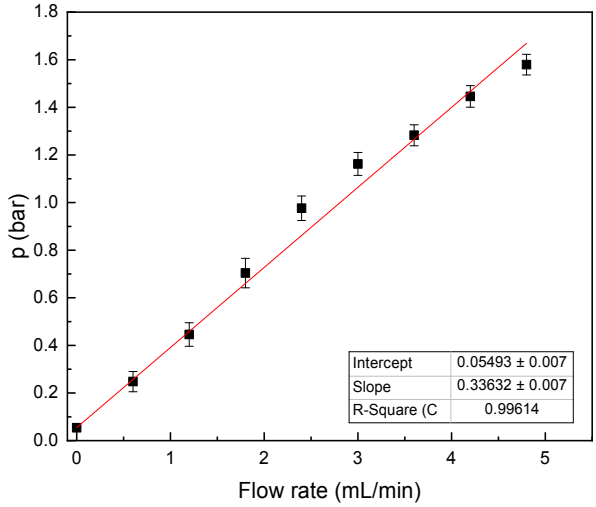

Figure S7. The pressure drop p of P5 micromixer from 0.6 to 4.8 mL/min water flow rate.

RTD of poly-Pickering-HIPE micromixers tested at various injection ratios

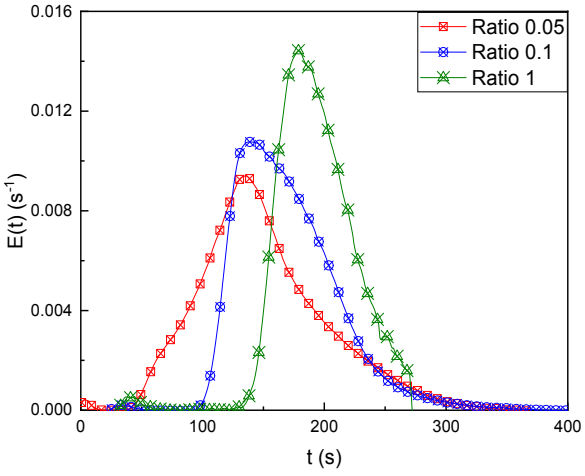

Figure S8. RTD curves of P10 micromixer with a diameter of 12 mm at Q = 1.2 mL/min

RTD of 25 mm diameter poly-Pickering-HIPE micromixer

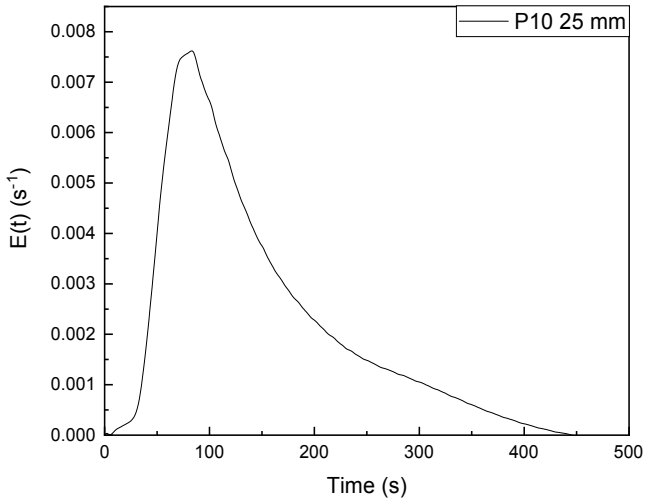

Figure S9. RTD curve of poly-Pickering-HIPE micromixer fabricated from P10 monolith having 25 mm diameter and 30 mm length

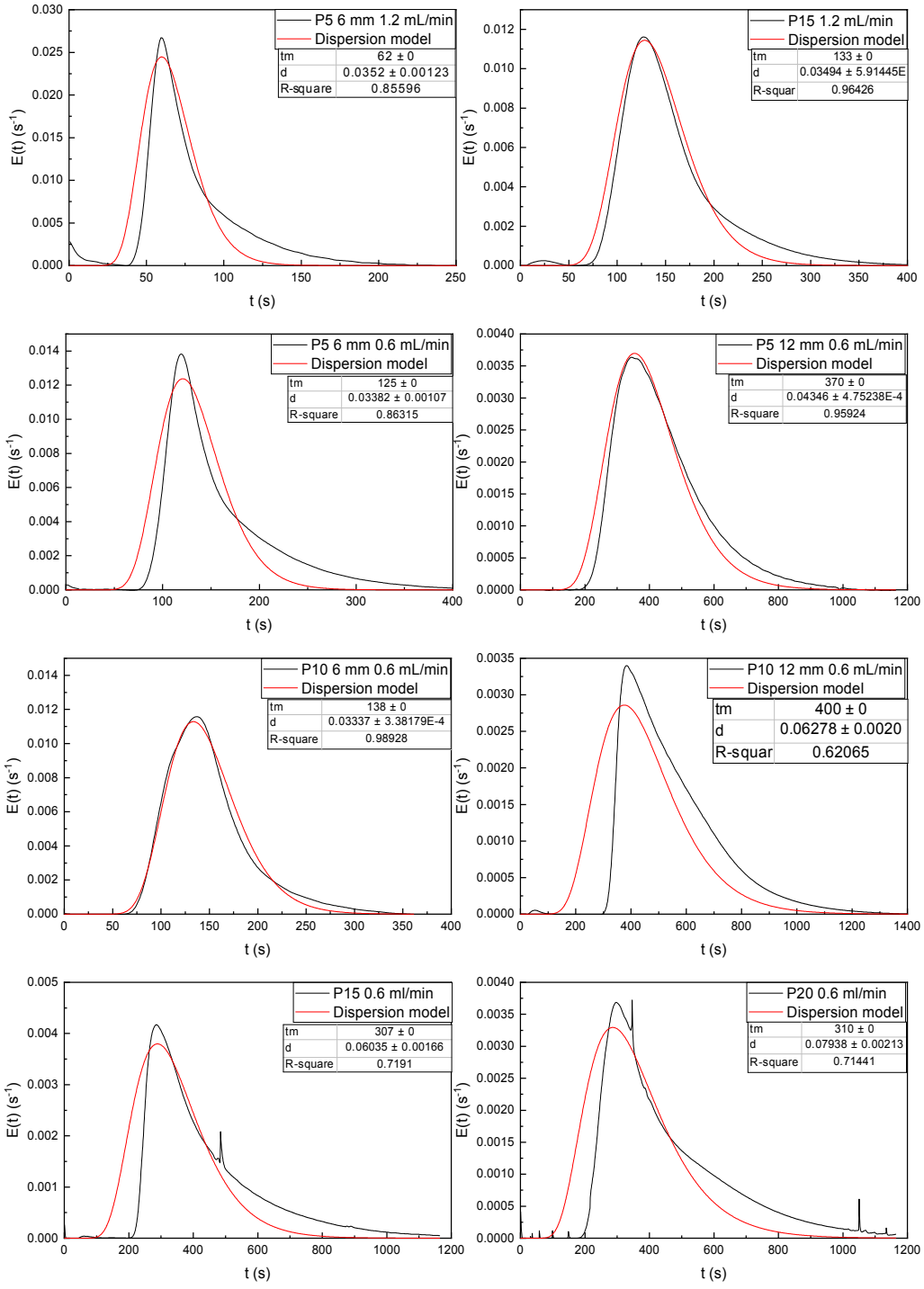

Figure S10. Fittings of the axial dispersion model to RTD ($E(t)$)

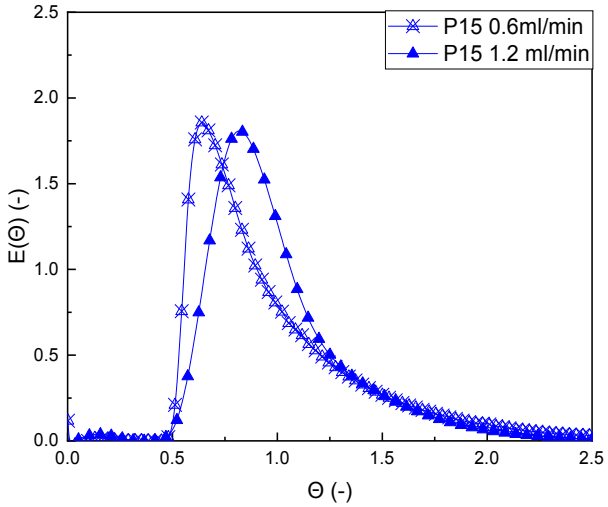

Figure S11. Dimensionless residence time distribution $E(\theta)$ curve

REFERENCES

(1) Manley, S. S.; Steindl, P.; Hewitt, G. F.; Bismarck, A. An Integrated Method for Measuring Gas Permeability and Diffusivity of Porous Solids. *Chem. Eng. Sci.* **2020**, *223*, 115725. DOI: 10.1016/j.ces.2020.115725.

(2) Danninger, D.; Hartmann, F.; Paschinger, W.; Pruckner, R.; Schwödiauer, R.; Demchyshyn, S.; Bismarck, A.; Bauer, S.; Kaltenbrunner, M. Stretchable Polymerized High Internal Phase Emulsion Separators for High Performance Soft Batteries. *Adv. Energy Mater.* **2020**, 2000467. DOI: 10.1002/aenm.202000467.

Chemical Engineering Science 252 (2022) 117296

Publication II

Contents lists available at ScienceDirect

Chemical Engineering Science

journal homepage: www.elsevier.com/locate/ces

Polymerised high internal phase emulsion micromixers for continuous emulsification

Hande Barkan-Öztürk [a], Angelika Menner [a], Alexander Bismarck [a,b,*]

[a] Polymer and Composite Engineering (PaCE) Group, Institute of Material Chemistry and Research, Faculty of Chemistry, University of Vienna, Währinger Strasse, 42, 1090 Vienna, Austria
[b] Department of Chemical Engineering, Imperial College London, South Kensington Campus, London SW7 2AZ, United Kingdom

HIGHLIGHTS

- Emulsion templates were generated with poly-Pickering-HIPE micromixers.
- The porosities of the resulting polyHIPEs were depend on the flow rate ratios.
- Openness of poly-Pickering-HIPEs affects the droplet diameters of emulsions.
- Macroporous polymers having graded porosities were fabricated with micromixers.
- 3D shapes were emulsified, printed and photopolymerised, simultaneously.

GRAPHICAL ABSTRACT

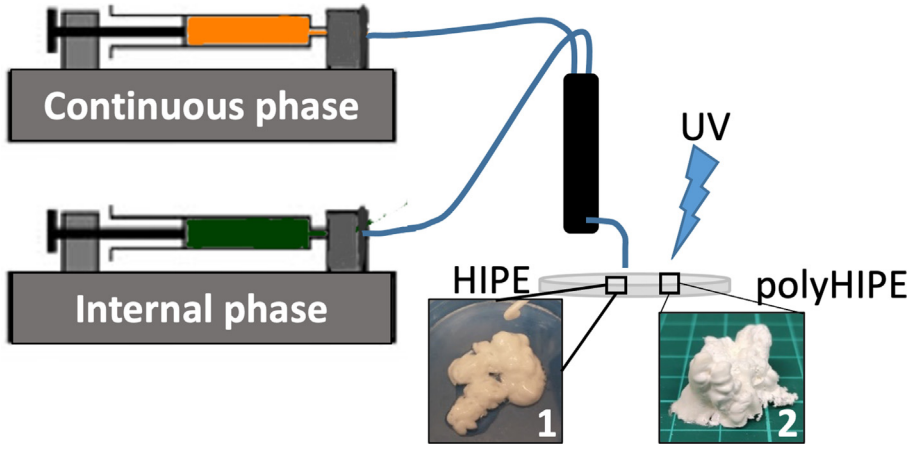

ARTICLE INFO

Article history:
Received 10 July 2021
Received in revised form 3 November 2021
Accepted 18 November 2021
Available online 23 November 2021

Keywords:
Emulsion templating
polyHIPEs
Macroporous polymers
Micromixer
Continuous emulsification

ABSTRACT

Micromixers made from emulsion templated macroporous polymers (poly-Pickering-HIPEs) were used to continuously produce polymerizable high internal phase emulsions (HIPE) by injecting a monomer containing continuous phase and aqueous internal phase into micromixers. The interconnected and complex flow path through poly-Pickering-HIPE micromixers resulted in effective mixing by creating local vortices and shear. The emulsion phase volume fraction of the produced HIPE templates can be varied during the process. PolyHIPEs with a porosity gradient ranging from 74% to 89% were produced by altering the phase volume ratio during emulsification in poly-Pickering-HIPE micromixers. The average pore size of the produced polyHIPEs can be tailored by using poly-Pickering-HIPE micromixers with degrees of interconnectivity ranging from 0.028 to 0.06. The lower the degree of interconnectivity of the micromixer the smaller the droplet size of the produced HIPEs and thus the average pore size of the resulting polyHIPEs.

1. Introduction

Polymerised High Internal Phase Emulsions (polyHIPEs) are macroporous polymers produced by polymerisation of the monomer-containing continuous phase of high internal phase

* Corresponding author at: Polymer and Composite Engineering (PaCE) Group, Institute of Material Chemistry and Research, Faculty of Chemistry, University of Vienna, Währinger Strasse, 42, 1090 Vienna, Austria.
E-mail address: alexander.bismarck@univie.ac.at (A. Bismarck).

https://doi.org/10.1016/j.ces.2021.117296
0009-2509/

emulsions (HIPEs) and subsequent removal of the internal phase, which exceeds 74% of the total volume of the emulsion. (Menner et al., 2006; Cameron, 2005; Foudazi, 2021) Emulsions are used as a template to produce macroporous polymers with tailored mechanical and morphological properties. PolyHIPEs are useful macroporous polymers, which are of interest for a wide range of applications both in laboratories and industries, such as filters, (Ikem et al., 2014) stationary phase in chromatography, (Desire et al., 2017) separators in energy harvesters, (Jiang et al., 2017) in flexible batteries, (Danninger et al., 2020) or as tissue engineering scaffolds, (Owen et al., 2016) or as adsorbent pats in diapers. (Hubbard, 2014) Researchers also started to explore polyHIPEs as a flow-through reactors or micromixers. (Tebboth et al., 2015; Brown et al., 2005; Tebboth et al., 2015; Bolton et al., 2006; Barkan-Öztürk et al., 2021) Tebboth et al. (Tebboth et al., 2015) produced micromixers from polyHIPEs and showed its effectiveness to extract caffeine from an aqueous solution with ethyl acetate.

PolyHIPEs are permeable; When fluids pass through the pore structure of polyHIPEs, the flow is split and recombined at pore throats resulting in well-mixed fluids. (Barkan-Öztürk et al., 2021) Usually micromixers consist of microscale channels, in which the flow is laminar. Fluids to be mixed flow parallel to each other and mixing occurs by molecular diffusion. The high surface-to-volume ratio in microscale channels enhances the contact area between fluids thus improving heat and mass transfer efficiency. (Bayareh et al., 2020) Moreover, the contact area between mixing species, thus the interface for molecular diffusion, can be increased by designing the microchannel allowing to manipulate the flow redirecting it so that small vortices occur along the channel. In general, micromixers have many advantages over macroscale mixers, including better control of physical reaction parameters, fast and controllable mixing, lower energy consumption and, therefore, reduced costs. (Capretto et al., 2011; Nimafar et al., 2012) These advantages of micromixers made them attractive microreactors for continuous production of pharmaceuticals and miniaturized analytical systems for chemistry and biology. (Bayareh et al., 2020; Capretto et al., 2011; Nguyen, 2012) Moreover, micromixers and static mixers were used for laminar flow emulsification. (Christopher and Anna, 2007; Elsing et al., 2017; Kiss et al., 2011) The flow of the oil and water phases is controlled via complex microscale geometries of micromixers, which enable the deformation of the dispersed phase and droplet breakup resulting in stable emulsions. (Christopher and Anna, 2007) Most of these emulsifying micromixers are microfluidic devices, in which droplet formation occurs because the viscous shear forces exceed the interfacial tension force rather than by mixing the fluids. (Capretto et al., 2011; Nimafar et al., 2012; Christopher and Anna, 2007) Droplets are created in such devices by breaking up the dispersed phase using an orifice or an obstacle by co- or cross-flowing streams or stretching dominated flow. However, the production speed is very low (ml h^{-1}) due to the microscale single channel flow, (Christopher and Anna, 2007; Stubenrauch et al., 2018) and furthermore the structure of the micromixer limits the average droplet size of the emulsions to 50 μm. (Elsing et al., 2017; Kiss et al., 2011) On the contrary, static mixers consist of motionless mixer elements that generate emulsions by dividing and re-uniting fluid flow, which can be laminar or turbulent depending on the hydraulic diameter of the device. (Kiss et al., 2011)

Emulsions have found many application areas, including food products,(Muijlwijk et al., 2015) pharmaceutical and agrochemical formulations, as well as paints (Tadros, 2010) or as templates to produce macroporous polymers. (Menner et al., 2006) In order to create a stable emulsion, an interface between the immiscible phases needs to be created and stabilised. The interface is generally produced by turbulent agitation methods both in industry and laboratory (Menner et al., 2006; Foudazi, 2021; Paul et al., 2004) and stabilised using suitable emulsifiers, such as surfactants or particles. According to Kolmogorov (Kolmogorov, 1949) and Hinze, (Hinze, 1955) large shear and pressure gradients lead to droplet break-up of liquid–liquid dispersions in turbulent flow by generating eddies in the fluid usually by homogenizers, ultrasonicators or mixing devices. Static mixers are also used to create emulsions continuously in either laminar or turbulent regime. (Kiss et al., 2011) However, according to the literature their application is mainly limited to dilute systems with less than 35 vol%. (Chabanon et al., 2017) HIPEs were produced using T-shape junction microfluidic devices using cross-flowing streams, (Montillet et al., 2013) flow focusing devices, (Elsing et al., 2017; Costantini et al., 2019) or co-flow geometries. (Lapierre et al., 2015; Gokmen et al., 2009) However, the droplet size of those HIPEs was strongly dependent on the orifice and channel diameters of the microfluidic devices, their flow rates and also the rheological properties of the phases. (Costantini et al., 2019; Gokmen et al., 2009; Kim et al., 2014) Another bottleneck of microfluidic devices is that the dispersed phase volume fraction of the produced emulsions cannot be tailored during emulsification. Thus in order to produce HIPEs it is necessary for the emulsion droplets to sediment at the end of the emulsification to achieve the desired volume fraction followed by removal of excess continuous phase, which limits the applicability of the process. (Elsing et al., 2017; Dabrowski et al., 2020)

Alternatively, polyHIPE monoliths can be used as micromixers because of their interconnected 3-dimentional porous structure in which miscible fluids can be successfully mixed in laminar flow regime. (Barkan-Öztürk et al., 2021; Tebboth et al., 2015) The interconnected structure of polyHIPEs redistributes fluids through the pore throats in the radial direction, thereby creating eddies in the fluid by the pressure drop between pores across pore throats. Increased shear and pressure gradients can cause droplet break-up, which leads to liquid–liquid dispersion and, therefore, emulsification. We quantified the micromixing performance of high porosity, permeable poly-Pickering-HIPEs, which were produced by polymerisation of Pickering-HIPE templates stabilised by hydrophobized silica nanoparticles. (Barkan-Öztürk et al., 2021)

Herein we show that poly-Pickering-HIPE micromixers can be used to produce HIPEs continuously. HIPEs were created faster than most used flow-focusing microfluidic devices with an adjustable emulsion phase volume fraction. (Christopher and Anna, 2007; Costantini et al., 2014) We analysed the effect of flow rate, immiscible fluid ratio and the morphology of poly-Pickering-HIPE micromixers on the average droplet size, which was studied after polymerisation of the produced HIPE templates. (Lissant, 1966) Moreover, we will prove that the three-dimensional structure of poly-Pickering-HIPE micromixers is well suited to create highly viscous emulsions, which can be used directly as ink in printing processes. We will also demonstrate that it is possible to produce a continuous porosity gradient in macroporous polymers by changing the flow parameters during emulsification.

2. Experimental section

2.1. Materials

Styrene (St) ≥ 99%, divinylbenzene (DVB) 80%, α,α′-azoisobutyronitrile (AIBN), calcium chloride dihydrate ($CaCl_2{\cdot}2H_2O$) ≥ 99%, sorbitan monooleate (Span 80), ethylhexyl acrylate (EHA), ethylene glycol dimethacrylate (EGDMA) were purchased from Sigma-Aldrich. Hydrophobic pyrogenic silica particles HDK H20 were kindly provided by Wacker Chemie AG (Germany), polyurethane diacrylate (Ebecryl 8402, PUDA) by Cytec (Diegem, Belgium) and

the surfactant Hypermer B246 by Croda (East Yorkshire, UK). 2-Hydroxy-2-methyl-1-phenyl-propan-1-one (Darocur 1173) was purchased from BASF (Kaisten, Germany). Araldite rapid adhesive was purchased from Rapid Electronics Limited (Essex, UK) and Araldite 2020 from Farnell Element14 (Salzburg, Austria). The shrink tube was supplied by Conrad Electronic GmbH (Vienna, Austria). All materials were used as received.

2.2. Preparation of poly-Pickering HIPEs

The procedure for the preparation of poly-Pickering-HIPEs was described in detail elsewhere. (Barkan-Öztürk et al., 2021) Briefly, the continuous phase (CP) of Pickering-HIPEs was prepared by homogenising styrene and DVB (1:1) and 3% (w/v) HDK H20 using a dispenser (Kinematica POLYTRON PT 1600 E, Malterz, Switzerland) for 15 min at 15,000 rpm. Afterwards, the mixture was transferred into a reaction vessel and 1 mol% AIBN (with respect to the double bonds of the monomers) was added. The aqueous internal phase contained 40 g/L $CaCl_2$ and was added slowly into the CP under constant agitation at 400 rpm. After complete addition of dispersed phase, the mixture was emulsified at 400 rpm for 3 min. To obtain interconnected poly-Pickering-HIPEs, (Ikem et al., 2010) different amounts of surfactant (Span 80) (5, 10, 15 or 20 vol% with respect to the continuous phase amount) were added to the Pickering-HIPEs and mixed for an additional 30 s to disperse the surfactant. Afterwards, the emulsions were transferred from the reaction vessel into polypropylene centrifuge tubes (D_i = 12 mm) and polymerised at 70 °C in a convection oven for 4 h. Afterwards, the monoliths were removed from the tubes and washed with water and then with acetone to remove the electrolyte and impurities, respectively. Monoliths were called P05, P10, P15 and P20 based on the surfactant amount added to the Pickering-HIPEs formulation.

2.3. Preparation of poly-Pickering-HIPE micromixers

The micromixers were designed heuristically by placing the inlets and outlet tubes into various places in poly-Pickering-HIPE monoliths as shown in Fig. 1 to access their emulsification performance. Initially, two holes for inlet tubes were drilled to a depth of 5 mm in 3 different positions into the top of the monolith as indicated in **Figure 1.1** (positioned vertical V and horizontal H). In total, three different arrangements for the inlet tube positions were tried; parallel to each other on top of the monolith (V1 and V1), or perpendicular to each other (V1 and H2), of which one of the tubes was on top, the other 5 mm below the top of the monolith as well as opposite to each other 5 mm below the top of the monolith (H1 and H2). Two PTFE 1/16″ tubes were sealed into the holes with highly viscous Araldite® Rapid two-phase epoxy resin. The same procedure as described above was performed for the outlet tube (position O1 and O2 were tested). The monolith surface was sealed with highly viscous epoxy resin to create an impermeable barrier (**Figure 1.2**). The sealed monolith was placed into a heat shrink tube to provide extra protection (**Figure 1.3**). Finally, the feed tubes were additionally sealed with Araldite® 2020 (**Figure 1.4**) and the epoxy resin was cured in a convection oven at 70 °C for 4 h.

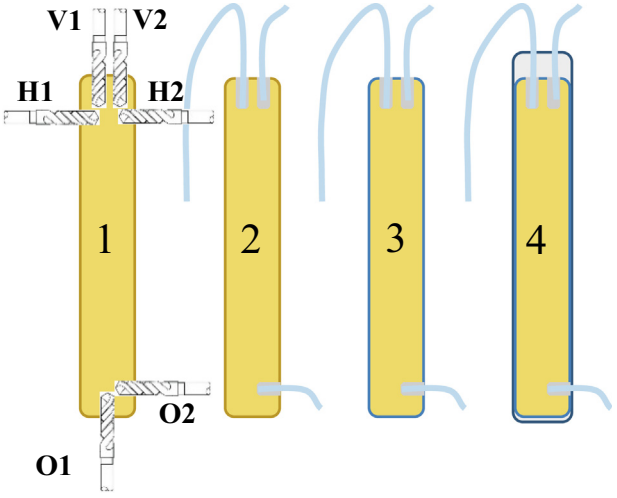

Fig. 1. Schematic showing the fabrication process of poly-Pickering-HIPE micromixers: 1) drilling inlet and outlet connector holes (V for vertical placing, H for horizontal and O for outlet tube positions), 2) sealing the tubes into the drilled holes with epoxy resin, 3) covering the outer surface of the monolith with epoxy resin, 4) sealing with shrink tube and pouring epoxy resin on top of the flow cell.

The micromixing performance of poly-Pickering-HIPE micromixers was characterised in previous work. (Barkan-Öztürk et al., 2021)

2.4. Experimental setup of emulsification with poly-Pickering-HIPE micromixers

Continuous emulsification of an aqueous and organic (monomer) phase using poly-Pickering-HIPE micromixers was performed in the setup schematically shown in Fig. 2. The micromixer was connected to two syringes placed into syringe pumps (PHD Ultra, Harvard Apparatus, UK, and Masterflex® Touch-Screen Syringe Pump, Cole-Parmer, Germany, respectively) via separate inlet tubes. One syringe contained monomers, surfactant and initiator and the other aqueous electrolyte (Table 1). The flow rates of the aqueous internal phase (IP) and organic monomer phase (CP) was varied between 0.1 and 3 mL/min. We confirmed that total flow rate is the sum up of individual flow rates (**Table S1-3**). To identify the optimal micromixer design for emulsification, P5 and P10 micromixers fabricated using the designs shown in **Figure 1.1** were tested using a PUDA-EHA mixture as CP and an aqueous IP using flow rates of 0.2 and 0.6 mL/min, respectively. The most effective micromixer design was found to be design 4 in Fig. 1, where inlets were positioned vertical (V1-V2) at the top and outlet horizontally into the bottom part of the micromixer (O2). HIPEs were produced using three different CP formulations (Table 1) at various flow rates and flow ratios between CP and IP (see ESI **Table S1-3**). Emulsions were collected at the outlet tube after the mean residence time t_m of the liquids in the micromixers (Table 2) and polymerised either by UV initiation using a UV pen (365 nm, 5% intensity, UV-Gröbel GmbH, Ettlingen, Germany) placed 2 cm away or in an oven operated at 70 °C depending on the initiator used in the formulation (Table 1). The pressure drop along the poly-Pickering-HIPE micromixers was measured using a pressure transducer (Tecsis GmbH, Offenbach am Main, Germany) fitted between both CP and IP syringes and micromixer during emulsifications (**Table S4-5**). Between each set of experiments the micromixers were rinsed with water. At the end of the emulsification, micromixers were cleaned by injecting water followed by ethanol. Each micromixer was used at least 10 times and re-tested 3 months later after the first set of experiments.

The energy dissipation rate ε (W/kg) per unit mass of fluid is related to the pressure drop Δp across a micromixer and the flow rate Q as follows: (Falk and Commenge, 2010)

$$\varepsilon = \frac{Q \cdot \Delta p}{\rho \cdot V} \quad (1)$$

where ρ is the average density of the emulsion, and V the fluid volume in the micromixer. The energy dissipation rate for HIPEs pro-

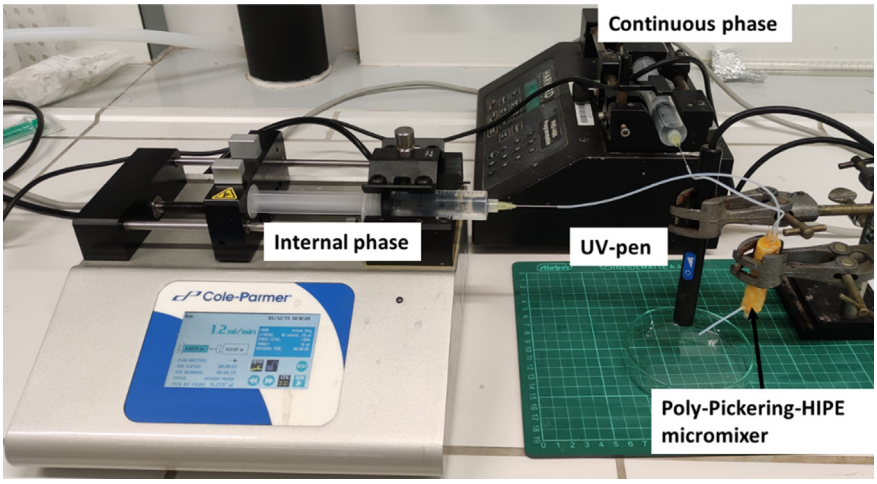

Fig. 2. Photo showing the experimental setup used for continuous HIPE production in a poly-Pickering-HIPE micromixer followed by subsequent UV polymerisation of the HIPE template.

Table 1
Formulations of CP and IP used to produce HIPEs using poly-Pickering-HIPE micromixers.

Formulation name	CP							IP
	monomer		crosslinker		surfactant		initiator	
	name	vol%	name	vol%	name	vol%	name	g/L $CaCl_2$
PUDA-EHA	EHA	60	PUDA	36	B246	3	Darocur 1173	10
EGDMA-EHA	EHA	57.5	EGDMA	38.5	B246	3.5	Darocur 1173	40
St-DVB	St	66.6	DVB	16.5	Span 80	16.5	AIBN	40

Table 2
Effect of increasing surfactant volumes added to primary Pickering-HIPE templates on the morphology descriptors (average pore d_p and pore throat diameter d_{pt}, degree of interconnectivity (or openness) *DoI*, and porosity *P*) as well as gas permeability *k* and mean residence time t_m of poly-Pickering-HIPE micromixers.

Sample	d_p μm	d_{pt} μm	*DoI* $\cdot 10^{-2}$	*P* %	*k* $\cdot 10^{-12}$ m^2	t_m s
P05	78 ± 38	12 ± 9	2.8 ± 0.6	84.3 ± 0.4	0.4 ± 0.1	195 ± 14
P10	80 ± 29	20 ± 12	4.3 ± 0.2	86.7 ± 1.2	1.5 ± 0.2	233 ± 8
P15	96 ± 33	17 ± 10	4.6 ± 0.7	87.2 ± 0.5	3.2 ± 0.5	151 ± 6
P20	68 ± 30	13 ± 8	6 ± 0.8	88.2 ± 1.2	3.7 ± 0.1	197 ± 5

duced using a conventional stirrer emulsification method is described in **ESI S1**.

2.5. Characterisation of poly-Pickering-HIPEs and polyHIPEs

2.5.1. Determination of morphology of poly-Pickering-HIPE micromixers and polyhipes

The morphology of the poly-Pickering-HIPE micromixers and polyHIPEs produced by polymerisation of HIPEs produced using the poly-Pickering-HIPE micromixers was investigated using scanning electron microscopy (SEM, JCM-6000, JEOL GmbH, Eching, Germany). Fractured sample surfaces were gold coated using JFC-1200 (JEOL GmbH, Eching, Germany) to guarantee sufficient electrical conductivity. SEM images were further analysed using an image analysis software package (ImageJ©, https://imagej.nih.gov/ij/download.html) to determine the average pore (d_p) and pore throat (d_{pt}) sizes of the samples. At least 100 pore and pore throat diameters were measured. The average degree of interconnectivity (*DoI*) of poly-Pickering-HIPEs was calculated as described by Pulko and Krajnc: (Pulko and Krajnc, 2012)

$$DoI = \frac{N \cdot d_{pt}^2}{4 \cdot d_p^2}. \quad (2)$$

where *N* is the average number of pore throats per pore. The Sauter mean pore diameter (d_{32}) of polyHIPEs produced by polymerisation of HIPEs generated with micromixers was calculated as follows:

$$d_{32} = \frac{\sum_{i=1}^{n} d_{p_i}^3}{\sum_{i=1}^{n} d_{p_i}^2}. \quad (3)$$

2.5.2. Density of poly-Pickering-HIPEs and polyHIPEs

The skeletal density (ρ_s) of poly-Pickering-HIPEs and polyHIPEs was determined using helium pycnometry (Accupyc 1330, Micrometrics, Dunstable, UK) using ground (about 0.1 g) samples. The foam density (ρ_f) of the poly(-Pickering-)HIPEs was analysed using an envelope density analyser (Geopyc 1360, Micrometrics, Dunstable, UK). The porosity of the monoliths was calculated as follows:

$$P\% = \left(1 - \frac{\rho_f}{\rho_s}\right) \cdot 100. \quad (4)$$

However, the porosities of the poly-(PUDA-EHA)H/MIPEs prepared by polymerisation of M/HIPEs produced using our micromixers could not be determined using the envelope density analyser because of their high compressibility. (Jiang et al., 2017) Therefore,

their foam densities were measured by cutting them into cuboids. The specimens were weighed and their dimensions measured from these values the foam density (ρ_f) was calculated:

$$\rho_f = \frac{m}{V}. \quad (5)$$

where m is the sample weight and V the sample volume. Their porosities were calculated using Eq. (4).

2.5.3. Viscosity of continuous emulsion phases and HIPE templates

The viscosity of the continuous HIPE phases (St-DVB, PUDA-EHA and EGDMA-EHA) was measured using a rheometer (Discovery Hybrid Rheometer HR-3, TA Instrument, Eschborn, Germany) equipped with a cone-cup geometry at 25 °C. The gap between rotor and cylinder was 0.52 mm. The dynamic viscosity of CPs was measured using a shear rate sweep between 10^{-2} s^{-1} and 100 s^{-1}. The rheology of HIPEs was measured using a shear rate sweep between 10^{-1} and 1000 s^{-1} for St-DVB as CP and 10^{-2} and 100 s^{-1} for HIPEs with a CP containing PUDA-EHA (Fig. S2-3).

3. Results and discussion

3.1. The morphology of poly-Pickering HIPEs

Macroporous polymers produced from Pickering-HIPEs stabilised by nanoparticles to which surfactant was added possess an interconnected structure (Fig. 3 and **Figure S1**). Having the same dispersed phase volume fraction and formulations (except the surfactant volume) resulted in poly-Pickering-HIPEs with the same porosities and average pore and pore throat diameters within error (Table 2). Varying the surfactant volume, which was added to the Pickering-HIPE template after emulsification, allowed to vary the *DoI* (or openness) of the poly-Pickering-HIPEs; an increasing *DoI* resulted in an increased gas permeability (Manley et al., 2020) of the monoliths (Table 2). Emulsions were produced continuously using our poly-Pickering-HIPE micromixers, whose micromixing performance was quantified in our previous work. (Barkan-Öztürk et al., 2021) We determined that an increasing *DoI* of poly-Pickering-HIPEs enhanced the radial dispersion of micromixers resulting in a higher tailing and asymmetry in their residence time distribution curve, which led to a larger deviation from the axial dispersion model. (Barkan-Öztürk et al., 2021)

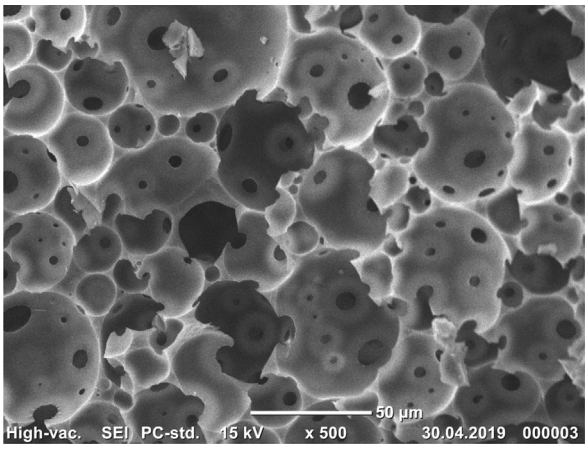

Fig. 3. Characteristic SEM image of poly-Pickering-HIPE (P5) prepared by polymerisation of the continuous phase of Pickering-HIPE templates to which 5 vol% surfactant had been added.

3.2. Effect of micromixer design

Poly-Pickering-HIPE micromixers were fabricated by placing an outlet tube into the bottom part of the monolith parallel to the inlet tubes (**Figure 1.1, O**1). Unfortunately, having the inlet tubes and outlet tube in the same direction resulted in fewer obstacles to redirect the flow, thus effective mixing could not be achieved. However, highly viscous HIPEs were obtained by placing the outlet tube in the side wall of the monolith 5 mm above its base (**Figure 1.1, O**2). In this case, the outlet tube is not facing the flow direction. Hence, the produced emulsion is redirected perpendicular to the flow causing additional mixing in the bottom part of the micromixer, resulting in a continuous stable emulsion stream.

3.3. Producing HIPEs using poly-Pickering-HIPE micromixers

The injected aqueous IP and monomer CP were effectively emulsified in a poly-Pickering-HIPE micromixer after the mean residence time (Table 2) as can be seen in the measured pressure drop across the micromixer (**Figure S2**). **Figure S2** shows the pressure drop across a P20 micromixer during formation of a stable water-in-St-DVB HIPE with an internal phase volume ratio of 83.3% (Fig. 4**a-b**); Please note that the initial pressure increase is due to the formation of water droplets in the monomer phase while the subsequent pressure drop is due to the shear thinning behaviour of the formed HIPE (Fig. S3-4). Also noticeable are pressure fluctuations which were caused by partial pore (throat) blocking by larger droplets prior to droplet breakup. (Cobos et al., 2009; Romero, 2009) Doubling the total flow rate caused a slight increase of the steady-state pressure drop across the micromixer from 0.56 bar to 0.63 bar (**Figure S2**; **Table S4**). The viscosity of the produced HIPE increased when doubling the total flow rate (from 1.2 mL/min to 2.4 mL/min) resulting in a higher shear rate (**Table S4-5**) causing droplet breakup and thus a higher resistance against flow (Fig. 4**a** showing a creamy HIPE and highly viscous mayonnaise-like HIPE in Fig. 4**b)**. Moreover, the HIPE did not spread on a glass plate because of its high viscosity (Fig. 4**b**), which can be helpful to produce 3-dimensional objects when polymerising its CP subsequently. The increased flow rate and thus increased shear (**Table S4-5**) caused the breakup of larger droplets resulting in a narrower droplet size distribution (as discussed below). Even though the energy dissipation rate during emulsification increased from 1.85 W/kg to 4.16 W/kg, the Sauter diameter d_{32} of the produced HIPEs remained identical within error. The increased flow (and thus shear) rate resulted in a reduction of the number of large droplets with size around 50 µm (Fig. 4**c-d**). Cobos et al. (Cobos et al., 2009) and Romero (Romero, 2009) already showed that emulsions can be produced in capillaries with decreasing diameter and in porous media, respectively, where droplet breakup was caused by partial pore blocking phenomena occurring when forcing immiscible fluids through flow constrictions. When a fluid volume (of a multiphase fluid) is forced though the pore throats of poly-Pickering-HIPE micromixers, acting as orifice in a tube, both in the axial and radial flow direction, pore blockage did occur resulting in an increased pressure drop across the micromixer (**Figure S2**) and thus in droplet elongation and breakup and, hence, the formation of emulsions. Further discussions on possible droplet breakup mechanisms can be found in **ESI S3** (and associated **Tables S4-5**).

After polymerisation of these HIPEs in a centrifuge tube and subsequent purification and drying, interconnected polyHIPEs were obtained (Fig. 4**c-d**), which had a porosity of 86% slightly higher than their nominal phase volume ratio (flow rate ratio which is determined by the flow ratio of CP:IP, in this case 1:5) because the surfactant used was removed during the purification. Methacrylate-based (Dabrowski et al., 2020) and St-DVB based

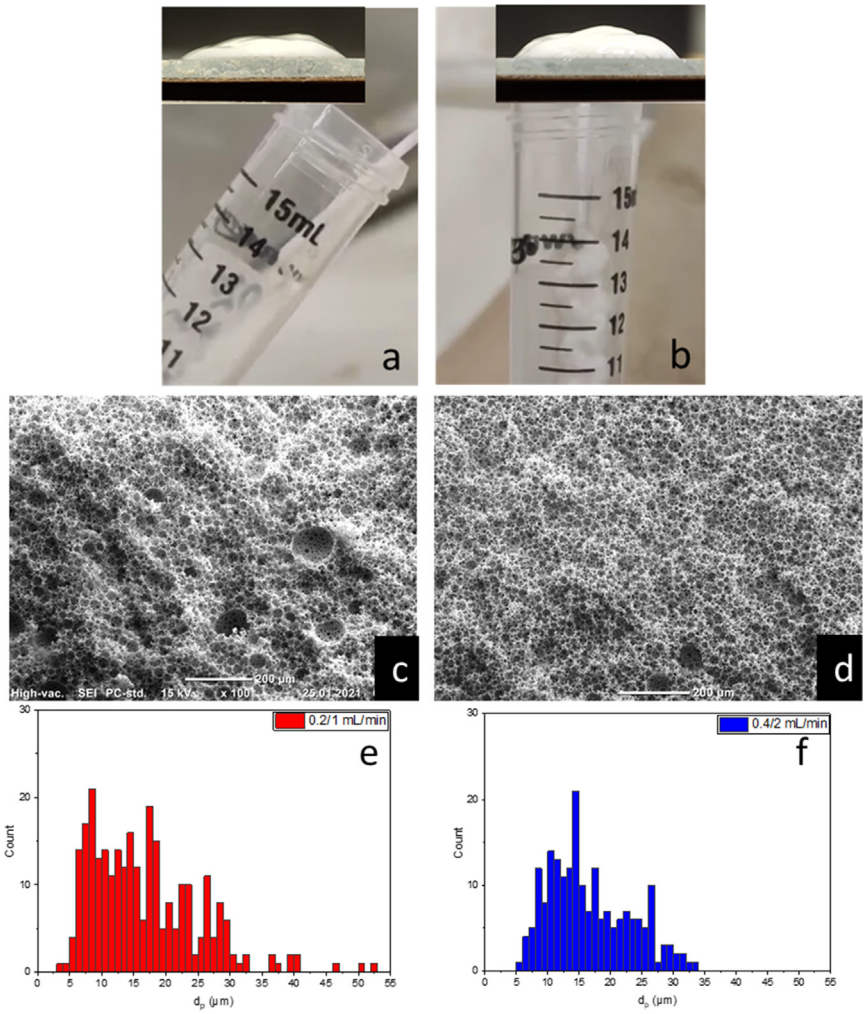

Fig. 4. Photographs of water-in-St-DVB HIPEs generated using a P20 micromixer at a) a flow rate ratio of CP/IP of 0.2/1 mL/min and b) of 0.4/2 mL/min. The inserts show HIPEs applied onto a glass substrate. Videos (ESI **Video S1 and S2**) showing the production of HIPEs shown in a) and b) are included in the ESI. Characteristic SEM micrographs c) and d) of poly(St-co-DVB)HIPEs produced by polymerisation of the HIPEs shown in a) and b). e) and f) show the pore size distribution of produced polyHIPEs, templated by HIPE droplets and thus reflecting the original droplet size distribution in the emulsion template.

(Quell et al., 2015) emulsions were produced using a flow-focusing microfluidic device by injecting a 1:1 ratio of IP and CP. However, prior to polymerisation of the emulsion templates the droplets were required to sediment to produce polyHIPEs with a porosity of 74%. The use of flow-focusing microfluidic devices does not allow to alter the internal phase volume ratio and, thus, porosity gradients cannot be produced. (Dabrowski et al., 2020; Quell et al., 2015)

The average pore diameters of our polyHIPEs (Fig. 4**c-d**), were templated by droplets with indentical Sauter mean dimeters (Eq. (3)) (23.4 ± 1.7 µm and 22.3 ± 0.7 µm) and did not depend on flow rate. Even though the increased flow rate did not have any effect on the average droplet diameter (which were determined after polymerisation of the HIPEs from the pore diameters following Lissant's suggestion (Lissant, 1966), the HIPEs produced with a lower total volume flow rate (1.2 mL/min) possessed a broader droplet diameter distribution (Fig. 4**e-f**) as can be seen in the low magnification SEM micrographs of the polyHIPE produced (Fig. 4**c-d**).

Fig. 5 shows the average pore sizes of poly(St-co-DVB)HIPEs produced by polymerisation of w/St-DVB HIPEs made using P5 (Fig. 5**A**) and P20 (Fig. 5**B**) micromixers. It is apparent that HIPEs produced using P5 micromixers possessed a smaller average droplet diameter as compared to those produced using P20. Increasing the *DoI* (or openness) of poly-Pickering-HIPE micromixers from 0.03 to 0.06 (P20 and P5, respectively) results in higher radial mixing but also lower shear rates resulting in less droplet breakup by forcing the fluids between pores through larger and more pore throats in a P20 micromixer. Nevertheless, d_p of poly(St-co-DVB) HIPEs produced by polymerisation of HIPEs made using poly-Pickering-HIPE micromixers remained similar when increasing the total flow rate (Fig. 5, **Figure S5** and **Table S1**); only a slight decrease of the average d_p with increasing total flow rate can be seen when using P10 and P20 as microemulsification device. When using a P5 micromixer the total flow rate could not be increased above 1.4 mL/min because of its low *DoI*, which resulted in a significant backpressure. However, w/St-DVB HIPEs could be produced up to total flow rate of 2.4 mL/min using P20 micromixers having the highest *DoI* without significant backpressure on the syringe pumps. Literature reports the production of emulsions with different droplet diameters by altering the orifice and channel dimensions of microfluidic emulsification devices, which can only be minimized up to hundreds of micrometres because of limitations of their production techniques. (Elsing et al., 2017; Kim et al., 2014; Costantini et al., 2014) The orifice diameter of those micromixers affect the average droplet size and as far as we know, HIPEs with the same formulation, after polymerisation polyHIPEs,

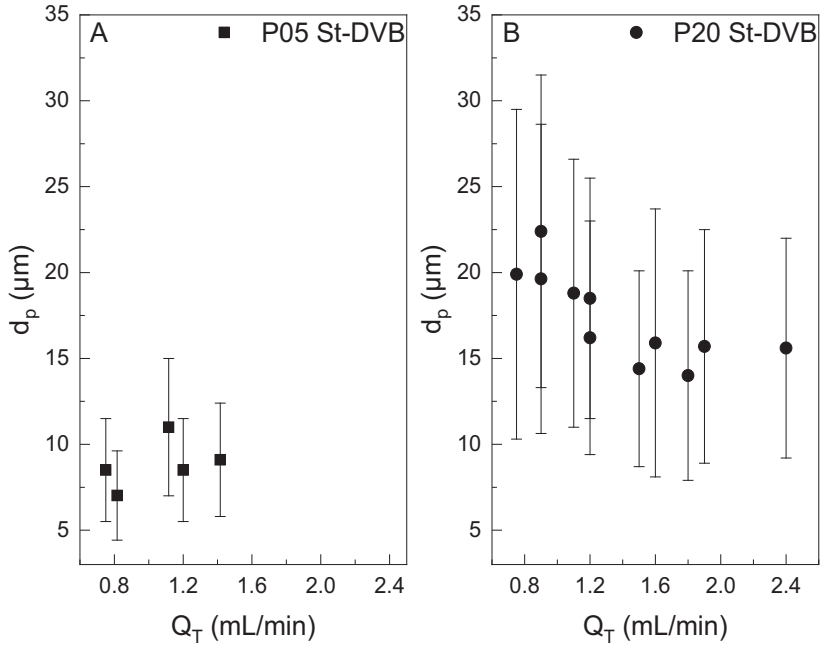

Fig. 5. Average pore diameter d_p of poly(St-co-DVB)HIPEs synthesised by polymerisation of emulsions produced using various total flow rates using P05 (A) and P20 (B) micromixers.

having d_p of less than 60 μm diameter were not reported. (Elsing et al., 2017) However, using poly-Pickering-HIPE microemulsification devices enabled the direct production of HIPE (without the need for droplet sedimentation) with much smaller average droplet diameters, which after polymerisation resulted in poly(St-co-DVB)HIPEs with an average d_p in the range of 5 to 22 μm (Fig. 5). Moreover, P10 and P15 micromixers were used to produce w/St-DVB HIPEs confirming that the average d_p of the poly(St-co-DVB) HIPEs produced by polymerisation of emulsion templates decreased with decreasing *DoI* of poly-Pickering-HIPE monoliths employed as micromixers (**Figure S6)**.

Acrylate-based HIPE templates can be UV polymerised and thus printing of HIPE templates can be used to create net-shaped polyHIPEs. (Jiang et al., 2017) Emulsification of an aqueous electrolyte in PUDA-EHA was tested to create 3D shapes by photopolymerising the continuous emulsion phase (ESI **Video S3**). It was possible to print a cage pattern when fitting the microemulsification device into the movable head of a CNC machine (Stepcraft 420 Construction Kit, Iserlohn, Germany) allowing for the continuous production of a w/PUDA-EHA HIPE with a phase volume ratio of 75% at a total flow rate of 0.8 mL/min, which was printed and immediately UV polymerised (see upper corner of Fig. 6**a**). With increasing total flow rate, we observed again an increase of the HIPE viscosity. The high viscosity of the w/PUDA-EHA HIPEs enabled us to print complex 3D shapes, which could be photopolymerised into poly(PUDA-co-EHA)HIPEs (Fig. 6**b**).

As discussed above, also in case of the microemulsification of w/PUDA-EHA the morphology of the micromixers (Table 2) affected the drop breakup. w/PUDA-EHA HIPEs were produced using poly-Pickering-HIPE micromixers at various flow rates and flow ratios (ESI **Table S2**). The average droplet sizes, and thus d_p of the resulting polyHIPEs increased from 5 μm to 14 μm with increasing *DoI* of the poly-Pickering-HIPE micromixers at the same flow rates (Figs. 7 and 8 and **Figure S7**). Methacrylate-based HIPEs were generated using a flow focusing microfluidic device. (Dabrowski et al., 2020) After polymerisation of these HIPEs the resulting polyHIPEs possessed average d_p ranging from 70 μm to 120 μm, which is much larger than d_p of polyHIPEs that we produced from acrylate-based HIPEs using poly-Pickering-HIPE micromixers. In general, during droplet breakup, droplets are stretched and thinned, which causes them to breakup, which depend on the critical capillary number and viscosity ratio between the IP and CP, as well as physical parameters of the micromixer. (Grace, 1982) The orifice of their flow-focusing microfluidic device was 100 μm, (Dabrowski et al., 2020) while the pore throats of our poly-Pickering-HIPE micromixers were approximately 15 μm, which results in increased shear on the droplets leading to smaller droplets when compared to flow-focusing micromixers. We also compared d_{32} of our polyHIPEs with those produced by polymerisation of HIPEs made using our standard emulsification procedure (i.e. with an overhead stirrer) using the same formulation at different agitation rates (400 rpm, 1000 rpm and 2000 rpm) resulting in increased energy dissipation (Fig. 8; **Eq. (1)** and **Eq. S1**). Poly(PUDA-co-EHA)HIPEs produced by polymerisation of HIPEs made using an agitation rate of 400 rpm had a Sauter pore diameter of 10 μm, which was comparable to that of polyHIPEs prepared from HIPEs made using the P15 micromixer operated at a total flow rate of 1.2 mL/min, or when using P10 at 0.8 mL/min and P15 at 1.5 mL/min (**Figure S7**). PolyHIPEs made from HIPEs created using the P5 micromixer operated at total flow rate of 1.5 mL/min had d_{32} of 6 μm, which was similar to d_{32} of polyHIPEs produced from HIPEs emulsified at 1000 rpm (Fig. 8). The increase in the flow rate resulted in a higher energy dissipation rate along the micromixer, causing d_{32} of HIPEs (and thus polyHIPEs) to decrease. The critical capillary number Ca_{crit} (**Table S5**) and the viscosity ratio between IP and CP ($\lambda = \eta_{IP}/\eta_{CP}$) determine the droplet breakup by shear forces in laminar flow. (Grace, 1982) However, Ca_{crit} was between 0.0013 and 0.0028 for the emulsification of water-in-PUDA-EHA with poly-Pickering-HIPE micromixers (**Table S4-5**), which was significantly lower compared to Grace's droplet breakup model in laminar flow . (Grace, 1982) Therefore, elongational forces need to be considered for the droplet breakup in poly-Pickering-HIPE micromixer (ESI S3). d_{32} of water droplets in St-DVB HIPEs (determined after polymerisation from SEM images) was not affected by doubling of the total flow rate during the emulsification. However, d_{32} of w/PUDA-EHA HIPEs decreased significantly with increasing

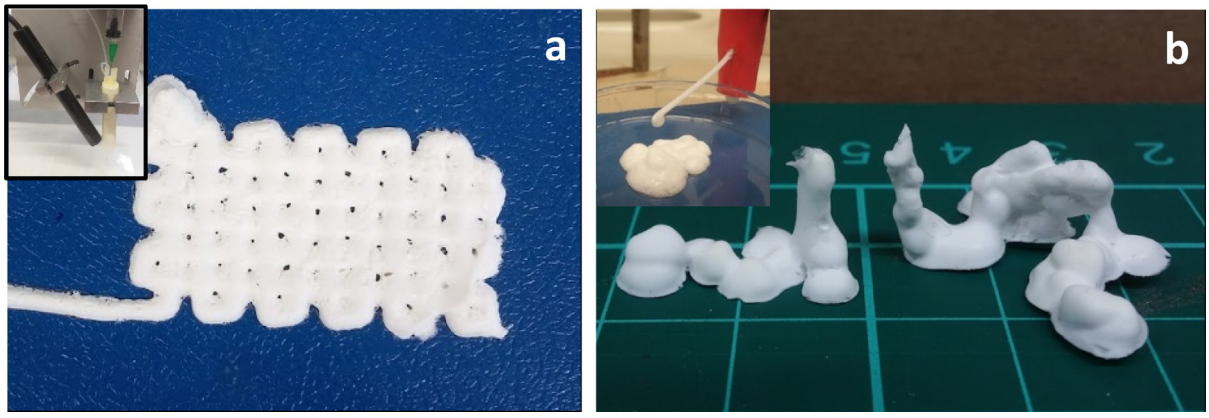

Fig. 6. Photographs of a) a water-in-PUDA-EHA HIPE produced continuously using a P10 micromixer fitted into the CNC tabletop machine (insert). This HIPE could be printed into a cage pattern and was simultaneously polymerised using a UV-pen, b) a HIPE flowing out of the P10 micromixer and photopolymerised simultaneously into complex shapes.

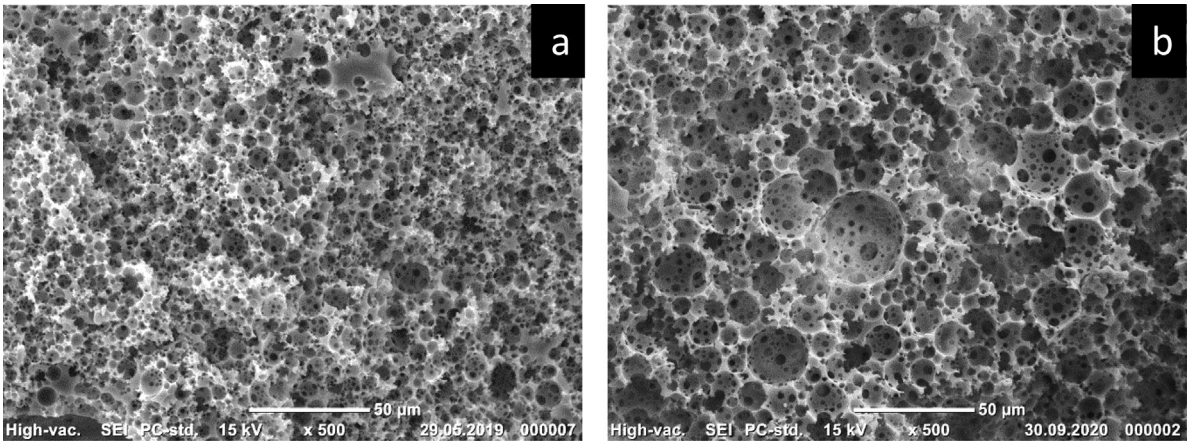

Fig. 7. Characteristic SEM images of poly(PUDA-co-EHA)HIPEs produced by polymerisation of w/PUDA-EHA HIPEs made using the P5 (a) and P20 (b) micromixer operated at a total flow rate of 1.2 mL/min and a CP:IP flow rate ratio of 1:3 corresponding to an emulsion phase volume ratio of 75%.

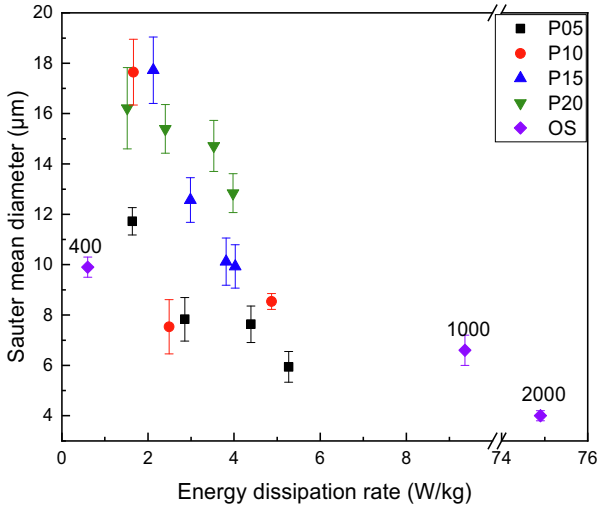

Fig. 8. Sauter pore diameter d_{32} of poly(PUDA-co-EHA)HIPEs produced by polymerisation of HIPEs made by using poly-Pickering-HIPE micromixers as function of energy dissipation rate. For comparison we show d_{32} of polyHIPEs made by polymerisation of w/PUDA-EHA HIPEs generated using an overhead stirrer (OS) operated with increasing agitation rates (400, 1000 and 2000 rpm).

energy dissipation rate (Fig. 8). The reason might be λ of the emulsions, which is for w/St-DVB 0.37 and for PUDA-EHA 0.023.

We demonstrated that it is possible to control the emulsion phase volume ratio of HIPEs and, therefore, the porosity of polyHIPEs produced therefrom, by adjusting the flow rate ratio of internal and continuous emulsion phases (Fig. 9 and **Table S2**) during microemulsification. The flow rate ratio of IP and CP did not affect the Sauter mean diameter of polyHIPEs at same total flow rate, however d_{32} decreased with increasing total flow rate (**Figure S8**). Since the shear force applied to breakup droplets mainly depended on the total flow rate for the same micromixer.

The exceptions from this, were polyHIPEs produced from HIPEs produced using P5 and P10 micromixers operated at a total flow rate of 1.5 mL/min. The porosities of those polyHIPEs were lower (67% made with P5) or higher (87% made with P10) caused by inefficient mixing of the HIPEs at high flow rates, due to limiting radial fluid dispersion through the smaller pore throats of the monoliths having the lowest *DoI* (**Figure S8**). P05 and P10 micromixers could emulsify the immiscible phases only up to total flow rates of 0.55 mL/min, whereas stable HIPEs could not be produced using P15 and P20 micromixers with the highest *DoI* at a total flow rate lower than 0.95 mL/min (**Table S2, 4**). Effective mixing through the micromixers was achieved by generating chaotic advection and local vortices in the flow path of poly-Pickering-HIPEs owing to their complex pore structure.

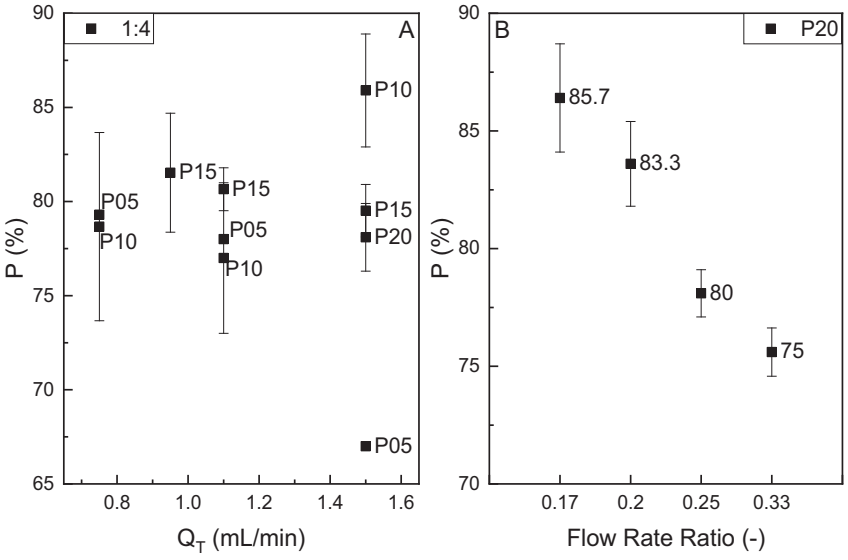

Fig. 9. Porosities of poly(PUDA-co-EHA)HIPEs produced by polymerisation of HIPEs made using various poly-Pickering-HIPE micromixers operated at various total flow rates at a 1:4 flow ratio (CP:IP) (A), and using P20 by changing the emulsion phase volume ratio, which was achieved by adjusting the flow rate ratio of continuous and internal phase to 1:3, 1:4, 1:5 and 1:6 (CP:IP) (B).

The P20 micromixer was also used to produce w/EGDMA-EHA HIPEs at various flow ratios and rates. The resulting HIPEs were subsequently UV polymerised after emulsification (Fig. 10 and **Table S2**). In this case, total flow rates up to 3.5 mL/min could be tested during emulsification for emulsion phase volume ratios as high as 83.3% and 85.7%, which was possible because of the relatively low viscosity (4 mPa·s at 25 °C) of EGDMA-EHA used as CP when compared to PUDA-EHA (43 mPa·s at 25 °C). The low viscosity of the crosslinker resulted in low viscosity HIPEs, which spread further on a glass substrate resulting in thinner polyHIPEs (Fig. 10**B**) after polymerisation as compared to poly(PUDA-co-EHA)HIPEs (Fig. 6). Again, we observed that the viscosity of HIPEs increased with increasing total flow rates. The porosity of poly (EGDMA-co-EHA)HIPEs can be controlled by controlling the flow rate ratios (CP:IP), which determines the emulsion phase volume ratio, during the emulsification using a P20 micromixer (Fig. 11**B**). Chanonon et al. (Chabanon et al., 2017) reported that the dispersed phase volume fraction of oil-in-water emulsions made using a SMX + commercial static mixer can be controlled in the range from 5 to 60 vol.%. However, phase inversion occurred in their experiments when the phase volume fraction exceeded 60%. We, on the other hand, managed to produce stable HIPEs with phase volume fractions of up to 85.7% (Fig. 11). In case of our emulsification devices it is possible to control the dispersed phase volume fraction, which controls the porosity of the produced polyHIPEs, continuously simply by changing the CP:IP flow rate ratio (Fig. 9 and Fig. 11**B**). Poly(EGDMA-co-EHA)HIPEs had similar average d_p to poly(PUDA-co-EHA)HIPEs made by polymerisation of HIPEs produced at a total flow rate of 1.5 mL/min (Fig. 8 and Fig. 11**A**). Even though the very high viscosity of PUDA resulted in highly viscous HIPEs, it was possible to operate the P20 micromixer at the same total flow rate, which resulted in similar shear forces on the droplets during emulsification. This indicated that the viscosity of the CP did not play an important role on the average droplet diameters but allows to increase the total flow rate during the emulsification when using lower viscosity emulsion phases to produce HIPEs.

Another advantage of being able to change the phase volume fraction during emulsification, which allows to tailor the porosity of the polyHIPEs produced by polymerisation of the HIPE template, is that macroporous polymers with graded morphology/porosity can be produced. We produced both w/St-DVB (**Figure S9**) and

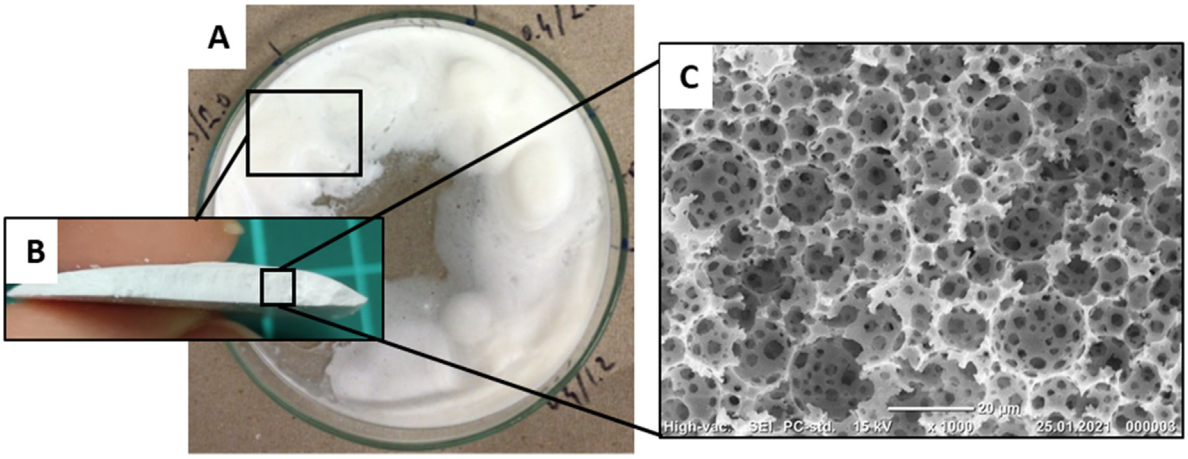

Fig. 10. Photographs of a) polyHIPE made by UV polymerisation of w/EGDMA-EHA HIPEs prepared using P20 micromixers operated at various flow rates and CP:IP flow rate ratios, b) cross-section of polyHIPE and c) a characteristic SEM image showing the pore structure of a poly(EGDMA-co-EHA)HIPE.

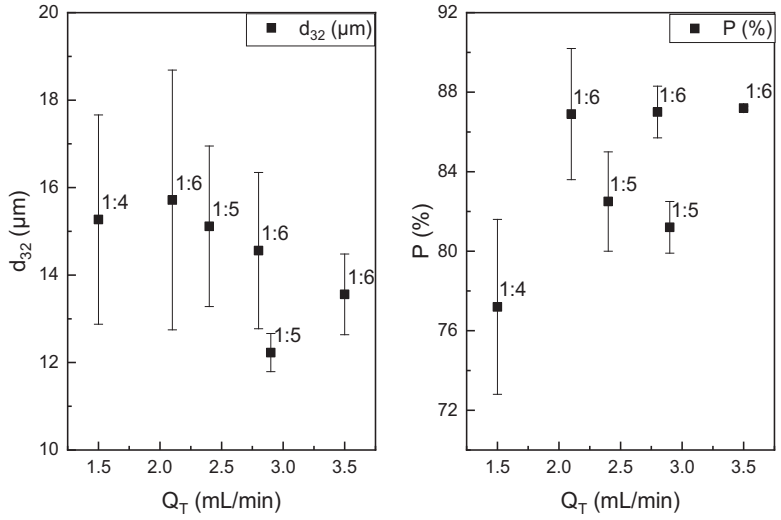

Fig. 11. Sauter pore diameter d_{32} and porosity P(%) of poly(EGDMA-co-EHA)HIPEs made by polymerisation of HIPEs produced using a P20 micromixer operated at phase flow rate (CP:IP) ratios of 1:4, 1:5 and 1:6 as function of total flow rates Q_T.

w/PUDA-EHA HIPEs altering the dispersed phase volume fraction during emulsification and polymerised these templates. No separation between regions with different porosities in the polyHIPEs could be observed, after slicing them perpendicular to the gradient or during bending and breaking. Moreover, the targeted porosities (determined by the flow rate ratio) were achieved on both sides of the transition zone (**Figure 12 and S9**). The continuous emulsification and smooth transition between the layers resulted in monolithic macroporous polymers with a porosity by no pore size gradient containing no separation layers, while other methods used to produce graded macroporous polymers result in interpenetrating layers, which negatively affect the mechanical properties of the material. (Naebe and Shirvanimoghaddam, 2016) However, the relatively high mean residence time in the poly-Pickering-HIPE micromixers (t_m = 150–212 s for 1.2 mL/min total flow rate) (Barkan-Öztürk et al., 2021) results in a broad transition zone across the gradient. During the production of w/PUDA-EHA HIPEs the flow rate of the IP was changed from 1.2 to 1.8 mL/min while keeping the CP flow rate constant (0.3 mL/min) (**ESI Video S4**), which resulted in a porosity gradient of the macroporous polymer produced from this HIPE template (Fig. 12). A video record of increasing Q_{CP} from 0.3 to 0.4 mL/min and increasing Q_{IP} from 1.5 to 2 mL/min is shown in the ESI (**Video S5**).

SEM micrographs of all micromixers were taken after using them repeatedly at least 17 times to produce a range of HIPEs, with approximately one month break between the various experiments. As can be seen in **Figure S10** (exemplary shown for P5) no morphological changes as result of exposure to the chemicals and shear force during the emulsifications were observed. Moreover, poly-Pickering-HIPEs were stable against the continuous phase formulation (i.e. no swelling was observed after immersion into St-DVB and PUDA-EHA over a period of 2 h) owing to their heavily crosslinked nature. Moreover, the mechanical performance of poly-Pickering-HIPEs used as micromixers were compared with pristine monoliths and no change was observed (**Figure S11**).

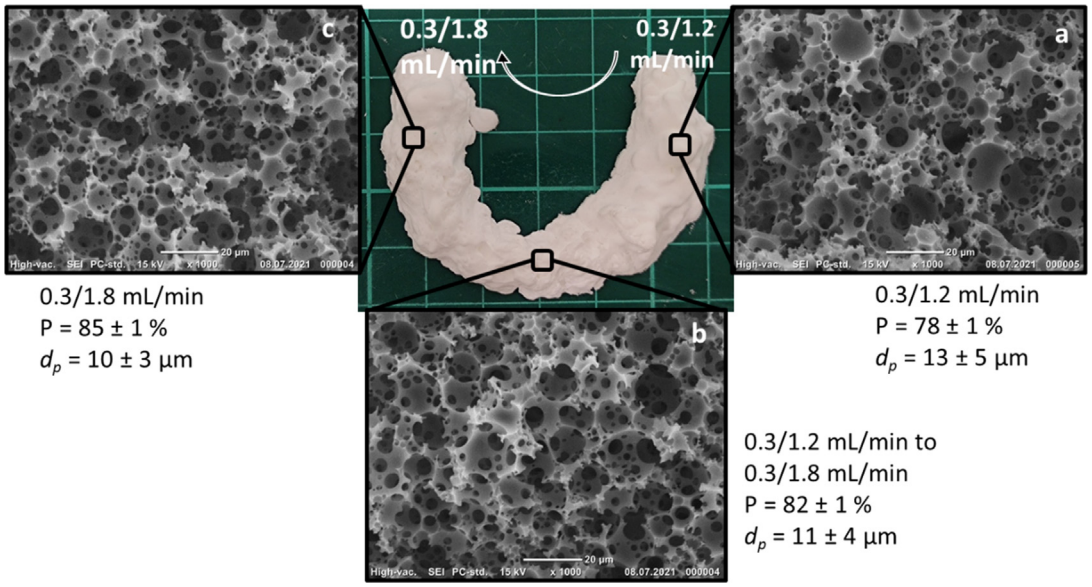

Fig. 12. Photograph of a poly(PUDA-co-EHA)HIPE with a porosity gradient made by polymerisation of a HIPE with was produced using a P20 micromixer operated at flow rate ratios increasing from 0.3/1.2 mL/min to 0.3/1.8 mL/min (CP/IP) and characteristic SEM images taken from the corresponding places shown in the photograph (a) 0.3/1.2 mL/min, b) transition area and c) 0.3/1.8 mL/min (CP/IP)).

4. Conclusions

Macroporous polymers were produced by polymerising the monomer-containing continuous phase of HIPEs generated using poly-Pickering-HIPE micromixers, which were operated continuously. Water-in-PUDA-EHA, w/EGDMA-EHA and w/St-DVB HIPEs could be successfully generated using macroporous micromixers and polymerised into polyHIPEs. The phase volume fraction of the HIPEs could be adjusted during the emulsification process, which provides a means to tailor the porosity of the resulting polyM/HIPEs. This is in contrast to literature reports in which the porosity had to be adjusted by sedimentation of the emulsion droplets prior to polymerisation. (Elsing et al., 2017; Costantini et al., 2014) Consequently, we produced macroporous polymers with porosities ranging from 70% to 88%, which could be altered continuously, resulting in macroporous polymers with graded porosity. Furthermore, the average pore sizes of the produced polyHIPEs can be controlled by using poly-Pickering-HIPE micromixers with various degrees of interconnectivity (*DoI*). Using micromixers with a higher *DoI* resulted in larger average pore sizes of the resulting polyHIPEs, due to decreased shear force on the droplets during the emulsification. Increasing the total flow rate used for emulsification resulted in a slight decrease of the average pore size. Additionally, the viscosity of emulsions produced using microemulsification increased with increasing total flow rate. HIPEs with a high viscosity can be used directly as ink in 3D printing processes and can be UV-polymerised in-situ.

CRediT authorship contribution statement

Hande Barkan-Öztürk: Investigation, Data curation, Formal analysis, Methodology, Validation, Visualization, Writing – original draft. **Angelika Menner:** Conceptualization, Methodology, Resources, Project administration, Supervision, Writing – review & editing. **Alexander Bismarck:** Conceptualization, Methodology, Funding acquisition, Supervision, Writing – review & editing.

Declaration of Competing Interest

The authors declare that they have no known competing financial interests or personal relationships that could have appeared to influence the work reported in this paper.

Acknowledgements

We acknowledge the financial support through the Institute of Materials Chemistry (371300) of Faculty of Chemistry of University of Vienna.

Funding

We acknowledge the financial support through the Institute of Materials Chemistry (371300) of Faculty of Chemistry of University of Vienna

Appendix A. Supplementary material

Supplementary data to this article can be found online at https://doi.org/10.1016/j.ces.2021.117296.

References

Barkan-Öztürk, H., Menner, A., Bismarck, A., 2021. Emulsion-templated macroporous polymer micromixers. Ind. Eng. Chem. Res. 60 (39), 14013–14025. https://doi.org/10.1021/acs.iecr.1c0194910.1021/acs.iecr.1c01949.s001.

Bayareh, M., Ashani, M.N., Usefian, A., 2020. Active and passive micromixers: a comprehensive review. Chem. Eng. Process. - Process Intensif. 147, 107771. https://doi.org/10.1016/j.cep.2019.107771.

Bolton, K.F., Canty, A.J., Deverell, J.A., Guijt, R.M., Hilder, E.F., Rodemann, T., Smith, J. A., 2006. Macroporous monolith supports for continuous flow capillary microreactors. Tetrahedron Lett. 47 (52), 9321–9324. https://doi.org/10.1016/j.tetlet.2006.10.113.

Brown, J.F., Krajnc, P., Cameron, N.R., 2005. PolyHIPE supports in batch and flow-through suzuki cross-coupling reactions. Ind. Eng. Chem. Res. 44 (23), 8565–8572. https://doi.org/10.1021/ie048843c10.1021/ie048843c.s001.

Cameron, N.R., 2005. High internal phase emulsion templating as a route to well-defined porous polymers. Polymer 46 (5), 1439–1449. https://doi.org/10.1016/j.polymer.2004.11.097.

Capretto, L., Cheng, W., Hill, M., Zhang, X., 2011. Micromixing within microfluidic devices. In: Lin, B. (Ed.), Microfluidics, Vol. 304. Springer, Berlin, Heidelberg, pp. 27–68. https://doi.org/10.1007/128_2011_150.

Chabanon, E., Sheibat-Othman, N., Mdere, O., Valour, J.P., Urbaniak, S., Puel, F., 2017. Drop size distribution monitoring of oil-in-water emulsions in SMX+ static mixers: effect of operating and geometrical conditions. Int. J. Multiph. Flow 92, 61–69. https://doi.org/10.1016/j.ijmultiphaseflow.2017.03.001.

Christopher, G.F., Anna, S.L., 2007. Microfluidic methods for generating continuous droplet streams. J. Phys. Appl. Phys. 40 (19), R319–R336. https://doi.org/10.1088/0022-3727/40/19/R01.

Cobos, S., Carvalho, M.S., Alvarado, V., 2009. Flow of oil-water emulsions through a constricted capillary. Int. J. Multiph. Flow 35 (6), 507–515. https://doi.org/10.1016/j.ijmultiphaseflow.2009.02.018.

Costantini, M., Colosi, C., Guzowski, J., Barbetta, A., Jaroszewicz, J., Święszkowski, W., Dentini, M., Garstecki, P., 2014. Highly ordered and tunable PolyHIPEs by using microfluidics. J. Mater. Chem. B 2 (16), 2290. https://doi.org/10.1039/c3tb21227k.

Costantini, M., Jaroszewicz, J., Kozoń, Ł., Szlązak, K., Święszkowski, W., Garstecki, P., Stubenrauch, C., Barbetta, A., Guzowski, J., 2019. 3D-printing of functionally graded porous materials using on-demand reconfigurable microfluidics. Angew. Chem. Int. Ed. 58 (23), 7620–7625. https://doi.org/10.1002/anie.v58.2310.1002/anie.201900530.

Dabrowski, M.L., Jenkins, D., Cosgriff-Hernandez, E., Stubenrauch, C., 2020. Methacrylate-based polymer foams with controllable connectivity, pore shape, pore size and polydispersity. Phys. Chem. Chem. Phys. 22 (1), 155–168. https://doi.org/10.1039/C9CP03606G.

Danninger, D., Hartmann, F., Paschinger, W., Pruckner, R., Schwödiauer, R., Demchyshyn, S., Bismarck, A., Bauer, S., Kaltenbrunner, M., 2020. Stretchable polymerized high internal phase emulsion separators for high performance soft batteries. Adv. Energy Mater. 10 (19), 2000467. https://doi.org/10.1002/aenm.v10.1910.1002/aenm.202000467.

Desire, C.T., Hilder, E.F., Arrua, R.D., 2017. Monolithic high-performance liquid chromatography columns. In: Meyers, R.A. (Ed.), Encyclopedia of Analytical Chemistry. John Wiley & Sons, Ltd, Chichester, UK, pp. 1–37. https://doi.org/10.1002/9780470027318.a9386.

Elsing, J., Quell, A., Stubenrauch, C., 2017. Toward functionally graded polymer foams using microfluidics. Adv. Eng. Mater. 19 (8), 1700195. https://doi.org/10.1002/adem.201700195.

Falk, L., Commenge, J.-M., 2010. Performance comparison of micromixers. Chem. Eng. Sci. 65 (1), 405–411. https://doi.org/10.1016/j.ces.2009.05.045.

Foudazi, R., 2021. HIPEs to PolyHIPEs. React. Funct. Polym. 164, 104917. https://doi.org/10.1016/j.reactfunctpolym.2021.104917.

Gokmen, M.T., Van Camp, W., Colver, P.J., Bon, S.A.F., Du Prez, F.E., 2009. Fabrication of porous "clickable" polymer beads and rods through generation of high internal phase emulsion (HIPE) droplets in a simple microfluidic device. Macromolecules 42 (23), 9289–9294. https://doi.org/10.1021/ma9018679.

Grace, H.P., 1982. Dispersion phenomena in high viscosity immiscible fluid systems and application of static mixers as dispersion devices in such systems. Chem. Eng. Commun. 14 (3–6), 225–277. https://doi.org/10.1080/00986448208911047.

Hinze, J.O., 1955. Fundamentals of the hydrodynamic mechanism of splitting in dispersion processes. AIChE J. 1 (3), 289–295. https://doi.org/10.1002/(ISSN)1547-590510.1002/aic.v1:310.1002/aic.690010303.

Hubbard, Jr., W.M. 2014. High internal phase emulsion foam associated with polyurethane foam. US20150374876A1.

Ikem, V.O., Menner, A., Horozov, T.S., Bismarck, A., 2010. Highly permeable macroporous polymers synthesized from pickering medium and high internal phase emulsion templates. Adv. Mater. 22 (32), 3588–3592. https://doi.org/10.1002/adma.201000729.

Ikem, V.O., Menner, A., Bismarck, A., Norman, L.R., 2014. Liquid screen: a novel method to produce an in-situ gravel pack. SPE J. 19 (03), 437–442. https://doi.org/10.2118/141256-PA.

Jiang, Q., Barkan, H., Menner, A., Bismarck, A., 2017. Micropatterned, macroporous polymer springs for capacitive energy harvesters. Polymer 126, 419–424. https://doi.org/10.1016/j.polymer.2017.04.018.

Kim, N., Murphy, M.C., Soper, S.A., Nikitopoulos, D.E., 2014. Liquid-liquid segmented flows in polycarbonate microchannels with cross-sectional expansions. Int. J. Multiph. Flow 58, 83–96. https://doi.org/10.1016/j.ijmultiphaseflow.2013.09.002.

Kiss, N., Brenn, G., Pucher, H., Wieser, J., Scheler, S., Jennewein, H., Suzzi, D., Khinast, J., 2011. Formation of O/W emulsions by static mixers for pharmaceutical applications. Chem. Eng. Sci. 66 (21), 5084–5094. https://doi.org/10.1016/j.ces.2011.06.065.

Kolmogorov, A., 1949. On the breakage of drops in a turbulent flow. Dokl. Akad. Navk. SSSR 66, 825–828.
Lapierre, F., Cameron, N.R., Zhu, Y., 2015. Ready... set, flow: simple fabrication of microdroplet generators and their use in the synthesis of PolyHIPE microspheres. J. Micromechanics Microengineering 25 (3), 035011. https://doi.org/10.1088/0960-1317/25/3/035011.
Lissant, K.J., 1966. The geometry of high-internal-phase-ratio emulsions. J. Colloid Interface Sci. 22 (5), 462–468.
Manley, S.S., Steindl, P., Hewitt, G.F., Bismarck, A., 2020. An integrated method for measuring gas permeability and diffusivity of porous solids. Chem. Eng. Sci. 223, 115725. https://doi.org/10.1016/j.ces.2020.115725.
Menner, A., Powell, R., Bismarck, A., 2006. Open porous polymer foams via inverse emulsion polymerization: should the definition of high internal phase (ratio) emulsions be extended? Macromolecules 39 (6), 2034–2035. https://doi.org/10.1021/ma052705x.
Montillet, A., Nedjar, S., Tazerout, M., 2013. Continuous production of water-in-oil emulsion using micromixers. Fuel 106, 410–416. https://doi.org/10.1016/j.fuel.2012.11.018.
Muijlwijk, K., Berton-Carabin, C., Schroën, K., 2015. How microfluidic methods can lead to better emulsion products. Lipid Technol. 27 (10), 234–236. https://doi.org/10.1002/lite.201500052.
Naebe, M., Shirvanimoghaddam, K., 2016. Functionally graded materials: a review of fabrication and properties. Appl. Mater. Today 5, 223–245. https://doi.org/10.1016/j.apmt.2016.10.001.
Nguyen, N.-T., 2012. Micromixers: Fundamentals, Design, and Fabrication, 2nd ed. Micro & nano technologies series. Elsevier/William Andrew, Amsterdam, Boston.
Nimafar, M., Viktorov, V., Martinelli, M., 2012. Experimental investigation of split and recombination micromixer in confront with basic T- and O- type micromixers. Int. J. Mech. Appl. 2 (5), 61–69. https://doi.org/10.5923/j.mechanics.20120205.02.
Owen, R., Sherborne, C., Paterson, T., Green, N.H., Reilly, G.C., Claeyssens, F., 2016. Emulsion templated scaffolds with tunable mechanical properties for bone tissue engineering. J. Mech. Behav. Biomed. Mater. 54, 159–172. https://doi.org/10.1016/j.jmbbm.2015.09.019.
Paul, E.L., Atiemo-Obeng, V.A., Kresta, S.M. (Eds.), 2004. Handbook of Industrial Mixing: Science and Practice. Wiley-Interscience, Hoboken, N.J..
Pulko, I., Krajnc, P., 2012. High internal phase emulsion templating – a path to hierarchically porous functional polymers. Macromol. Rapid Commun. 33 (20), 1731–1746. https://doi.org/10.1002/marc.v33.2010.1002/marc.201200393.
Quell, A., Elsing, J., Drenckhan, W., Stubenrauch, C., 2015. Monodisperse polystyrene foams via microfluidics - a novel templating route: monodisperse polystyrene foams via microfluidics. Adv. Eng. Mater. 17 (5), 604–609. https://doi.org/10.1002/adem.201500040.
Romero, M.I., 2009. Flow of emulsions in porous media. In: All Days; SPE, New Orleans, Louisiana, p. SPE-129519-STU. https://doi.org/10.2118/129519-STU.
Stubenrauch, C., Menner, A., Bismarck, A., Drenckhan, W., 2018. Emulsion and foam templating-promising routes to tailor-made porous polymers. Angew. Chem. Int. Ed. 57 (32), 10024–10032. https://doi.org/10.1002/anie.v57.3210.1002/anie.201801466.
Tadros, T.F., 2010. Rheology of Dispersions: Principles and Applications. Wiley-VCH-Verl, Weinheim.
Tebboth, M., Kogelbauer, A., Bismarck, A., 2015. Liquid-liquid extraction within emulsion templated macroporous polymers. Ind. Eng. Chem. Res. 54 (29), 7284–7291. https://doi.org/10.1021/acs.iecr.5b01346.
Tebboth, M., Kogelbauer, A., Bismarck, A., 2015. Effectiveness of emulsion-templated macroporous polymer micromixers characterized by the bourne reaction. Ind. Eng. Chem. Res. 54 (22), 5974–5981. https://doi.org/10.1021/acs.iecr.5b00493.

Supporting Information

Polymerised High Internal Phase Emulsion Micromixers for Continuous Emulsification

Hande Barkan-Öztürk,[1] *Angelika Menner,*[1] *Alexander Bismarck*[1,2,*]

[1] Polymer and Composite Engineering (PaCE) Group, Institute of Material Chemistry and Research, Faculty of Chemistry, University of Vienna, Währinger Strasse, 42, 1090, Vienna, Austria.

[2] Department of Chemical Engineering, Imperial College London, South Kensington Campus, London SW7 2AZ, United Kingdom

* Corresponding author: Alexander Bismarck, e-mail: alexander.bismarck@univie.ac.at

S2 Mean energy dissipation rate during emulsification using an overhead stirrer. The energy dissipation rate $\overline{\varepsilon}$ during the preparation of HIPEs using an overhead stirrer was calculated as follows:[2]

$$\overline{\varepsilon} = \frac{W}{\rho V_T} \qquad (Eq.S1)$$

where ρ $(= \phi_{IP} \cdot \rho_{IP} + \phi_{CP} \cdot \rho_{CP})$ is the apparent density of the agitated fluid, V_T the total fluid volume and W the power input, which was calculated as follows:

$$W = W_0 \rho N^3 D^5 \qquad (Eq.S2)$$

where W_0 is power number dependent on impeller type (0.22),[3] N the impeller speed, D the impeller diameter.

SEM images of poly-Pickering-HIPEs

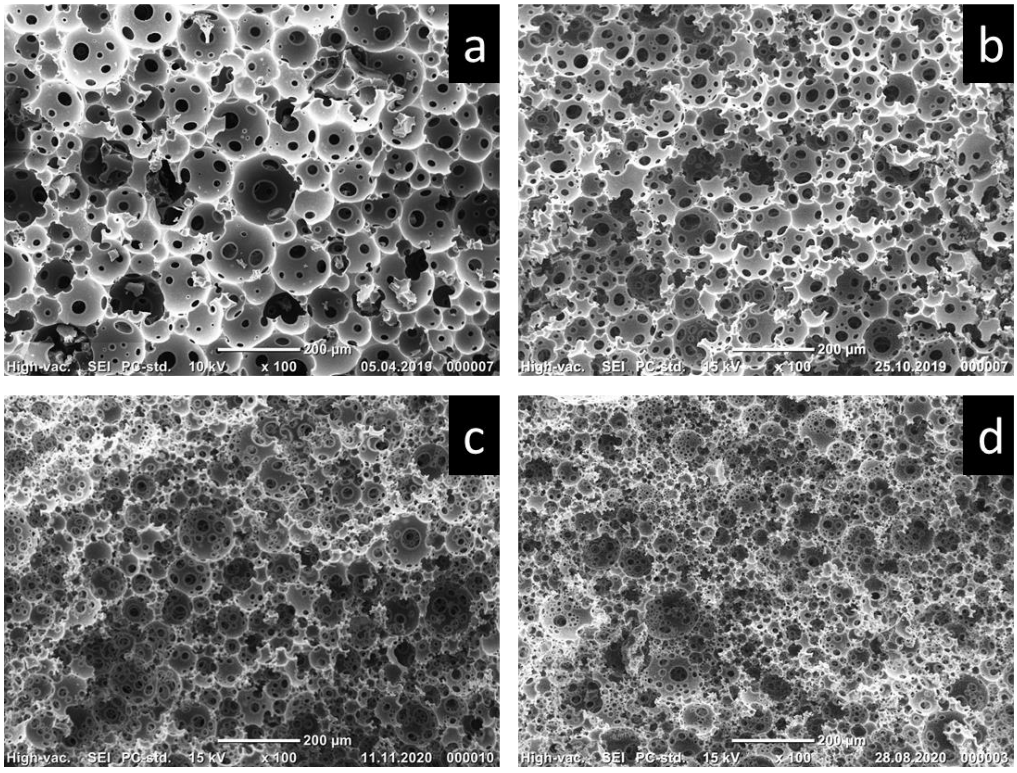

Figure S1. Characteristic SEM images of poly-Pickering-HIPEs (P5 (a), P10 (b), P15 (c) and P20 (d)) prepared by polymerization of the continuous phase of Pickering-HIPE templates to which increasing amounts of surfactant was added.

S1 Gas permeability of poly-Pickering-HIPEs. The permeability coefficient K was calculated as described by Manley et al.:[1]

$$K = \frac{Q_2 P_2 L}{\Delta P A} = \frac{V\left(\frac{dP_2}{dt}\right)L}{P_1 A} = \frac{k}{\mu} P_m + \frac{4}{3} K_0 \sqrt{\frac{8RT}{\pi M}} \qquad \text{(Eq. S3)}$$

where, Q_2 is the volumetric flow rate downstream, P_2 the downstream pressure, ΔP the pressure difference across the samples, A cross-sectional area of sample, L length of sample, P_1 beginning pressure, μ fluid viscosity, V a known volume, K_0 the slip coefficient, M the molecular weight of the transport species, R the gas constant, T the absolute temperature and t the time.

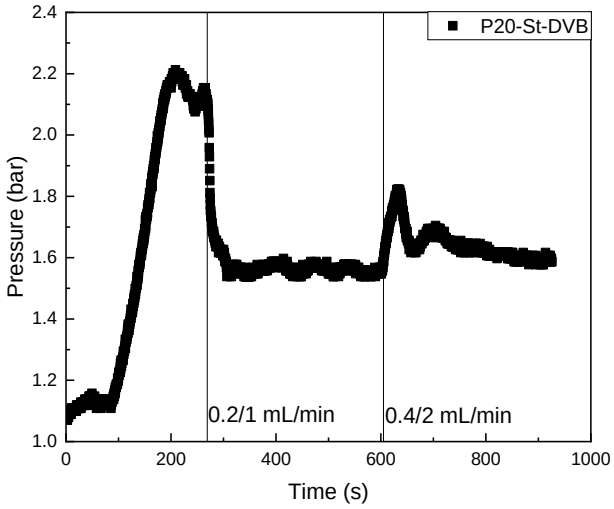

Figure S2: The inlet pressure as function of flow rate. Evolution of inlet pressure with varying flow rate for water-in-St-DVB emulsification in a P20 micromixer. Flow rate range: Q_T = 1.2 mL/min and 2.4 mL/min at a fixed IP:CP ratio of 5

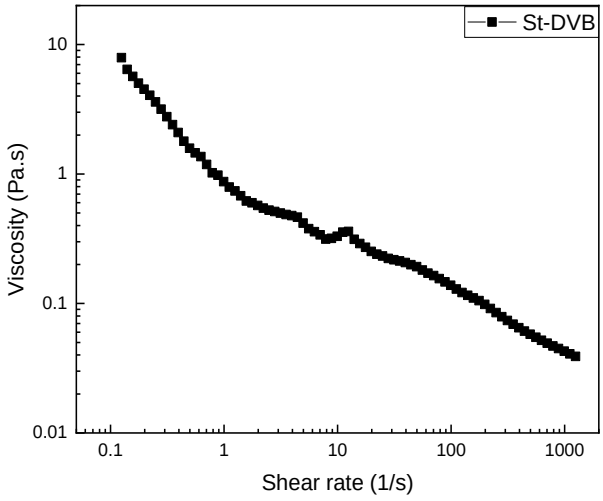

Figure S3: Dynamic viscosity of water-in-St-DVB HIPE (75 vol% IP, emulsified at 1000 rpm) as function of shear rate.

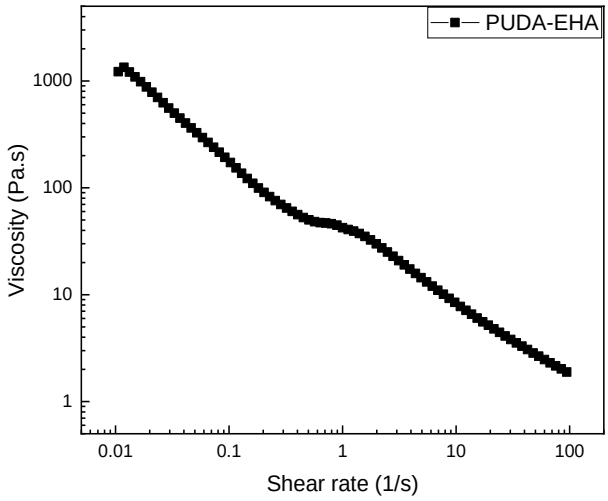

Figure S4: Dynamic viscosity of water-in-PUDA-EHA HIPE (75 vol% IP, emulsified at 1000 rpm) as a function of shear rate.

Table S1: CP flow rate (Q_{CP}), IP flow rate (Q_{IP}) and total flow rate (Q_T) of water-in-St-DVB HIPEs generated with P5, P10, P15 and P20 micromixers.

Q_{CP}	Q_{IP}	Q_T	CP : IP	Micromixer name			
(mL/min)	(mL/min)	(mL/min)	ratio	P5	P10	P15	P20
0.1	0.4	0.5	1:4	-	+	-	-
0.15	0.4	0.55	1.5:4	-	+	-	-
0.15	0.5	0.65	1.5:5	-	+	-	-
0.15	0.60	0.75	1:4	+	+	-	-
0.20	0.50	0.70	1:2.5	+	-	-	-
0.20	0.60	0.80	1:3	+	+	+	-
0.30	0.60	0.90	1:2	-	-	+	-
0.20	0.75	0.95	1:3.5	-	+	+	-
0.30	0.75	1.05	1:2.5	-	-	+	-
0.15	0.75	0.90	1:5	-	-	-	+
0.30	0.80	1.10	1:2.5	+	-	-	-
0.20	0.90	1.10	1:4.5	+	+	-	+
0.30	0.90	1.20	1:3	+	-	+	-
0.20	1.00	1.20	1:5	-	-	-	+
0.20	1.20	1.40	1:6	+	-	-	-
0.30	1.20	1.50	1:3	-	-	-	+
0.40	1.20	1.60	1:4	-	-	+	+
0.30	1.50	1.80	1:5	-	-	+	+
0.40	1.50	1.90	1:4.2	-	-	+	-
0.40	1.60	2.00	1:4	-	-	-	+
0.40	2.00	2.40	1:5	-	-	-	+

Table S2: CP flow rate (Q_{CP}), IP flow rate (Q_{IP}) and total flow rate (Q_T) of water-in-PUDA-EHA HIPEs generated with P5, P10, P15 and P20 micromixers.

Q_{CP}	Q_{IP}	Q_T	CP : IP	Micromixer			
(mL/min)	(mL/min)	(mL/min)	ratio	P5	P10	P15	P20
0.13	0.40	0.53	1:3.5	+	+	-	-
0.15	0.40	0.55	1:3.3	-	+	-	-
0.15	0.50	0.65	1:3.7	-	+	-	-
0.15	0.60	0.75	1:4	+	+	-	-
0.18	0.60	0.78	1:3.5	+	-	-	-
0.20	0.60	0.80	1:3	+	+	-	-
0.20	0.75	0.95	1:3.5	-	-	+	+
0.30	0.75	1.05	1:2.5	-	-	+	+
0.15	0.90	1.05	1:6	-	+	-	+
0.20	0.90	1.10	1:4.5	-	+	+	-
0.23	0.90	1.13	1:4.5	+	-	-	-
0.27	0.90	1.17	1:3.3	+	+	-	-
0.30	0.90	1.20	1:3	+	+	+	+
0.15	1.00	1.15	1:6.2	-	-	-	+
0.20	1.00	1.20	1:5	-	-	-	+
0.34	1.20	1.54	1:3.5	+	+	-	-
0.40	1.20	1.60	1:3	-	+	+	+
0.30	1.50	1.80	1:5	-	-	-	+
0.40	1.50	1.90	1:4.2	-	-	-	+
0.30	1.80	2.10	1:6	-	-	-	+

Table S3: CP flow rate (Q_{CP}), IP flow rate (Q_{IP}) and total flow rate (Q_T) of water-in-EGDMA-EHA HIPEs generated with P20 micromixer.

Q_{CP} (mL/min)	Q_{IP} (mL/min)	Q_T (mL/min)	CP : IP ratio	Micromixer
0.30	1.20	1.50	1:4	P20
0.30	1.80	2.10	1:6	
0.40	2.00	2.40	1:5	
0.40	2.40	2.80	1:6	
0.50	2.40	2.90	1:5	
0.50	3.00	3.50	1:6	

S3 Shear stress and Critical Capillary Number during emulsification in Poly-Pickering-HIPE micromixers. Assuming a simple flow-in-tube model, the wall shear stress τ_w along a pipe, can be determined from the pressure drop Δp measured during emulsification as follows:

$$\tau_w = \frac{\Delta p \cdot D \cdot P}{4 \cdot l \cdot \tau}, \qquad (Eq.S4)$$

where D is micromixer diameter and P its porosity, l is the length of the poly-Pickering-HIPE micromixer and τ its tortuosity[4]. Over the length of the micromixer a HIPE forms. However, HIPEs are heavily shear thinning fluids (**Figure S2** and **S3**) but the wall shear stress corresponds to a dynamic viscosity η, from which the mean wall shear rate $\dot{\gamma}_w$ can be calculated as follows:[5]

$$\dot{\gamma}_w = \left(\frac{\varepsilon\rho}{2\eta}\right)^{1/2} \qquad (Eq.S5)$$

where ε is energy dissipation calculated using **Eq. 1**. In laminar pipe flow, droplet generation is promoted by shear forces opposed by capillary forces, thus their ratio can control continuous emulsification.[6] The calculated $\dot{\gamma}_w$ corresponds well (< factor 1.5) the shear rate applied to the HIPEs during rheology measurements. The critical capillary number Ca_{crit} determines the critical value for droplet breakup in laminar flow and calculated:

$$Ca_{crit} = \frac{d_m \cdot \eta_c \cdot \dot{\gamma}}{\sigma} \qquad (Eq.S6)$$

where d_m is the maximum stable drop diameter, which in our case cannot exceed the pore diameter d_p of the used poly-Pickering-HIPE micromixers, η_c the viscosity of the CP, and σ (= 24 ± 0.1 mN/m for St-DVB as CP and 26.1 ± 0.5 mN/m for PUDA-EHA as CP, respectively) interfacial tension between the aqueous IP and organic CP, which was measured using a tensiometer (K11, Krüss GmbH, Hamburg, Germany) using the Wilhelmy-plate method.

Table S4: Effect of flow rate and CP to IP ratio on the measured pressure drop Δp across poly-Pickering-HIPE micromixers during emulsification of water-in-St-DVB, from which wall shear stress τ_w, energy dissipation ε, wall shear rate $\dot{\gamma}$, and critical capillary number were calculated.

Micromixer	Q_{CP} mL/min	Q_{IP} mL/min	Q_T mL/min	Δp bar	τ_w Pa	ε W/kg	$\dot{\gamma}$ s^{-1}	Ca_{crit}	We_h
P05	0.2	0.6	0.8	1.75	20.8	1.73	70.2	$6.32 \cdot 10^{-4}$	$1.28 \cdot 10^{-4}$
	0.3	0.9	1.2	1.87	24.2	3.01	111.3	$10.02 \cdot 10^{-4}$	$4.33 \cdot 10^{-4}$
	0.3	1.2	1.5	1.95	26.4	4.11	124.9	$11.24 \cdot 10^{-4}$	$8.46 \cdot 10^{-4}$
P10	0.2	0.6	0.8	1.65	18.1	1.48	70.2	$6.32 \cdot 10^{-4}$	$1.25 \cdot 10^{-4}$
	0.3	0.9	1.2	1.86	23.9	2.94	99.2	$8.93 \cdot 10^{-4}$	$4.23 \cdot 10^{-4}$
	0.4	1.2	1.6	1.96	26.7	4.37	140.1	$12.61 \cdot 10^{-4}$	$1.00 \cdot 10^{-3}$
P15	0.2	0.6	0.8	1.46	12.8	1.04	55.8	$5.02 \cdot 10^{-4}$	$1.22 \cdot 10^{-4}$
	0.3	0.9	1.2	1.64	17.8	2.16	88.4	$7.96 \cdot 10^{-4}$	$4.13 \cdot 10^{-4}$
	0.3	1.5	1.8	1.64	17.8	3.24	111.3	$10.02 \cdot 10^{-4}$	$1.40 \cdot 10^{-3}$
	0.4	1.2	1.6	1.6	16.7	2.70	99.2	$8.93 \cdot 10^{-4}$	$9.80 \cdot 10^{-4}$
P20	0.3	0.9	1.2	1.65	18.1	2.15	88.4	$7.96 \cdot 10^{-4}$	$3.95 \cdot 10^{-4}$
	0.2	1	1.2	1.56	15.6	1.85	78.8	$7.09 \cdot 10^{-4}$	$3.95 \cdot 10^{-4}$
	0.4	2	2.4	1.63	17.5	4.16	140.1	$12.61 \cdot 10^{-4}$	$3.16 \cdot 10^{-3}$

Table S5: Effect of flow rate and CP to IP ratio on the measured pressure drop Δp across poly-Pickering-HIPE micromixers during emulsification of water-in-PUDA-EHA, from which wall shear stress τ_w, energy dissipation ε, wall shear rate $\dot{\gamma}$, and critical capillary number were calculated.

Micromixer	Q_{CP} mL/min	Q_{IP} mL/min	Q_T mL/min	Δp bar	τ_w Pa	ε W/kg	$\dot{\gamma}$ 1/s	Ca_{crit} -	We_h
P05	0.2	0.6	0.8	0.73	20.3	1.64	9.7	$12.8 \cdot 10^{-4}$	$1.22 \cdot 10^{-4}$
	0.3	0.9	1.2	0.85	23.6	2.86	15.3	$20.2 \cdot 10^{-4}$	$4.10 \cdot 10^{-4}$
	0.4	1.2	1.6	0.98	27.2	4.39	21.5	$28.4 \cdot 10^{-4}$	$9.73 \cdot 10^{-4}$
	0.4	1.5	1.9	0.99	27.5	5.27	24.2	$31.8 \cdot 10^{-4}$	$1.63 \cdot 10^{-3}$
P10	0.2	0.6	0.8	0.75	20.8	1.66	9.7	$12.8 \cdot 10^{-4}$	$1.19 \cdot 10^{-4}$
	0.3	0.9	1.2	0.75	20.8	2.49	13.7	$18.0 \cdot 10^{-4}$	$4.01 \cdot 10^{-4}$
	0.4	1.2	1.6	1.1	30.6	4.87	21.5	$28.4 \cdot 10^{-4}$	$9.50 \cdot 10^{-4}$
P15	0.2	0.6	0.8	0.97	26.9	2.12	12.2	$16.1 \cdot 10^{-4}$	$1.16 \cdot 10^{-4}$
	0.3	0.9	1.2	0.91	25.3	2.99	15.3	$20.2 \cdot 10^{-4}$	$3.91 \cdot 10^{-4}$
	0.3	1.2	1.5	0.93	25.8	3.82	19.2	$25.4 \cdot 10^{-4}$	$7.65 \cdot 10^{-4}$
	0.4	1.2	1.6	0.92	25.6	4.03	21.5	$28.4 \cdot 10^{-4}$	$9.28 \cdot 10^{-4}$
P20	0.2	0.6	0.8	0.71	19.7	1.52	9.7	$12.8 \cdot 10^{-4}$	$1.11 \cdot 10^{-4}$
	0.3	0.9	1.2	0.75	20.8	2.41	13.7	$18.1 \cdot 10^{-4}$	$3.74 \cdot 10^{-4}$
	0.3	1.2	1.5	0.88	24.4	3.53	17.2	$22.7 \cdot 10^{-4}$	$7.30 \cdot 10^{-4}$
	0.4	1.2	1.6	0.93	25.8	3.98	19.2	$25.4 \cdot 10^{-4}$	$8.86 \cdot 10^{-4}$

S4 Droplet breakup in poly-Pickering-HIPE micromixers: Grace[7] did show that the droplet breakup in a simple shear flow that droplet breakup occurs above a Ca_{crit} for a given viscosity ratio of IP to CP ($\lambda = \eta_{IP}/\eta_{CP}$). In our case the viscosity ratios for w: St-DVB and w:PUDA-EHA were $\lambda = 0.37$ and $\lambda = 0.023$, respectively. According to Grace showed that the lowest Ca_{crit} required for droplet breakup are 0.5 and 3, respectively. This would indicate that droplet breakup should not occur in simple shear flow. However, in our poly-Pickering-HIPE micromixers, Ca_{crit} was significantly lower compared to those predicted by Grace. This apparent disagreement was already discussed by Stegeman et al.[8] As mentioned above, in our case, the maximum stable

droplet diameter d_m cannot exceed the pore diameter d_p in the poly-Pickering-HIPE micromixers thus the Grace model does not apply to our type of micromixers.

However, emulsification in porous media,[6] such as our micromixers, is possible and can be explained by the hydraulic Weber number We_h, which is the ratio of inertial forces to the surface tension forces. We_h is defined as follows:[9,10]

$$We_h = \frac{\rho_{CP} \cdot u_s^2 \cdot d_p}{\sigma} \qquad (Eq.S7)$$

where ρ_{CP} is the density of the continuous emulsion phase, u_s the superficial velocity ($u_s = Q_T/\pi \cdot P \cdot r^2$, where P is the micromixer porosity and r its radius), d_p again the average pore size of our poly-Pickering-HIPE micromixer, assumed to be an average tube diameter. The lowest We_h was 0.00011 for P20 but it increased with increasing fluid flow rate. However, also in this case We_h is too low for a given λ to explain droplet breakup.

Cobos et al.[11] and Romero[12] already showed that emulsions can be produced by partial pore blocking phenomena occurring when forcing immiscible fluids through porous media. When a fluid volume (of a multiphase fluid) is forced though the pore throats of poly-Pickering-HIPE micromixers, acting as orifice in a tube, both in the axial and radial flow direction, pore blockage does occur resulting in a backpressure increase (**Figure S4**) and thus in droplet elongation and breakup and, hence, the formation of emulsions.

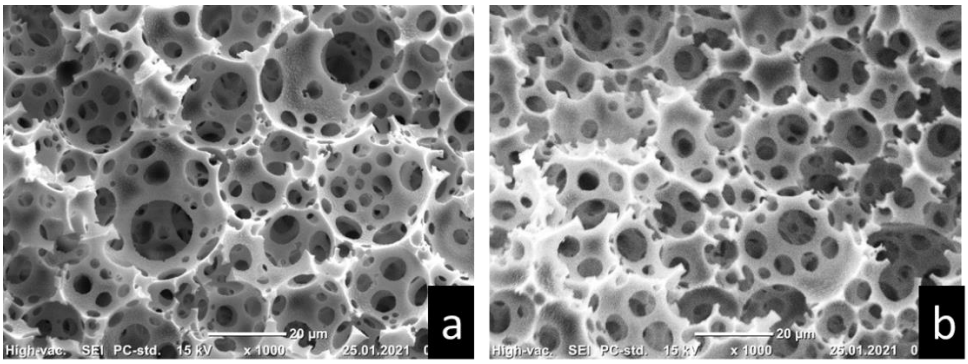

Figure S5: The SEM images of poly-(St-DVB)HIPEs produced by polymerizing the HIPEs made in a P20 micromixer at c) 0.2/1 mL/min, d) 0.4/2 mL/min (CP/IP) flow rates.

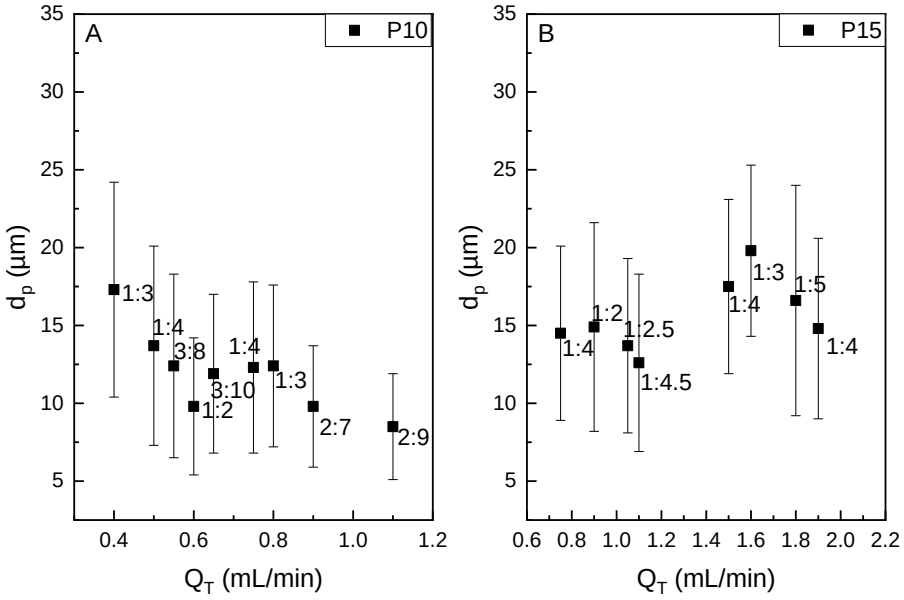

Figure S6: d_p of poly(St-co-DVB)HIPEs produced from polymerisation of HIPEs generated with P10 (A) and P15 (B) micromixers at various Q_T and ratios.

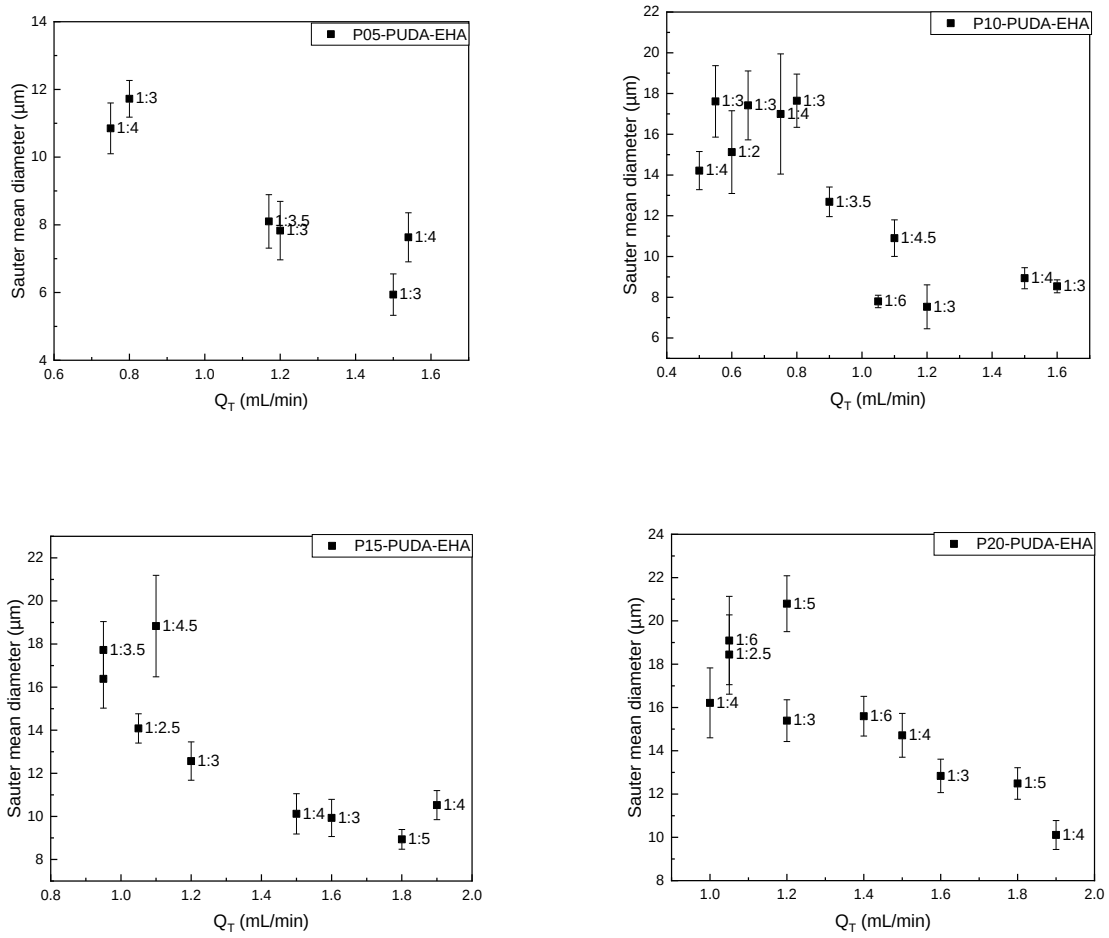

Figure S7: Sauter mean pore diameter d_{32} of poly-(PUDA-EHA)HIPEs produced by polymerisation of HIPEs generated in P5, P10, P15 and P20 micromixers at various Q_T and flow ratios.

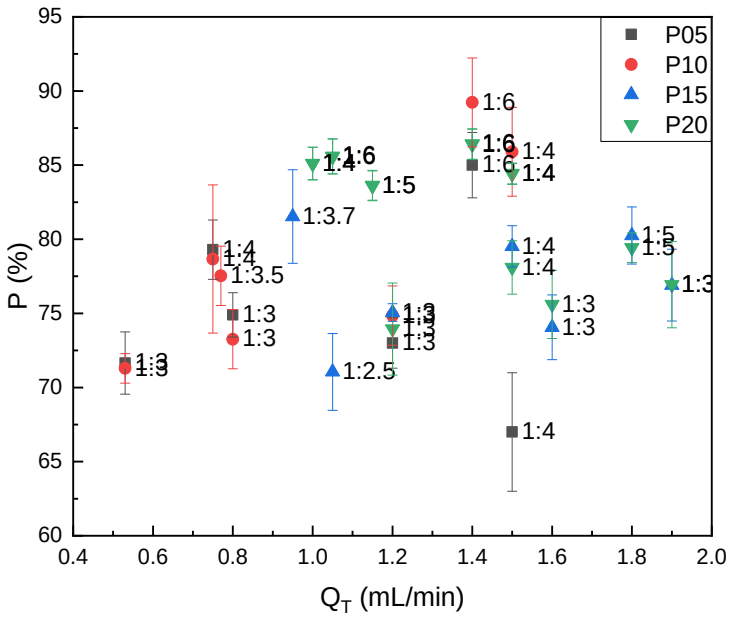

Figure S8: Porosities of poly-(PUDA-EHA)HIPEs produced by polymerisation of HIPEs generated in poly-Pickering-HIPE micromixers at various Q_T and ratios.

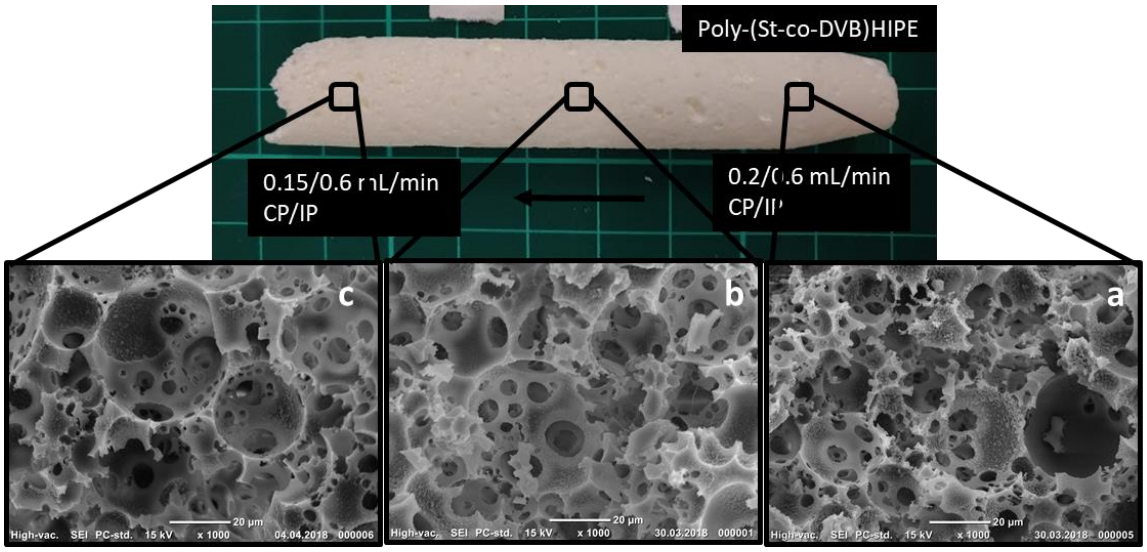

Figure S9: Photograph of a poly(St-co-DVB)HIPE with graded porosity made by polymerization of a HIPE with varying internal volume fraction produced in P20 micromixer operated at flow rate ratios of 0.2/0.6 and 0.15/0.6 (CP/IP) and SEM images taken from the corresponding places shown in the photograph (a: Q = 0.2/0.6 mL/min, b: transition area, and c: Q = 0.15/0.6 mL/min (CP/IP).

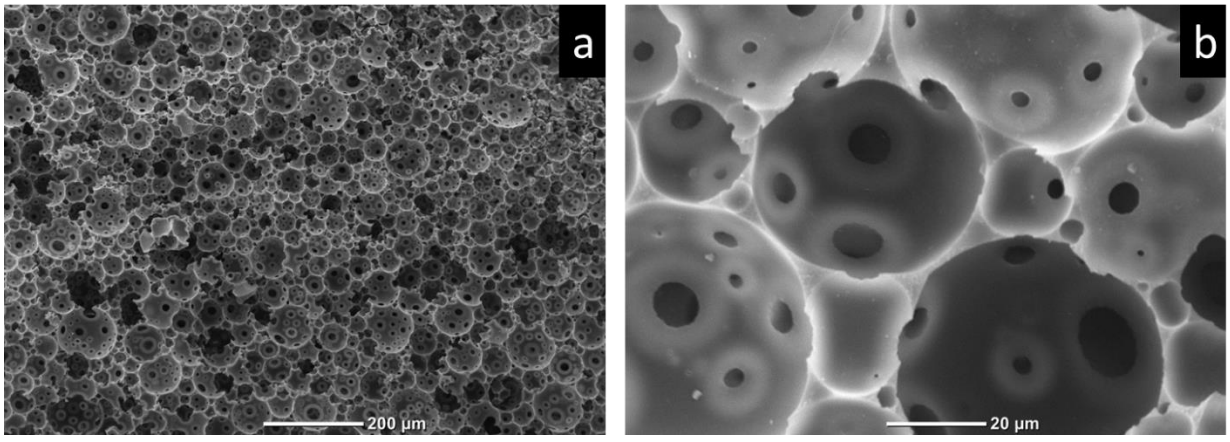

Figure S10: SEM images of a P05 micromixer taken after using it several times for emulsification at a) low magnification, and b) high magnification.

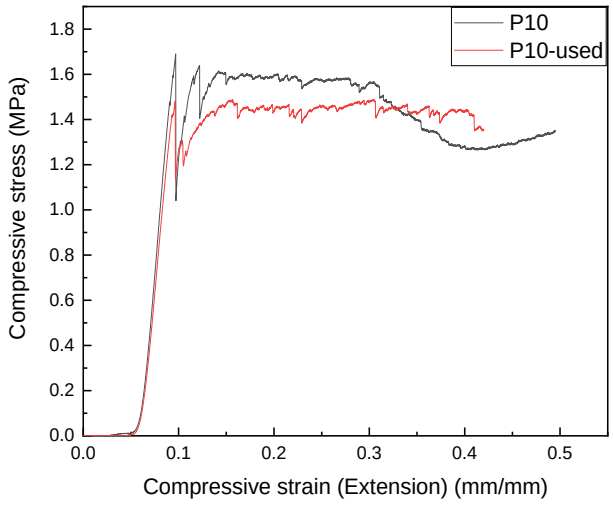

Figure S11: Stress-strain curves pristine and used P10 poly-Pickering-HIPEs micromixer monoliths measured in compression.

REFERENCES

(1) Manley, S.S.; Steindl, P.; Hewitt, G.F.; Bismarck, A. An Integrated Method for Measuring Gas Permeability and Diffusivity of Porous Solids. *Chem. Eng. Sci.* **2020**, *223*, 115725. https://doi.org/10.1016/j.ces.2020.115725.

(2) Kysela, B.; Konfrst, J.; Chara, Z.; Sulc, R.; Jasikova, D. Evaluation of the Turbulent Kinetic Dissipation Rate in an Agitated Vessel. *EPJ Web Conf.* **2017**, *143*, 02062. https://doi.org/10.1051/epjconf/201714302062.

(3) Hattou, S.; Costes, J. *Power, Macromixing and Micromixing in de Dietrich Standard Reactors*; Récents progrès en génie des procédés; Groupe français de génie des procédés diff. Lavoisier-Technique et documentation: Nancy Cachan, 1997.

(4) Barkan-Öztürk, H.; Menner, A.; Bismarck, A. Emulsion Templated Macroporous Polymer Micromixers. *Ind. Eng. Chem. Res.* **2021**, *Submitted*.

(5) Falk, L.; Commenge, J.-M. Performance Comparison of Micromixers. *Chem. Eng. Sci.* **2010**, *65* (1), 405–411. https://doi.org/10.1016/j.ces.2009.05.045.

(6) Gómora-Figueroa, A.P.; Camacho-Velázquez, R.G.; Guadarrama-Cetina, J.; Guerrero-Sarabia, T.I. Oil Emulsions in Naturally Fractured Porous Media. *Petroleum* **2019**, *5* (3), 215–226. https://doi.org/10.1016/j.petlm.2018.12.004.

(7) Grace, H.P. DISPERSION PHENOMENA IN HIGH VISCOSITY IMMISCIBLE FLUID SYSTEMS AND APPLICATION OF STATIC MIXERS AS DISPERSION DEVICES IN SUCH SYSTEMS. *Chem. Eng. Commun.* **1982**, *14* (3–6), 225–277. https://doi.org/10.1080/00986448208911047.

(8) Stegeman, Y.W.; Van De Vosse, F.N.; Meijer, H.E.H. On the Applicability of the Grace Curve in Practical Mixing Operations. *Can. J. Chem. Eng.* **2008**, *80* (4), 1–6. https://doi.org/10.1002/cjce.5450800414.

(9) Chabanon, E.; Sheibat-Othman, N.; Mdere, O.; Valour, J.P.; Urbaniak, S.; Puel, F. Drop Size Distribution Monitoring of Oil-in-Water Emulsions in SMX+ Static Mixers: Effect of Operating and Geometrical Conditions. *Int. J. Multiph. Flow* **2017**, *92*, 61–69. https://doi.org/10.1016/j.ijmultiphaseflow.2017.03.001.

(10) Kiss, N.; Brenn, G.; Pucher, H.; Wieser, J.; Scheler, S.; Jennewein, H.; Suzzi, D.; Khinast, J. Formation of O/W Emulsions by Static Mixers for Pharmaceutical Applications. *Chem. Eng. Sci.* **2011**, *66* (21), 5084–5094. https://doi.org/10.1016/j.ces.2011.06.065.

(11) Cobos, S.; Carvalho, M.S.; Alvarado, V. Flow of Oil–Water Emulsions through a Constricted Capillary. *Int. J. Multiph. Flow* **2009**, *35* (6), 507–515. https://doi.org/10.1016/j.ijmultiphaseflow.2009.02.018.

(12) Romero, M. I. Flow of Emulsions in Porous Media. In *All Days*; SPE: New Orleans, Louisiana, 2009; p SPE-129519-STU. https://doi.org/10.2118/129519-STU.

Publication III

Simultaneous hypercrosslinking and functionalization of polyHIPEs for use as catalyst supports

Hande Barkan-Öztürk,[1] Angelika Menner,[1] Alexander Bismarck,[1,2,] Robert Woodward, [1,*]*

[1] Polymer and Composite Engineering (PaCE) Group, Institute of Material Chemistry and Research, Faculty of Chemistry, University of Vienna, Währinger Strasse, 42, 1090, Vienna, Austria.

[2] Department of Chemical Engineering, Imperial College London, South Kensington Campus, London, SW7 2AZ, United Kingdom

KEYWORDS: Emulsion templating, polyHIPEs, hierarchical porous polymers, hypercrosslinking, heterogeneous catalyst support, Suzuki-Miyaura reaction.

ABSTRACT

Porous polymers offer desirable properties for heterogeneous catalysis, such as excellent stability, high active site density, and reusability. However, their synthesis is often complicated, requiring expensive reagents and laborious synthetic processes. We produce organophosphorus functionalized polyHIPEs by the polymerization of particle and surfactant stabilized water-in-styrene/divinylbenzene high internal phase emulsion templates, followed by post-functionalization using low-cost hypercrosslinking strategies. Three hypercrosslinking approaches were investigated, including knitting with an external crosslinker, solvent stitching and Scholl coupling reaction. Each approach's ability to simultaneously create micro/mesoporosity and incorporate organophosphorus moieties into the polyHIPE structure as catalyst anchor sites were assessed,

introducing surface areas of up to 410 m^2/g and phosphorus concentrations of up to 7.4 wt.%. After Pd-loading, the polyHIPEs displayed outstanding catalytic performance in a Suzuki-Miyaura coupling reaction, reaching turnover frequencies of 2440 h^{-1}. The coarse powder form of the polyHIPEs allowed for simple catalyst recovery from the reaction mixture for reuse.

INTRODUCTION

Hypercrosslinked polymers (HCPs), among porous organic polymers, are of significant interest due to their high porosity, broad monomer pool, excellent stability, and low cost.[1,2] These features allow for their use in a diverse array of applications including gas separation/storage,[3] as stationary phase in liquid chromatography separation,[4] light-harvesting,[5,6] and as heterogeneous catalyst supports.[7] HCPs have been prepared by a variety of bottom-up strategies to crosslink arene monomers, such as 'knitting' using external crosslinkers,[8–10] the solvent stitching method,[11,12] and the Scholl coupling reaction.[13] In the knitting strategy, rigid arene monomers are hypercrosslinked using external crosslinkers, such as dimethoxymethane (DMM), via simple Friedel-Crafts reactions in the presence of a Lewis acid catalyst.[9] Using this approach, a diverse number of micro/mesoporous HCPs with surface areas up to 2300 $m^2\ g^{-1}$ have been reported.[14] In the solvent stitching approach, the reaction medium (typically dichloromethane, (DCM)) acts also as external crosslinker, creating bridges between aromatic rings in the presence of a Lewis acid catalyst.[11] The Scholl reaction forms aryl-aryl bonds between aromatic rings by elimination of two aryl-bound hydrogens.[13] Many HCPs were employed as heterogeneous catalyst supports because of their desirable textural and chemical properties.[7,13,15] However, these HCPs are often as fine powder, requiring extra isolation steps for catalyst recycling.[7,16]

Polymerized high internal phase emulsions (polyHIPEs) are emulsion-templated macroporous polymers[17,18] employed for a wide variety of applications, ranging from filters[19] to tissue engineering scaffolds,[20] spring/separation units[21] and micromixers.[18,22–24] Prior to polymerization, HIPE templates consist of a continuous phase of monomer(s) and an aqueous internal phase, comprising ≥74% of the total emulsion volume. Surfactant-stabilized HIPEs yield emulsion-templated interconnected macroporous structures upon polymerization and drying.[17,22] Particle-stabilized HIPE templates (known as Pickering-HIPEs), typically yield closed pore structure upon adsorption, so called- poly-Pickering-HIPEs, caused by irreversible adsorption of particles at the w/o interface. Interconnected poly-Pickering-HIPEs can be produced by the addition of small amounts of surfactant after emulsification, yielding permeable structures upon polymerization, with improved mechanical performance when compared with common polyHIPEs.[23–25] High porosity macroporous polyHIPEs have relatively low surface areas (< 20 m^2 g^{-1}),[26] hindering their usefulness as heterogeneous catalyst supports.[16] Besides their low surface area, the lack of electron donors able to act as catalyst-complexing ligands result in decreased catalytic activity and stability on traditional polyHIPEs.[27,28] The introduction of hierarchical porosity and chemical functionality into such structures may offer desirable properties, such as rapid mass transport permitted by interconnected macroporous structures and high catalyst loadings due to high surface areas derived from micro/mesopores.[4,16,26]

The production of high surface area polyHIPEs was reported by hypercrosslinking of the polymer to impart micro/mesoporosity.[16,26,29] Poly(styrene-co-divinylbenzene)HIPEs can be further crosslinked by post-modification using external crosslinkers and a Lewis acid catalyst to induce extensive Friedel-Craft alkylation reactions, yielding interconnected polyHIPEs with high surface areas (up to 921 m^2/g).[26,29] Such materials are attractive for many applications, such as oil spill

clean-up[29] or heterogeneous catalysis.[16] Typically, hypercrosslinking is performed on small polyHIPE pieces (approximately 0.5 cm^3)[26,29,30] or even powdered materials,[16] using DMM as external crosslinker and an $FeCl_3$ catalyst. However, the isolation of such small polyHIPE pieces at the end of the reaction can be difficult, particularly when employing external crosslinkers also capable of self-condensation. Perhaps more crucially, the lack of monolithic hypercrosslinked porous polymers limits their applicability in applications, such as monolithic chromatography columns or in flow cells. Tan et al. recently reported the hypercrosslinking of pyridine-containing polyHIPEs, which were subsequently loaded with gold for use as heterogeneous catalysts.[31] Therein, they provide evidence that both hierarchical porosity and functionality are required for good catalytic activity. To test this hypothesis, we apply various crosslinking strategies to the same macroporous scaffold aiming to tailor micro/mesopore content while introducing suitable moieties to anchor catalyst particles functionality.

Using polyHIPE scaffolds, we synthesize catalyst supports containing hierarchical porosity and suitable binding sites by simultaneous hypercrosslinking and functionalization of macroporous poly(styrene-co-divinylbenzene). The hypercrosslinking strategies include knitting with an external crosslinker,[4,26] solvent stitching[11] and Scholl coupling reactions.[13] Various hypercrosslinking approaches are employed to vary polyHIPE surface areas while retaining their emulsion-templated macroporous structures, enabling simultaneous incorporation of aromatic organophosphorus moieties, to be loaded with Pd catalyst. The performance of these Pd-loaded hypercrosslinked polyHIPEs as heterogeneous catalysts is assessed using a model Suzuki-Miyaura coupling reaction. The use of coarse polyHIPE pieces enables easy recovery of the catalysts from the reaction medium for reuse.

EXPERIMENTAL

Materials. Styrene (St) (≥99%), divinylbenzene (DVB) (80%), sorbitan monooleate (Span 80), α,α′-azoisobutyronitrile (AIBN), calcium chloride dihydrate ($CaCl_2 \cdot 2H_2O$) (≥99%), 1,2-dichloroethane (DCE), dimethoxymethane (DMM), chloroform-d, anhydrous ferric chloride ($FeCl_3$), anhydrous aluminum chloride ($AlCl_3$), palladium acetate ($Pd(OAc)_2$), bromobenzene, phenylboronic acid, anhydrous potassium persulfate (K_3PO_4) and triphenylphosphine (PPh_3) were purchased from Sigma-Aldrich (Vienna, Austria). Hydrophobic pyrogenic silica particles (HDK H20) were kindly provided by Wacker Chemie AG (Germany). Dichloromethane (DCM), chloroform ($CHCl_3$), ethyl acetate, hydrochloric acid (37 wt.%) and methanol were purchased from Fisher Chemicals (Vienna, Austria). All materials were used as received.

Preparation of polyHIPEs. PolyHIPE monoliths were prepared by polymerization of the continuous phase of HIPEs consisting of St and DVB in an 8:2 ratio (v/v). H20 silica particles (3 wt.%) were dispersed in the continuous phase in a centrifuge tube (Falcon®) using a dispenser (Kinematica, POLYTRON PT 1600 E, Malters, Switzerland) for 15 min at 15000 rpm. The continuous phase was then transferred into a glass vessel and 1 mol% AIBN (relative to the monomer's polymerizable double bonds) was added. The aqueous internal phase containing 40 g/L $CaCl_2$ was added dropwise, while stirring at 400 rpm using an overhead stirrer fitted with an anchor stirrer. The final internal phase volume fraction was 80%. After addition, stirring continued for 3 min before 10 vol% Span 80 (relative to the continuous phase) was added and mixed for a further 30 s. The resulting emulsion templates were transferred into centrifuge tubes for polymerization in an oven at 70 °C for 4 h. Thereafter, the monoliths were removed and washed with water. The polyHIPEs were then purified via Soxhlet extraction using acetone for 16 h to remove surfactant and unreacted monomer. Finally, the polymers were dried in an oven at 70 °C for 24 h.

Hypercrosslinking of PolyHIPE monoliths

Knitting of macroporous polymers using an external crosslinker. Cylindrical polyHIPE monoliths (12 mm in diameter and 60 mm in length) were swollen for 24 h in DCE (swelling ratio[32] Q = 1.38 ± 0.04, See **ESI S1**). After swelling, DMM external crosslinker (2.9 g per 1 g monolith) and $FeCl_3$ catalyst (7 g per 1 g monolith) were added to reaction mixture. For functionalization with triphenylphosphine (PPh_3), the compound was also added to the mixture (3.7 g per 1 g monolith). Reactions were carried out at 80 °C for 24 h under reflux. After cooling to ambient temperature, the reaction was stopped by addition of methanol and the resulting materials were first washed using a solution of HCl in H_2O (v/v = 1:1 with HCl 37 w/w%) and then using methanol. The monoliths were further purified via Soxhlet extraction using methanol for 24 h. Hypercrosslinked polymers were oven dried at 70 °C for 24 h. We refer to the resulting materials **K-P**.

Solvent-stitching of macroporous polymers. Monoliths were first swollen in DCM (swelling ratio Q = 1.44 ± 0.03, See **ESI S1**) or DCE for 24 h. Afterwards, $AlCl_3$ (7.35 g per 1 g monolith) was added as hypercrosslinking catalyst under constant stirring while purging the reaction mixture with N_2. For organophosphorus functionalization, PPh_3 (3.7 g per 1 g monolith) was also added to the reaction mixture. The reaction was carried out under N_2 at 25 °C for 16 h, followed by 40 °C for 24 h and then 80 °C for a further 24 h. After cooling to room temperature, a HCl-H_2O solution (v/v = 1:1 with HCl 37 w/w%) was used to quench the reaction. The same washing, purification and drying procedure as described above was followed. Solvent stitched samples are denoted as **STM-P** when using DCM as solvent or **STE-P** when using DCE. The M and E in their nomenclature refer to the anticipated methyl- and ethyl-bridges to be formed during solvent stitching when using DCM and DCE, respectively.

Scholl coupling reaction of macroporous polymers. Monoliths were first swollen in $CHCl_3$ (swelling ratio Q = 1.41 ± 0.02, See **ESI S1**) for 24 h. $AlCl_3$ (7.35 g per 1 g monolith) was added as hypercrosslinking catalyst. For organophosphorus functionalization, PPh_3 (3.7 g per 1 g monolith) was also added to the solvent. After purging with N_2, the reaction was carried out at 60 °C for 48 h under reflux. Again, the washing and drying procedure remained unchanged. Scholl coupled polyHIPEs are denoted **SH-P**.

Preparation of Pd loaded polyHIPE catalyst supports

Pd catalyst was immobilized onto the hypercrosslinked (functionalized) polyHIPEs (0.1 g) by first soaking the pieces in DCM (10 mL) containing $Pd(OAc)_2$ (0.058 g, 0.26 mmol) followed by reflux for 2 h over stirring. Control experiments with non-functionalized hypercrosslinked scaffolds revealed that Pd is not successfully attached (see **ESI Figure S2.1**). Catalyst-loaded supports were collected using tweezers, dried in a fume hood and washed with acetone to remove residual non-bound Pd^{II} and afterwards were dried at 70 °C in an oven. The Pd-loaded supports are indicated by **Pd@**, for example **Pd@K-P**.

Suzuki-Miyaura coupling reaction using Pd@HCP-polyHIPEs catalysts

The catalytic properties of Pd-loaded hypercrosslinked polyHIPEs were tested using the Suzuki-Miyaura coupling reaction of bromobenzene with phenylboronic acid (**Figure 1**).[33] Bromobenzene (1 mmol), phenylboronic acid (1.1 mmol) and anhydrous K_3PO_4 (3 mmol) were added to 4 mL H_2O-EtOH (v/v = 1:1) solution. After the K_3PO_4 dissolved, a single piece of Pd@catalyst support (4 ± 0.4 mg) was added to the mixture. The reaction was allowed to proceed for 30 min at 80 °C while stirring. Afterwards, the Pd-loaded support was removed from the reaction mixture with tweezers and washed with ethanol, water, and ethyl acetate. The catalyst was then pat-dried with

tissue before reuse. Each sample was used six times to investigate catalyst recycling. To extract reaction products and unreacted educts from the reaction mixture, ethyl acetate was used. The organic ethyl acetate phase was dried over $MgSO_4$, filtered and the solvent removed using a rotary evaporator. The recovered solid residue was characterized by ^1H NMR and biphenyl yields were calculated by the ratio of the biphenyl spectral signal to the total signal including aryl halide. The reaction was repeated three times with fresh Pd-loaded supports and each repeat was recycled six times.

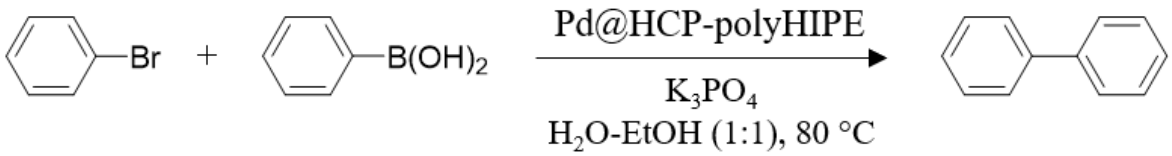

Figure 1. Suzuki-Miyaura coupling reaction of bromobenzene with phenylboronic acid at 80 °C using Pd-loaded catalyst support.

Characterization methods

High magnification images of fractured (hypercrosslinked) polyHIPEs (taken from three different locations) were recorded using scanning electron microscopy (JEOL SEM, JCM-6000) operated in high vacuum mode with an acceleration voltage of 15 kV. The samples were attached to a sample holder and sputtered with gold for 50 s, prior to imaging (JEOL JFC-1200). SEM images were further analyzed using an image analysis software package (ImageJ©, https://imagej.nih.gov/ij/download.html) to determine pore (d_p) and pore throat (d_{pt}) diameters. At least 100 pore and pore throat diameters were characterized for each sample and their mean value was used. The skeletal density (ρ_s) was measured using He displacement pycnometry (AccuPyc, 1330, Micromeritics Ltd.) after grinding (repeated three times with fresh samples). The

foam density (ρ_f) was analyzed using a foam density analyzer (GeoPyc 1360, Micromeritics Ltd.) using the volume displacement method (repeated five times with fresh samples). The porosity (*P*) was calculated:

$$P\% = \left(1 - \frac{\rho_f}{\rho_s}\right) \cdot 100\% \qquad \text{(Eq. 1)}$$

N_2 adsorption isotherms of (hypercrosslinked) polyHIPEs (repeated three times with fresh samples) were measured using a porosity analyzer (Tristar, Micromeritics Ltd.) at 77 K. Prior to analysis, samples were degassed under N_2 flow at 393 K overnight. Surface areas were calculated using the Brunauer-Emmett-Teller (BET) method.[34]

FT-IR spectra were recorded three times with new samples in the range of 4000-400 cm^{-1} (Bruker Tensor II fitted with an A225/Q Platinum ATR unit). The sample was pressed using a clamp onto ATR unit to achieve good contact. Solid-state ^{13}C cross polarization (CP) and ^{31}P high power decoupling (HPDEC) magic angle spinning (MAS) NMR spectra were collected (Bruker Biospin AV III 600 MHz NMR spectrometer) and integration was performed using OriginLab software using a Gaussian fit. The elemental composition of samples was analyzed by high resolution X-ray photoelectron spectroscopy (HR-XPS) (Nexsa, Thermo Fisher Scientific) using Al K_α radiation and the spectra analyzed (Avantage v5.9925 with Smart background, Simplex fitting and Gauss-Lorentz product). Reference values for functional group binding energies were sourced from the NIST Standard Reference Database.[35] Weight% of the detected atom ($wt._i\%$) was calculated from its atomic% ($at._i\%$) determined from the area under the XPS curve, which was given by the software:

$$wt_i\% = \frac{M_{W_i} \cdot at_i\%}{\sum_{j=1}^{k}(M_{W_j} \cdot at_j\%)} x100 \qquad (Eq.2)$$

Total Pd-loading was determined using total X-ray reflection fluorescence spectrometry (TXRF) (Bruker S2 PicoFox TXRF). The Pd-P complex was destroyed by dispersing powdered samples (~0.1 g) in HNO_3 for 48 h in air atmosphere. ^{1}H NMR spectra (Bruker BioSpin AV III HD 700) were collected in chloroform-d and product yields were calculated by peak integration. Elemental analysis (Eurovector EA 3000 CHNS-O Elemental Analyser) were performed using 0.75 and 3.0 mg of sample, weighed into tin vials (4×6 mm). Samples were run at least in duplicate. The operating temperatures for combustion and reduction were 1000 °C (1480 °C for O analysis) and 750 °C, respectively, using He (99.999+) as carrier gas.

RESULTS AND DISCUSSION

Morphology and mechanical performance of polyHIPEs

PolyHIPEs possessed interconnected pore structures (**Figure 2**) with average pore diameters d_p = 80.2 ± 29.1 μm and average pore throat diameters d_{pt} = 20 ± 12 μm. The structures had skeletal densities ρ_s = 1.12 g/cm^3 and possesses a porosity of 86%. The polyHIPEs prepared from an emulsion template stabilized using both particles and surfactant had improved mechanical properties (E = 48 MPa, σ_c = 2 MPa) compared with their equivalents prepared by polymerization of solely surfactant-stabilized HIPEs (E = 18 MPa, σ_c = 1 MPa) (See **ESI S3**). Although conventional poly(St-co-DVB)HIPEs are chemically stable and can be hypercrosslinked,[26,29] their structures are very brittle and friable, which did result in structural erosion during post-modification and use (See **ESI Figure S4.1**). In contrast, polyHIPEs derived from particle and surfactant-stabilized HIPEs, having the same chemical composition, were much more robust

during both hypercrosslinking and use as heterogeneous catalyst supports (**ESI Video S1**). Thus, we will only further consider the latter polyHIPEs and data for the conventional polyHIPE equivalents can be found in the **ESI S4**.

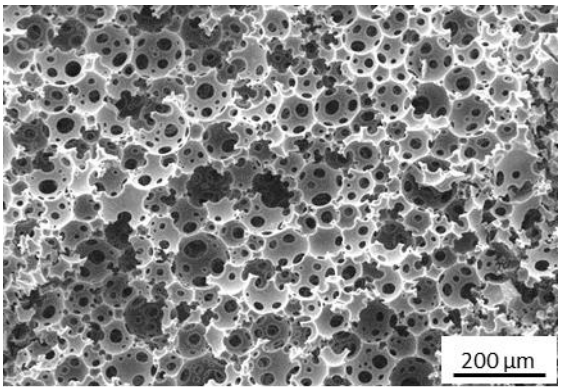

Figure 2. Characteristic SEM image of a polyHIPE prepared by polymerization of a HIPE simultaneously stabilized by H20 silica particles and Span 80.

Chemical and structural properties of hypercrosslinked and functionalized polyHIPEs

We produced polyHIPEs with functionalized hierarchical pore structures, i.e. possessing macro-, meso- and micropores, using three hypercrosslinking methods, in order to simultaneously increase their surface areas and incorporate triphenylphosphine moieties into their structures. Phosphines are known to form stable transition metal complexes, which can help stabilize catalyst performance, and improve leaching resistance and catalytic activity.[13,15,36] Triphenylphosphine was selected due to its aromaticity, enabling linkage to the polyHIPE and immobilizing organophosphorus functional group on the porous structure. After knitting with a DMM external crosslinker, **K-P** retained the monolith structure and turned from white to orange-brown (**Figure S5.1)**. After solvent stitching (**STM-P** or **STE-P**) and the Scholl coupling reaction (**SH-P**), all structures again had an orange-brown color, however the polyHIPE monoliths were cracked and/or

broken. This cracking may be due to rapid vapor release during the quenching of $AlCl_3$ within the rigid structures. However, the remaining pieces retained structural integrity and were not friable, which enabled their use as heterogeneous catalyst support in batch reactions. Moreover, hypercrosslinking approaches did not affect the emulsion-templated morphology (**Figure S5.2**). As a result of hypercrosslinking, the skeletal density of all networks increased (**Table 1**).

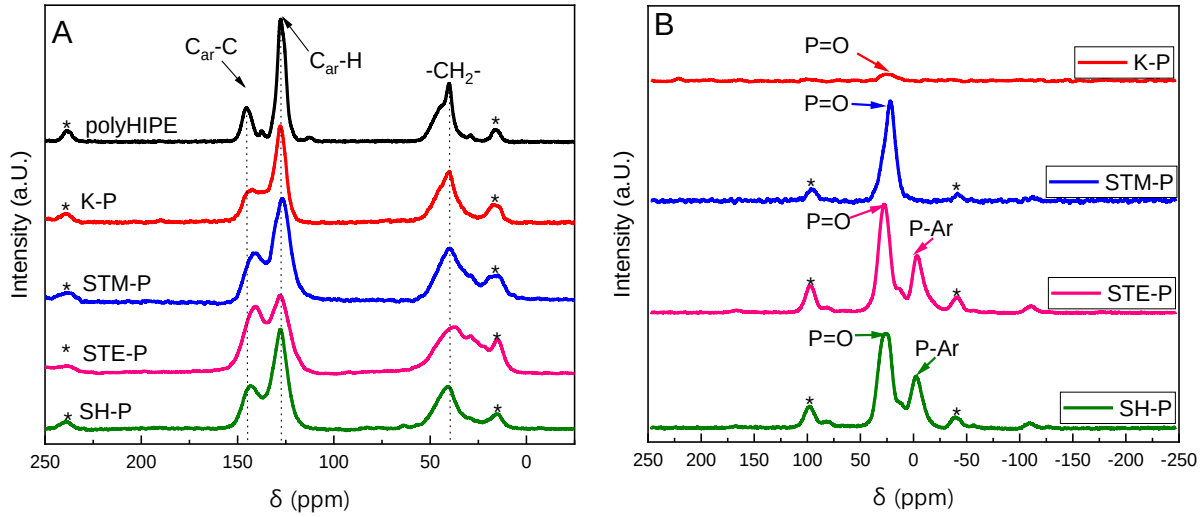

Figure 3. A) ^{13}C cross-polarization magic-angle spinning (CP/MAS) NMR spectra and B) ^{31}P (HPDEC/MAS) NMR of hypercrosslinked and functionalized polyHIPEs. (Asterisks denote spinning sidebands)

The successful simultaneous hypercrosslinking and functionalization of polyHIPE scaffolds was confirmed by ^{13}C CP/MAS NMR (**Figure 3A** – the spectra of only hypercrosslinked polyHIPEs are in **ESI S6**). Peaks at ~144 ppm and ~127 ppm were assigned to substituted (C_{ar}-C) and non-substituted (C_{ar}-H) aromatic carbons, respectively.[37] The peak area ratio between C_{ar}-H and C_{ar}-C decreased from 3.4 for pristine polyHIPEs to 1.1 in **K-P** and 2.0 in **STM-P** (for peak deconvolution see **ESI S7**). This change is indicative of an increase in substituted aromatic carbons, confirming successful crosslink formation.[38] The peak ratio was 1.0 and 1.7 for **STE-P** and **SH-P**,

respectively. Unfortunately, newly formed methylene/ethylene bridges are not easily identified due to peak overlap with the poly(St-co-DVB) backbone at ca. 40 ppm, only the emergence of a peak shoulder at ca. 35 ppm was observed.

We confirmed the simultaneous incorporation of phosphorus species using ^{31}P HPDEC/MAS NMR. In **K-P** and **STM-P**, a resonance peak at 26 ppm was observed, indicative of an oxidized triphenylphosphine ($PO(Ph)_3$) (**Figure 3B**).[39] A weak signal in the ^{31}P NMR spectrum of **K-P** shows significantly lower P incorporation, as confirmed by EA and XPS (**Table 1**). ^{31}P NMR spectra of **STE-P** and **SH-P** contained resonance peaks at both 27 ppm and -3.5 ppm, which were assigned to $O=P(Ph)_3$ and PPh_3, respectively. Peak area ratios of $O=P(Ph)_3$ and PPh_3were 0.6 for **STE-P** and 0.5 for **SH-P** (**Figure S8.1**). Unfortunately, the literature is ambiguous regarding the state of the organophosphorus species in hypercrosslinked networks prior to Pd-binding.[13,28,40] Either ^{31}P NMR of their supports are not reported or peaks are not specifically assigned. Therefore, we investigate further the organophosphorus species of our materials using XPS. HR-XPS spectra confirmed the presence of P in all functionalized hypercrosslinked polyHIPEs (**Figure S8.4** and **Table 1**). The P 2p spectra of **STM-P**, **STE-P** and **SH-P** all showed the linkage of P-C_{Ar} at binding energies of 130.4 eV and the presence of significant P=O at a binding energy of 132.5 eV (**Figure S8.4**). The oxidized triphenylphosphine species is also apparent in the O 1s spectra, where peaks at a binding energy of 531.1 eV are indicative of O=P bonds (**Figure S8.5**). **K-P** did not contain enough P to deduce reliable information.

Table 1. Morphological and structural properties of functionalized hypercrosslinked polyHIPEs, including skeletal density (ρ_s), foam density (ρ_f), porosity (P), specific surface area (A_S), and P content.

Sample name	ρ_s (g/cm^3)	ρ_f (g/cm^3)	P (%)	A_S (m^2/g)	P[i] (wt.%)	P[ii] (wt.%)	Pd-loading[iii] (wt.%)
polyHIPE	1.12 ± 0.02	0.11 ± 0.01	86 ± 2	7 ± 1	0	0	-
K-P	1.17 ± 0.04	0.11 ± 0.01	92 ± 4	370 ± 3	0.6	0.4	10.2
STM-P	1.30 ± 0.01	0.17 ± 0.01	86 ± 0.8	410 ± 30	3.2	2.6	3.4
STE-P	1.13 ± 0.01	0.23 ± 0.01	80 ± 1.3	9 ± 2	6.3	4.3	2.8
SH-P	1.28 ± 0.03	0.23 ± 0.03	82 ± 2.2	240 ± 7	7.4	5.6	2.1

[i] P content was determined using XPS.
[ii] P content was determined using Elemental Analysis.
[iii] Pd content was determined using TXRF.

FTIR spectra of all hypercrosslinked and functionalized polyHIPEs (**Figure S8.6**) contain a group of bands in the region 3000-2800 cm^{-1}, corresponding to aliphatic C-H stretching as well as bands at 3100-3000 cm^{-1}, attributed to aromatic C-H stretching. After crosslinking, aliphatic C-H bands increased in intensity compared to aromatic C-H due to the introduction of m/ethylene crosslinks. Bands in the region 1600-1400 cm^{-1} were assigned to substituted aromatic ring skeleton vibrations, which became broader after hypercrosslinking (**Figure 3B**). The intensity of the sharp band at 700 cm^{-1} decreased due to substitution of the aromatic ring in the *para* position. P-C_{Ar} stretching is observed as a sharp band at 1090 cm^{-1} in the FTIR spectrum of pure PPh_3,[41] however, the identification of P-C_{Ar} in hypercrosslinked and functionalized polyHIPEs is difficult due to overlap with the broad band at around 1100 cm^{-1} attributed to silica (**Figure S8.6**). Moreover, a broad band at around 600 cm^{-1} was observed in **SH-P**, which we assign to C-Cl stretching due to the incorporation of $CHCl_3$ (**Figure 3B**). It is often hypothesized in the literature that the Scholl coupling reaction for the formation of HCPs involves the elimination of two aryl-bound H atoms to form a direct bond between aryl groups.[13] However, HR-XP Cl 2p spectrum of **SH-P** showed

both metal-chloride bonds, evidence of residual $AlCl_3$ catalyst, and C-Cl bonds, indicative of possible solvent stitching of $CHCl_3$ to aromatic rings (**Figure S8.7**). This result suggests that methylene linkers as well as direct aryl-aryl bonds are formed in the Scholl coupling reaction in $CHCl_3$. Furthermore, Rozyyev et al.[42] showed recently that alky bridging reactions are more feasible than the aryl couplings when using $CHCl_3$ as solvent.

We probed the thermal stability of all hypercrosslinked and functionalized polyHIPEs using thermogravimetric analysis (TGA) in nitrogen. The TGA of **STM-P** and **STE-P** showed approximately 57% and 61% weight loss, respectively, of the polymers occurs at ~400 °C. **K-P** and **SH-P** displayed a weight loss of approximately 64% and 51%, respectively, at the same temperature, while non-crosslinked polyHIPE lost ~ 90% (See **ESI S9**), demonstrating improved thermal stability imparted by hypercrosslinking.

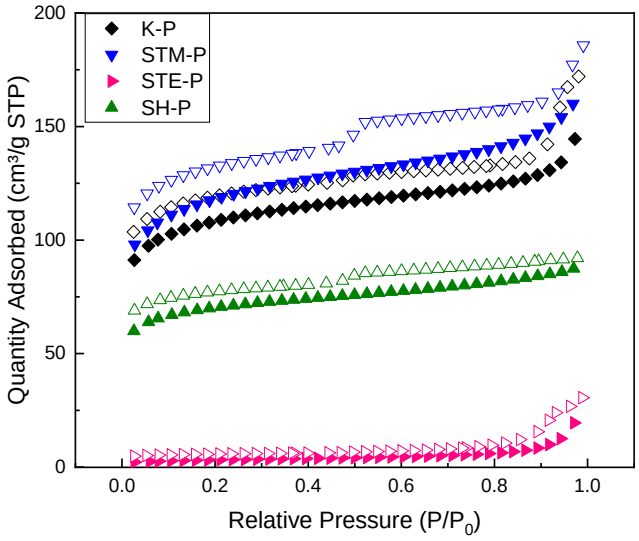

Figure 4: N_2 sorption isotherms at 77 K of hypercrosslinked and functionalized polyHIPEs.

The micro/mesoporosity of all hypercrosslinked (**Figure S6.2**) and functionalized polyHIPEs was analyzed using N_2 adsorption analysis (**Figure 4**). The adsorption isotherms of native polyHIPEs

show no significant N_2 uptake, suggesting low micro/mesoporosity (A_S = 7 m^2/g). With the exception of **STE-P**, all other hypercrosslinked (**Figure S6.2**) and functionalized polyHIPEs showed steep N_2 uptake at low relative pressures, indicative of significant microporosity. The presence of hysteresis upon desorption is also indicative of capillary condensation in mesopores.[43] **K-P** and **STM-P** showed the largest A_S increases, reaching 370 m^2/g and 410 m^2/g, respectively (**Table 1**). To the best of our knowledge, neither solvent stitching nor Scholl coupling has thus far been reported for the formation of hierarchically porous networks with such broad pore size distributions. **STE-P** showed no A_S increase after solvent stitching (A_S = 9 m^2/g), due to the formation of more flexible networks when crosslinking with ethylene bridges, allowing more efficient packing (**Table 1**). Additionally, some incomplete crosslink formation in **STE-P** was observed by XPS, as both metal-Cl (from $AlCl_3$) and C-Cl bonds were detected in the Cl 2p spectrum (3.25 wt.% Cl) (**Figure S8.7A**). Wang et al.[11] also observed a reduced A_S when stitching biphenyl using DCE (A_S = 536 m^2/g) as compared to DCM (A_S = 1475 m^2/g). Finally, the Scholl coupling/$CHCl_3$ solvent stitching and functionalization of polyHIPEs led to A_S of 240 m^2/g in **SH-P**.

Catalytic performance of hypercrosslinked and functionalized polyHIPEs

The simultaneous hypercrosslinking and introduction of organophosphorus moieties into polyHIPEs produced stable heterogeneous catalyst supports, which were Pd-loaded by soaking the samples in $Pd(OAc)_2$ solutions. Upon Pd-loading, the P peaks of **Pd@STE-P** and **Pd@SH-P** in ^{31}P HPDEC/MAS NMR consolidated into a single peak at 28.7 and 30 ppm, respectively (**Figure S10.1**). This is in-line with previous reports and indicative of the successful coordination of Pd^{II} to organophosphorus moieties.[13,28,40] Denmark et al.[44] demonstrated that triphenylphosphine oxide can in fact act as an efficient ligand for Pd in catalytic species. Therefore, we hypothesise that

although our hypercrosslinked and functionalized polyHIPEs mainly contain $O=P(Ph)_3$ species, they are still able to act as efficient ligands for Pd. High resolution P 2p XPS showed that the peak shifted from 132.4 eV to 133 eV upon Pd-loading in our polymers, confirming the formation of Pd complexes (**Figure S8.5**).[39] Furthermore, the Pd 3d HR-XP spectra revealed that Pd^0 and Pd^{II} species were present in **Pd@STM-P**, **Pd@STE-P**, and **Pd@SH-P** at binding energies of 335.9 eV and 337.6 eV in the Pd $3d_{5/2}$ level and 341.3 eV and 343.4 eV in the Pd $3d_{3/2}$ level, respectively (**Figure 5**).

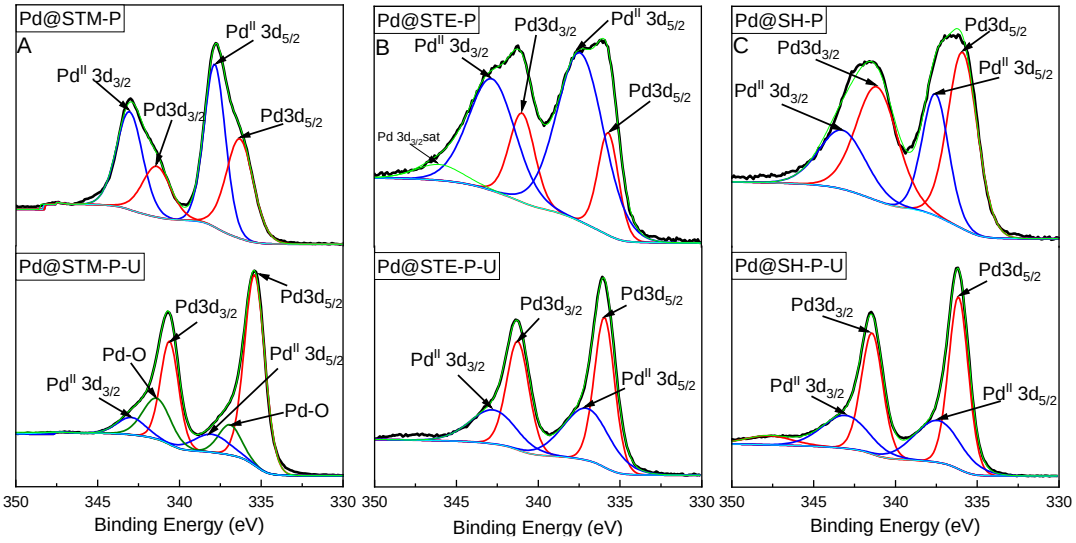

Figure 5: High resolution Pd 3d XP spectra of A) **Pd@STM-P**, B) **Pd@STE-P** and C) **Pd@SH-P**. Spectra of the Pd-loaded polymers after 6 reaction cycles are included (denoted with -U) (green line represents fitting and black line is the original data).

Pd-loaded hypercrosslinked and functionalized polyHIPEs (**Figure S10.4A**) were used as heterogeneous catalysts for Suzuki-Miyaura cross-coupling reactions of bromobenzene (

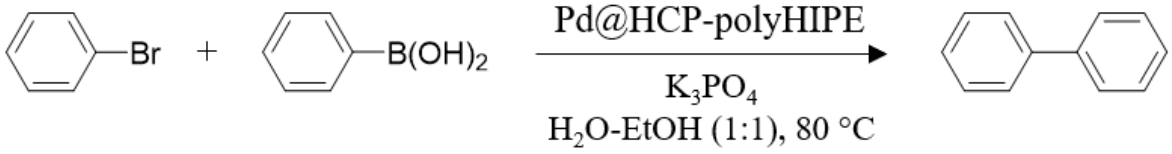

Figure 1). Homogeneous catalysis using $Pd(PPh_3)_4$ reached substrate conversions of just 15% after 30 min. Hypercrosslinked and functionalized polyHIPEs prior to Pd loading showed no catalytic activity. All Pd-loaded polyHIPEs, irrespectively of P content, resulted in yields of 98% in the first Suzuki-Miyaura coupling reaction cycle (**Table 2**). Pd-loaded non-organophosphorus functionalized hypercrosslinked polyHIPEs showed significant reductions in catalytic activity after the first reaction cycle due to a lack of Pd complexes resulting in catalyst leaching, as evidenced by the formation of a Pd black slurry. Although **Pd@K-P** contained the highest amount of Pd, as determined using TXRF (**Table 1**), the catalytic activity of **Pd@K-P** reduced dramatically after the first reaction cycle and was completely inactive after the third (**Table 2**). As **Pd@K-P** contained only 0.6 wt.% P, catalyst leaching occurred, which was again confirmed by the formation of a Pd black slurry (**Figure S10.4C**). Furthermore, 75% catalyst loss after the first reaction cycle was observed by XPS. High initial Pd concentrations may be due to the combined effect of the high A_S and swelling degree of **K-P** in DCM (See **ESI Video S2** and **Figure S10.5**). XPS showed that both fresh **Pd@K-P** and the same sample after three reaction cycles had binding energies of Pd $3d_{5/2}$ at 335.5 eV and 336.4 eV (**Figure S10.8**), indicative of Pd^0 and the formation of PdO, respectively.

Table 2. Suzuki-Miyaura coupling reaction yields obtained using Pd-loaded hypercrosslinked and functionalized polyHIPE catalysts.

#	**Pd@K-P** yield (%)	**Pd@STM-P** yield (%)	**Pd@STE-P** yield (%)	**Pd@SH-P** yield (%)
1	96 ± 1	98 ± 3	98 ± 1	98 ± 1
2	18 ± 3	83 ± 3	95 ± 2	96 ± 2
3	9 ± 2	83 ± 3	94 ± 2	97 ± 1
4	0	82 ± 4	94 ± 2	97 ± 1
5	-	81 ± 3	93 ± 1	96 ± 1
6	-	82 ± 4	92 ± 1	91 ± 6

In contrast to **Pd@K-P,** polyHIPE catalyst **Pd@STM-P** retained good catalytic activity upon reuse, decreasing slightly to 83% yield after reaction cycle one and then retaining its activity across five additional cycles. The initial drop in activity is attributed to oxidation and reducing of Pd during the reaction, which was observed by a shift in Pd^{II} binding energy from 337.6 eV to 336.5 eV and 335.3 eV in the Pd $3d_{5/2}$ level, respectively (**Figure 5**). On the other hand, polyHIPE catalysts **Pd@STE-P** and **Pd@SH-P** showed almost no activity loss upon reuse over six cycles (**Table 2** and **ESI S11**). After a reaction time of 30 min, a turnover frequency (TOF)[45] of 1880 h^{-1} and 2440 h^{-1} was calculated for **Pd@STE-P** and **Pd@SH-P**, respectively (See **ESI S12**). Moreover, the XPS binding energies of Pd $3d_{5/2}$ and $3d_{3/2}$ levels in **Pd@STE-P** and **Pd@SH-P** remained unchanged after re/use. Lei et al.[36] produced P-functionalized porous organic polymers in fine powder form as Pd catalyst supports for Suzuki-Miyaura coupling reactions. Their Pd 3d XP spectra revealed the presence of both Pd^0 and Pd^{II} states after the first reaction cycle which remained unchanged following further cycles. Our catalysts, containing both Pd^0 and Pd^{II} states, were also able to repeatedly perform Suzuki-Miyaura reactions to high conversion yields.

Although our hypercrosslinked and functionalized polyHIPEs possess lower A_S than many hypercrosslinked polymers produced from discreet aromatics, they nevertheless showed good catalytic performance in the Suzuki-Miyaura coupling reaction of bromobenzene with phenylboronic acid as compared to Pd-immobilized microporous organic polymers. Li et al.[28] reached a TOF of 162 h^{-1} using 0.7 wt.% Pd-loaded knitted aryl network synthesized by knitting benzene and triphenylphosphine with DMM external crosslinker. A microporous polymer produced via Scholl coupling of triphenylbenzene and PPh_3 contained 1.2 wt.% of Pd after loading and achieved an impressive TOF of 59400 h^{-1}.[13] Microporous copolymers of benzene and N-heterocyclic carbene knitted using DMM contained 5.1 wt.% Pd and resulted in TOFs of 990 h^{-1}.[46] Using similar copolymers, Xu et al. reached TOFs of 8684 h^{-1}, even with Pd loadings <0.06 mmol/g.[27] However, in both cases, N-heterocyclic carbene monomer needed to first be synthesized, somewhat complicating catalyst production. In all of these examples, the catalyst supports are produced in a fine powder form, which require laborious filtration steps. To try to eliminate this, Desforges et al.[47] functionalized polyHIPEs with various amino groups for use as Pd catalyst support, reporting yields of 60% for the Suzuki coupling of iodobenzene and phenylboronic acid after 23 h. Mrózka et al.[48] incorporated Pd into polyHIPEs modified with silica for hydrogenation reactions. However, their polyHIPEs disintegrated during stirring due to poor mechanical properties. Because of this, they crushed the materials into fine powder for use, negating the advantages of the emulsion-templated network and again requiring filtration. In addition to good catalyst activity, our coarse powder supports were easily recovered using tweezers, post-catalytic conversion (See ESI **Video S1**), and avoiding filtration. High organophosphorus concentrations permitted high Pd-loadings, irrespective of support surface area,

and emulsion templated macroporosity improved mass transport to active sites. Furthermore, we observed no decrease in catalytic activity after supports were exposed to air.

CONCLUSION

Inspired by encouraging reports in the literature, we attempted to discern the role of surface area and catalyst support functionality on the effectiveness of Pd-loaded heterogeneous catalyst supports. We report the simultaneous hypercrosslinking and functionalization of two polyHIPE supports using three different hypercrosslinking approaches. We successfully introduced micro/mesoporosity into macroporous polymers to produce hierarchical pore structures. We showed that incorporation of organophosphorus moieties was dependent upon hypercrosslinking approach. With the exception of **K-P**, which was knitted using DMM external crosslinker, high organophosphorus content was achieved in all simultaneously hypercrosslinked and functionalized polyHIPEs, increasing the stability of loaded Pd. By comparing the catalytic activity of **Pd@STE-P** (TOF = 1884, A_S = 9 m^2/g) with **Pd@STM-P** (TOF= 1544, A_S = 410 m^2/g) and **Pd@SH-P** (TOF = 2440, A_S = 240 m^2/g), it is clear that the presence of micro/mesoporosity, and hence high surface areas, is not crucial in the design of catalyst supports for Suzuki-Miyaura cross-coupling reactions. Solvent stitching with DCE followed by Pd-loading produced excellent macroporous polyHIPE catalysts without the introduction of micro/mesoporosity. Our hypercrosslinked and functionalized polyHIPEs had excellent catalytic activities in mild conditions and aqueous media and could be successfully reused multiple times without significant performance reduction. Moreover, owing to their coarse powder form, they were easily and quickly separated from the reaction for reuse without filtration. This low-cost strategy to functionalized polyHIPEs provides a practical route to designable supports for various precious metals.

ASSOCIATED CONTENT

Supporting Information.

The following files are available free of charge.

Additional characterization methods and their results (i.e. swelling and mechanical tests of polyHIPEs) and chemical and structural properties of hypercrosslinked and/or functionalized conventional-polyHIPEs, hypercrosslinked polyHIPEs. The detail results of hypercrosslinked and functionalized polyHIPE are also included to the ESI.

Supporting_Information.pdf

AUTHOR INFORMATION

Corresponding Author

* Alexander Bismarck, E-mail: alexander.bismarck@univie.ac.at *Robert Woodward, E-Mail: robert@woodward.univie.ac.at

Author Contributions

All authors conceptualized the work, HBÖ performed all experimental work and analyzed the data. HBÖ, RW and AB wrote the manuscript and designed the figures. AM, RW and AB supervised the work. All authors contributed to manuscript review and editing.

Funding Sources

HBÖ gratefully acknowledges financial support by the University of Vienna.

ACKNOWLEDGMENT

We acknowledge the financial support from Faculty of Chemistry, University of Vienna. We thank Franz Jirsa for TXRF analysis, Andreas Mautner for XPS measurements, and Hanspeter Kählig for NMR and ssNMR measurements. We also thank the students who involved in the experimental and characterization parts, Maximilian Spitaler and Martin Gostner.

ABBREVIATIONS

A_S, surface area calculated using BET method; d_p, average pore diameter (μm); d_{pt}, average pore throat diameter (μm); P, porosity (%).

Greek Letters

ρ_s, skeletal density (g cm^{-3}); ρ_f, foam density (g cm^{-3}).

Acronyms

AIBN, α, α′-azoisobutyronitrile; BET, Brunauer, Emmett and Teller; CP/MAS, cross-polarization magic-angle spinning; DCE, 1,2-dichloroethane; DCM, dichloromethane; DMM, dimethoxymethane; DVB, divinylbenzene; FTIR, Fourier-transform infrared spectroscopy; HCP, hypercrosslinked polymers; HDK H20, hydrophobic pyrogenic silica particles; HIPE, high internal phase emulsion; HPDEC, high power decoupling; NMR, nuclear magnetic resonance; polyHIPE, polymerized high internal phase emulsion; SEM, scanning electron microscopy; Span 80, sodium monosorbitol; TGA, thermal gravimetric analysis; TOF, turnover frequency; TON, turnover number; TXRF, total X-ray reflection fluorescence; XPS, X-ray photoelectron spectroscopy.

REFERENCES

(1) Tan, L.; Tan, B. Hypercrosslinked Porous Polymer Materials: Design, Synthesis, and Applications. *Chem. Soc. Rev.* **2017**, *46* (11), 3322–3356. https://doi.org/10.1039/C6CS00851H.

(2) Davankov, V.; Rogozhin, V.; Tsjurupa, M. Macronet Polystyrene Structures for Ionites and Method of Producing Same. US3729457A, April 24, 1973.

(3) Liu, G.; Wang, Y.; Shen, C.; Ju, Z.; Yuan, D. A Facile Synthesis of Microporous Organic Polymers for Efficient Gas Storage and Separation. *J. Mater. Chem. A* **2015**, *3* (6), 3051–3058. https://doi.org/10.1039/C4TA05349D.

(4) Maya, F.; Svec, F. A New Approach to the Preparation of Large Surface Area Poly(Styrene-Co-Divinylbenzene) Monoliths via Knitting of Loose Chains Using External Crosslinkers and Application of These Monolithic Columns for Separation of Small Molecules. *Polymer* **2014**, *55* (1), 340–346. https://doi.org/10.1016/j.polymer.2013.08.018.

(5) Schukraft, G. E. M.; Woodward, R. T.; Kumar, S.; Sachs, M.; Eslava, S.; Petit, C. Hypercrosslinked Polymers as a Photocatalytic Platform for Visible-Light-Driven CO_2 Photoreduction Using H_2O. *ChemSusChem* **2021**, *14* (7), 1720–1727. https://doi.org/10.1002/cssc.202002824.

(6) Wang, S.; Xu, M.; Peng, T.; Zhang, C.; Li, T.; Hussain, I.; Wang, J.; Tan, B. Porous Hypercrosslinked Polymer-TiO2-Graphene Composite Photocatalysts for Visible-Light-Driven CO2 Conversion. *Nat. Commun.* **2019**, *10* (1), 676. https://doi.org/10.1038/s41467-019-08651-x.

(7) Xu, W.; Liu, C.; Xiang, D.; Luo, Q.; Shu, Y.; Lin, H.; Hu, Y.; Zhang, Z.; Ouyang, Y. Palladium Catalyst Immobilized on Functionalized Microporous Organic Polymers for C–C Coupling Reactions. *RSC Adv.* **2019**, *9* (59), 34595–34600. https://doi.org/10.1039/C9RA07303E.

(8) Davankov, V.; Tsyurupa, M.; Ilyin, M.; Pavlova, L. Hypercross-Linked Polystyrene and Its Potentials for Liquid Chromatography: A Mini-Review. *J. Chromatogr. A* **2002**, *965* (1–2), 65–73. https://doi.org/10.1016/S0021-9673(01)01583-7.

(9) Li, B.; Gong, R.; Wang, W.; Huang, X.; Zhang, W.; Li, H.; Hu, C.; Tan, B. A New Strategy to Microporous Polymers: Knitting Rigid Aromatic Building Blocks by External Cross-Linker. *Macromolecules* **2011**, *44* (8), 2410–2414. https://doi.org/10.1021/ma200630s.

(10) Prince, L.; Guggenberger, P.; Santini, E.; Kleitz, F.; Woodward, R. T. Metal-Free Hyper-Cross-Linked Polymers from Benzyl Methyl Ethers: A Route to Polymerization Catalyst Recycling. *Macromolecules* **2021**, *54* (19), 9217–9222. https://doi.org/10.1021/acs.macromol.1c01332.

(11) Wang, S.; Zhang, C.; Shu, Y.; Jiang, S.; Xia, Q.; Chen, L.; Jin, S.; Hussain, I.; Cooper, A. I.; Tan, B. Layered Microporous Polymers by Solvent Knitting Method. *Sci. Adv.* **2017**, *3* (3), e1602610. https://doi.org/10.1126/sciadv.1602610.

(12) Msayib, K. J.; McKeown, N. B. Inexpensive Polyphenylene Network Polymers with Enhanced Microporosity. *J. Mater. Chem. A* **2016**, *4* (26), 10110–10113. https://doi.org/10.1039/C6TA03257E.

(13) Li, B.; Guan, Z.; Yang, X.; Wang, W. D.; Wang, W.; Hussain, I.; Song, K.; Tan, B.; Li, T. Multifunctional Microporous Organic Polymers. *J. Mater. Chem. A* **2014**, *2* (30), 11930. https://doi.org/10.1039/C4TA01081G.

(14) Hou, S.; Razzaque, S.; Tan, B. Effects of Synthesis Methodology on Microporous Organic Hyper-Cross-Linked Polymers with Respect to Structural Porosity, Gas Uptake Performance and Fluorescence Properties. *Polym. Chem.* **2019**, *10* (11), 1299–1311. https://doi.org/10.1039/C8PY01730A.

(15) Song, K.; Jiang, Y.; Zou, Z. Effect of Vesicle Structure on Catalytic Activity of Suzuki-Miyaura Cross-Coupling Reaction: Impact of Framework and Morphology. *ChemistrySelect* **2020**, *5* (37), 11438–11445. https://doi.org/10.1002/slct.202003233.

(16) Pulko, I.; Wall, J.; Krajnc, P.; Cameron, N. R. Ultra-High Surface Area Functional Porous Polymers by Emulsion Templating and Hypercrosslinking: Efficient Nucleophilic Catalyst Supports. *Chem. - Eur. J.* **2010**, *16* (8), 2350–2354. https://doi.org/10.1002/chem.200903043.

(17) Menner, A.; Bismarck, A. New Evidence for the Mechanism of the Pore Formation in Polymerising High Internal Phase Emulsions or Why PolyHIPEs Have an Interconnected Pore Network Structure. *Macromol. Symp.* **2006**, *242* (1), 19–24. https://doi.org/10.1002/masy.200651004.

(18) Menner, A.; Powell, R.; Bismarck, A. Open Porous Polymer Foams via Inverse Emulsion Polymerization: Should the Definition of High Internal Phase (Ratio) Emulsions Be Extended? *Macromolecules* **2006**, *39* (6), 2034–2035. https://doi.org/10.1021/ma052705x.

(19) Vásquez, L.; Davis, A.; Gatto, F.; Ngoc An, M.; Drago, F.; Pompa, P. P.; Athanassiou, A.; Fragouli, D. Multifunctional PDMS PolyHIPE Filters for Oil-Water Separation and Antibacterial Activity. *Sep. Purif. Technol.* **2021**, *255*, 117748. https://doi.org/10.1016/j.seppur.2020.117748.

(20) Aldemir Dikici, B.; Dikici, S.; Reilly, G. C.; MacNeil, S.; Claeyssens, F. A Novel Bilayer Polycaprolactone Membrane for Guided Bone Regeneration: Combining Electrospinning and Emulsion Templating. *Materials* **2019**, *12* (16), 2643. https://doi.org/10.3390/ma12162643.

(21) Jiang, Q.; Barkan, H.; Menner, A.; Bismarck, A. Micropatterned, Macroporous Polymer Springs for Capacitive Energy Harvesters. *Polymer* **2017**, *126*, 419–424. https://doi.org/10.1016/j.polymer.2017.04.018.

(22) Barbetta, A.; Cameron, N. R. Morphology and Surface Area of Emulsion-Derived (PolyHIPE) Solid Foams Prepared with Oil-Phase Soluble Porogenic Solvents: Span 80 as Surfactant. *Macromolecules* **2004**, *37* (9), 3188–3201. https://doi.org/10.1021/ma0359436.

(23) Barkan-Öztürk, H.; Menner, A.; Bismarck, A. Emulsion-Templated Macroporous Polymer Micromixers. *Ind. Eng. Chem. Res.* **2021**, *60* (39), 14013–14025. https://doi.org/10.1021/acs.iecr.1c01949.

(24) Barkan-Öztürk, H.; Menner, A.; Bismarck, A. Polymerised High Internal Phase Emulsion Micromixers for Continuous Emulsification. *Chem. Eng. Sci.* **2021**, 117296. https://doi.org/10.1016/j.ces.2021.117296.

(25) Ikem, V. O.; Menner, A.; Horozov, T. S.; Bismarck, A. Highly Permeable Macroporous Polymers Synthesized from Pickering Medium and High Internal Phase Emulsion Templates. *Adv. Mater.* **2010**, *22* (32), 3588–3592. https://doi.org/10.1002/adma.201000729.

(26) Woodward, R. T.; Jobbe-Duval, A.; Marchesini, S.; Anthony, D. B.; Petit, C.; Bismarck, A. Hypercrosslinked PolyHIPEs as Precursors to Designable, Hierarchically Porous Carbon Foams. *Polymer* **2017**, *115*, 146–153. https://doi.org/10.1016/j.polymer.2017.03.042.

(27) Xu, S.; Song, K.; Li, T.; Tan, B. Palladium Catalyst Coordinated in Knitting N-Heterocyclic Carbene Porous Polymers for Efficient Suzuki–Miyaura Coupling Reactions. *J. Mater. Chem. A* **2015**, *3* (3), 1272–1278. https://doi.org/10.1039/C4TA05265J.

(28) Li, B.; Guan, Z.; Wang, W.; Yang, X.; Hu, J.; Tan, B.; Li, T. Highly Dispersed Pd Catalyst Locked in Knitting Aryl Network Polymers for Suzuki-Miyaura Coupling Reactions of Aryl Chlorides in Aqueous Media. *Adv. Mater.* **2012**, *24* (25), 3390–3395. https://doi.org/10.1002/adma.201200804.

(29) Yang, X.; Tan, L.; Xia, L.; Wood, C. D.; Tan, B. Hierarchical Porous Polystyrene Monoliths from PolyHIPE. *Macromol. Rapid Commun.* **2015**, *36* (17), 1553–1558. https://doi.org/10.1002/marc.201500235.

(30) Park, J.; Kim, K.; Seo, M. Hyper-Cross-Linked Polymers with Controlled Multiscale Porosity *via* Polymerization-Induced Microphase Separation within High Internal Phase Emulsion. *Chem. Commun.* **2018**, *54* (57), 7908–7911. https://doi.org/10.1039/C8CC03508C.

(31) Tan, L.; Tan, B. Functionalized Hierarchical Porous Polymeric Monoliths as Versatile Platforms to Support Uniform and Ultrafine Metal Nanoparticles for Heterogeneous Catalysis. *Chem. Eng. J.* **2020**, *390*, 124485. https://doi.org/10.1016/j.cej.2020.124485.

(32) Steindl, P.; Menner, A.; Bismarck, A. Permeable Emulsion-Templated Porous Polyepoxides. *Polymer* **2022**, *240*, 124476. https://doi.org/10.1016/j.polymer.2021.124476.

(33) Suzuki, A. Organoboron Compounds in New Synthetic Reactions. *Pure Appl. Chem.* **1985**, *57* (12), 1749–1758. https://doi.org/10.1351/pac198557121749.

(34) Brunauer, S.; Emmett, P. H.; Teller, E. Adsorption of Gases in Multimolecular Layers. *J. Am. Chem. Soc.* **1938**, *60* (2), 309–319. https://doi.org/10.1021/ja01269a023.

(35) Powell, C. X-Ray Photoelectron Spectroscopy Database XPS,Version 4.1, NIST Standard Reference Database 20, 1989. https://doi.org/10.18434/T4T88K.

(36) Lei, Y.; Chen, Z.; Li, G. Palladium/Phosphorus-Functionalized Porous Organic Polymer with Tunable Surface Wettability for Water-Mediated Suzuki–Miyaura Coupling Reaction. *RSC Adv.* **2019**, *9* (63), 36600–36607. https://doi.org/10.1039/C9RA06680B.

(37) Law, R. V.; Sherrington, D. C.; Snape, C. E.; Ando, I.; Kurosu, H. Solid-State ^{13}C MAS NMR Studies of Hyper-Cross-Linked Polystyrene Resins. *Macromolecules* **1996**, *29* (19), 6284–6293. https://doi.org/10.1021/ma951606o.

(38) Joseph, R.; Ford, W. T.; Zhang, S.; Tsyurupa, M. P.; Pastukhov, A. V.; Davankov, V. A. Solid-State 13C-NMR Analysis of Hypercrosslinked Polystyrene. *J. Polym. Sci. Part Polym. Chem.* **1997**, *35* (4), 695–701. https://doi.org/10.1002/(SICI)1099-0518(199703)35:4<695::AID-POLA12>3.0.CO;2-I.

(39) Zhou, Y.-B.; Li, C.-Y.; Lin, M.; Ding, Y.-J.; Zhan, Z.-P. A Polymer-Bound Monodentate-P-Ligated Palladium Complex as a Recyclable Catalyst for the Suzuki-Miyaura Coupling Reaction of Aryl Chlorides. *Adv. Synth. Catal.* **2015**, *357* (11), 2503–2508. https://doi.org/10.1002/adsc.201500070.

(40) Wang, X.; Min, S.; Das, S. K.; Fan, W.; Huang, K.-W.; Lai, Z. Spatially Isolated Palladium in Porous Organic Polymers by Direct Knitting for Versatile Organic Transformations. *J. Catal.* **2017**, *355*, 101–109. https://doi.org/10.1016/j.jcat.2017.08.030.

(41) Larkin, P. *Infrared and Raman Spectroscopy: Principles and Spectral Interpretation*; Elsevier: Amsterdam ; Boston, 2011.

(42) Rozyyev, V.; Thirion, D.; Ullah, R.; Lee, J.; Jung, M.; Oh, H.; Atilhan, M.; Yavuz, C. T. High-Capacity Methane Storage in Flexible Alkane-Linked Porous Aromatic Network Polymers. *Nat. Energy* **2019**, *4* (7), 604–611. https://doi.org/10.1038/s41560-019-0427-x.

(43) Thommes, M.; Kaneko, K.; Neimark, A. V.; Olivier, J. P.; Rodriguez-Reinoso, F.; Rouquerol, J.; Sing, K. S. W. Physisorption of Gases, with Special Reference to the Evaluation of Surface Area and Pore Size Distribution (IUPAC Technical Report). *Pure Appl. Chem.* **2015**, *87* (9–10), 1051–1069. https://doi.org/10.1515/pac-2014-1117.

(44) Denmark, S. E.; Smith, R. C.; Tymonko, S. A. Phosphine Oxides as Stabilizing Ligands for the Palladium-Catalyzed Cross-Coupling of Potassium Aryldimethylsilanolates. *Tetrahedron* **2007**, *63* (26), 5730–5738. https://doi.org/10.1016/j.tet.2007.02.017.

(45) Kozuch, S.; Martin, J. M. L. "Turning Over" Definitions in Catalytic Cycles. *ACS Catal.* **2012**, *2* (12), 2787–2794. https://doi.org/10.1021/cs3005264.

(46) Liu, X.; Xu, W.; Xiang, D.; Zhang, Z.; Chen, D.; Hu, Y.; Li, Y.; Ouyang, Y.; Lin, H. Palladium Immobilized on Functionalized Hypercrosslinked Polymers: A Highly Active and Recyclable Catalyst for Suzuki–Miyaura Coupling Reactions in Water. *New J. Chem.* **2019**, *43* (31), 12206–12210. https://doi.org/10.1039/C9NJ02444A.

(47) Desforges, A.; Backov, R.; Deleuze, H.; Mondain-Monval, O. Generation of Palladium Nanoparticles within Macrocellular Polymeric Supports: Application to Heterogeneous Catalysis of the Suzuki-Miyaura Coupling Reaction. *Adv. Funct. Mater.* **2005**, *15* (10), 1689–1695. https://doi.org/10.1002/adfm.200500146.

(48) Mrówka, J.; Gackowski, M.; Lityńska-Dobrzyńska, L.; Bernasik, A.; Kosydar, R.; Drelinkiewicz, A.; Hasik, M. Poly(Methylvinylsiloxane)-Based High Internal Phase Emulsion-Templated Materials (PolyHIPEs)—Preparation, Incorporation of Palladium, and

Catalytic Properties. *Ind. Eng. Chem. Res.* **2020**, *59* (44), 19485–19499. https://doi.org/10.1021/acs.iecr.0c03429.

Supporting Information

Simultaneous hypercrosslinking and functionalization of polyHIPEs for catalyst supports

Hande Barkan-Öztürk,[1] Angelika Menner,[1] Alexander Bismarck,[1,2,] Robert Woodward [1,*]*

[1] Polymer and Composite Engineering (PaCE) Group, Institute of Material Chemistry and Research, Faculty of Chemistry, University of Vienna, Währinger Strasse, 42, 1090, Vienna, Austria.

[2] Department of Chemical Engineering, Imperial College London, South Kensington Campus, London SW7 2AZ, United Kingdom

* Corresponding author: Alexander Bismarck, e-mail: alexander.bismarck@univie.ac.at, Robert Woodward, e-mail: robert.woodward@univie.ac.at

S1 Swelling experiments of polyHIPEs

Swelling tests were performed on polyHIPEs to evaluate the resistance against dichloroethane (DCE), dichloromethane (DCM) and chloroform (CF). PolyHIPE monoliths were cut into shorter cylindrical shape (diameter = ~4.5 mm and height = ~13 mm) with 5 samples were prepared for each solvent. After measuring their dry weight and dimensions, the samples were placed in vials and 4 mL of solvent was added. Weight and dimensions of swollen polyHIPEs were recorded after 24 h. Afterwards, the samples were dried in a conventional oven for 24 h at 70 °C and their weight

and dimensions were measured again to determine possible material loss. Swelling ratios Q were calculated from the ratio of volume of the swollen V_{SM} to initial dry polyHIPEs:

$$Q = \frac{V_{SM}}{V_0} \qquad \text{(Eq. S1)}$$

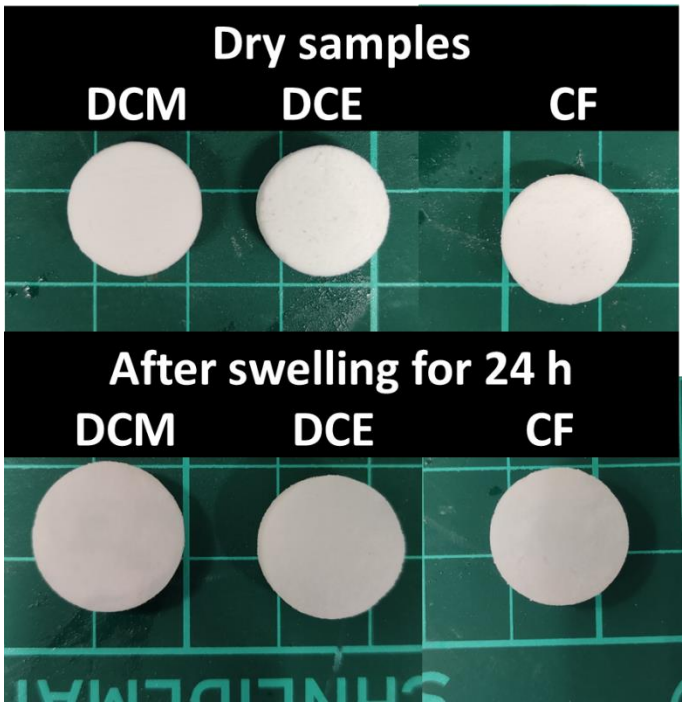

Figure S1.1. Photograph of dry polyHIPEs and after swelling them in appropriate solvent for 24 h.

Table S1.1. Swelling ratios (Q) of polyHIPEs in DCE, DCM and CF.

	Q_{DCE}	Q_{DCM}	Q_{CF}
PPH	1.38 ± 0.04	1.44 ± 0.03	1.41 ± 0.02

S2 Suzuki-Miyaura cross-coupling reaction with Pd-loaded hypercrosslinked polyHIPE catalyst

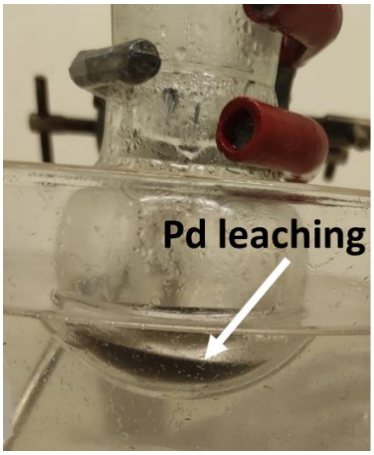

Figure S2.1. Suzuki-Miyaura cross-coupling reaction using Pd-loaded hypercrosslinked polyHIPE catalyst. Due to the Pd-leaching reaction mixture turned to black color.

S3 Mechanical testing of conventional polyHIPEs and polyHIPEs

Compression tests were carried out at room temperature using an Instron series 5584 testing machine (Instron Ltd., Norwoord, U.K.) equipped with a 1 kN load cell. The specimens had a diameter of 12 mm and height of 10 mm. Samples were compressed at an extension rate of 1 mm/min until the height was reduced by 30% of its original value. Elastic modulus was determined from the slope of the initial linear elastic region in the stress/strain plot. The crush

strength was determined from the maximum compressive strength of the sample at the end of the initial linear elastic region, normalized with respect to the cross-sectional area.

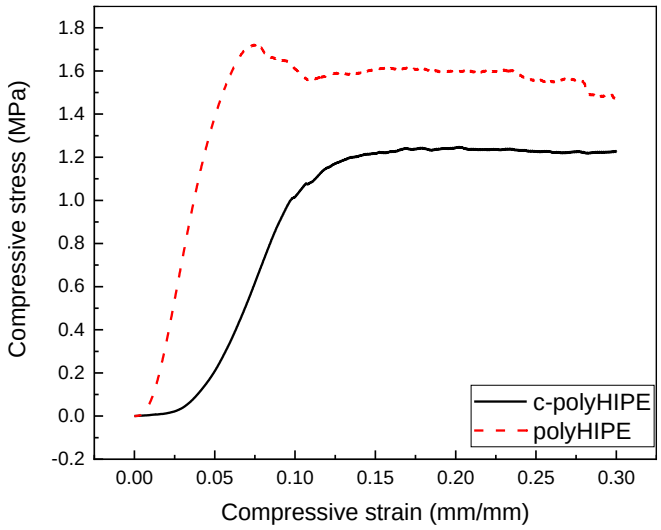

Figure S3.1. The stress-strain curves of conventional (c-)polyHIPEs and polyHIPEs monoliths during the compression test.

Table S3.1. Young's modulus (E) and crush strength (σ_c), of c-polyHIPEs and polyHIPEs.

Sample	E (MPa)	σ_c (MPa)
c-polyHIPEs	19 ± 2	1 ± 0.2
polyHIPEs	48 ± 8	1.6 ± 0.2

S4 chemical and structural properties of hypercrosslinked and/or functionalized conventional polyHIPEs

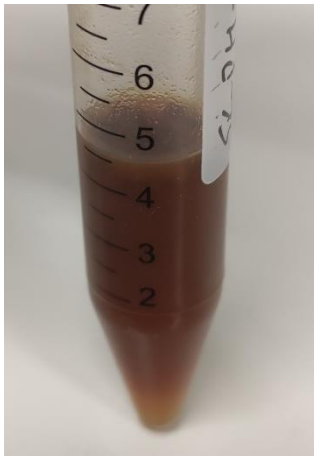

Figure S4.1. The photograph of hypercrosslinked and functionalized c-polyHIPE produced from solely surfactant-stabilized HIPEs eroded during the post-modification with $Pd(OAc)_2$ in DCM.

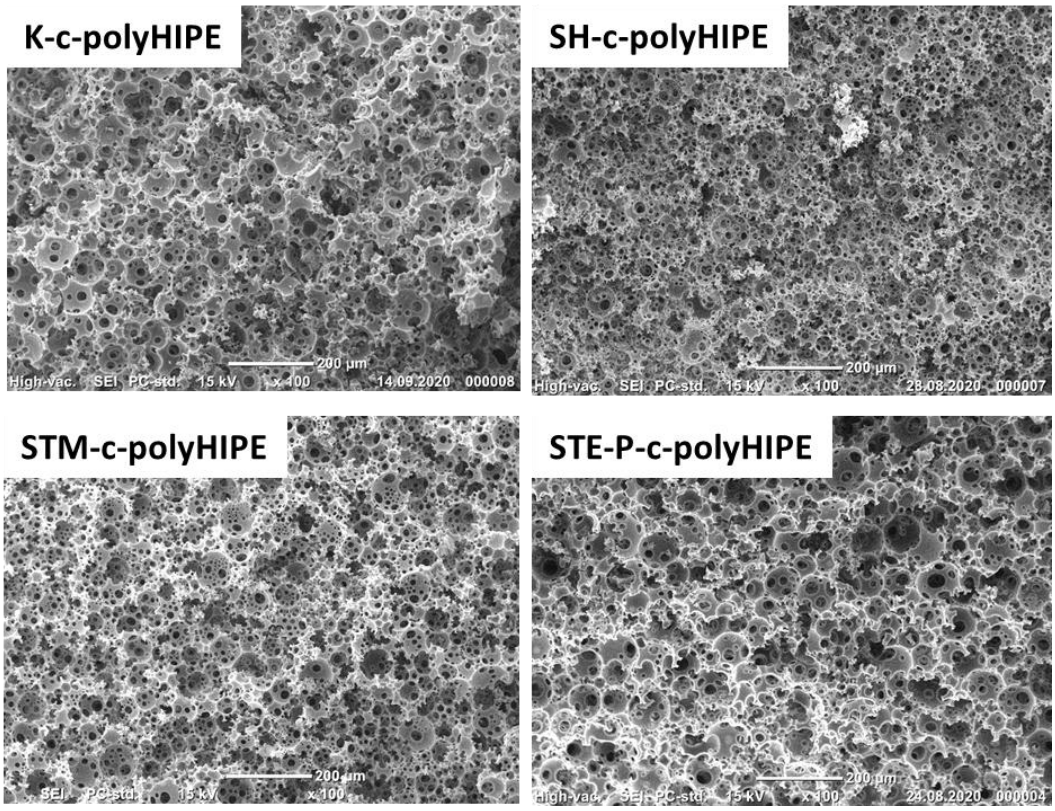

Figure S4.2. Characteristic SEM images of hypercrosslinked (**K-c-polyHIPE**, **SH-c-polyHIPE** and **STM-c-polyHIPE**) and/or functionalized (**STE-P-c-polyHIPE**) conventional polyHIPEs.

Table S4.1. Morphological characteristics, skeletal density (ρ_s) and foam density (ρ_f), porosity (P) and structural properties, specific surface area (A_s), and phosphorus content of hypercrosslinked and functionalized conventional (c-) polyHIPEs.

Sample name	ρ_s (g/cm^3)	ρ_f (g/cm^3)	P (%)	As (m^2/g)	P^{i} (wt.%)	P^{ii} (wt.%)
c-polyHIPE	1.10 ± 0.02	0.16 ± 0.02	86 ± 2	10 ± 2	0	0
K-c-polyHIPE	1.09 ± 0.02	0.11 ± 0.01	90 ± 1	496 ± 15	0	0
STM-c-polyHIPE	1.2 ± 0.07	0.11 ± 0.01	90 ± 0.6	448 ± 15	0	0
SH-c-polyHIPE	1.21 ± 0.04	0.13 ± 0.02	91 ± 4	163 ± 1	0	0
STM-P-c-polyHIPE	1.27 ± 0.02	0.15 ± 0.02	88 ± 1.7	399 ± 45	1.7	0.7
STE-P-c-polyHIPE	1.11 ± 0.01	0.16 ± 0.01	88 ± 6.4	23 ± 1	2.7	1.9

[i] P content was determined using XPS.
[ii] P content was determined using Elemental Analysis.

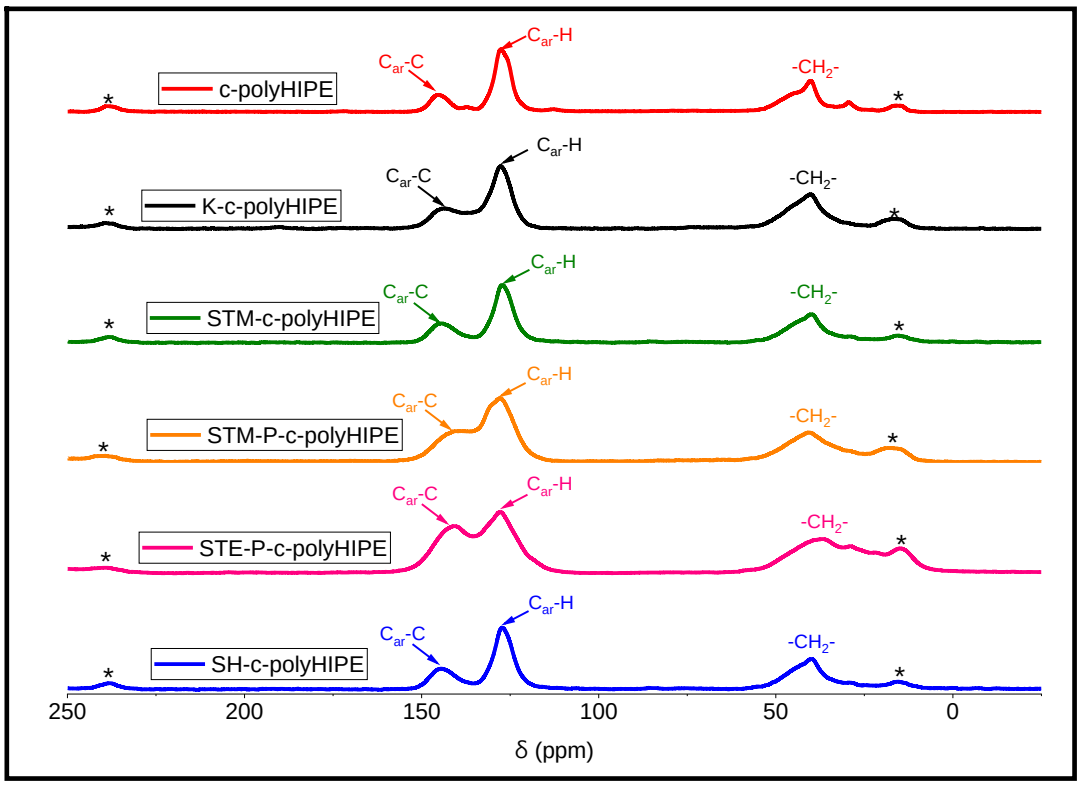

Figure S4.3. ^{13}C cross-polarization magic-angle spinning (CP/MAS) NMR of c-polyHIPE and hypercrosslinked and/or functionalized c-polyHIPEs. Asterisks denote spinning sidebands.

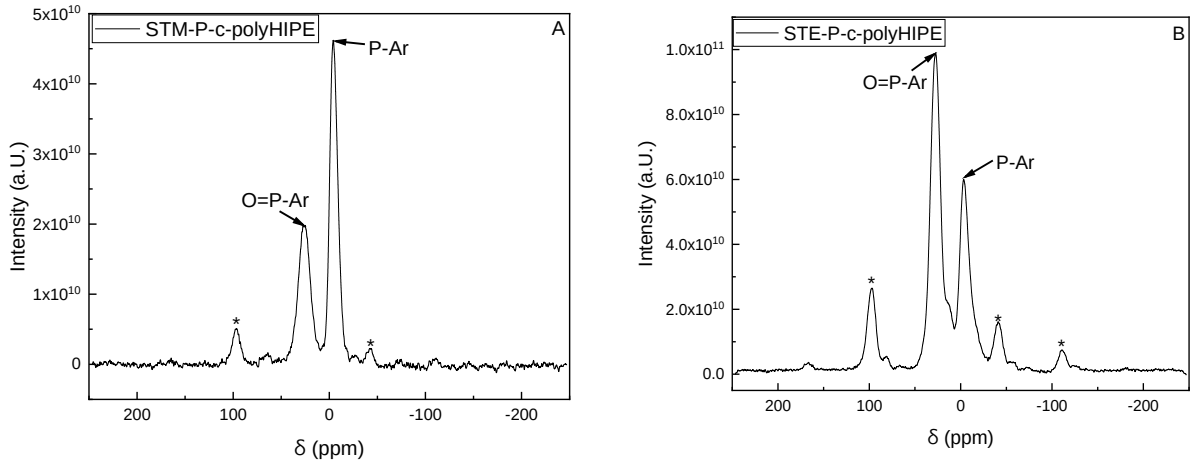

Figure S4.4. ^{31}P HPDEC/MAS NMR of knitted and functionalized A) STM-P-c-polyHIPE and B) STE-P-c-polyHIPE (Asterisks denote spinning sidebands).

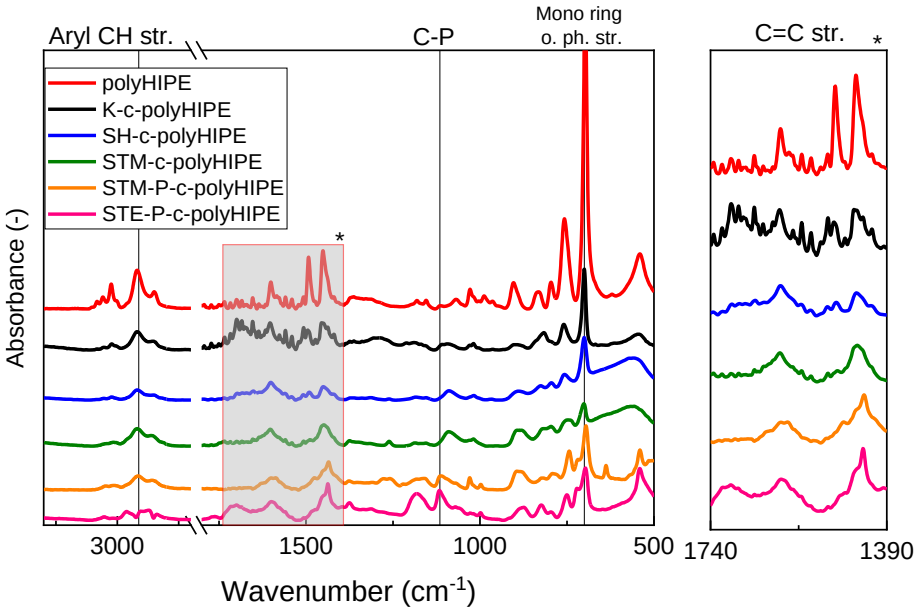

Figure S4.5. The FT-IR spectra of polyHIPE and hypercrosslinked and/or functionalized c-polyHIPEs. The right spectra represent zoomed area in the main FT-IR spectra indicated in the grey box to show the details of the C=C stretching vibrations of the benzene ring.

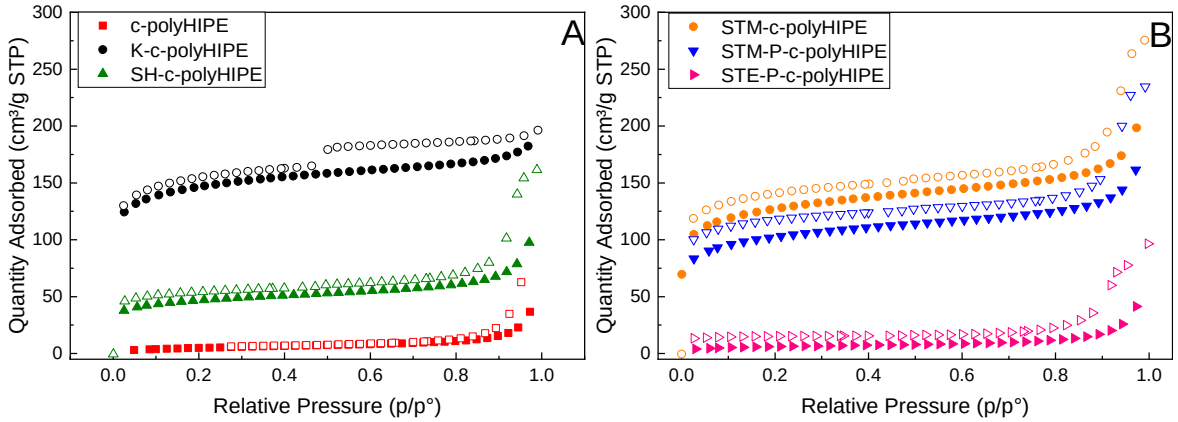

Figure S4.6. N_2 sorption isotherms of c-polyHIPE and hypercrosslinked and/or functionalized c-polyHIPEs.

S5 Pictures and high magnification SEM images of hypercrosslinked and functionalized polyHIPEs

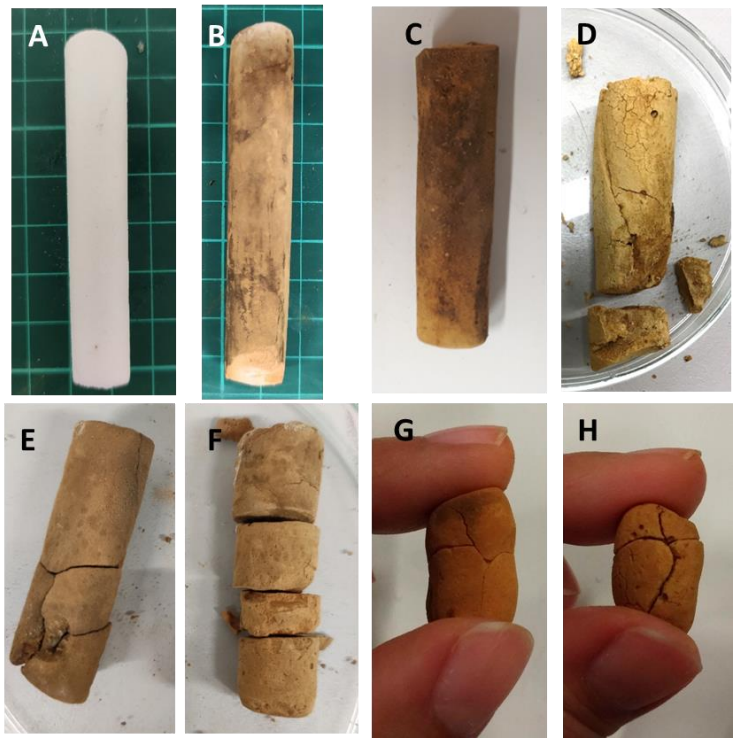

Figure S5.1. Photographs of A) polyHIPE, B) **K**, C) **K-P**, D) **STE-P**, E) **STM**, F) **STM-P**, G) **SH**, H) **SH-P**.

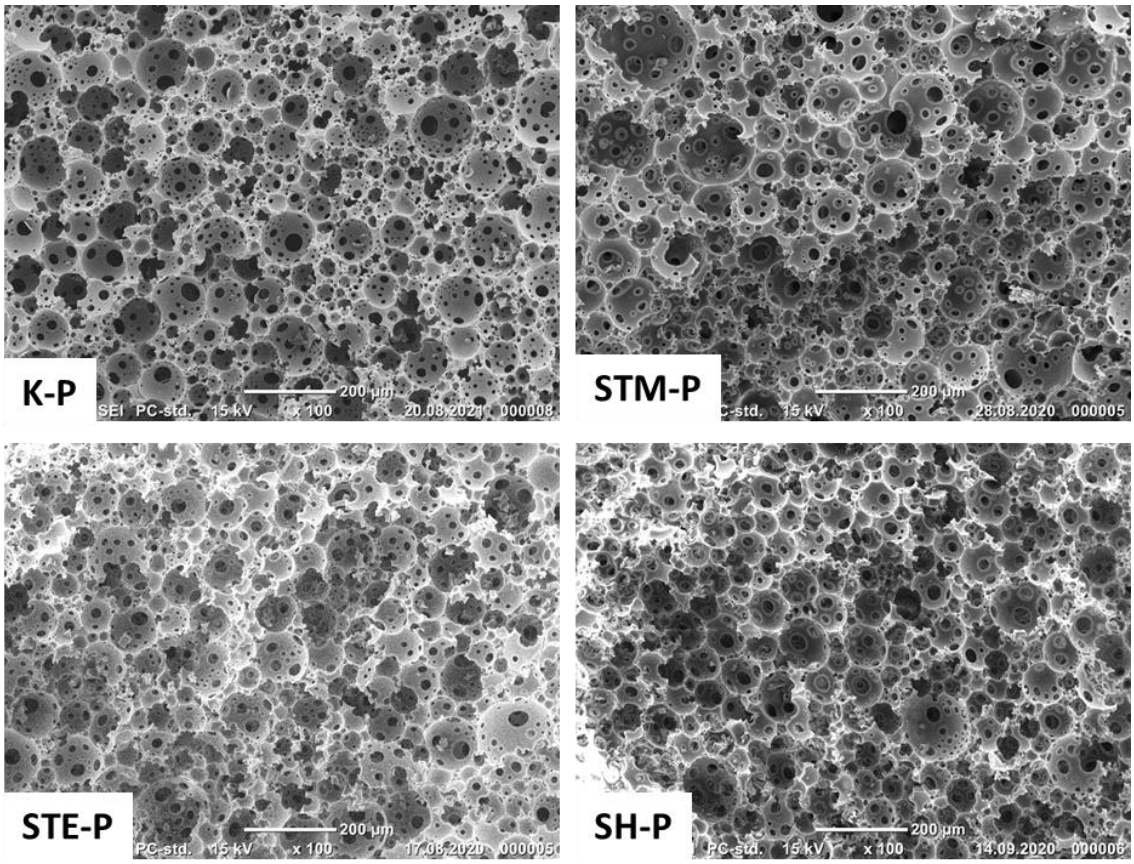

Figure S5.2. Characteristic SEM images of **K-P**, **STM-P**, **STE-P** and **SH-P**.

S6 Chemical and structural properties of hypercrosslinked polyHIPEs

Table S6.1. Morphological and structural properties of hypercrosslinked polyHIPEs, including skeletal density (ρ_s), foam density (ρ_f), porosity (P), specific surface area (A_S), and P content.

Sample name	ρ_s (g/cm^3)	ρ_f (g/cm^3)	P (%)	A_S (m^2/g)	P[iii] (wt.%)	P[iv] (wt.%)
DMM-PPH	1.15 ± 0.03	0.13 ± 0.01	89 ± 0.7	536 ± 51	0	0
STM-PPH	1.24 ± 0.06	0.16 ± 0.01	87 ± 1	391 ± 32	0	0
SH-PPH	1.21 ± 0.01	0.21 ± 0.01	86 ± 7	150 ± 45	0	0

[iii] P content was determined using XPS.
[iv] P content was determined using Elemental Analysis.

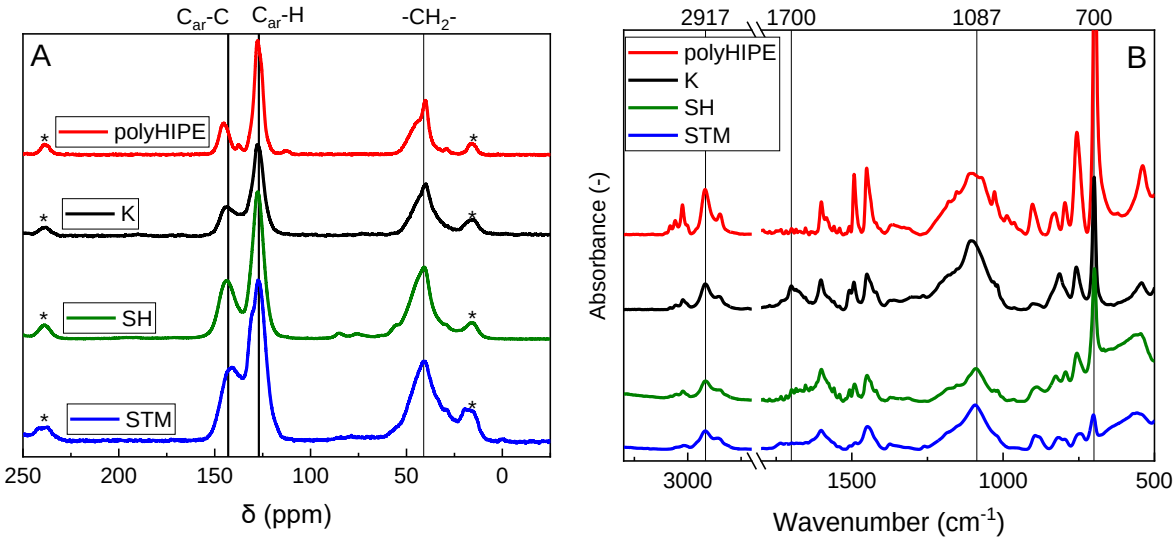

Figure S6.1. A) ^{13}C cross-polarization magic-angle spinning (CP/MAS) NMR spectra (Asterisks denote spinning sidebands) and B) FT-IR spectra of polyHIPE and hypercrosslinked polyHIPEs.

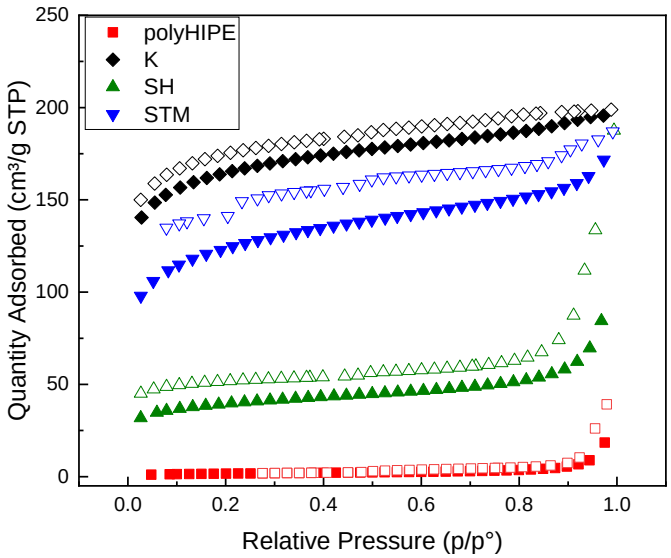

Figure S6.2. N_2 sorption isotherms at 77 K of hypercrosslinked polyHIPEs.

S7 Deconvolution of ^{13}C CP/MAS NMR spectra of P(P)Hs and HCP- P(P)Hs

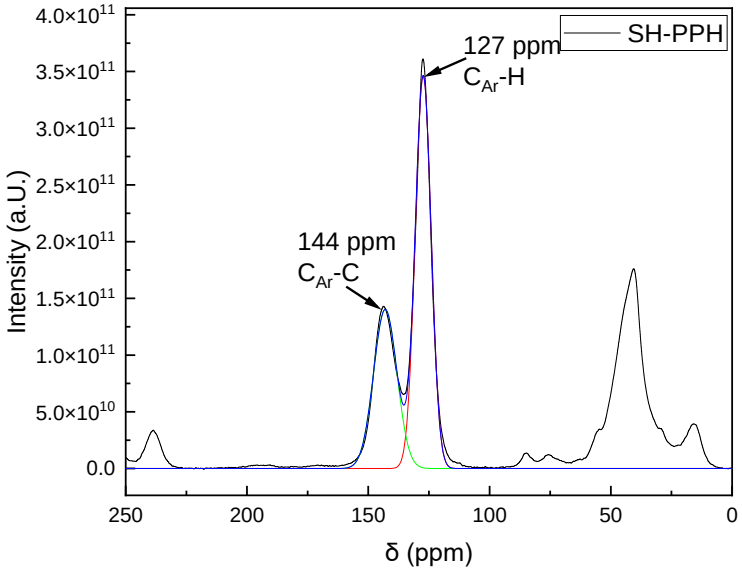

name	A_{127}/A_{144}
polyHIPE	3.42
K	1.79
K-P	1.13
STM	1.22
STM-P	2.02
STE-P	0.97
SH	1.68
SH-P	1.74

Figure S7.1. Deconvoluted ^{13}C CP/MAS NMR spectrum of SH-PPH (blue line represents deconvolution, red line represents C_{Ar}-H peak at 127 ppm, and green line represents C_{Ar}-C peak at 144 ppm). In the table, the ratio of area of C_{Ar}-H (A_{127}) to area of C_{Ar}-C (A_{144}) is given for the corresponding samples.

S8 Chemical properties of hypercrosslinked and functionalized polyHIPEs

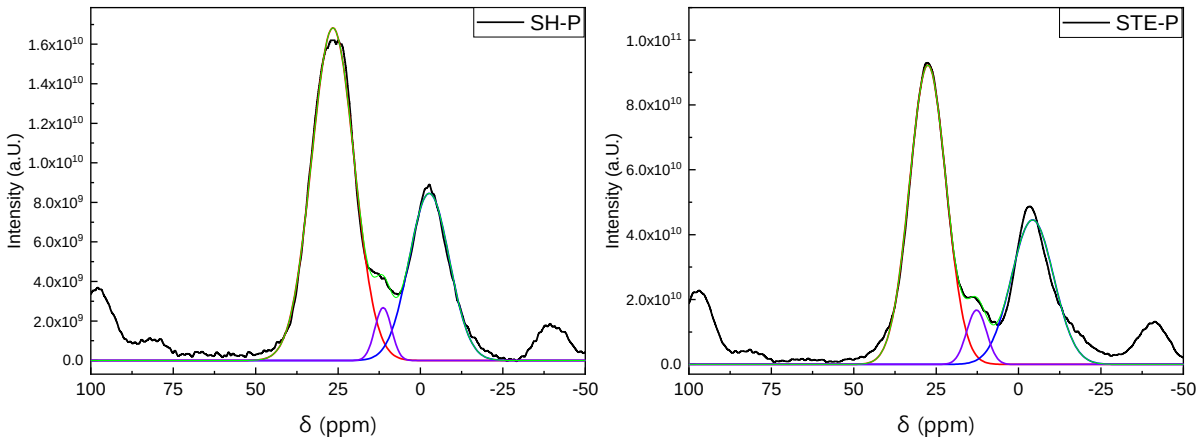

Figure S8.1 Deconvoluted ^{31}P CP/MAS NMR spectrum of SH-P and STE-P (green line represents the fitting, while black line is the original data).

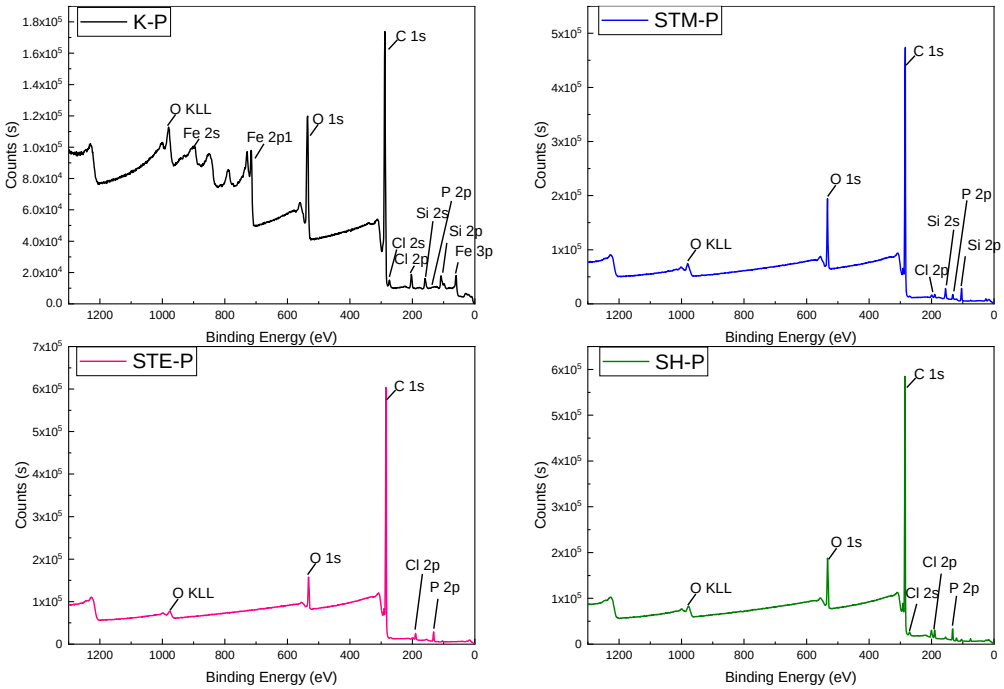

Figure S8.2. XP survey spectra of hypercrosslinked and functionalized polyHIPEs.

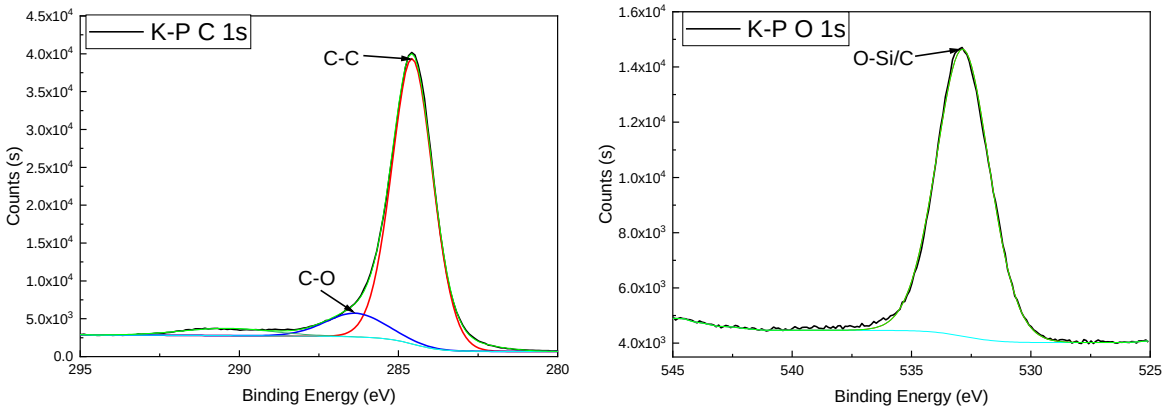

Figure S8.3. High resolution C 1s and O 1s XP spectra **K-P** (green line represents the fitting and black line is the original data).

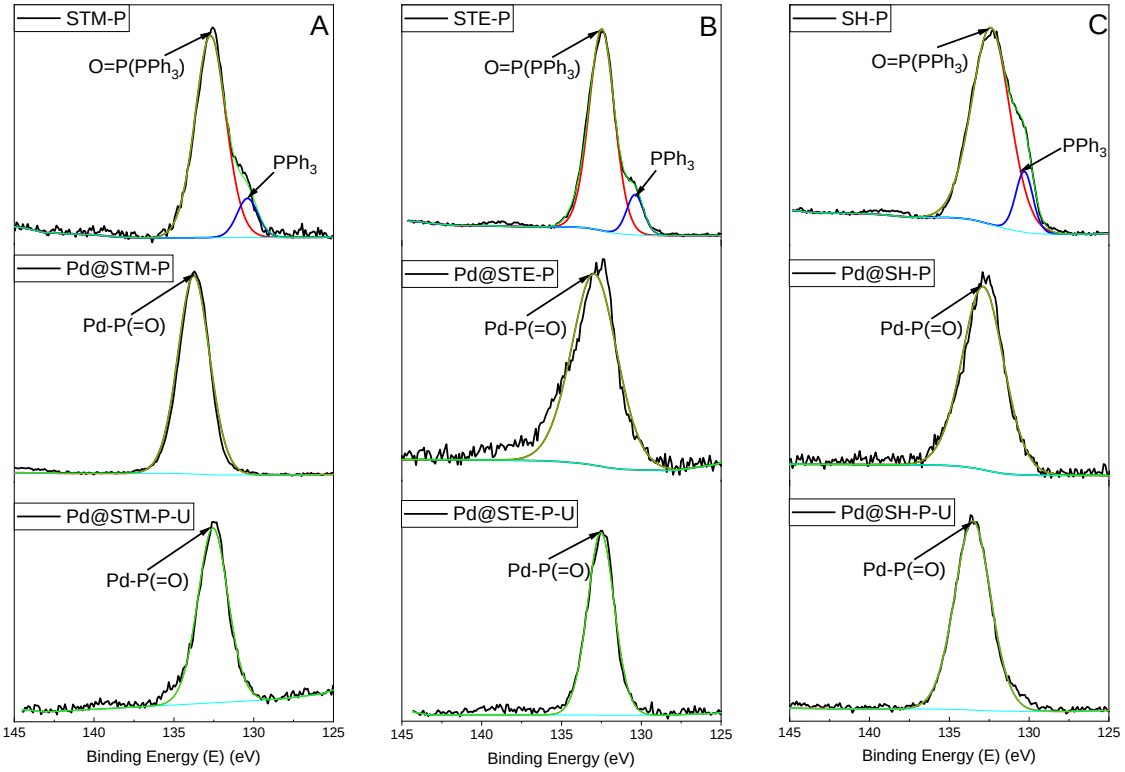

Figure S8.4. High resolution P 2p XPS spectra of A) STM-P, fresh Pd@STM-P, and Pd@STM-P after 6 runs, B) STE-P, fresh Pd@STE-P, and Pd@STE-P after 6 runs, and C) SH-P, fresh Pd@SH-P, and Pd@SH-P after 6 runs (green line represents the fitting, while black line is the original data).

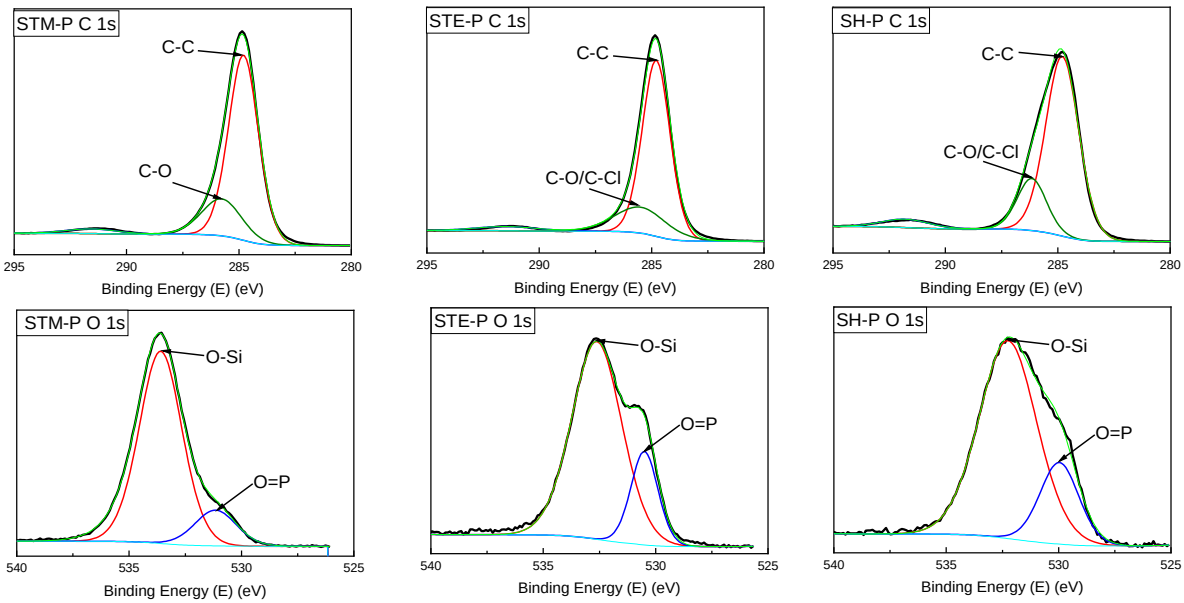

Figure S8.5. High resolution C 1s and O 1s XPS spectra of **STM-P**, **STE-P** and **SH-P** (green line represents the fitting and black line is the original data).

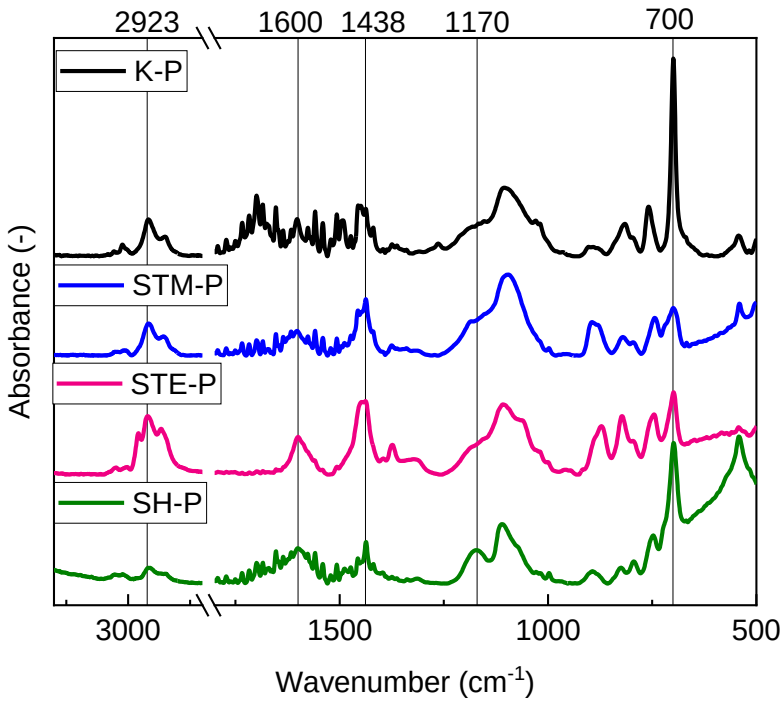

Figure S8.6. FT-IR spectra of hypercrosslinked and PPh_3 functionalized polyHIPEs.

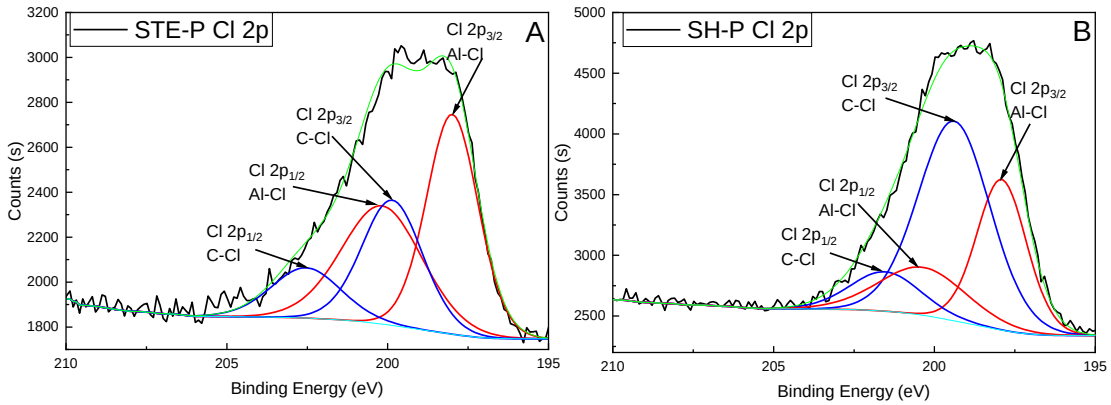

Figure S8.7. High resolution Cl 2p XP spectra of A) **STE-P** and B) **SH-P** (green line represents the fitting and black line is the original data).

S9 Thermal gravimetric analysis of (hypercrosslinked) poly-Pickering-HIPEs

Thermal gravimetric analysis (TGA) of poly-Pickering-HIPEs was performed across the range of 50 °C to 800 °C using a TA instrument Discovery TGA (Discovery SA, TA Instrument, Eschborn, Germany) with a heating rate of 10 °C/min under a nitrogen atmosphere.

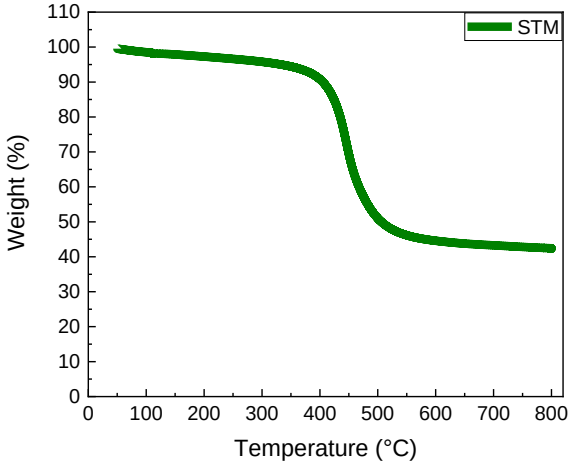

Sample name	Weight loss wt.%
polyHIPE	90
K	74
STM	55
SH	70
K-P	64
STM-P	57
STE-P	61
SH-P	51

Figure S9.15. TGA plot of SK-PPH from 50 °C to 800 °C under N_2 atmosphere, and in the table the weight loss at 800 °C of polyHIPE, and hypercrosslinked and/or functionalized polyHIPEs.

S10 Catalyst performance of hypercrosslinked and functionalized polyHIPEs

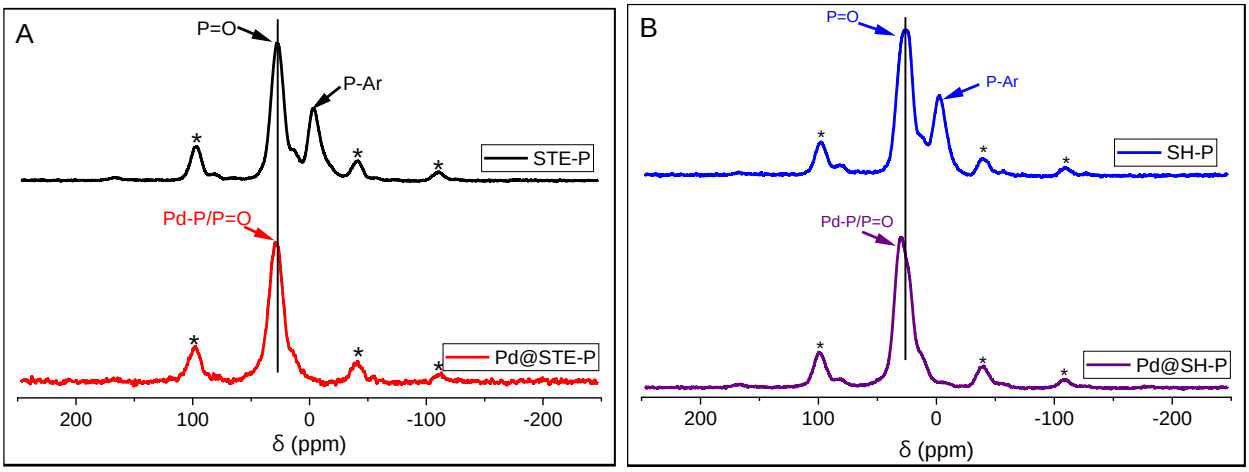

Figure S10.1. ^{31}P NMR CP/MAS of A) **STE-P** and after coating them with **Pd@STE-P**, B) **SH-P** and after coating them with **Pd@SH-P**. Asterisks denote spinning sidebands.

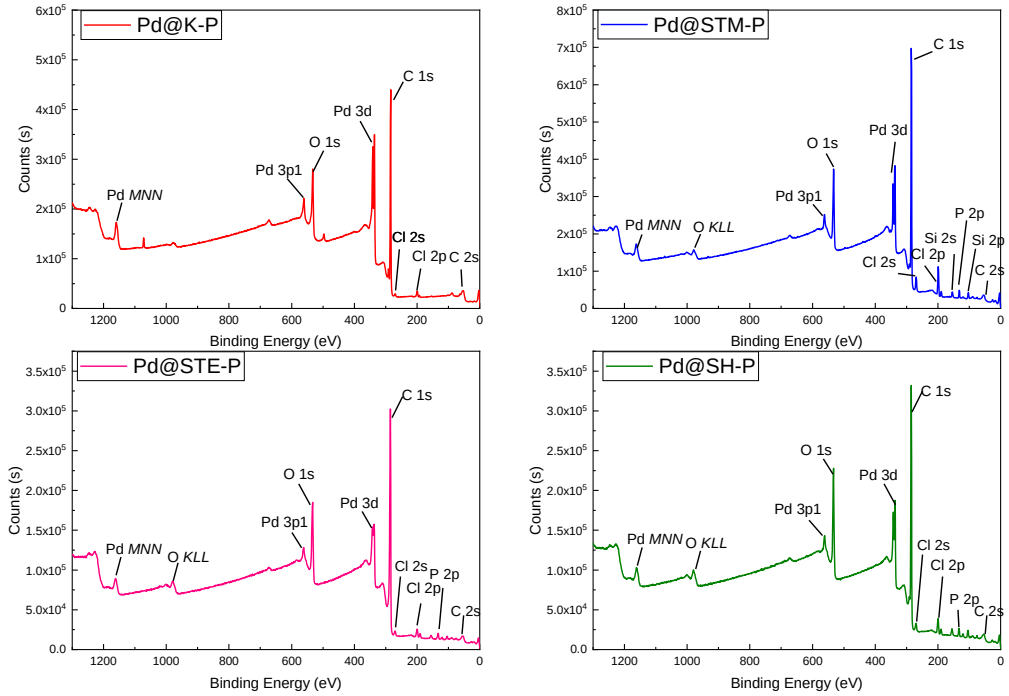

Figure S10.2. XPS survey spectra of Pd-loaded hypercrosslinked and functionalized polyHIPEs.

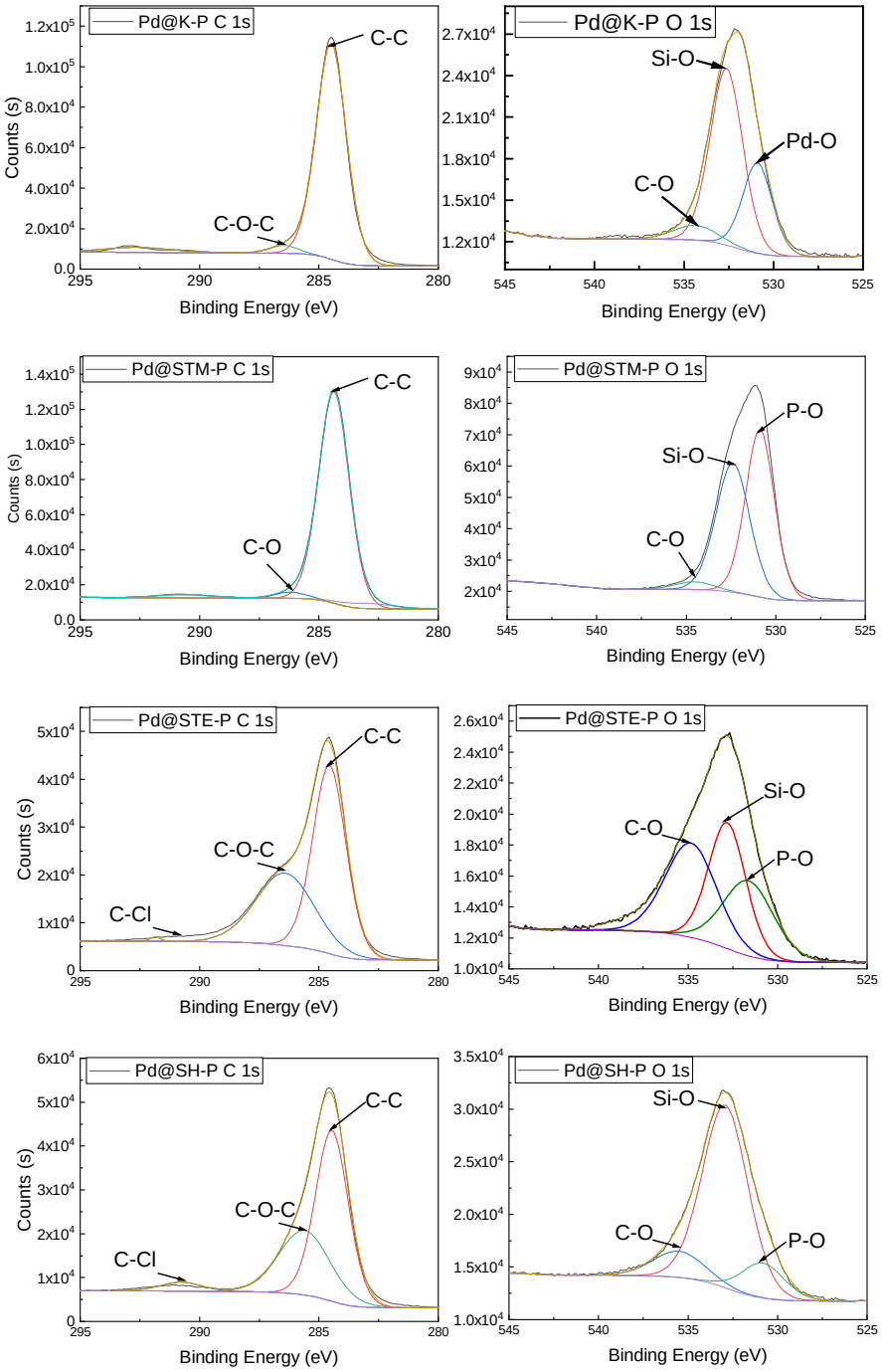

Figure S10.3. HR C 1s and O 1s XP spectra of Pd-loaded hypercrosslinked and functionalized polyHIPEs.

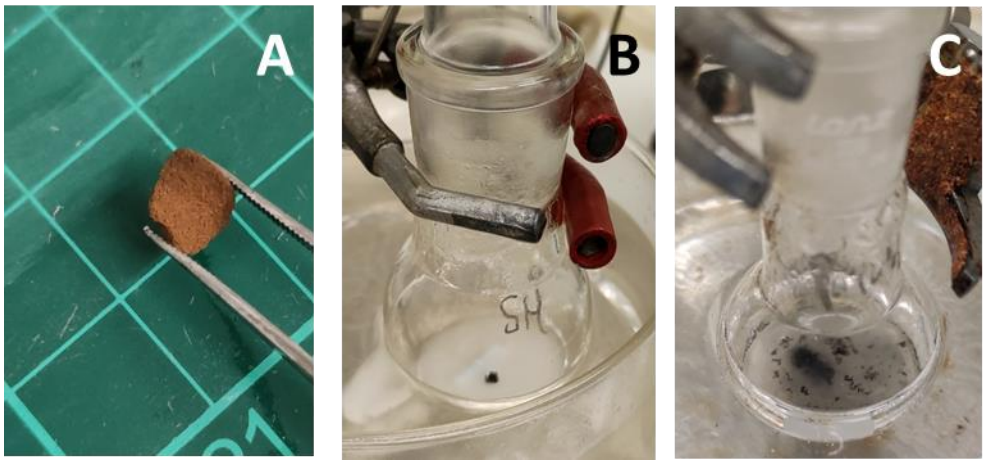

Figure S10.4. Photograph of A) Pd loaded **STE-P** piece, B) Suzuki-Miyaura reaction using **Pd@SH-P** as catalyst and C) Suzuki-Miyaura reaction using **Pd@K-P** as catalyst and black slurry as a result of leaching of Pd.

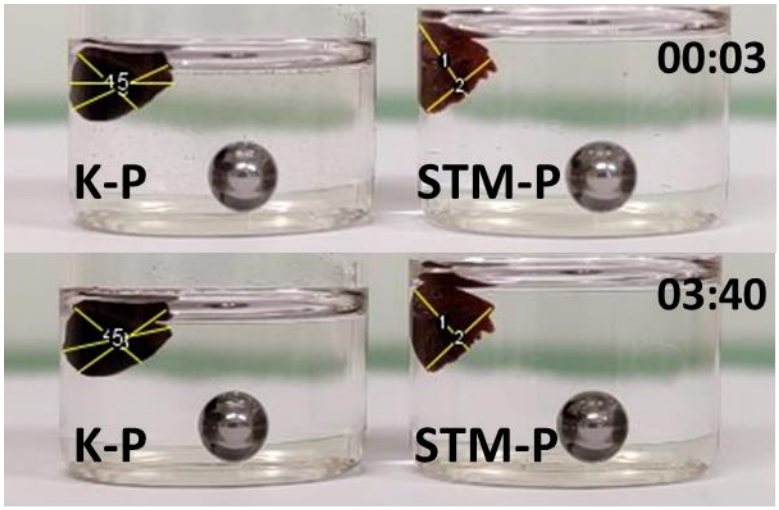

	00:03 (-)	03:40 (-)
STM-P-1	1.178	1.09
STM-P-2	1.128	1.233
K-P-3	1.434	1.473
K-P-4	1.124	1.201
K-P-5	1.438	1.521

Figure S10.5. Photographs of **K-P** and **STM-P** taken from the time-lapse video (x30) (**ESI Video S2**) at 00:03 and 03:40 (mm:ss) to determine their swelling ratios in DCM solvent, of which corresponding lengths are displayed in the table. The diameter of the metal ball to determine swelling.

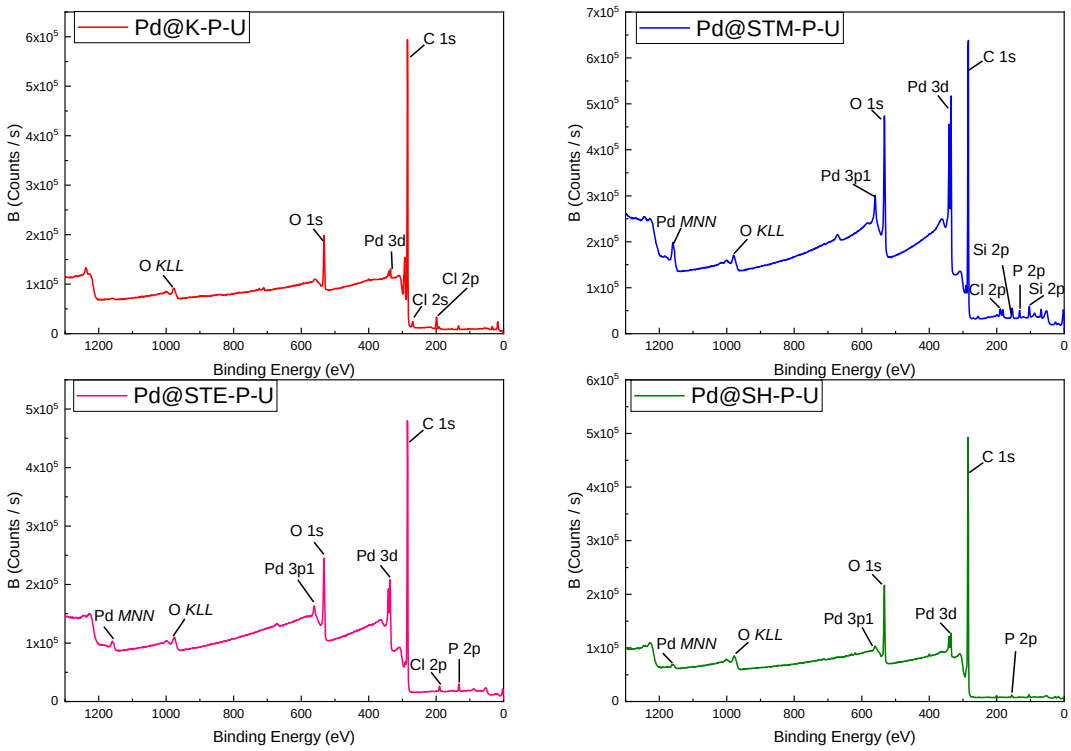

Figure S10.6. XPS survey spectra of Pd-loaded hypercrosslinked and functionalized polyHIPEs after six Suzuki-Miyaura cross-coupling reactions.

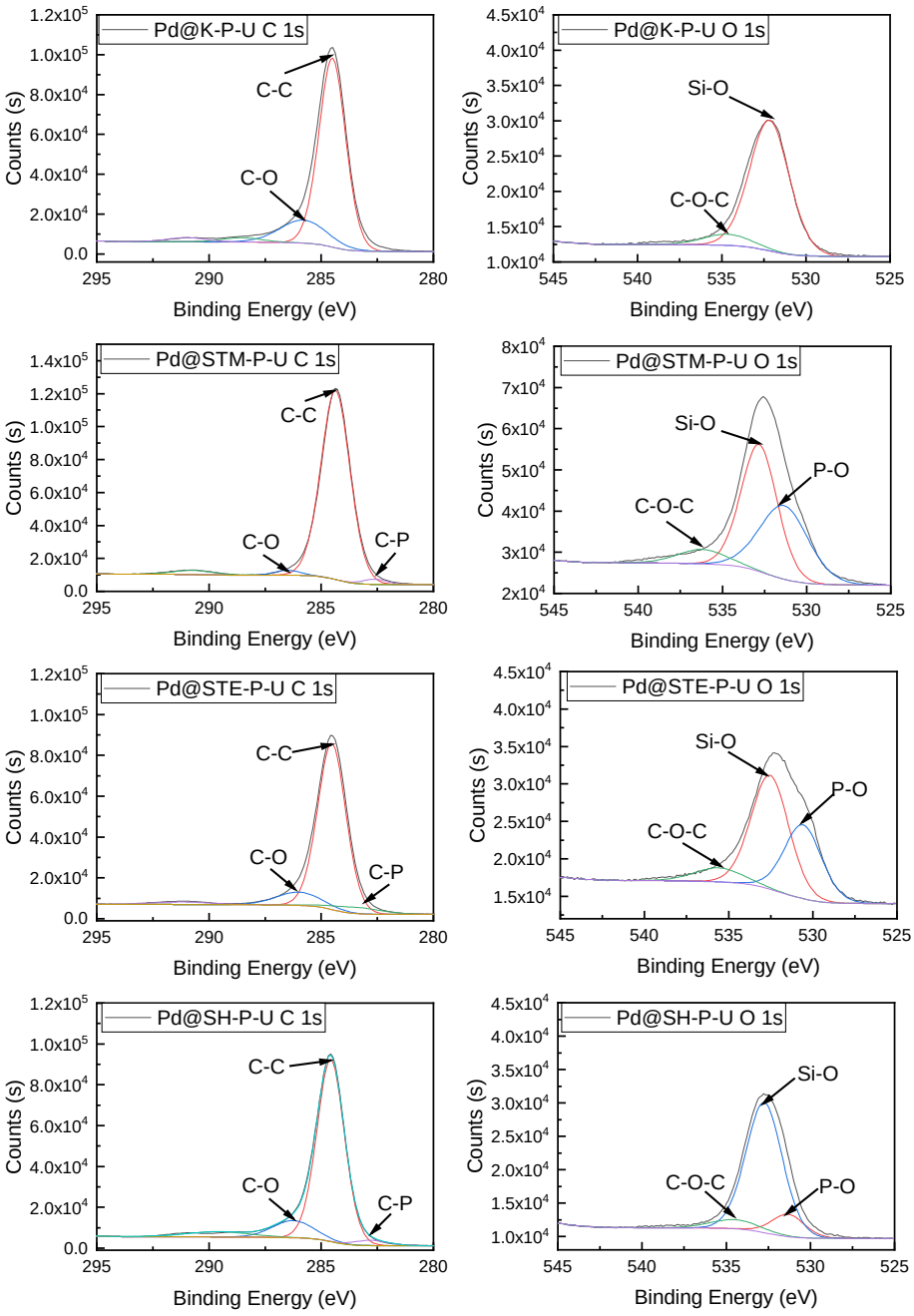

Figure S10.7. HR C 1s and O 1s XP spectra of Pd-loaded hypercrosslinked and functionalized polyHIPEs after six Suzuki-Miyaura cross-coupling reactions.

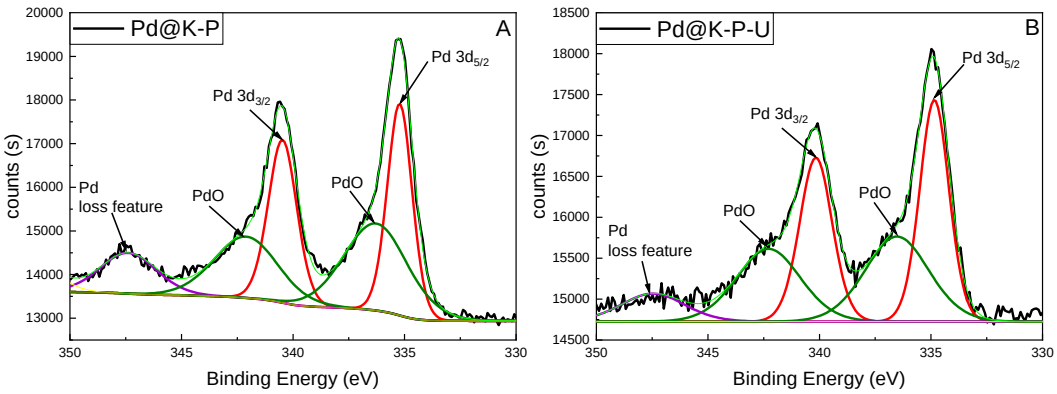

Figure S10.8. XPS spectra for Pd 3d of A) **Pd@K-P** and B) **Pd@K-P** after 3 reaction cycles (green line represents the fitting, while black line is the original data).

S11 ^{1}H NMR of Suzuki-Miyaura cross-coupling reaction of bromobenzene using Pd@hypercrosslinked and functionalized polyHIPEs

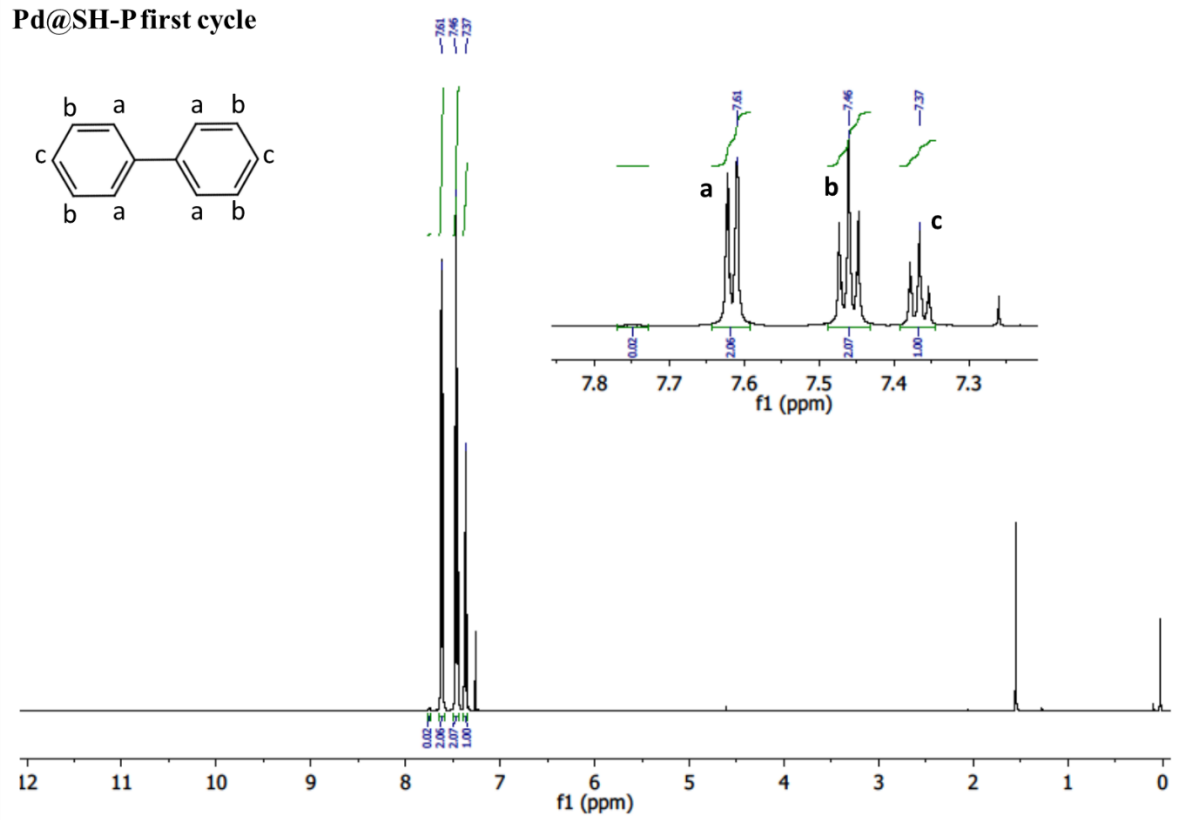

Figure S11.1. ^{1}H NMR spectra of Suzuki-Miyaura coupling reaction of bromobenzene with phenylboronic acid using **Pd@SH-Pd** for the 1st time as catalyst support.

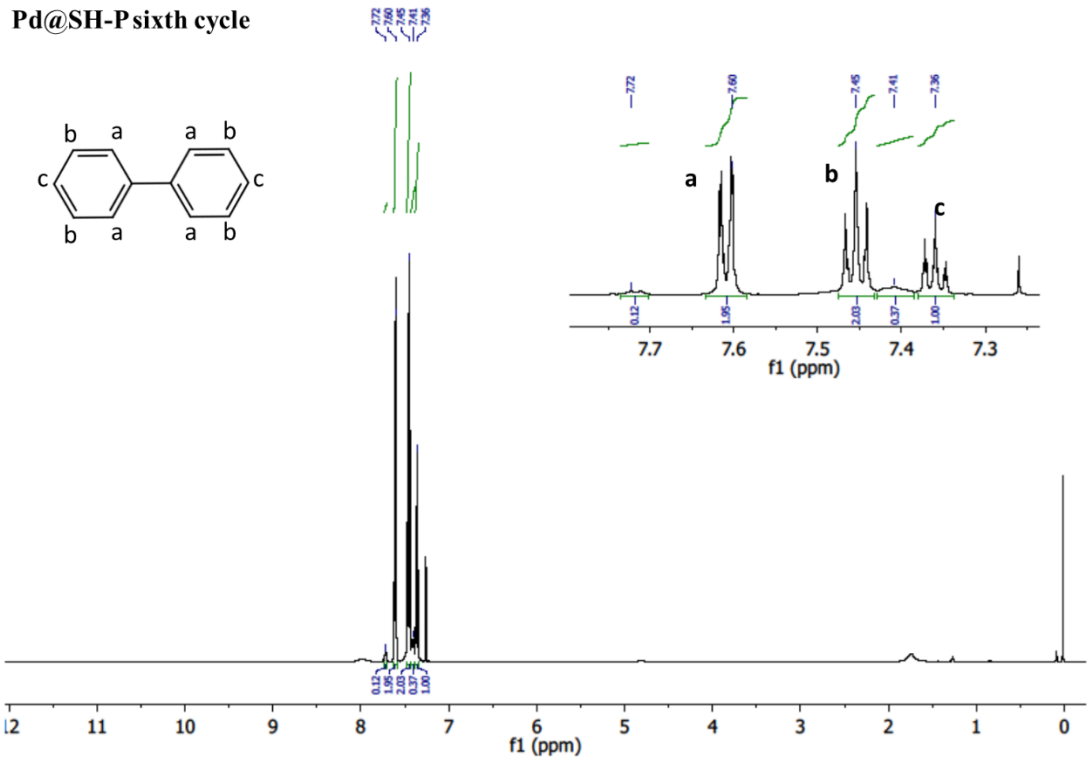

Figure S11.2. ^{1}H NMR spectra of Suzuki-Miyaura coupling reaction of bromobenzene with phenylboronic acid using **Pd@SH-P** for the 6th time as catalyst support.

S12 Turnover frequency (TOF) of Pd@HCP-polyHIPEs

TOF quantifies how many catalytic reaction cycles proceed per site and per unit of time, or per gram of catalyst. The number of cycles that a catalyst can run through before it deactivates is determined by the turnover number (TON). It quantifies the number of A molecules transformed into B molecules using one molecule of catalyst. TOF can be determined by dividing TON to reaction time:

$$TON\ (-) = \frac{\%conversion\ \cdot \#\ of\ moles\ of\ substrate}{\#\ of\ moles\ of\ catalyst} \qquad (Eq.S2)$$

$$TOF\ (h^{-1}) = \frac{TON}{t} \qquad (Eq.S3)$$

Table S12.1. Pd-loading of hypercrosslinked and functionalized poly-Pickering-HIPEs determined using TXRF and their turnover frequency (TOF) in the Suzuki-Miyaura coupling reaction.

Supports	Pd (w%)	TON (-)	TOF (h^{-1})
DMM-Pd	10.2	1200	510
STM-Pd	3.4	3088	1544
STE-Pd	2.8	3768	1884
SH-Pd	2.1	4880	2440

Publication IV

Liquid-liquid extraction using combined hydrophilic-hydrophobic emulsion templated macroporous polymer micromixer-settlers

Hande Barkan-Öztürk,[1] Joanna Delorme,[1,†] Angelika Menner,[1] Alexander Bismarck[1,2,]*

[1] Polymer and Composite Engineering (PaCE) Group, Institute of Material Chemistry and Research, Faculty of Chemistry, University of Vienna, Währinger Strasse, 42, 1090, Vienna, Austria.

[2] Department of Chemical Engineering, Imperial College London, South Kensington Campus, London SW7 2AZ, United Kingdom

[†] Placement student from Sigma-Cermont, 20 Avenue Blaise Pascal, 63178 Aubiere Cedex, France.

* Corresponding author: Alexander Bismarck, e-mail: alexander.bismarck@univie.ac.at

Abstract

Continuous liquid-liquid extraction and separation of 4-aminoacetophenone, a product of the hydrogenation of 4-nitroacetophenone, was performed within emulsion templated macroporous polymer (polyHIPE) extraction units using a miniaturized gravity-based settler. PolyHIPEs with interconnected and tailorable macroporous structures are effective micromixers allowing to mix fluids in both axial and radial directions. We fabricated extraction units by combining hydrophilic and hydrophobic polyHIPEs, which improved the extraction efficiency by inverting the liquid/liquid dispersion type from oil/water to water/oil (or vice versa) during the extraction, which

is governed by the wettability of the porous medium. The extraction efficiency of our combined polyHIPE micromixer reached 98%, while that of control experiments performed using a blank tube or commercial Kenics® static mixer was 78%. The overall volumetric mass transfer coefficient k_La in polyHIPE micromixer-settlers was significantly higher 0.011 s^{-1} reaching interfacial areas a of 17900 m^2/m^3, much larger compared to a blank tube (k_La = 0.0035 s^{-1} and a = 5700 m^2/m^3) and static mixer (k_La = 0.0041 s^{-1} and a = 6800 m^2/m^3). PolyHIPE micromixer-settlers could be potentially useful to intensify continuous L-L extractions.

Keywords: L-L extraction, polyHIPEs, volumetric mass transfer coefficient, extraction efficiency.

1 Introduction

Process intensification is a set of innovative principles used to develop sustainable and cost-effective chemical process systems,[1] which can be summed up in the "mnemonic safer, cleaner, and smaller".[2] One aim of process intensification is to downsize plants to microreactors to overcome bottlenecks in heat and mass transfer by utilising the advantages of micromixers. Micromixers mix fluids in microscale channels, where mass transport occurs by molecular diffusion and chaotic advection. Micromixers and -reactors play a significant role to reduce the dimensions of chemical reactors because of their well-defined flow patterns, better temperature control resulting in a uniform process environment, which leads to lower energy consumption, less raw material usage and thus less waste generation.[2] Micromixers provide many benefits over conventional processes, e.g. high mass transport rates, rapid mixing and high selectivity and conversion.[3–5] Because of those advantages, micromixers can be used in various chemical process units, e.g., mixers,[6,7] microreactors with embedded catalyst[8–10] or liquid-liquid extractors.[11,12]

Liquid-liquid extraction plays an important role both in laboratories and industry to separate compounds which cannot be separated directly or when direct separation, such as crystallization or distillation, is too costly.[13] Based on the partial miscibility of liquids, dissolved compounds can be separated by liquid-liquid extraction from a process solvent to a second solvent by mass transfer.[13,14] However, macroscale L-L extraction has drawbacks, including necessity for large amount of solvents with its associated risks especially when using volatile solvents and it is labor intensive.[15,16] Besides employing L-L extraction in laboratories to purify synthesized compounds, or to be able to characterize compounds in a suitable solvent,[17,18] it is curial process step in industries, including recovery of metals, extraction of organic compounds, refining radioactive isotopes, oil recovery, etc.[14] In extraction unit designs, immiscible liquids are dispersed by energy input to increase the contact (interfacial) area to enhance mass transfer efficiency. Liquid-liquid extraction operations are usually performed using countercurrent columns, centrifugal extractors and mixer-settlers.[13] However, large liquid volumes require high energy input for efficient mixing and volatile liquids result in increased pressures in the extraction unit. In contrast, micromixers allow for advanced process control and high contact area to volume ratio resulting in enhanced mass transfer between two immiscible phases.[19]

Various micromixer designs have been disclosed. The simplest micromixers use Y or T connector of empty tubes, while more elaborate designs use etching of metal or silicon substrates, molding or CNC milling of polymer substrates.[3] However, in order to achieve effective mixing in small dimensions, vortices have to be generated in microchannels, which is possible by adding split-and-recombination channels or obstacles. Design and dimensions of such complex channel structures are limited by machine accuracy.[20] We already demonstrated that micromixers can be fabricated from emulsion templated macroporous polymers, called polymerized high internal phase

emulsions (polyHIPEs).[21–24] Their interconnected pore structures can be tailored to create parallel mixing paths along the micromixer, which allows for effective micromixing in a co-flow arrangement.[6]

PolyHIPEs are produced by polymerization of HIPEs comprising a monomer containing continuous phase and an aqueous internal phase (>74 vol.% of the total emulsion), which after removal of the templating phase results in macroporous polymers.[25–27] The pore structure of polyHIPEs can be tailored by choice of emulsifier,[28,29] the emulsion phase volume ratio,[21,30] and the energy input during emulsification.[30,31] Their interconnected pore structure allows for fluid transport through their monolithic structure rendering them useful as stationary phase in column chromatography,[32–34] as filters,[35–37] or microreactors.[21,23,38] During liquid-liquid extraction, effective mixing results in increased interfacial area between immiscible liquids, which is necessary to increase the mass transfer rates and thus extraction performance of desired compounds.

Herein, we introduce a design of a co-flow contactor liquid-liquid micromixer-settler separation unit comprising both hydrophilic and hydrophobic polyHIPEs. In order to improve the mass transfer between raffinate and extract phase, we will alter droplet form during L-L extraction by changing the wettability of polyHIPE extraction unit from oil to water-wet. Therefore, the effect of polyHIPE wettability on the droplet formation is investigated by generating emulsions via injecting surfactant containing aqueous and oil solutions to polyHIPE extraction units. The continuous L-L extraction of 4-aminoacetophenone, which is a typical product of the hydrogenation of 4-nitroacetophenone, is performed using the polyHIPE micromixer-settler. We investigated the effect of the location of hydrophilic and hydrophobic polyHIPEs in the extraction unit at two different flow rates. The extraction efficiency and overall volumetric mass transfer of

polyHIPE micromixer-settlers are calculated by determination the 4-AAP concentration in the exit raffinate and extract phases and will be compared with a blank tube and commercial static mixer.

2 Experimental Part

2.1 Materials

Styrene (St) ≥99%, divinylbenzene (DVB) 80%, α,α′-azoisobutyronitrile (AIBN), calcium chloride dihydrate ($CaCl_2 \cdot 2H_2O$) ≥99%, sorbitan monooleate (Span 80), trifluoroethyl methacrylate (TFEMA), 2-hydroxyethyl methacrylate (HEMA), N,N'-methylene bisacrylamide (MBAA), ammonium persulfate (APS), the surfactant poly-(ethylenglycole)-block-poly-(propyleneglycole)-block-poly-(ethyleneglycole) (Kolliphor® P 188 (P188)), cyclohexane, N,N,N′,N′-tetramethylethylenediamine (TEMED), hexadecane, surfactant polysorbate 80 (Tween 80), 4-nitroacetophenone (4-NAP), 4-aminoacetophenone (4-AAP), ammonium formate (AF) and caffeine were purchased from Sigma-Aldrich (Vienna, Austria). Ethanol, ethyl acetate and isopropanol were purchased from Fischer Chemicals (Vienna, Austria), Araldite Rapid adhesive® from Rapid Electronics Limited (Essex, UK), Araldite 2020 from Farnell Element14 (Salzburg, Austria), shrink tubing from Conrad Electronic GmbH (Vienna, Austria), 3/8" Kenics static mixer (12 helix) from Cole-Parmer (Germany), and 1/16" PTFE tubes from VWR (Vienna, Austria). All materials were used as received.

2.2 Preparation of polyHIPEs

2.2.1 Hydrophilic polyHIPEs

Hydrophilic polyHIPEs were produced adapting the procedure published by Kovačič et al.[39] Briefly, the continuous phase (CP) of o/w HIPEs was prepared by dissolving HEMA (1.7 g, 0.013

mol) in H_2O (5.2 g) in a glass mixing vessel equipped with an anchor paddle attached to an overhead stirrer (Phoenix Instruments RSO-20D, Garbsen, Germany). The crosslinker MBAA (0.8 g, 0.0052 mol), surfactant P188 (1 or 1.5 g) and initiator APS (1 mol%, with respect to total amount of double bonds of the monomers) were dissolved in the HEMA solution. Cyclohexane (17.34 g) as internal phase (IP) was added slowly into the CP under constant agitation at 400 rpm. Thereafter, HIPEs were agitated further for 30 min at 400 rpm, producing a stable emulsion. The reducing agent (TEMED, 0.0465 g, 0.52 mmol) was added to the emulsion and further mixed for 30 s. O/w HIPEs were transferred into polypropylene centrifuge tubes (Falcon®, D_i = 12 mm) and polymerised at room temperature in a fume hood for 24 h. Afterwards, the monoliths were removed from the tubes and immersed into isopropanol for 16 h, and further purified by Soxhlet extraction with isopropanol for 16 h. PolyHIPEs were dried first in the fume hood overnight, then in a convection oven at 70 °C for 24 h. The hydrophilic polyHIPE monoliths are called HM10 and HM15, were the number indicates the surfactant amount used to stabilise the HIPE templates.

2.2.2 Hydrophobic polyHIPEs

Hydrophobic polyHIPEs were prepared by polymerisation of the continuous monomer phase of w/o HIPEs prepared by mixing St (8 mL, 0.07 mol), DVB (2 mL, 0.014 mol), TFEMA (0, or 2 mL, 0.014 mol) and Span 80 (2 mL) in a reaction vessel while adding AIBN (0.16 g or 0.2 g, 1 mol% with respect to the double bonds of the monomers). The aqueous IP consisted of 40 g/L $CaCl_2$ and was added dropwise into the CP under constant agitation at 400 rpm. After complete addition of dispersed phase (77 vol.%), it was further stirred at 400 rpm for 3 min. Then the emulsion templates were transferred into centrifuge tubes and polymerised at 70 °C in an oven for 4 h. Afterwards, the monoliths were removed and washed with water and acetone to remove the electrolyte and impurities (surfactant and unreacted monomers), respectively. PolyHIPEs were

dried in an oven at 70 °C for 16 h. The hydrophobic poly(St-co-DVB) and poly(St-co-TFEMA-co-DVB) monoliths were called S and SF, respectively.

2.3 Fabrication of micromixer-settler units

Micromixer units with a total length of 40 mm were fabricated using either a hydrophilic or hydrophobic polyHIPEs, or a combination of both polyHIPEs (Stage 1 in **Figure 1A**). After cutting the polyHIPEs to either 20 mm or 40 mm, two inlet holes with diameters of 2 mm were drilled 5 mm deep into the top of the monolith (Stage 2 in **Figure 1A**). An outlet hole of the same diameter and depth was drilled into the bottom of the monolith. PTFE tubes (outer diameter 1/16", VWR, Vienna, Austria) were sealed into the holes using Araldite® Rapid adhesive, which cured in 30 min at room temperature (Stage 3 in **Figure 1A**). The adhesive was also used to coat the surface of the monolith to avoid fluid bypassing the polyHIPEs (Stage 3 in **Figure 1A**). Afterwards, the monoliths were sealed to provide extra protection with a high temperature shrink tube using a heat gun (Stage 4 in **Figure 1A**). The top and the bottom parts of the extraction unit were sealed using epoxy resin (Araldite® 2020), which also provided stability to the in- and outlet tubes (Stage 4 in **Figure 1A**). The device was placed into a convection oven at 70 °C for 4 h to cure the epoxy resin. Extraction units were named by adding "E" to their name.

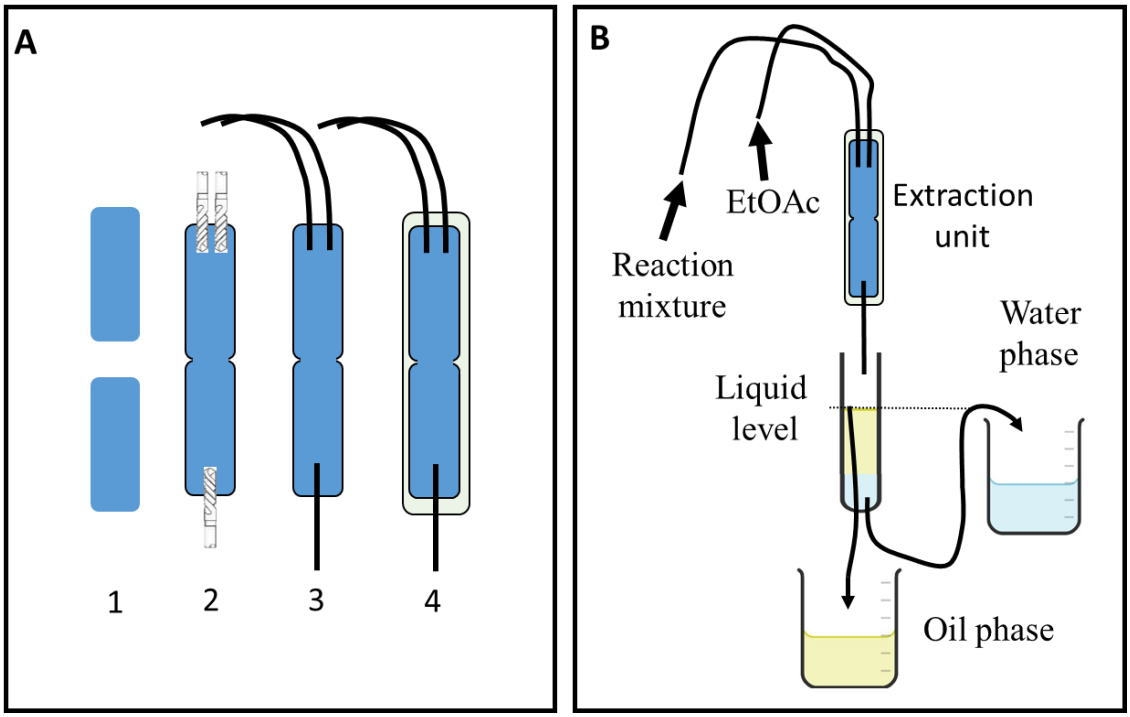

Figure 1. A) Schematic showing the fabrication of polyHIPE extraction units; stage 1: hydrophilic and hydrophobic polyHIPEs, stage 2: drilling inlets and outlet, and coating outside of polyHIPEs with Rapid adhesive, stage 3: sealing inlet and outlet tubes, stage 4: covering outside with a shrink tube and applying epoxy resin to upper and bottom parts. B) Schematic of the continuous micromixer-settler unit for extraction of 4-AAP from a simulated aqueous reaction medium with ethyl acetate.

The settler unit, shown in **Figure 1B**, was fabricated using a 12 mm centrifuge tube. Two holes were drilled into the bottom part of the centrifuge tube and flexible tubes (outer diameter 1/8", VWR, Vienna, Austria) were inserted and sealed using Araldite® Rapid adhesive. One of the tubes was placed 5 mm into the centrifuge tube as siphon to the collect the denser aqueous phase and the other one 40 mm above the bottom to collect the oil phase. Both phases were collected continuously.

2.4 Characterization methods

2.4.1 Characterization of hydrophilic and hydrophobic polyHIPEs

The morphology of polyHIPEs was investigated using scanning electron microscopy (SEM, JCM-6000, JEOL GmbH, Eching, Germany). Fractured sample surfaces were gold coated (JFC-1200, JEOL GmbH, Eching, Germany) to guarantee sufficient electrical conductivity. SEM images were further analysed using the image analysis software package (ImageJ©, https://imagej.nih.gov/ij/download.html). To determine the average pore (d_p) and pore throat (d_{pt}) diameters of the samples at least 100 pore and pore throat diameters were measured. The skeletal density (ρ_s) of polyHIPEs was determined using helium pycnometry (Accupyc 1330, Micrometrics, Dunstable, UK) using ground (about 0.1 g) samples. The foam density (ρ_f) of the polyHIPEs was analysed using an envelope density analyser (Geopyc 1360, Micrometrics, Dunstable, UK). The porosity of the monoliths was calculated as follows:

$$P\,\% = \left(1 - \frac{\rho_f}{\rho_s}\right) \cdot 100 \qquad \text{(Eq. 1)}$$

All other methods used for polyHIPE characterisation are detailed in the Supplementary Information; swelling ratio (ESI **S1**), mechanical properties (ESI **S2**), fluorine content (ESI **S3**) and contact angle measurements (ESI **S4**).

2.4.2 4-Aminoacetophenone partition and mass transfer coefficients

The method to determine the partition coefficient P_C of 4-AAP between an aqueous and ethyl acetate phase and mass transfer coefficients was adapted from our previous work.[22] P_C is the ratio of the equilibrium concentration of 4-AAP in extract $C_{i^{eq},E}$ and in raffinate phase $C_{i^{eq},R}$:

$$P_C = \frac{C_{i^{eq},E}}{C_{i^{eq},R}} \quad (Eq.2)$$

The equilibrium concentration of 4-AAP in both phases was determined using UV-vis spectroscopy (Agilent 8453, Agilent Technologies Österreich GmbH, Vienna, Austria). 10 mL of simulated reaction mixture (4-AAP (0.05 M in EtOH), 4-NAP (0.05 M in EtOH) and AF (0.06 M in H_2O) in a 1:1:2 volume ratio) was agitated with 10 mL ethyl acetate using a vortex mixer. Afterwards we waited for phase separation to occur prior to taking samples of both phases. The solute concentration C_i in the effluent was calculated using the Lambert-Beer law:

$$[C_i] = \frac{A}{\varepsilon_i l} \quad (\text{Eq.}3)$$

where A is the absorbance, l the optical path length, and ε_i the molar extinction coefficient of 4-AAP at 310 nm (22634 $L \cdot mol^{-1} \cdot cm^{-1}$) determined using a known concentration of substances in H_2O and ε_i = 28220 $L \cdot mol^{-1} \cdot cm^{-1}$ in ethyl acetate (**Figure S5-1**).

The mass transfer coefficient of 4-AAP (k_L) was calculated from the 4-AAP concentration in ethyl acetate phase after extraction of a 20 mL simulated reaction mixture with 80 mL ethyl acetate in a cylindrical vessel agitated with a sawtooth impeller at 300 rpm. During the extraction, 100 µL samples were taken at certain time intervals using a micropipette. [4-AAP] in ethyl acetate (extract) phase C_E was calculated from the absorbance measured using UV-vis spectroscopy. The overall mass transfer coefficient ($k_L a$) could then be calculated:[22]

$$C_E = \left(\frac{1}{1+\alpha}\right) P_C C_{i^{in},R}(1 - \exp(-(1+\alpha)k_L a \cdot t)) \quad (Eq.4)$$

with

$$\alpha = \frac{V_{org} P_C}{V_{aq}} \qquad (Eq. 5)$$

where $C_{i^{in},R}$ is the initial [4-AAP] in the aqueous raffinate phase, a interfacial area per unit volume, *t* the extraction time, V_{org} and V_{aq} the volumes of organic and aqueous phases, respectively. The interfacial area per volume a was calculated from the Sauter mean droplet diameter $\bar{d}_{32}$, which was determined using the correlation for a sawtooth impeller reported by El-Hamouz et al.:[40]

$$a = \frac{6\theta}{\bar{d}_{32}} \qquad (Eq. 6)$$

$$\frac{\bar{d}_{32}}{D} = 0.187 We^{-0.6} = 0.187 \left(\frac{\rho_c N^2 D^3}{\sigma} \right)^{-0.6} \qquad (Eq. 7)$$

where θ is the dispersed phase volume fraction, *D* the impeller diameter, *We* the Weber number, ρ_c the density of the continuous phase, *N* the rate of impeller rotation and σ the interfacial tension ($\sigma_{ow} = 7.37\ mN/m$).[41]

The overall mass transfer coefficient ($k_L a$) for the extraction using a sawtooth impeller was calculated from the gradient of the natural logarithm of C_E as a function of time (**Figure S6-1**). The mass transfer coefficient for this solution (k_L) was found by dividing $k_L a$ by a obtained using Eq. 6. The interfacial area per volume created within the polyHIPEs was estimated using the known mass transfer coefficient k_L assuming similar film transfer coefficients between the agitated vessel and the polyHIPE micromixer.[22]

2.5 Emulsification using polyHIPE extraction units

To test the hypothesis that the wettability of the porous medium determines dispersed liquid phase type – either w/o or o/w we used polyHIPE extraction units fabricated using either only hydrophilic

or both hydrophilic and hydrophobic polyHIPEs to create emulsions. The effect of wettability of the polyHIPE on the droplet formation was characterized by emulsification of an aqueous and oil phase. Water containing 2 wt.% Tween 80 and hexadecane containing 2 wt.% Span 80 were injected into the polyHIPE extraction units using a double syringe pump (Masterflex® Touch-Screen Syringe Pump, Cole-Parmer, Germany) at a flow rate of 0.3 mL/min. Emulsions were collected in water dyed with red food color and/or in sunflower seed oil to determine the produced emulsion type: w/o or o/w, respectively. Videos of the experiments are available in the Supplementary Information (**Video S1-S3**).

2.6 L-L Extraction using polyHIPE micromixer-settler units

Liquid-liquid extraction using polyHIPE micromixer-settlers was performed with two different solutions. In the first extraction experiment, caffeine was extracted from an aqueous solution (1 g/L caffeine) with ethyl acetate. Solutions were saturated with the other solvent prior to extraction to avoid volume changes, since they have some degree of mutual solubility. The two phases were injected into the extraction unit using a double syringe pump at a flow rate of 0.3 mL/min. The effluent was separated continuously using our settler and collected in vials. After extraction the water phase was characterized using UV-Vis spectroscopy to determine the caffeine concentration.

In a second extraction experiment, 4-AAP was extracted from a simulated process fluid of a 4-NAP hydrogenation reaction containing 4-AAP (0.05 M in EtOH), 4-NAP (0.05 M in EtOH) and AF (0.06 M in H_2O) in a 1:1:2 volume ratio into ethyl acetate using the polyHIPE micromixer-settler. The aqueous mixture and ethyl acetate were injected at the same flow rate simultaneously using a double syringe pump at a flow rate of 0.2 and 0.3 mL/min (total flow rate 0.4 or 0.6 mL/min, respectively). Control experiments were performed using a commercial Kenics mixer and

an empty tube (d_i = 1.5 mm, L = 2.1 m, i.e. having the same volume as the pore volume of the polyHIPE micromixer) at the same extraction conditions. The effluent was separated continuously using our homemade settler (**Video S4**) and the 4-AAP concentration in the aqueous phase was determined as before.

The extraction efficiency *E* was determined by the [4-AAP] concentration in extract phase using the following equation:[42]

$$E = \frac{C_{i_{out},E} - C_{i_{in},E}}{C_{i^{eq},E} - C_{i_{in},E}} \qquad (Eq.8)$$

where $C_{i_{out},E}$ is the [4-AAP] concentration in the extract phase collected at the outlet, $C_{i_{in},E}$ the [4-AAP] concentration in the extraction solvent (ethyl acetate). Moreover, the mass transfer performance of droplets generated in the extraction units were estimated from the overall volumetric mass transfer coefficient $k_L a$ of the polyHIPE micromixer-settlers, the blank tube and the Kenics mixer. The overall volumetric mass transfer coefficient $k_L a$ is expressed as follows:[42,43]

$$k_L a = \frac{1}{\tau} \ln\left(\frac{C_{i^{eq},R} - C_{i_{in},R}}{C_{i^{eq},R} - C_{i_{out},R}}\right) \qquad (Eq.9)$$

where τ is the extraction time determined by the ratio of extraction unit volume and volumetric flow rate, $C_{i_{in},R}$ the [4-AAP] concentration in the inlet of the raffinate phase and $C_{i_{out},R}$ the [4- AAP] concentration in the exit stream of the raffinate phase.

Energy dissipation rate ε of polyHIPE extraction units, the blank tube and Kenics mixer were calculated from pressure drop measurements (ΔP):

$$\varepsilon = \frac{\Delta P Q_{tot}}{\rho_c V_R} \qquad (Eq.10)$$

where Q_{tot} is the total volumetric flow rate during L-L extraction, ρ_c density of CP of the extracted system and V_R the extractor volume. The Reynolds number of the polyHIPE extraction units was calculated as follows:

$$Re = \frac{\rho_c d_p u_{tot}}{\mu_c} \qquad (Eq. 11)$$

where d_p is average pore size of polyHIPEs used in the extraction unit, u_{tot} total superficial velocity and μ_c dynamic viscosity of CP.

3 Results and Discussion

Morphology and mechanical properties of hydrophilic polyHIPEs

Macroporous poly(HEMA-co-MBAA)HIPE monoliths were produced by polymerization of continuous phase, which was stabilized either 10 or 15 vol.% surfactant (with respect to the CP volume) and subsequent removal of the templating oil phase resulting in an interconnected macroporous structure (**Figure 2**). As a result of increasing surfactant amount used to stabilise the HIPE template, the average pore diameter d_p of the polyHIPEs decreased from 16 µm (HM10) to 8 µm (HM15) (**Table 1**), which are extremely significantly different according to Student's *t*-test. Their skeletal densities were identical within the error since they were produced using the same monomer to crosslinker ratio. The porosity of the monoliths increased with increasing surfactant amount from 86.5% to 89.3% (**Table 1**). We adapted the formulation of o/w HIPE templates from the literature,[39] however, monomer to crosslinker ratio was decreased from 6.5 to 2.5 in order to increase the chemical stability and the mechanical properties of these polyHIPEs. The increased

crosslinker concentration caused a slight increase of the pore diameter of the polyHIPEs; from 5.5 µm in the literature to 8 µm for our polyHIPEs (HM15) (**Table 1**).

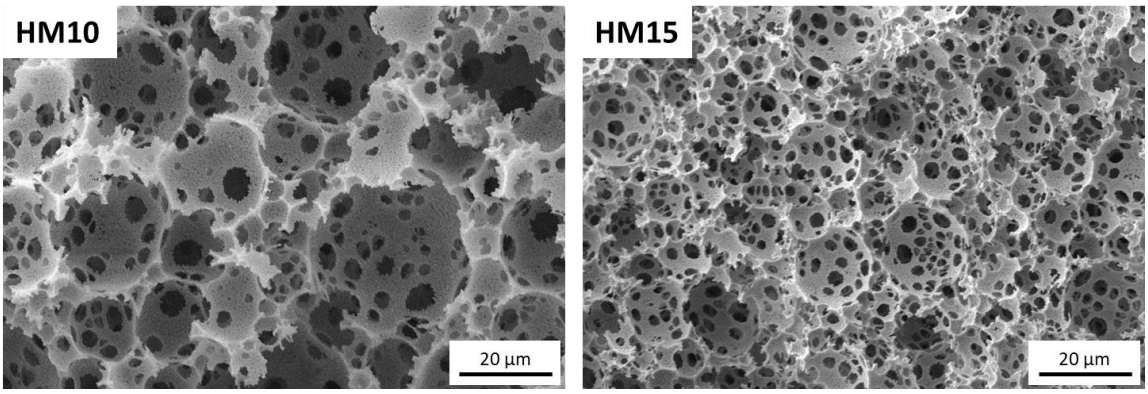

Figure 2. Characteristic SEM images of hydrophilic polyHIPEs produced by polymerization of o/w HIPEs.

Water spread on and imbibed immediately into hydrophilic polyHIPEs. Swelling ratios *Q* of polyHIPEs determined by immersion of dry polyHIPEs into water for 24 h were 1.4 ± 0.2 and 1.3 ± 0.2 for HM10 and HM15, respectively. Their water uptake was 8.7 ± 0.5 and 7.1 ± 0.7 g of water per gram of polyHIPEs for HM10 and HM15, respectively, which was lower compared to literature data (Q = 1.5 and water uptake = 10.95 g/g) because of much lower monomer to crosslinker ratio;[39] the higher degree of crosslinking restricts swelling. The Young's moduli of HM10 and HM15 were 12 MPa to 9 MPa and crush strengths 0.45 MPa and 0.31 MPa, respectively (**Table 1**) (stress strain curves are shown **Figure S2-1**).

Table 1. Morphological characteristics, average pore (d_p) and pore throat (d_{pt}) diameter, skeletal density (ρ_s), foam density (ρ_f), porosity (P), Young's moduli (E), and crush strength (σ_c), of polyHIPEs used for micromixer fabrication.

Samples	d_p (μm)	d_{pt} (μm)	ρ_s (g/cm^3)	ρ_f (g/cm^3)	P (%)	E (MPa)	σ_c (MPa)
HM10	16 ± 7	3 ± 1	1.32 ± 0.03	0.18 ± 0.01	86 ± 1	12 ± 6	0.45 ± 0.1
HM15	8 ± 3	2 ± 1	1.35 ± 0.02	0.16 ± 0.01	89 ± 1	9 ± 2	0.31 ± 0.1
S	11 ± 3	3 ± 1	1.12 ± 0.02	0.16 ± 0.01	83 ± 2	19 ± 2	1.3 ± 0.1
SF	10 ± 5	1.3 ± 1	1.19 ± 0.01	0.23 ± 0.01	80 ± 1	52 ± 4	1.8 ± 0.2

Morphology and mechanical properties of hydrophobic polyHIPEs

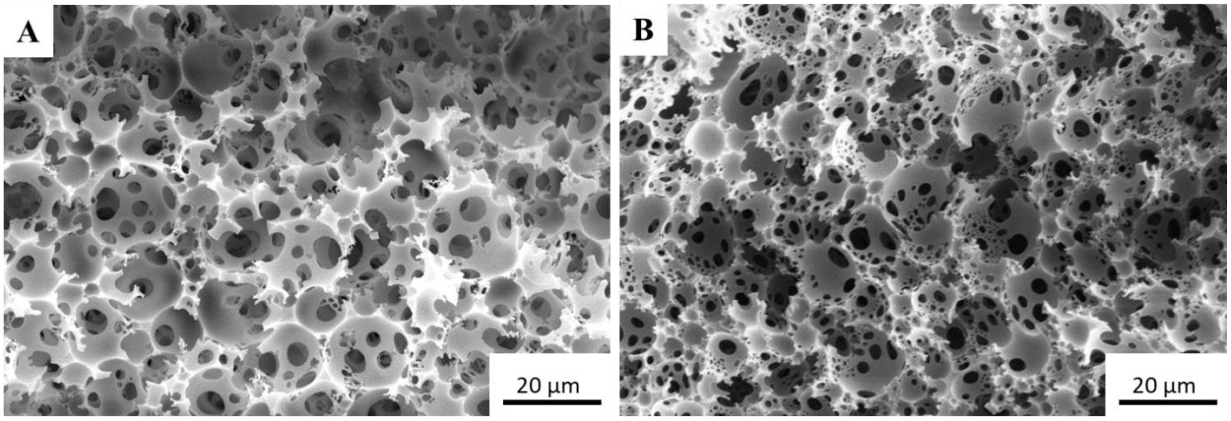

Figure 3. Characteristic SEM images of hydrophobic polyHIPEs produced A) by polymerization of St-DVB (S) and B) of St-DVB-TFEMA based HIPEs (SF).

Macroporous hydrophobic polymers also possess the typical interconnected macroporous structure of polyHIPEs (**Figure 3**). To increase the hydrophobic nature of crosslinked polystyrene fluorine containing monomer (TFEMA) was added to the St-DVB mixture. Even though the average pore diameters of the hydrophobic polyHIPEs S and SF were same within the error (**Table 1**), they were still significantly different according to Student's *t*-test. The successful incorporation of TFEMA into the polyHIPE was determined using FTIR (**ESI S3**). In the FTIR spectra (**Figure S3-1**), a carbonyl band appeared at 1750 cm^{-1}, whilst C-O-C stretching was observed at 1280 cm^{-1} and C-F stretching at 1163 cm^{-1}, which indicated the presence of TFEMA in the polymer network. The fluorine content of SF was determined by elemental analysis to be 3.6 wt.%, and 1.2 wt.% using

X-ray photoelectron spectroscopy (XPS) (**Table S3-1**). As result of TFEMA, thus fluorine, incorporation the hydrophobicity of the resultant polyHIPEs increased as determined by contact angle measurement. **Figure S4-1** shows an increase of the water contact angle on the polyHIPE surface from 117° to 135°. Please note, because of the porous nature of polyHIPEs the wetting regime is Cassie-Baxter as air is entrapped below water droplets.

The incorporation of TFEMA into the poly(St-co-DVB) resulted in a slight increase of ρ_s due to the higher density of TFEMA (1.18 g/cm^3) compared to styrene (0.91 g/cm^3) and DVB (0.91 g/cm^3). However, both polyHIPEs (S and SF) had similar porosities (**Table 1**). Furthermore, the incorporation of TFEMA into poly(St-co-DVB) resulted in significantly better mechanical properties of the polyHIPEs (**Table 1** and **Figure S2-2**).

Effect of polyHIPE wettability on micromixing performance

The micromixing efficiency of polyHIPE extraction units was first tested by determining the residence time distribution (**ESI S7**). Since those extraction units were fabricated by combining hydrophilic and hydrophobic polyHIPEs, their mixing performance differed slightly from that of micromixers fabricated using only a single polyHIPE type (**Figure S7-2**). Because of their high surface area to volume ratio of microfluidic systems, the interfacial tension between microchannels and liquid determines the type of liquid-liquid dispersion that forms; either o/w or w/o.[44] By changing the polyHIPE wettability from water to oil-wet (or vice versa) we assumed to increase the mass transfer effectiveness during L-L extraction. To test the influence of polyHIPE wettability on the type of droplet dispersion we investigated emulsion formation in the extraction units. Using a micromixer fabricated using a single unit hydrophilic polyHIPE resulted in the formation of hexadecane-in-water emulsion (**Video S1**, showing that emulsion droplets did not spread on sunflower seed oil but sediment). In case of using an extraction unit fabricated by combination of

both hydrophilic and hydrophobic polyHIPEs, the emulsion type was dependent on the wettability of the polyHIPE at the bottom of the extraction unit (**Video S2** (E-SF/HM15, hydrophilic polyHIPE at the bottom) and **Video S3** (E-HM15/SF, hydrophobic polyHIPE at the bottom)); Emulsion created by forcing the same oil and water solutions through E-SF/HM15 remained stable in sunflower seed oil indicating the formation of an o/w emulsion (**Video S2**), whilst a w/o emulsion was produced when using E-HM15/SF with the hydrophobic part at the bottom (**Video S3**). Those findings support that the polyHIPE wettability influences the droplet dispersion type.

Continuous liquid-liquid extraction using polyHIPE micromixer-settlers

Previously we extracted caffeine with an efficiency of 86% from an aqueous solution into ethyl acetate using poly(St-co-DVB)HIPE micromixers having a permeability of 7.6 mD ($0.0076 \cdot 10^{-12}$ m^2).[22] These extractors were fabricated by placing epoxy resin coated polyHIPEs into a stainless steel tube (D_i = 7.5 mm, L = 70 mm). During L-L extraction using those polyHIPE micromixers, fluids were injected through the open end of the tube with pipe connections, and effluent was collected directly from the other open end of the tube. However, more recently we did show that placing inlet and outlet tubes into the micromixer significantly increased their micromixing performance, even when using polyHIPEs with higher permeability.[6] We tested our poly(St-co-DVB) micromixers E-S to extract caffeine from an aqueous solution using ethyl acetate to compare the extraction performance with previous work. Using E-S having a liquid permeability of 190 mD an 85% extraction efficiency was achieved: the same efficiency but using a shorter micromixer with a higher permeability.

We studied the L-L extraction of 4-AAP from a simulated hydrogenation reaction of 4-NAP medium (**Figure S9-1**), which included the unreacted 4-NAP, salt from the hydrogen source and reaction product (4-AAP). We achieved an 88% extraction efficiency using E-S operated at a total

flow rate of 0.6 mL/min, which was significantly higher compared with the blank tube having the same mixing volume as the polyHIPE extraction units and a Kenics mixer (**Table 2**). Fluids split and recombine through the polyHIPE pore throats in the extraction unit, thus the mixing performance improved considerably compared to the blank tube, in which fluids mixed in a combination of slug and parallel flow. In the static mixer, fluid was re-oriented through the channel, which resulted a slight increase in the extraction efficiency compared with the blank tube (**Table 2**).

Table 2. L-L extraction performance of polyHIPE micromixer-settlers, a blank tube and static mixer operated at total flow rates of 0.4 and 0.6 mL/min for extraction of 4-AAP from an aqueous medium into ethyl acetate; extraction efficiency, overall volumetric mass transfer coefficient k_La, interfacial area a, and permeability k. Please note the colour code next to the sample name, which is used in the graphs.

Extraction unit	Extraction efficiency (%)		k_La (s^{-1} x 10^{-3})		a (m^2/m^3 x 10^4)		k (mD) (· 10^{-12} m^2)	
	0.4 mL/min	0.6 mL/min	0.4 mL/min	0.6 mL/min	0.4 mL/min	0.6 mL/min	0.4 mL/min	0.6 mL/min
E-HM10 *	85 ± 4	96 ± 2	3.5 ± 0.2	9.1 ± 0.2	0.59 ± 0.04	1.51 ± 0.4	59 ± 2	76 ± 4
E-HM15 *	79 ± 4	96 ± 2	2.8 ± 0.3	8.6 ± 0.2	0.46 ± 0.9	1.42 ± 0.4	39 ± 3	35 ± 3
E-S *	78 ± 6	88 ± 4	2.2 ± 0.4	4.5 ± 0.3	0.37 ± 0.8	0.75 ± 0.7	145 ± 3	192 ± 2
E-SF *	88 ± 3	90 ± 2	3.4 ± 0.3	5.7 ± 0.2	0.57 ± 0.7	0.95 ± 0.5	122 ± 2	109 ± 5
E-SF/HM10 *	91 ± 5	95 ± 3	4.1 ± 0.2	8.1 ± 0.2	0.68 ± 0.4	1.34 ± 0.4	112 ± 1	106 ± 3
E-HM10/SF *	84 ± 2	98 ± 4	3.2 ± 0.2	11 ± 0.2	0.53 ± 0.4	1.79 ± 0.4	78 ± 2	74 ± 4
E-SF/HM15 *	87 ± 3	97 ± 4	3.4 ± 0.3	9.1 ± 0.4	0.57 ± 0.9	1.51 ± 0.8	51 ± 1	78 ± 2
E-HM15/SF *	90 ± 3	96 ± 3	4.0 ± 0.3	8.4 ± 0.3	0.66 ± 0.9	1.39 ± 0.9	47 ± 5	49 ± 1
Blank tube *	76 ± 2	78 ± 2	2.2 ± 0.1	3.5 ± 0.1	0.36 ± 0.1	0.57 ± 0.1	660 ± 10	112 ± 10
Static mixer *	76 ± 2	80 ± 1	2.4 ± 0.1	4.1 ± 0.1	0.40 ± 0.1	0.68 ± 0.1	1.3 ± 0.1	0.2 ± 0.1

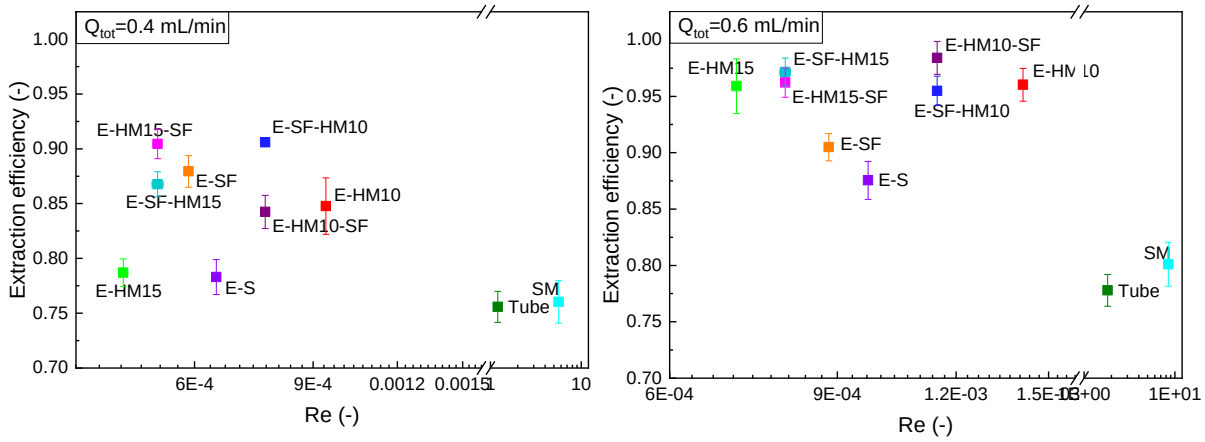

Figure 4. L-L extraction efficiency of 4-AAP from its simulated reaction medium into ethyl acetate as function of Re-number using various polyHIPE micromixer-settlers, a blank tube and static mixer at two different total volumetric flow rates A) 0.4 mL/min and B) 0.6 L/min.

The extraction efficiency of all polyHIPE micromixer-settlers increased when increasing the total flow rate from 0.4 mL/min to 0.6 mL/min (**Table 2**). The increased flow rate resulted in increased shear rates on the droplets which formed in the polyHIPE resulting in droplet break-up[24] and thus in increased interfacial area *a* between the two phases (**Table 2**). The Capillary number ($3.4 \cdot 10^{-6}$ at 0.6 mL/min flow rate) indicated that the viscous forces are much smaller than the interfacial forces in polyHIPE extraction units, thus droplet flow was generated by droplet elongation and break-up in the pore throats of polyHIPEs. In this work, we could not investigate the droplet diameters in the extraction unit since the mixture phase separated immediately after leaving the extraction unit. However, in previous work we showed that droplet diameters decreased with increasing flow rate during emulsifying of immiscible phases using polyHIPE micromixers, due to increased shear forces acting on the droplets.[24] When using extraction units fabricated from hydrophilic polyHIPEs with a permeability of 76 mD for E-HM10 and 35 mD for E-HM15, the extraction efficiency increased to 96% at the same flow rate. The lower permeability of E-HM15

was due to the significantly smaller average pore and pore throat diameters of HM15 compared to HM10 (**Table 2** and **Table 1**). Even though pore throat diameters of hydrophilic polyHIPEs were significantly larger than the pore throat diameters of hydrophobic polyHIPEs, they possessed a much lower permeability but improved extraction efficiency (**Table 2**). One of the reasons for the improved extraction efficiency was likely that the extract (ethyl acetate) phase formed the dispersed/droplet phase in the hydrophilic polyHIPE extraction units, which is often the case in other microfluidic micromixers used for L-L extraction.[11,12,42] The reason for the lower permeability of hydrophilic polyHIPEs when compared with hydrophobic polymers is that they swell significantly in contact with an aqueous phase, which results in decreased pore and pore throat diameters during extraction. The hydrophilic polyHIPEs remained intact, which was checked after using these extraction units several times over five-month period; no morphological changes could be observed (**Figure S10-1**). However, the low permeability of the hydrophilic extraction units might be a drawback when using them in-line with a microreactor.

To address the permeability limitations of hydrophilic polyHIPEs, we shortened them and combined hydrophilic with hydrophobic polyHIPE sections. This hydrophilic-hydrophobic polyHIPE extraction units had a higher permeability compared to single hydrophilic extraction unit while retaining the high extraction efficiency. Placing the hydrophilic polyHIPE in the inlet part and the hydrophobic portion in the outlet part of the extraction unit results in a lower permeability as compared to extractor which was assembled vice versa. However, irrespectively of the assembly their extraction efficiencies remained same within the error (**Table 2**).

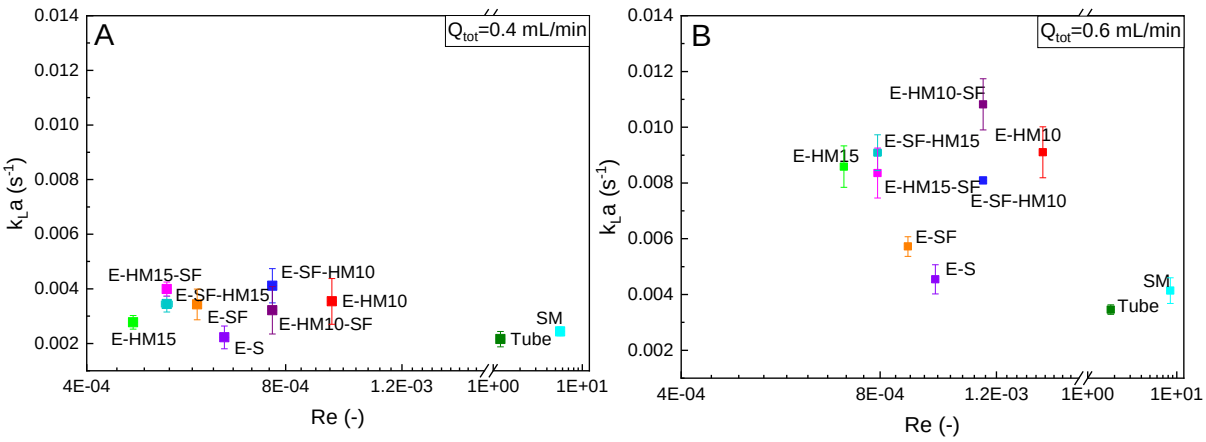

Figure 5. Overall volumetric mass transfer coefficient kLa as function of Re-number of the L-L extraction of 4-AAP using polyHIPE micromixer-settlers, a blank tube and commercial static mixer at total flow rates of A) 0.4 mL/min and B) 0.6 mL/min.

The overall volumetric mass transfer coefficient for each extraction unit is plotted as a function of the Re number in **Figure 5**; k_La more than doubled when increasing the flow rate, which was caused by increased shear forces acting on the droplets resulting in droplet break-up and hence increased interfacial areas enhancing mass transfer.

Literature reports that the volumetric mass transfer of L-L extractions in T- and Y-shaped micromixers improve when flow transitions from parallel flow to slug flow, which improve the internal recirculation within slugs,[2,12] and increases further droplet formation occurs in the micro-channel. However, in this case the average energy dissipation rate increases by 100 times but the interfacial area only doubles.[11] Our control, the blank tube with a Y-junction, had the lowest k_La since mass transfer occurred through the interfacial area in parallel flow and/or slug flow. k_La and interfacial area a within the blank tube and the static mixer were comparable with our previous results for the extraction of caffeine.[22] PolyHIPE extraction units possessing an interconnected

macroporous structure resulted in higher mass transfer coefficients because mixing of the fluids occurs both in axial and in radial directions. Extraction units fabricated using combined hydrophobic and hydrophilic polyHIPEs had higher k_La than single polyHIPE extraction units when operated at a total flow rate of 0.6 mL/min (**Table 2**).

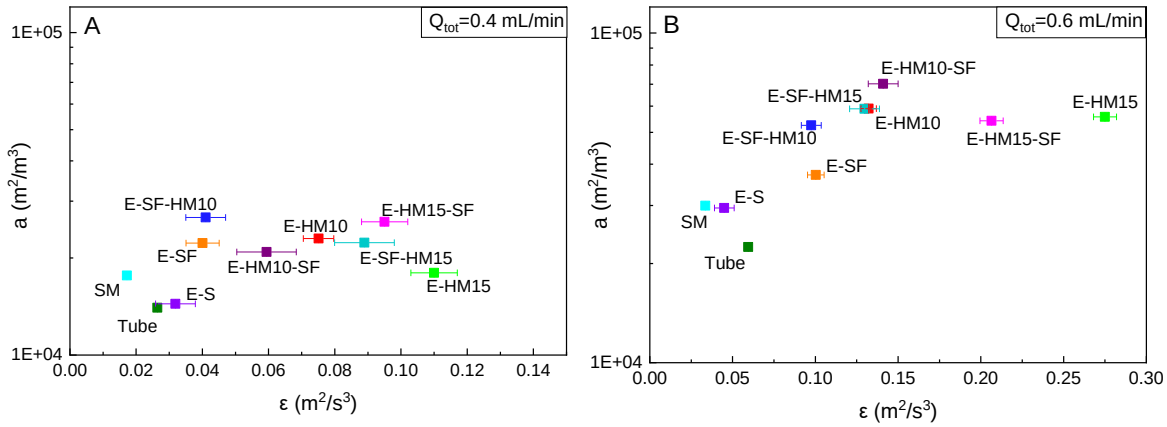

Figure 6. Interfacial area of polyHIPE micromixer-settler, a blank tube and static mixer as a function of energy dissipation rate during the extraction of 4-AAP from its simulated reaction mixture into ethyl acetate.

When using a hydrophilic-hydrophobic polyHIPE extraction unit the overall mass transfer coefficient increased up to $11 \cdot 10^{-3}$ s^{-1}, almost a sixfold increase over our previous work[22] ($1.92 \cdot 10^{-3}$ s^{-1}) using a hydrophobic polyHIPE extraction unit with a permeability of only 7.6 mD but the same morphological properties as our E-S micromixer. Nevertheless, despite having lowest k_La value ($4.5 \cdot 10^{-3}$ s^{-1}) among the polyHIPE micromixer-settlers, k_La of E-S micromixer-settler was still double that of a poly(St-co-DVB)HIPE with a lower permeabilty.[22]

Literature on L-L extraction of a single compound report higher overall volumetric mass transfer coefficients compared to our polyHIPE micromixer-settler (**Table 3**) but have in some cases still lower extraction efficiencies. The higher k_La values are a consequence of significantly lower

extraction times (see Eq. 9). Energy dissipation rates also need to be taken into account; in case of generating droplet flow in microchannels it can be as high as 100 m^2/s^3,[11] while in our polyHIPE micromixer-settlers we only reached energy dissipation rates of 0.28 m^2/s^3 (**Figure 6**). Kaske et al.[42] investigated L-L extraction performance of a blank tube with Y-junction, which had a similar internal diameter d_i as our blank tube but a significantly shorter length (L = 90 mm). They reached the same extraction efficiency for the extraction of acetone from water using toluene as we found for our blank tube at similar flow velocities.

Table 3. Comparison of overall volumetric mass transfer coefficient and interfacial area with published data.

	Regime and system	Conditions	Overall volumetric mass transfer and interfacial area
This work	Drop flow Nonreacting system Water-Ethanol/4-AAP/EtOAc	d_H = 8-16 µm macroporous polymer Q_{tot} = 0.4-0.6 mL/min	k_La = 0.002-0.011 s^{-1} a = 3700-17900 m^2/m^3
This work	Drop flow? Nonreacting system Water-Ethanol/4-AAP/EtOAc	d_H = 8.5 mm helical static mixer Q_{tot} = 0.4-0.6 mL/min	k_La = 0.0021-0.0041 s^{-1} a = 4000-6800 m^2/m^3
Kashid et al. (2007)[2]	Slug flow Nonreacting system Kerosene/acetic acid/water	d_H = 0.5-1 mm Y-junction u = 10-70 mm/s	k_La = 0.13-0.98 x 10^{-4} s^{-1} a = 2510-4800 m^2/m^3
Xie (2020)[45]	Disordered flow Reacting system 30%TBP-70%kerosene/ Zr(IV)/HNO_3 aq. solution	d_H = 400 µm Oscillating micromixer Q_{tot} = 6-21 mL/min	k_La = 3-13 x 10^{-4} s^{-1} a = N/A
Plouffe et al. (2016)[11]	Slug flow Reacting system Water/4-nitropheny acetate/Toluene …	d_H = 0.7 mm serpentine channel Q_{tot} = 1-8 mL/min	k_La = ~ 0.02-0.2 s^{-1} a = 8000-40000 m^2/m^3
Plouffe et al. (2016)[11]	Drop flow Reacting system Water/4-nitropheny acetate/Toluene …	d_H = 0.7 mm serpentine channel Q_{tot} = 12-32 mL/min	k_La = ~ 0.5-1.9 s^{-1} a = 10000-80000 m^2/m^3

Kaske et al. (2016)[42]	Slug flow	d_H = 0.5-1 mm	k_La = ~ 0.12-0.27 s^{-1}
	Nonreacting system Water/acetone/toluene	Y-junction Q_{tot} = 0.17-2 mL/min	a = N/A
Darekar et al. (2014)[46]	Parallel to slug flow	d_H = 184 µm	k_La = $7.36 \cdot 10^{-4}$-$2.18 \cdot 10^{-2}$ s^{-1}
	Reacting system Water/Zinc-D2EHPAH/dodecane	Split and recombine u = 0.02-0.4 m/s	a = N/A

Jafari et al.[47] extracted $CuSO_4$ aqueous solution by reactive extraction into kerosene containing di-(2-ethylhexyl) phosphoric acid (5 vol.%) using a twisted micromixer. The k_La value increased approximately from 1 s^{-1} to 8 s^{-1} with *Re* increasing from 75 to 450 but their extraction efficiency decreased from 97% to 60% due to a decrease in slug size, while the energy dissipation rate increased dramatically from 1200 Pa/s to 100000 Pa/s. This shows that a high k_La does not necessarily result in an efficient extraction performance. Xie et al.[45] disclosed a design of a passive L-L miniextraction unit consisting of four-stage oscillating micromixers including a minisettler. The fluids entered the mixing chambers through much smaller channels at high enough speed, causing fluid recirculation induced by the Coanda effect. Their system was similar to our porous media, since a fluid volume enters pores through much smaller pore throats. However, even though they tested their system at significantly higher flow rates, their extraction efficiencies were only between ~20-45% (**Table 3**), resulting in a much lower k_La value compared with our polyHIPE micromixer-settlers consisting of many more interconnected pores in which mixing, and thus extraction occurs.

4 Conclusions

We investigated a new micromixer-settler design consisting of water- and oil-wet sections of porous polymers. Compared to micromixers consisting only of a single hydrophobic section, the

mass transfer efficiency is significantly improved when using hydrophilic macroporous polymers but this comes at the expense of much lower permeability. This permeability limitation can be addressed by combining shorter sections of hydrophilic and hydrophobic macroporous polymers into a single micromixer. The mass transfer efficiency was studied using a simulated reaction mixture of a typical 4-NAP hydrogenation reaction resulting in 4-AAP.

We proved the effect of the wettability of polyHIPEs on the dispersion type of two immiscible liquids using a test emulsification of Tween 80 containing aqueous solution and Span 80 containing oil solution. When using hydrophilic polyHIPEs only or at the bottom part of extraction unit, the aqueous solution wetted the polyHIPE walls, which resulted in formation of oil-in-water emulsions. When using hydrophobic polyHIPEs at the bottom part of extraction unit water-in-oil emulsion formed. Thus, our proposed micromixer-settler design allows to invert the liquid-liquid dispersion type during an extraction.

Micromixer-settlers fabricated using polyHIPEs whose pore structure and composition can be tuned to adjust both permeability as well as wettability, allow for significant improvements in mass transfer rates and extraction efficiency as compared to conventional micro-channel and static mixer extractors. Microreactors could potentially be combined with polyHIPE micromixer-settlers allowing for significant process intensification of continuous flow reactions.

5 Appendices

Supporting Information. The following files are available free of charge.

Additional experimental details, materials, and methods, and their results.

Supporting_Information.docx

Corresponding Author

*Alexander Bismarck, E-mail: alexander.bismarck@univie.ac.at

Acknowledgements: We acknowledge the financial support by the Faculty of Chemistry of University of Vienna.

Funding: This research did not receive any specific grant from funding agencies in the public, commercial, or not-for-profit sectors.

6 References

(1) Van Gerven, T.; Stankiewicz, A. Structure, Energy, Synergy, Time—The Fundamentals of Process Intensification. *Ind. Eng. Chem. Res.* **2009**, *48* (5), 2465–2474. https://doi.org/10.1021/ie801501y.

(2) Kashid, M. N.; Harshe, Y. M.; Agar, D. W. Liquid−Liquid Slug Flow in a Capillary: An Alternative to Suspended Drop or Film Contactors. *Ind. Eng. Chem. Res.* **2007**, *46* (25), 8420–8430. https://doi.org/10.1021/ie070077x.

(3) Nguyen, N.-T. *Micromixers: Fundamentals, Design, and Fabrication*, 2nd ed.; Micro & nano technologies series; Elsevier/William Andrew: Amsterdam ; Boston, 2012.

(4) Nieves Remacha, M. J. Microreactor Technology : Scale-up of Multiphase Continuous Flow Chemistries, Massachusetts Institute of Technology, 2014.

(5) Chauhan, G.; Kaur, P. J.; Pant, K. K.; Nigam, K. D. P. *Sustainable Metal Extraction from Waste Streams*; 2020.

(6) Barkan-Öztürk, H.; Menner, A.; Bismarck, A. Emulsion-Templated Macroporous Polymer Micromixers. *Ind. Eng. Chem. Res.* **2021**, *60* (39), 14013–14025. https://doi.org/10.1021/acs.iecr.1c01949.

(7) Capretto, L.; Cheng, W.; Hill, M.; Zhang, X. Micromixing Within Microfluidic Devices. In *Microfluidics*; Lin, B., Ed.; Springer Berlin Heidelberg: Berlin, Heidelberg, 2011; Vol. 304, pp 27–68. https://doi.org/10.1007/128_2011_150.

(8) Cantillo, D.; Kappe, C. O. Immobilized Transition Metals as Catalysts for Cross-Couplings in Continuous Flow-A Critical Assessment of the Reaction Mechanism and Metal Leaching. *ChemCatChem* **2014**, *6* (12), 3286–3305. https://doi.org/10.1002/cctc.201402483.

(9) Brown, J. F.; Krajnc, P.; Cameron, N. R. PolyHIPE Supports in Batch and Flow-Through Suzuki Cross-Coupling Reactions. *Ind. Eng. Chem. Res.* **2005**, *44* (23), 8565–8572. https://doi.org/10.1021/ie048843c.

(10) Gömann, A.; Deverell, J. A.; Munting, K. F.; Jones, R. C.; Rodemann, T.; Canty, A. J.; Smith, J. A.; Guijt, R. M. Palladium-Mediated Organic Synthesis Using Porous Polymer

Monolith Formed in Situ as a Continuous Catalyst Support Structure for Application in Microfluidic Devices. *Tetrahedron* **2009**, *65* (7), 1450–1454. https://doi.org/10.1016/j.tet.2008.12.007.

(11) Plouffe, P.; Roberge, D. M.; Sieber, J.; Bittel, M.; Macchi, A. Liquid–Liquid Mass Transfer in a Serpentine Micro-Reactor Using Various Solvents. *Chem. Eng. J.* **2016**, *285*, 605–615. https://doi.org/10.1016/j.cej.2015.09.115.

(12) Dessimoz, A.-L.; Cavin, L.; Renken, A.; Kiwi-Minsker, L. Liquid–Liquid Two-Phase Flow Patterns and Mass Transfer Characteristics in Rectangular Glass Microreactors. *Chem. Eng. Sci.* **2008**, *63* (16), 4035–4044. https://doi.org/10.1016/j.ces.2008.05.005.

(13) Müller, E.; Berger, R.; Blass, E.; Sluyts, D.; Pfennig, A. Liquid-Liquid Extraction. In *Ullmann's Encyclopedia of Industrial Chemistry*; Wiley-VCH Verlag GmbH & Co. KGaA, Ed.; Wiley-VCH Verlag GmbH & Co. KGaA: Weinheim, Germany, 2008; p b03_06.pub2. https://doi.org/10.1002/14356007.b03_06.pub2.

(14) Zhang, J.; Wang, Y.; Stevens, G. W.; Fei, W. A State-of-the-Art Review on Single Drop Study in Liquid–Liquid Extraction: Experiments and Simulations. *Chin. J. Chem. Eng.* **2019**, *27* (12), 2857–2875. https://doi.org/10.1016/j.cjche.2019.03.025.

(15) Rawa-Adkonis, M.; Wolska, L.; Przyjazny, A.; Namieśnik, J. Sources of Errors Associated with the Determination of PAH and PCB Analytes in Water Samples. *Anal. Lett.* **2006**, *39* (11), 2317–2331. https://doi.org/10.1080/00032710600755793.

(16) Urkude, R.; Dhurvey, V.; Kochhar, S. Pesticide Residues in Beverages. In *Quality Control in the Beverage Industry*; Elsevier, 2019; pp 529–560. https://doi.org/10.1016/B978-0-12-816681-9.00015-1.

(17) Szabó, B. S.; Jakab, P. P.; Hegedűs, J.; Kirchkeszner, C.; Petrovics, N.; Nyiri, Z.; Bodai, Z.; Rikker, T.; Eke, Z. Determination of 24 Primary Aromatic Amines in Aqueous Food Simulants by Combining Solid Phase Extraction and Salting-out Assisted Liquid–Liquid Extraction with Liquid Chromatography Tandem Mass Spectrometry. *Microchem. J.* **2021**, *164*, 105927. https://doi.org/10.1016/j.microc.2021.105927.

(18) Shahrestani, M.; Tehrani, M. S.; Shoeibi, S.; Aberoomand Azar, P.; Waqif Husain, S. Comparison between Different Extraction Methods for Determination of Primary Aromatic Amines in Food Simulant. *J. Anal. Methods Chem.* **2018**, *2018*, 1–9. https://doi.org/10.1155/2018/1651629.

(19) Aoki, N.; Mae, K. Extraction. In *Micro Process Engineering*; Hessel, V., Renken, A., Schouten, J. C., Yoshida, J.-I., Eds.; Wiley-VCH Verlag GmbH & Co. KGaA: Weinheim, Germany, 2013; pp 323–345. https://doi.org/10.1002/9783527631445.ch12.

(20) Lapierre, F.; Cameron, N. R.; Zhu, Y. Ready… Set, Flow: Simple Fabrication of Microdroplet Generators and Their Use in the Synthesis of PolyHIPE Microspheres. *J. Micromechanics Microengineering* **2015**, *25* (3), 035011. https://doi.org/10.1088/0960-1317/25/3/035011.

(21) Tebboth, M.; Kogelbauer, A.; Bismarck, A. Effectiveness of Emulsion-Templated Macroporous Polymer Micromixers Characterized by the Bourne Reaction. *Ind. Eng. Chem. Res.* **2015**, *54* (22), 5974–5981. https://doi.org/10.1021/acs.iecr.5b00493.

(22) Tebboth, M.; Kogelbauer, A.; Bismarck, A. Liquid–Liquid Extraction within Emulsion Templated Macroporous Polymers. *Ind. Eng. Chem. Res.* **2015**, *54* (29), 7284–7291. https://doi.org/10.1021/acs.iecr.5b01346.

(23) Barkan-Öztürk, H.; Menner, A.; Bismarck, A. Emulsion Templated Macroporous Polymer Micromixers. *Ind. Eng. Chem. Res.* **2021**, *Submitted*.

(24) Barkan-Öztürk, H.; Menner, A.; Bismarck, A. Polymerised High Internal Phase Emulsion Micromixers for Continuous Emulsification. *Chem. Eng. Sci.* **2021**, 117296. https://doi.org/10.1016/j.ces.2021.117296.
(25) Lissant, K. J. Continuous Process for the Preparation of Emulsions. US3565817A.
(26) Menner, A.; Powell, R.; Bismarck, A. Open Porous Polymer Foams via Inverse Emulsion Polymerization: Should the Definition of High Internal Phase (Ratio) Emulsions Be Extended? *Macromolecules* **2006**, *39* (6), 2034–2035. https://doi.org/10.1021/ma052705x.
(27) Mert, H. H.; Mert, E. H. Emulsion Templated Hierarchical Macroporous Polymers. In *Advanced Functional Porous Materials: From Macro to Nano Scale Lengths*; Uthaman, A., Thomas, S., Li, T., Maria, H., Eds.; Engineering Materials; Springer International Publishing: Cham, 2022; pp 43–86. https://doi.org/10.1007/978-3-030-85397-6_3.
(28) Ikem, V. O.; Menner, A.; Bismarck, A. High-Porosity Macroporous Polymers Sythesized from Titania-Particle-Stabilized Medium and High Internal Phase Emulsions. *Langmuir* **2010**, *26* (11), 8836–8841. https://doi.org/10.1021/la9046066.
(29) Wong, L. L. C.; Ikem, V. O.; Menner, A.; Bismarck, A. Macroporous Polymers with Hierarchical Pore Structure from Emulsion Templates Stabilised by Both Particles and Surfactants. *Macromol. Rapid Commun.* **2011**, *32* (19), 1563–1568. https://doi.org/10.1002/marc.201100382.
(30) Tebboth, M.; Kogelbauer, A.; Bismarck, A. Highly Permeable Macroporous Polymers via Controlled Agitation of Emulsion Templates. *Chem. Eng. Sci.* **2015**, *137*, 786–795. https://doi.org/10.1016/j.ces.2015.06.047.
(31) Mert, H. H.; Mert, M. S.; Mert, E. H. A Statistical Approach for Tailoring the Morphological and Mechanical Properties of Polystyrene PolyHIPEs: Looking through Experimental Design. *Mater. Res. Express* **2019**, *6* (11), 115306. https://doi.org/10.1088/2053-1591/ab437f.
(32) Desire, C. T.; Arrua, R. D.; Mansour, F. R.; Bon, S. A. F.; Hilder, E. F. Effect of Shearing Stress on the Radial Heterogeneity and Chromatographic Performance of Styrene-Based Polymerised High Internal Phase Emulsions Prepared in Capillary Format. *RSC Adv.* **2019**, *9* (13), 7301–7313. https://doi.org/10.1039/C8RA06188B.
(33) Choudhury, S.; Connolly, D.; White, B. Application of Polymeric High-Internal-Phase-Emulsion-Coated Stationary-Phase Columns in Open-Tubular Capillary Electrochromatography. *J. Appl. Polym. Sci.* **2016**, *133* (48). https://doi.org/10.1002/app.44237.
(34) Desire, C. T.; Hilder, E. F.; Arrua, R. D. Monolithic High-Performance Liquid Chromatography Columns. In *Encyclopedia of Analytical Chemistry*; Meyers, R. A., Ed.; John Wiley & Sons, Ltd: Chichester, UK, 2017; pp 1–37. https://doi.org/10.1002/9780470027318.a9386.
(35) Chaleshtari, Z. A.; Foudazi, R. Polypyrrole@polyHIPE Composites for Hexavalent Chromium Removal from Water. *ACS Appl. Polym. Mater.* **2020**, *2* (8), 3196–3204. https://doi.org/10.1021/acsapm.0c00362.
(36) Eslek, A.; Kekevi, B.; Mert, H. H.; Mert, E. H. Emulsion Templated Polymer Monoliths Containing Cellulose Nanocrystals: Synthesis and Adsorption Properties. *J. Appl. Polym. Sci.* **2022**, *139* (11), 51802. https://doi.org/10.1002/app.51802.
(37) Mert, E. H.; Kaya, M. A.; Yıldırım, H. Preparation and Characterization of Polyester–Glycidyl Methacrylate PolyHIPE Monoliths to Use in Heavy Metal Removal. *Des. Monomers Polym.* **2012**, *15* (2), 113–126. https://doi.org/10.1163/156855511X615001.

(38) Bolton, K. F.; Canty, A. J.; Deverell, J. A.; Guijt, R. M.; Hilder, E. F.; Rodemann, T.; Smith, J. A. Macroporous Monolith Supports for Continuous Flow Capillary Microreactors. *Tetrahedron Lett.* **2006**, *47* (52), 9321–9324. https://doi.org/10.1016/j.tetlet.2006.10.113.
(39) Kovačič, S.; Štefanec, D.; Krajnc, P. Highly Porous Open-Cellular Monoliths from 2-Hydroxyethyl Methacrylate Based High Internal Phase Emulsions (HIPEs): Preparation and Void Size Tuning. *Macromolecules* **2007**, *40* (22), 8056–8060. https://doi.org/10.1021/ma071380c.
(40) EL-Hamouz, A.; Cooke, M.; Kowalski, A.; Sharratt, P. Dispersion of Silicone Oil in Water Surfactant Solution: Effect of Impeller Speed, Oil Viscosity and Addition Point on Drop Size Distribution. *Chem. Eng. Process. Process Intensif.* **2009**, *48* (2), 633–642. https://doi.org/10.1016/j.cep.2008.07.008.
(41) Shahid, M. Z.; Usman, M. R.; Akram, M. S.; Khawaja, S. Y.; Afzal, W. Initial Interfacial Tension for Various Organic–Water Systems and Study of the Effect of Solute Concentration and Temperature. *J. Chem. Eng. Data* **2017**, *62* (4), 1198–1203. https://doi.org/10.1021/acs.jced.6b00703.
(42) Kaske, F.; Dick, S.; Pajoohi, S. A.; Agar, D. W. The Influence of Operating Conditions on the Mass Transfer Performance of a Micro Capillary Contactor with Liquid–Liquid Slug Flow. *Chem. Eng. Process. Process Intensif.* **2016**, *108*, 10–16. https://doi.org/10.1016/j.cep.2016.06.010.
(43) Xu, J. H.; Tan, J.; Li, S. W.; Luo, G. S. Enhancement of Mass Transfer Performance of Liquid–Liquid System by Droplet Flow in Microchannels. *Chem. Eng. J.* **2008**, *141* (1–3), 242–249. https://doi.org/10.1016/j.cej.2007.12.030.
(44) Shui, L.; van den Berg, A.; Eijkel, J. C. T. Interfacial Tension Controlled W/O and O/W 2-Phase Flows in Microchannel. *Lab Chip* **2009**, *9* (6), 795–801. https://doi.org/10.1039/B813724B.
(45) Xie, T.; Ma, Y.; Xu, C. Passive Continuous-Flow Microextraction/Stripping System with High Throughput. *Chem. Eng. Sci.* **2020**, *223*, 115745. https://doi.org/10.1016/j.ces.2020.115745.
(46) Darekar, M.; Sen, N.; Singh, K. K.; Mukhopadhyay, S.; Shenoy, K. T.; Ghosh, S. K. Liquid–Liquid Extraction in Microchannels with Zinc–D2EHPA System. *Hydrometallurgy* **2014**, *144–145*, 54–62. https://doi.org/10.1016/j.hydromet.2014.01.010.
(47) Jafari, O.; Rahimi, M.; Kakavandi, F. H. Liquid–Liquid Extraction in Twisted Micromixers. *Chem. Eng. Process. Process Intensif.* **2016**, *101*, 33–40. https://doi.org/10.1016/j.cep.2015.12.013.

Supporting Information

Liquid-liquid extraction using combined hydrophilic-hydrophobic emulsion templated macroporous polymer micromixer-settlers

Hande Barkan-Öztürk,[1] Joanna Delorme,[1,†] Angelika Menner,[1] Alexander Bismarck[1,2,]*

[1] Polymer and Composite Engineering (PaCE) Group, Institute of Material Chemistry and Research, Faculty of Chemistry, University of Vienna, Währinger Strasse, 42, 1090, Vienna, Austria.

[2] Department of Chemical Engineering, Imperial College London, South Kensington Campus, London SW7 2AZ, United Kingdom

[†] Placement student from Sigma-Cermont, 20 Avenue Blaise Pascal, 63178 Aubiere Cedex, France.

* Corresponding author: Alexander Bismarck, e-mail: alexander.bismarck@univie.ac.at

S1. Swelling experiments of polyHIPEs

Swelling tests were performed on polyHIPEs to evaluate the resistance against ethyl acetate and water. PolyHIPE monoliths were cut into cubical shape (height = ~10 mm). After measuring the

dry weight and dimensions, five samples were placed into vials and 10 mL of solvent (water or ethyl acetate) was added. Weight and dimensions of swollen polyHIPEs were recorded after 24 h. Afterwards, the samples were dried in a conventional oven for 24 h at 70 °C and their weight and dimensions were re-measured to determine possible material loss. Swelling ratios Q were calculated from the ratio of volume of the swollen V_{SM} to initial dry volume V_0 of the polyHIPEs:

$$Q = \frac{V_{SM}}{V_0} \qquad \text{(Eq. S1)}$$

Table S1-1. Swelling ratios (Q) of polyHIPEs in H_2O and EtOAc.

	Q_{H_2O}	Q_{EtOAc}
HM-10	1.38 ± 0.04	1.04 ± 0.03
HM-15	1.33 ± 0.15	1.03 ± 0.03
S	1.02 ± 0.03	1.03 ± 0.02
SF	1.02 ± 0.02	1.01 ± 0.01

S2. Mechanical properties of polyHIPEs

Compression tests were carried out at room temperature using a universal dual column testing frame (5584, Instron Ltd., Norwoord, UK) equipped with a 1 kN load cell. The specimens had a diameter of 12 mm and height of 10 mm. Samples were compressed at a rate of 1 mm/min until the height reduced by 60% of its original value. Elastic moduli were determined from the slope of the initial linear elastic region of the stress-strain plot. The crush strength was determined from the maximum compressive strength of the sample at the end of the initial linear elastic region.

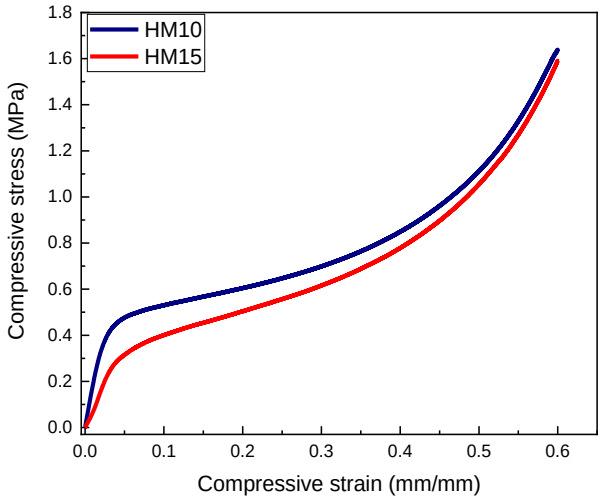

Figure S2-1. Compression stress-strain curves of hydrophilic polyHIPEs produced by polymerization of o/w HIPE templates.

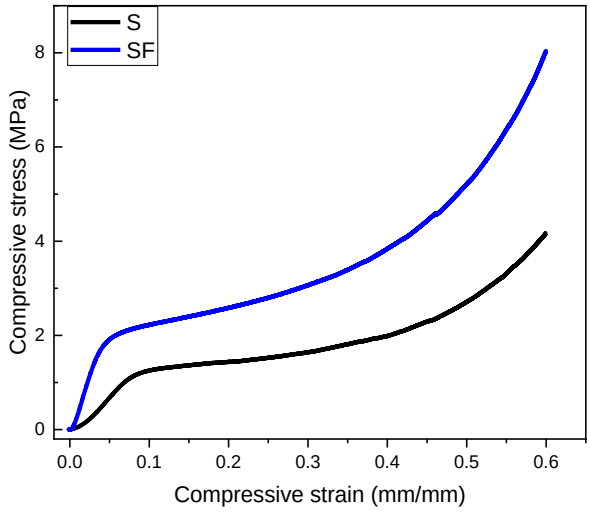

Figure S2-2. Compression stress-strain curves of hydrophobic polyHIPEs produced by polymerization of w/o HIPE templates.

S3. Determination of fluorine content of hydrophobic polyHIPEs

Elemental analysis (Eurovector EA 3000 CHNS-O Elemental Analyser) was performed using 0.75 and 3.0 mg of sample, weighed into tin vials (4×6 mm). Samples were run at least in duplicate. The operating temperatures for combustion and reduction were 1000 °C (1480 °C for O analysis) and 750 °C, respectively, using He (99.999+) as carrier gas. FT-IR spectra were recorded three times with new samples in the range of 4000-400 cm^{-1} (Bruker Tensor II fitted with an A225/Q Platinum ATR unit). The sample was pressed using a clamp onto ATR unit to achieve good contact. The elemental composition of samples was analyzed by high resolution X-ray photoelectron spectroscopy (HR-XPS) (Nexsa, Thermo Fisher Scientific) using Al K_α radiation and the spectra analyzed (Avantage v5.9925 with Smart background, Simplex fitting and Gauss-Lorentz product). Reference values for functional group binding energies were sourced from the NIST Standard Reference Database.[1] Weight% of the detected atom ($wt._i\%$) was calculated from its atomic% ($at._i\%$) determined from the area under the XPS curve, which was given by the software:

$$wt_i\% = \frac{M_{W_i} \cdot at_i\%}{\sum_{j=1}^{k}(M_{W_j} \cdot at_j\%)} x100 \qquad (Eq.S3.1)$$

Table S3-1. F content of hydrophobic polyHIPEs determined using EA and XPS, and their static contact angles.

Sample	F amount (wt.%)[i]	F amount (wt.%)[ii]	Contact angle (-)
S	0	0	116.6 ± 1.8
SF	3.6 ± 0.1	1.19	134.8 ± 3.7

[i] F content was determined using EA.
[ii] F content was determined using XPS.

FT-IR spectra were recorded three times with new samples in the range of 4000-400 cm^{-1} (Bruker Tensor II fitted with an A225/Q Platinum ATR unit). The sample was pressed using a clamp onto ATR unit to achieve good contact.

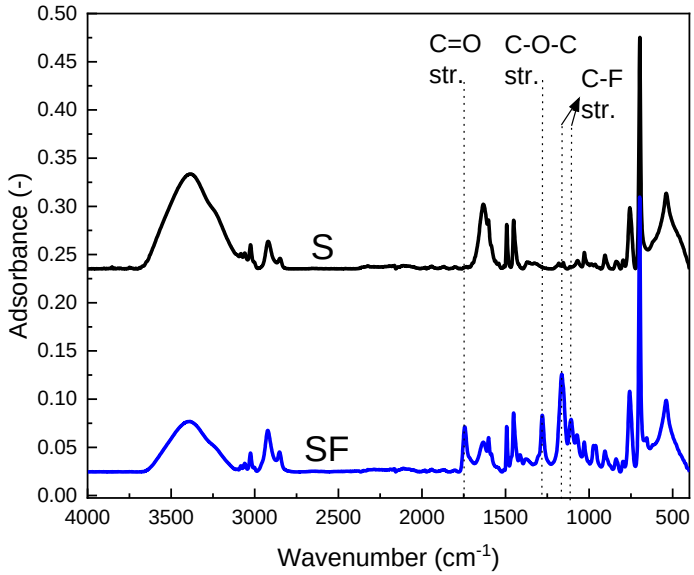

Figure S3-1. FTIR spectra of polyHIPEs produced by polymerization of HIPE containing 0 (S) or 2 vol% (SF) TFEMA.

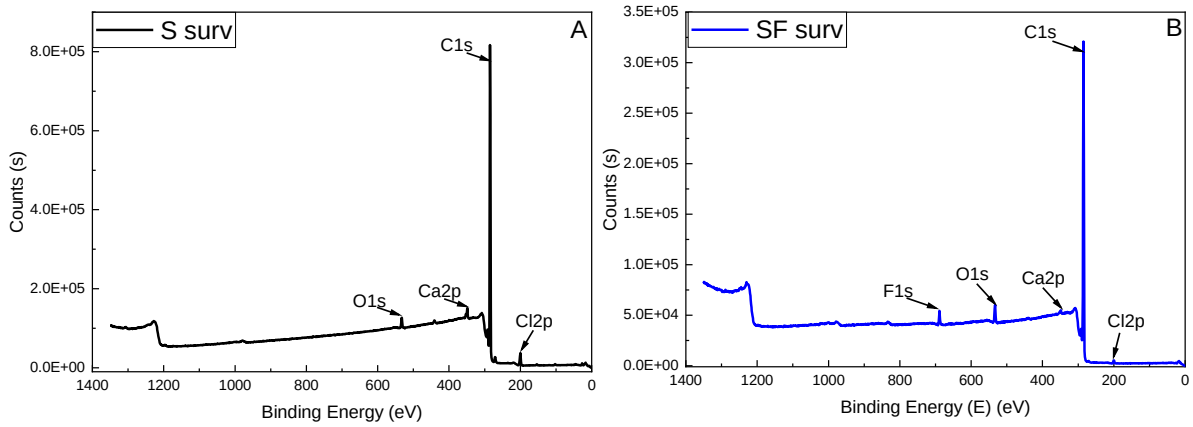

Figure S3-2. XP survey spectra of A) poly(St-co-DVB)HIPEs (S) and B) poly(St-co-DVB-co-TFEMA)HIPEs (SF).

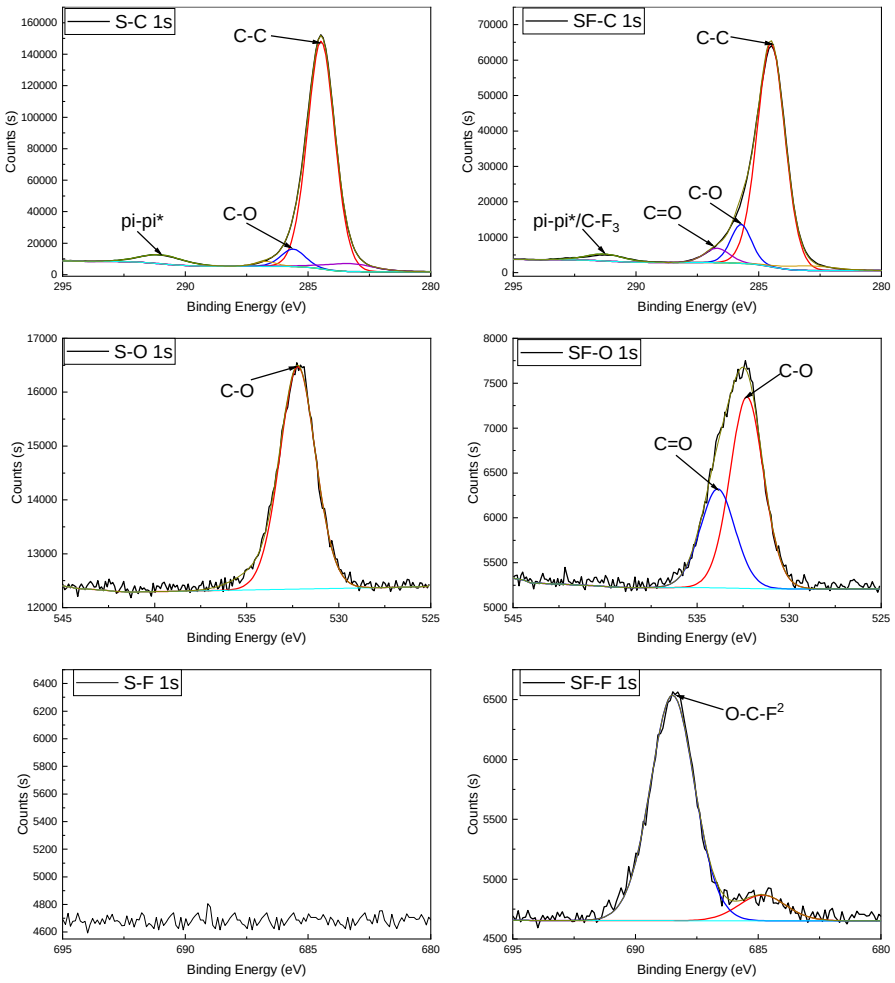

Figure S3-3. High resolution C1s, O1s and F1s XP spectra of S and SF polyHIPEs. O-C-F peak assignment indicates polymerization of TFEMA.[2]

S4. Static contact angle measurements of polyHIPEs

Static contact angles of water droplets on polyHIPEs were determined using a drop shape analyzer (DSA30, Krüss GmbH, Hamburg, Germany). The initial contact angle was recorded 5 s after dosing (2 µL drop of each test liquid), followed by measurements after 60 s. At least 30 measurements at three sites were taken.

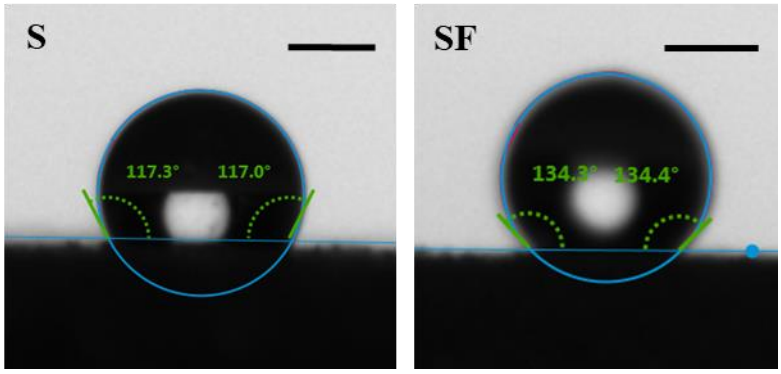

Figure S4-1. Static contact angle measurement of poly(St-co-DVB)HIPEs (S) and poly(St-co-DVB-co-TFEMA)HIPEs (SF).

S5. Calibration curve of 4-Aminoacetophenone by UV-Vis Spectroscopy

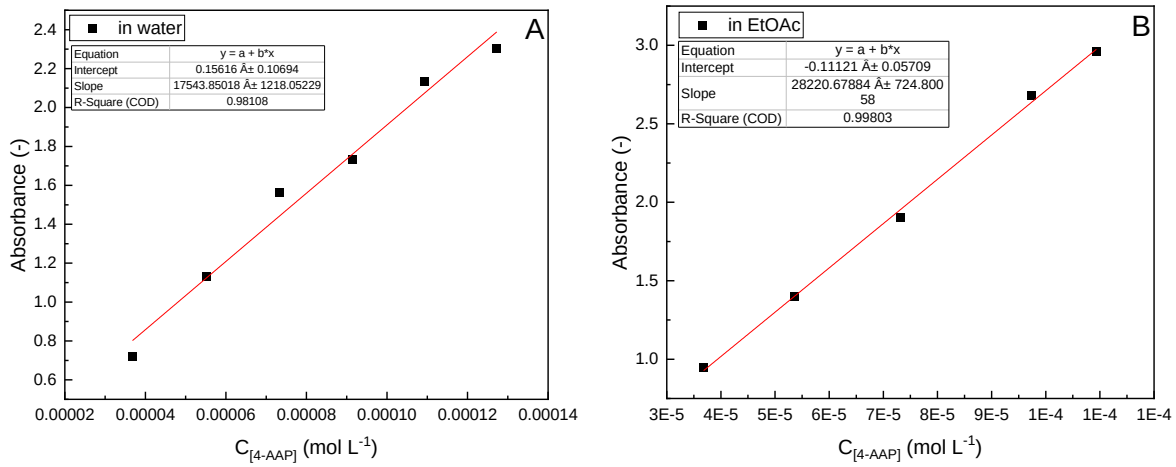

Figure S5-1. Absorbance measured by UV-Vis spectroscopy of known [4-AAP] concentrations A) in water and B) in ethyl acetate. Using this calibration curve unknown [4-AAP] concentrations could be determined from measured absorbance using the Beer-Lambert law.

S6. Determination of mass transfer coefficient k_L of 4-AAP

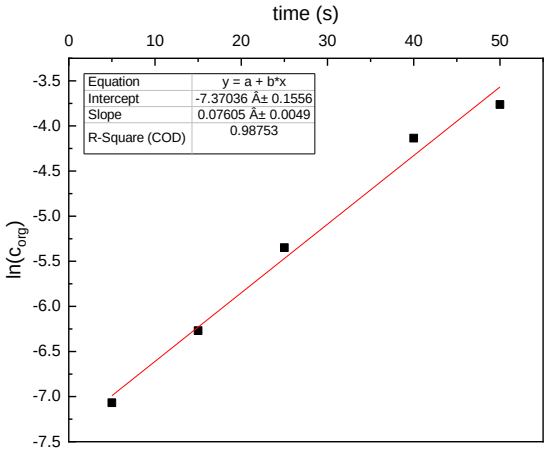

Figure S6-1. Determination of k_L in a vessel agitated with sawtooth impeller to show the variation of [4-AAP] concentration in the organic phase.

S7. Residence time distribution and permeability of extraction units

The RTD of polyHIPE extraction units was determined as mentioned in our previous study.[3] Briefly, an inert tracer (aqueous KCl solution) was injected into the extraction unit, whilst water flowing though the other inlet. A differential refractometer (DnDc, WGE Dr Bures, Dallgow-Doeberitz, Germany) was used to monitor the tracer concentration in the effluent by refractive index measurements as function of time. Since the measured refractive index is proportional to the tracer concentration, the tracer concentration in the exit stream was determined from the refractive index increment (dn/dc) of KCl solutions with known concentrations. While demineralized water was feed continuously through one of the inlet tubes using a syringe pump (PHD Ultra, Harvard Apparatus, UK) at a flow rate of 0.4 or 0.6 mL/min, through the other inlet 0.2 mL tracer (25 mg/mL KCl) was injected as pulse input. The refractive index of the effluent of extraction unit was recorded continuously against water. The measured refractive index was converted to concentration $c(t)$ using the calibration curve **Figure S7-1**.

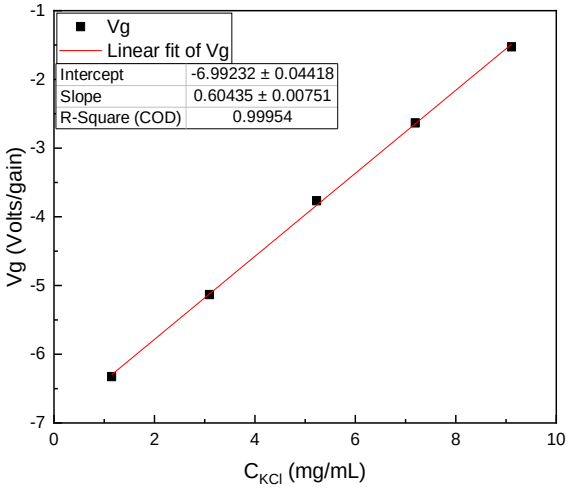

Figure S7-1: Refractive index increment (dn/dc) of KCl solutions with various concentrations obtained from the refractive index measurement (Vg).

The RTD function E(t) was determined using:[4]

$$E(t) = \frac{c(t)}{\int_0^\infty c(t)dt} \qquad \text{(Eq. S7.1)}$$

The mean residence time t_m and average residence time τ were calculated as follows:[4]

$$t_m = \int_0^\infty tE(t)dt \qquad \text{(Eq. S7.2)}$$

$$\tau = \frac{PV}{Q} \qquad \text{(Eq. S7.3)}$$

where t is the time of each measured $c(t)$, P the porosity, V the pore volume of the monolith and Q the volumetric flow rate.

The permeability k of the extraction units was calculated using Darcy's law from the measured pressure drop ΔP during water flooding of the extractor:

$$Q = \frac{k \cdot A}{\mu} \frac{\Delta P}{L} \qquad (Eq.S7.4)$$

where Q is the total flow rate, A cross-sectional area of polyHIPE extractor, μ the viscosity of the water and L the length of the extraction unit.

Table S7-1. Pressure drop (ΔP) and energy dissipation rate (ε) of extraction units fabricated using either single polyHIPEs or combination of hydrophilic and hydrophobic polyHIPEs.

Extraction unit	ΔP (bar)		ε (m^2/s^3)	
	0.4 mL/min	0.6 mL/min	0.4 mL/min	0.6 mL/min
E-HM10	1.40 ± 0.01	1.47 ± 0.02	0.4	0.6
E-HM15	1.61 ± 0.02	2.02 ± 0.03	0.08	0.13
E-S	1.16 ± 0.03	1.18 ± 0.01	0.11	0.28
E-SF	1.19 ± 0.01	1.32 ± 0.03	0.03	0.05
E-SF-HM10	1.21 ± 0.01	1.33 ± 0.01	0.04	0.10
E-HM10-SF	1.30 ± 0.01	1.48 ± 0.04	0.04	0.10
E-SF-HM15	1.47 ± 0.01	1.45 ± 0.01	0.06	0.14
E-HM15-SF	1.50 ± 0.03	1.72 ± 0.01	0.09	0.13
Blank tube	0.12 ± 0.01	0.14 ± 0.01	0.10	0.21
Static mixer	0.09 ± 0.01	0.11 ± 0.02	0.03	0.06

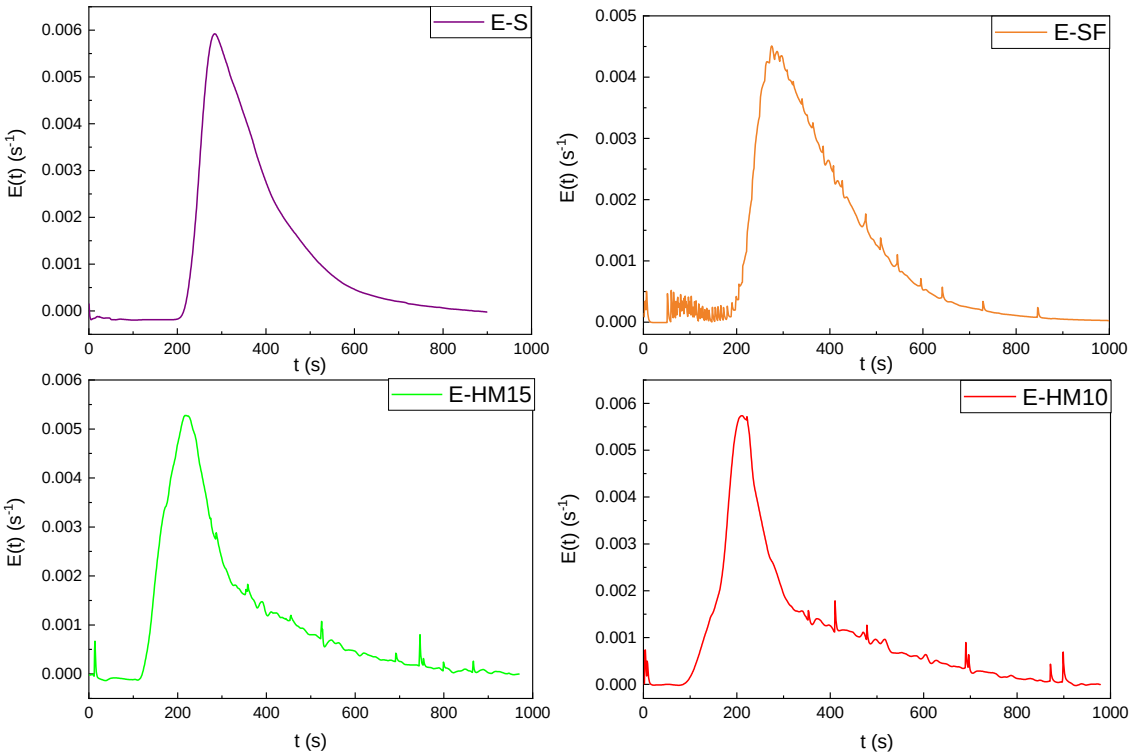

Figure S7-2. Residence time distribution functions of polyHIPE extraction units fabricated using single polyHIPEs.

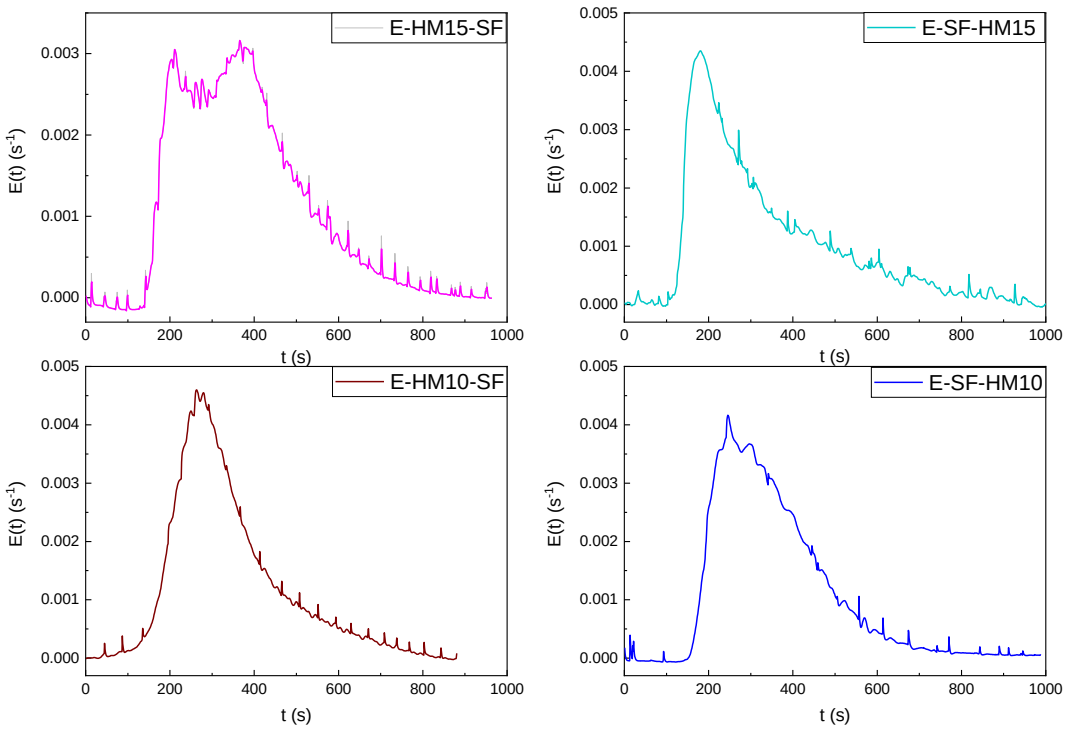

Figure S7-3. Residence time distribution functions of polyHIPE extraction units fabricated using both hydrophilic and hydrophobic polyHIPEs.

S8. Effect of polyHIPE wettability on liquid-liquid dispersion type

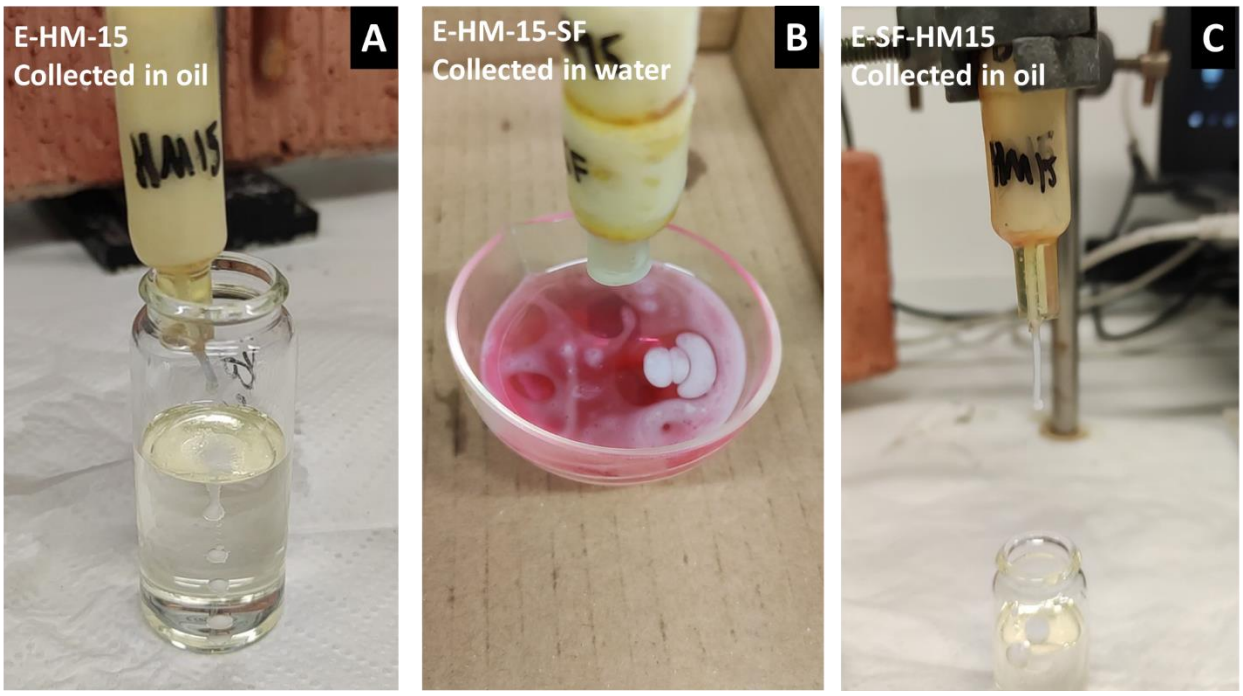

Figure S8-1. Photographs of emulsions generated with polyHIPE extraction units having various wettability, which resulted in A) o/w emulsions collected in sunflower seed oil using hydrophilic polyHIPE extraction unit (Video S1), B) w/o emulsions collected in dyed water using hydrophilic-hydrophobic polyHIPE extraction unit (Video S3), and C) o/w emulsions collected in sunflower seed oil using hydrophobic-hydrophilic polyHIPE extraction unit (Video S2).

S9. Simulated hydrogenation reaction of 4-nitroacetophenone

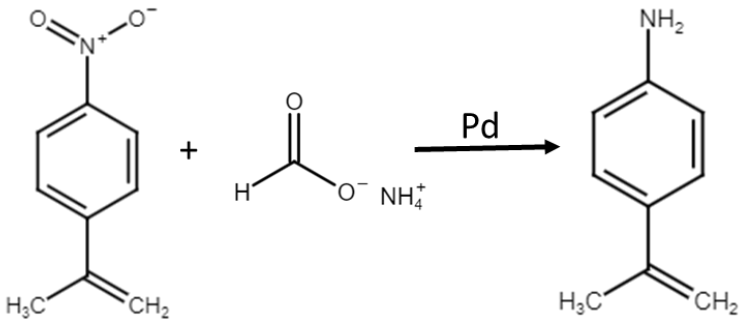

Figure S9-1. Hydrogenation reaction of 4-nitroacetophenone (4-NAP) with ammonium formate as hydrogen source catalyzed by Pd yielding 4-aminoacetophenone (4-AAP). This reaction mixture was simulated, and 4-AAP was extracted from it using ethyl acetate.

S10. Morphology of used polyHIPE micromixer-settlers

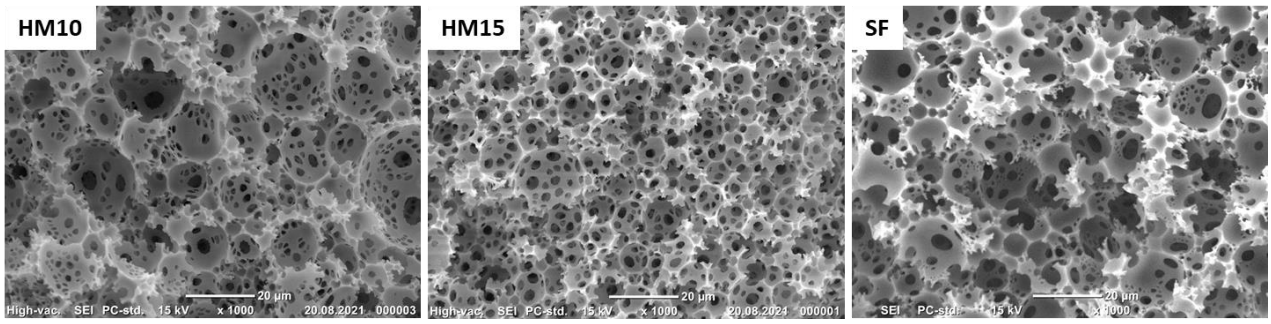

Figure S10-1. Characteristic SEM images of polyHIPEs after using them in micromixer-settlers to extract 4-AAP.